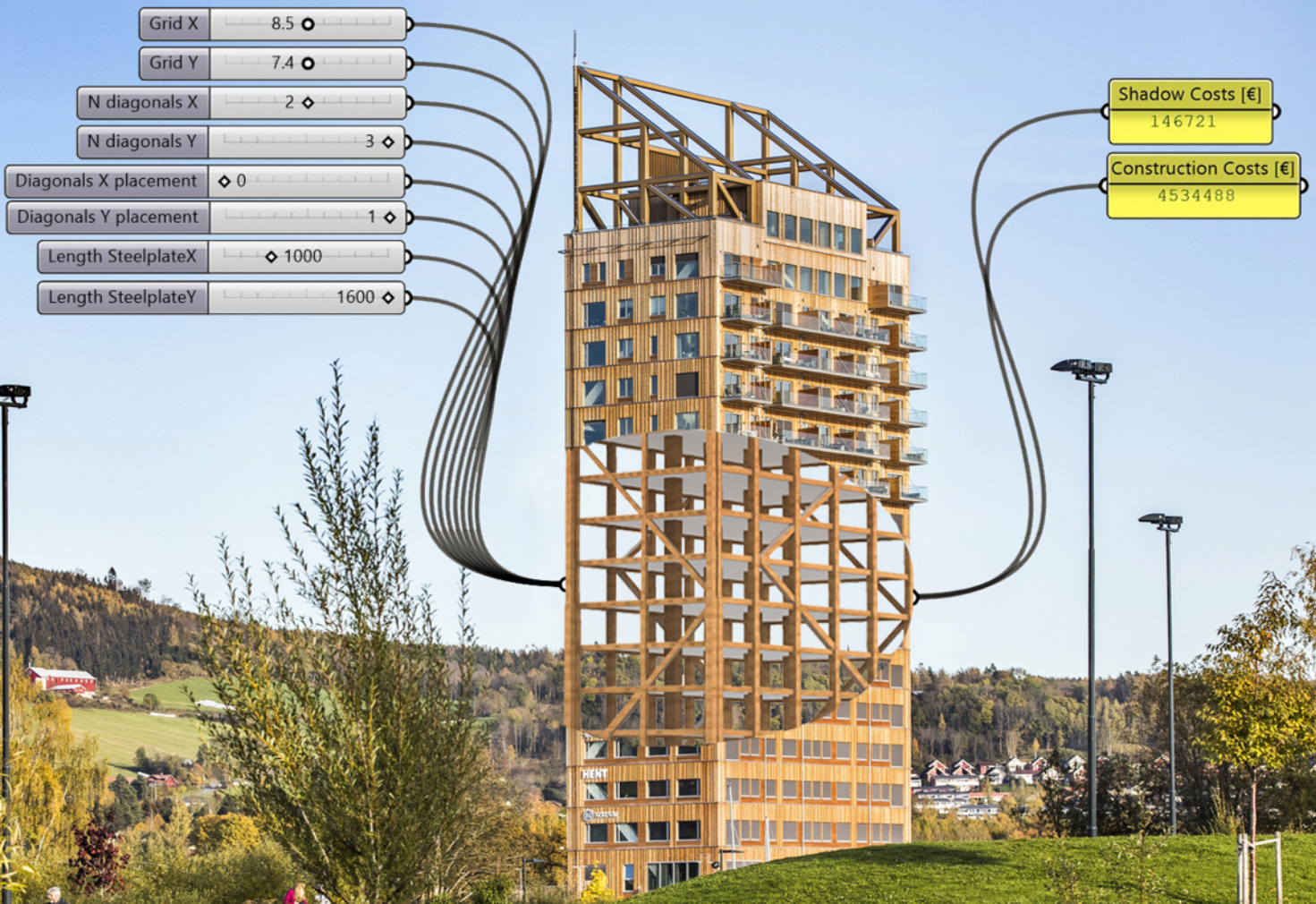


Multidisciplinary Design Optimization of Timber High-Rise

Research and Development of a Multidisciplinary Design Optimization Tool



J.F. de Gaaij

Multidisciplinary Design Optimization of Timber High-Rise

Research and Development of a
Multidisciplinary Design Optimization Tool

by

Joris Frank de Gaaij

to obtain the degree of Master of Science
at the Delft University of Technology,
to be defended publicly on Wednesday, June 16, 2021 at 9:00 AM

Student number:	4441206
Project duration:	September 1, 2020 – June 16, 2021
Thesis committee:	dr.ir. M.A.N. Hendriks, TU Delft, chair
	ir. L.P.L. van der Linden, TU Delft
	ir. C. Noteboom, TU Delft
	ing. T. Borst, Arcadis, daily supervisor
	dr. Ir. J.L. Coenders, White Lioness technologies

An electronic version of this thesis is available at <http://repository.tudelft.nl/>.

Abstract

In June 2019, the Netherlands presented their national Climate Agreement, aiming to meet the strict goals as agreed at the Paris Agreement. One of these goals is a reduction of CO_2 emittance of 3.4 Mton in 2030 compared to a reference scenario [43]. These goals for carbon emission reductions have a great impact on the construction industry. Since the construction industry is responsible for around 39% of the worlds total carbon emissions [146] [69]. Another major challenge in the coming decades is the growing trend of urbanization. The United Nations predicts 2.5 billion people will move to urban areas by 2050 [112], which results in densification in cities. Timber high-rise might prove as a suitable solution to both these problems.

However, there is a lack of implementation of timber high-rise. Bayne (2006), Giesekam et al. (2016), and Gosselin et al. (2017) conducted interviews and investigated articles to identify the cause for this lack of implementation [19], [56], [58]. Based on these findings the presence of a feedback loop is assumed, which hinders the implementation of timber high-rise.

It is argued that a lack of thorough analysis of timber design alternatives in the conceptual design phase is the root of this feedback loop, which results in the exclusion of further evaluation of timber building designs. This research intends to break this feedback loop through a thorough consideration of timber design alternatives in the conceptual design phase. This is achieved by the development of a tool, based on the Multidisciplinary Design Optimization (MDO) method. Using MDO, "high performing designs can be identified through the exploration of both geometric and non-geometric variables according to established design objectives and constraints" [132], [40]. In Grasshopper, a parametric model is created with which timber building designs are generated, validated, and optimized. As it is not possible to assess all of the disciplines in the Architecture, Engineering, and Construction industry, the most important disciplines are selected, resulting in two main optimization objectives and two constraints:

- **Structural - Constraint** Each building must be designed according to the constraints as determined in the Eurocode.
- **Architectural - Constraint** Each building must satisfy the architectural design requirements for acoustics, building height, and daylight entrance.
- **Environmental - Optimization objective** The environmental optimization objective is to minimize shadow costs, which are determined according to the MPG methodology. The MPG methodology uses Life Cycle Analysis data to assess the embodied energy impact of structural materials. This embodied energy impact is expressed in shadow costs [22].
- **Economical - Optimization objective** The economical optimization objective is to minimize construction costs.

Based on the mentioned constraints, the tool aims to indicate the design situations in which timber high-rise can be competitive to an assessed concrete design alternative, considering the combination of properties for shadow costs and construction costs. This leads to the main research question:

"For which design situation can a timber braced tube system be economically and environmentally competitive with a concrete design alternative for a 50 to 70 meter tall building?"

This research aims to answer this research question by following three steps:

1. **Theoretical Framework** A combination of literature study and unstructured interviews provided the required information to develop an accurate tool. It was found that a braced tube system is the most appropriate stability system to use when designing a full timber high-rise building. Furthermore, Kerto-Ripa floors were found to be the most suitable floor system. The theoretical framework also provided three methods for consideration of carbon sequestration in shadow costs calculations. Carbon sequestration is the storage of carbon dioxide outside of the atmosphere which takes place during the growth of a tree. The Dutch norms do not allow for the inclusion of this effect of carbon sequestration in the

calculation of shadow costs. It was also concluded that for two conflicting optimization objectives, a Pareto front will be found when performing an MDO [41]. This Pareto front consists of Pareto optimal building designs, which depict the designs containing the most favourable combination of properties for shadow costs and construction costs.

2. **Development of the Multidisciplinary Design Optimization tool** The design problem is translated into logic based on the information obtained in the theoretical framework. Using input parameters, the tool generates and evaluates timber building designs. These building designs are evaluated based on two optimization objectives: the environmental performance, represented in shadow costs, and the economical performance, represented in construction costs. Next, a Multi-Objective Genetic Algorithm (MOGA) optimizes the building design for both objectives. The dimensioning of the structural system, the construction costs calculation, and the shadow cost calculation, as performed in the tool, were found to be accurate when verified using Mjøstårnet as a reference project.
3. **Case study** Two concrete buildings, which are based on a current Arcadis project, are used as case studies. Both concrete buildings represent a design situation. The main difference between these design situations is the building dimensions. Building A3 represents timber building designs that are created for a design situation with a floor area of 28.8 x 28.8 m and a height of 60 meters. Building B3 represents timber building designs that are created for a design situation with a floor area of 21.6 x 43.2 m and a height of 50 meters. For both case studies, an optimization will obtain timber building designs with an optimal combination of properties for shadow costs and construction costs. Next, the competitiveness of the timber building designs and the concrete building design were analysed for both design situations.

Following these three steps, the following results were obtained. The Octopus plug-in is used in the tool. The Multi-Objective Genetic Algorithm used in this plug-in is the SPEA-2 algorithm as proposed by Zitzler et al. in 2001 [171]. The created tool was found to generate and evaluate timber building designs rapidly. The structural layout of the obtained Pareto optimal buildings is according to expectations. A full generation, evaluation, and verification of a timber building design requires 1.22 seconds on average using a 2.4 GHz processor. Furthermore, the Octopus plug-in is found to efficiently determine Pareto optimal building designs since half of the Pareto optimal building designs are obtained when only 6.25% of all possible building designs have been analysed.

When the effect of carbon sequestration is excluded in the calculation of shadow costs, the use of timber and concrete in the structural system was found to generate comparable results considering their shadow costs. The inclusion of the effect of carbon sequestration during the lifetime of a timber building results in a reduction of shadow costs of approximately 40% compared to a similar concrete building.

Considering the boundary conditions and scope of this research the ULS is found to be normative for a slenderness up to 2.35. When the slenderness is greater than 2.35, the along-wind acceleration was found to become normative. For all Pareto optimal building designs, the ULS check was found to be normative over the SLS check. The mass of the Pareto optimal timber building designs was found to be approximately 8 times smaller than their respective concrete design alternatives. The stability system used was found to be favourable considering construction costs compared to the construction costs of the assessed reference projects as obtained by Jackson (2019) and Tupenaite (2019) [85], [145].

Finally, the main research question can be answered. For the design situation based on the concrete building "The Rectangle", the Pareto optimal timber building designs, referred to as Building B3, were found to be competitive with "The Rectangle". For the other analysed design situation, the Pareto optimal timber building designs referred to as Building A3, were not found to be competitive with the concrete building "The Square". Considering the boundary conditions and scope of this research, it can be concluded that a design situation with a rectangular floor plan is favourable over a design situation with a square floor plan and a design situation with a building height of 50 meter is favourable over a design situation with a building height of 60 meter.

In future research, it would be interesting to compare the obtained results with a building design containing a stability system with a concrete core and timber floors, beams, and columns. This research recommends the Dutch government to create legislation resulting in a financial incentive, as is done for electric cars, to increase the implementation of timber buildings. Lastly, it is recommended to research several missing or conservative regulations in timber design and revise them if required.

Preface

This thesis was written in conclusion of my studies in Civil Engineering, master track Building Engineering, with specialization in Structural design at Delft University of Technology. The research was carried out in collaboration with the Faculty of Civil Engineering and Geosciences and the engineering firm Arcadis.

I would like to express my gratitude to Arcadis, where this research project was performed. Without the advice and insight from Tom Borst and other colleagues at Arcadis this thesis would not have been the same.

Furthermore, I would like to thank my other supervisors, Max Hendriks, Chris Noteboom, and Lennert van der Linden, who together have answered over two hundred questions. Their insightful answers, comments, and remarks have guided me through this research project. This has helped me tremendously with both staying on track and exploring the possibilities for additional analysis which increases the breadth of this research project. First, I would like to express my gratitude to Max Hendriks, who was always ready to help me keep an overview on this research and the scientific argumentation and background. Next, I would like to thank Chris Noteboom for his knowledge, feedback, and for the numerous conversations we have had regarding the effects of connection design on the stability system. Lastly, I would like to thank Lennert van der Linden who has helped me with parametric modelling and numerous other questions.

Thanks, Jeroen Coenders, for introducing me to the Multidisciplinary Design Optimization method, which formed the start of this research. Sadly, the circumstances did not allow for the implementation of this tool in the White Lioness online platform. Nevertheless, your feedback and insights, especially in the Multidisciplinary Design Optimization method have been of great help to me.

Thanks to my family and friends for their support during my thesis. Thanks for your genuine interest regarding my thesis, but also thanks for all the times you helped me unwind in this 10-month-process. Special thanks to my parents Maarten and Anita, my brother Casper and my girlfriend Roos, for their support during this thesis. Thank you Maarten and Anita, not only for your support during this thesis but more importantly for your motivation, help, and support throughout my whole life. This has helped me enormously to finish my studies and obtain the title Master of Science in Building Engineering at the Faculty of Civil Engineering at Delft University of Technology.

*J.F. de Gaaij
Delft, June 2021*

Contents

Abstract	iii
Glossary	xi
1 Introduction	1
1.1 Research context	1
2 Problem Analysis	3
2.1 Problem definition	3
2.1.1 Common decision-making method	3
2.1.2 Multidisciplinary Design Optimization method	4
2.2 Aim	6
3 Approach	7
3.1 Research question	7
3.1.1 Sub-questions	7
3.2 Methodology	7
3.3 Scope	9
4 Theory	11
4.1 Multidisciplinary Design Optimization	11
4.1.1 Introduction	11
4.1.2 Design optimization	13
4.1.3 MDO architecture	14
4.1.4 Design choices	16
4.2 Timber	18
4.2.1 Types of timber building materials	18
4.2.2 Properties and costs	20
4.3 High-Rise	22
4.3.1 Reference projects	22
4.3.2 Lateral stability systems	23
4.4 Building Elements	26
4.4.1 Connections	26
4.4.2 Floor	30
4.4.3 Beam	31
4.4.4 Column	31
4.4.5 Diagonals	31
4.4.6 Core	31
4.5 Disciplines	32
4.5.1 Structural	32
4.5.2 Architectural	33
4.5.3 Environmental	33
4.5.4 Economical	37
4.6 Structural design considerations	39
4.6.1 General	39
4.6.2 Serviceability Limit State	42
4.6.3 Ultimate Limit State	42

4.6.4	Fire safety	42
4.6.5	Scope	42
4.7	Architectural design considerations	43
4.7.1	Acoustics	43
4.7.2	Storey height	43
4.7.3	Daylight	43
5	Development of Multidisciplinary Design Optimization Tool	45
5.1	Introduction	45
5.1.1	Design problem	45
5.1.2	Design choices	47
5.2	Overview of modelling	49
5.3	Input parameters	51
5.4	Building geometry	53
5.4.1	Storey height	53
5.4.2	Geometry	54
5.5	Gravitational system	55
5.6	Floor system	56
5.7	Stability system	57
5.7.1	Grouping of members	58
5.8	Economical performance	61
5.9	Environmental performance	62
5.10	Post optimization verification	63
5.11	Multidisciplinary Design Optimization	64
5.12	Tool verification	65
5.12.1	Structural	66
5.12.2	Economical	66
5.12.3	Environmental	68
6	Case Studies	69
6.1	Introduction	69
6.1.1	Case studies	69
6.1.2	Tool guideline	71
6.1.3	Methodology	72
6.2	Genetic Algorithm analysis	73
6.2.1	Computational time and accuracy	73
6.3	Stability system analysis	76
6.3.1	150 meter tall building	76
6.3.2	Diagonal layout	80
6.4	Timber buildings analysis	82
6.4.1	Unity Checks	85
6.4.2	Angle of diagonals	89
6.4.3	Comparison to reference projects	90
6.4.4	Comparison to case studies	92
6.5	Case study analysis	95
6.5.1	Construction costs and shadow costs comparison	95
6.5.2	Carbon sequestration calculation methods	100
6.6	Conclusion	102
7	Discussion	105
7.1	Discussion of tool	105
7.2	Discussion of results	107
8	Conclusion	109
8.1	Answer to research questions	109
8.1.1	Sub-questions	109
8.2	Research question	111

9 Recommendations	113
9.1 Recommendations for future research	113
9.2 Recommendations for policy makers	114
Bibliography	115
A Theory	125
A.1 Properties and costs of timber	125
A.1.1 Structural properties	125
A.1.2 Sustainability	126
A.1.3 Durability	127
A.1.4 Fire safety	127
A.1.5 Acoustics	129
A.1.6 Additional properties	129
A.1.7 Costs	130
A.2 Reference projects	131
A.2.1 Introduction	131
A.2.2 25 King	131
A.2.3 Treet	132
A.2.4 Murray Grove Stadthaus	133
A.2.5 Mjøstårnet	133
A.2.6 Brock Commons Project	134
A.3 Connection types	135
A.3.1 Steel plate and dowels	135
A.4 Structural design considerations	139
A.4.1 Loads	139
A.4.2 Serviceability Limit State	142
A.4.3 Ultimate Limit State	147
A.4.4 Fire safety	150
A.5 Level Of Development	153
A.6 Optimize Cross Section	154
A.6.1 Verification	155
B Calculation of Building Elements	157
B.1 Steel plate and dowel connection	157
B.1.1 Custom node calculation	157
B.1.2 Verification	160
B.2 Knapp connection	165
B.3 Floors	166
B.3.1 Vibrations	166
B.3.2 Shear and tension	168
B.4 Beams	171
B.4.1 Custom node calculation	171
B.5 Columns	172
B.5.1 Custom node calculation	172
B.6 Diagonals	174
B.6.1 Force estimation	175
B.7 Core	176
B.7.1 Custom node calculation	176
B.7.2 Verification	179
B.8 Stability system	180
B.8.1 Verification	180
C Environmental and Economical Data	183
C.1 Environmental performance calculation	183
C.1.1 EPD data	183
C.2 Economical performance calculation	185

C.2.1 Construction costs per building element	185
C.2.2 Example of MAMO calculation	185
D Case Study	187
D.1 Construction cost calculations	187
D.2 MPG calculations	187
D.3 Building weight calculations	192
E Grasshopper Model Overview	193
E.1 Fixed model input parameters	193
E.2 Input parameters Mjøstårnet model	195
E.3 Figures of Grasshopper model	197
F Interviews	217

Glossary

AEC	Architecture, Engineering, and Construction
ARBO	<i>Arbeidsomstandighedenwet</i>
BECCS	BioEnergy with Carbon Capture and Storage
CLT	Cross Laminated Timber
CNC	Computer numerical control
EPD	Environmental Product Declaration
FSC	Forest stewardship council
GA	Genetic Algorithm
GFA	Gross Floor Area
Glulam	Glued laminated timber
GWP	Global Warming Potential
HypE	Hypervolume estimation algorithm for multi-objective optimization
IIC	Impact Insulation Class
LCA	Life Cycle Assessment
LOD	Level Of Development
MAMO	<i>Materiaal, Arbied, Materieel, Onderaanneming</i>
MDO	Multidisciplinary Design Optimization
MKI	<i>Milieu Kosten Indicator</i>
MOGA	Multi-Objective Genetic Algorithm
MPG	<i>MilieuPrestatie Gebouwen</i>
NMD	<i>Nationale Milieu Database</i>
ODP	Stratospheric Ozone Depletion Potential
SLS	Serviceability Limit State
SPEA-2	Strength Pareto Evolutionary Algorithm 2
STC	Sound Transmission Class
ULS	Ultimate Limit State

1

Introduction

1.1. Research context

Timber high-rise In June 2019, the Netherlands presented their national Climate Agreement, intending to meet the strict goals as agreed at the Paris Agreement. This national Climate Agreement contains various goals for the Netherlands. In 2030 the goal is to emit 3.4 Mton CO_2 less than in a reference scenario [43]. These goals for carbon emission reductions have a great impact on the construction industry. Since the construction industry is responsible for around 39% of the world's total carbon emissions [146] [69]. These carbon emissions can be divided into operational energy, responsible for 28%, and embodied energy, responsible for 11% [35]. With the rise of energy-neutral buildings, the emissions caused by operational energy decreases, thus increasing the relative impact of embodied energy. The usage of sustainably harvested timber as a building material can help lower carbon emissions for two reasons. Firstly, the primary energy consumption of timber is relatively low compared to traditional building materials such as concrete and steel [143]. Secondly, timber stores carbon dioxide, which retains the carbon dioxide outside the atmosphere for a period of at least the lifetime of the building.

Another major challenge in the coming decades is the growing trend of urbanization. In 2018, 55% of the world's population lived in cities. This percentage is expected to grow to 68% by 2050. Furthermore, the world's population is expected to grow by 2.2 billion people by 2050. Altogether, this results in an expected 2.5 billion people moving to urban areas by 2050 [112]. This urbanization results in densification in cities, which increases the demand for high-rise buildings. The creation of timber high-rise buildings can provide a solution to both these challenges.

Implementation of timber high-rise Although timber high-rise can help meet the urbanization demands and reduce carbon emissions, timber high-rise buildings are rarely realized. The reasons for this lack of implementation are identified in various researches. Bayne (2006) summarized the issues of timber building design by conducting interviews and focus groups with 34 designers and specifiers [19]. Giesekam et al. (2016) surveyed architects and engineers, receiving 32 full responses and 15 partial responses [56]. Gosselin et al. (2017) investigated 53 scientific articles, 13 documents, and concerns in the meeting minutes of non-residential timber buildings [58]. All researches report the following main reasons for lack of implementation of timber buildings:

- Lack of technical knowledge.
- Lack of economic certainty.
- Lack of established standards.
- Negative perceptions by other project professionals.
- Durability concerns

This research argues that these five reasons are coupled and can be presented with a feedback loop, as shown in Figure 1.1. The feedback loop suggests that a lack of thorough design considerations of timber design alternatives in the conceptual design phase results in the exclusion for further evaluation. This causes a

lack of experience, as timber buildings are rarely realised. This lack of experience results in a lack of knowledge in timber design. The lack of knowledge creates an economic risk, thus a lack of economic certainty. By breaking this feedback loop the implementation of timber high rise increases. This research aims to break this feedback loop by researching how timber design alternatives can be more thoroughly considered in the conceptual design phase, as is indicated with the red rectangle in Figure 1.1

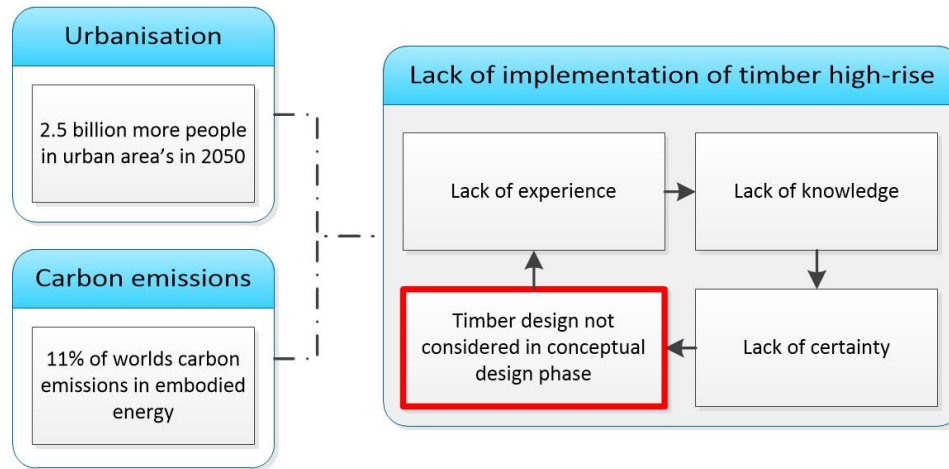


Figure 1.1: Feedback loop preventing consideration of timber high-rise design alternatives in the conceptual design phase.

Conceptual design phase The design process differs per project and company. To create more clarity, the basic model of the design process as shown in Figure 1.2 is used for this research. The conceptual design phase, as defined in Figure 1.2, has the main focus of this research. This phase is the first phase in the design stage, where the basis of design is created [151]. In the conceptual design phase, various design alternatives are generated and evaluated. This evaluation provides insight regarding the advantages and disadvantages of the various design alternatives.

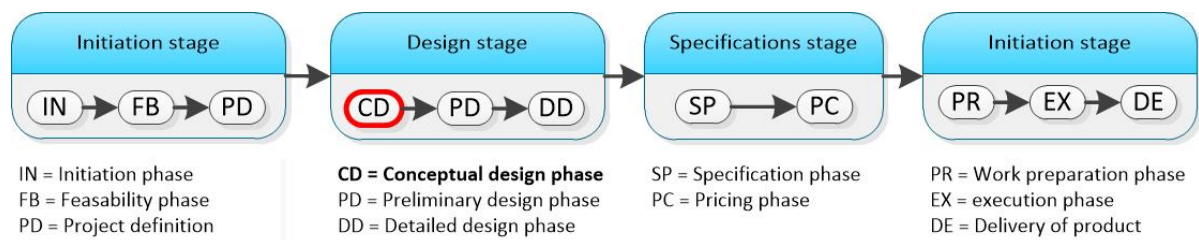


Figure 1.2: Design Process [151].

As stated above, timber high-rise buildings can help solve the urbanization demands and the carbon emission reductions. A feedback loop is identified as the cause of a lack of implementation of timber high-rise buildings. This research aims to transform this feedback loop preventing implementation in a feedback loop encouraging implementation, by researching how timber design alternatives can be more thoroughly considered in the conceptual design phase. Since it is argued that a more thorough consideration increases the implementation of timber buildings, thus increasing the experience, knowledge, and certainty of timber buildings.

2

Problem Analysis

2.1. Problem definition

Timber high-rise can aid with reducing carbon emissions and meet the increased demands for high-rise buildings in cities caused by urbanization. This research argues a feedback loop is preventing the realization of timber high-rise. It aims to break this feedback loop by researching how timber design alternatives can be more thoroughly considered in the conceptual design phase. To achieve this, first, the common decision-making method and its disadvantages are analysed. Next, based on these found disadvantages, another decision-making method is introduced which is argued to be more suitable for this particular design problem.

2.1.1. Common decision-making method

In theory, the conceptual design phase provides the possibility to evaluate an infinite amount of design alternatives. However, in practice on average less than three design alternatives are fully evaluated [50]. The main cause for this is the considerable amount of time that is required for managing information in the AEC (Architecture, Engineering, and Construction) industry caused by the performance-based analysis methods that are commonly used, see Figure 2.1.

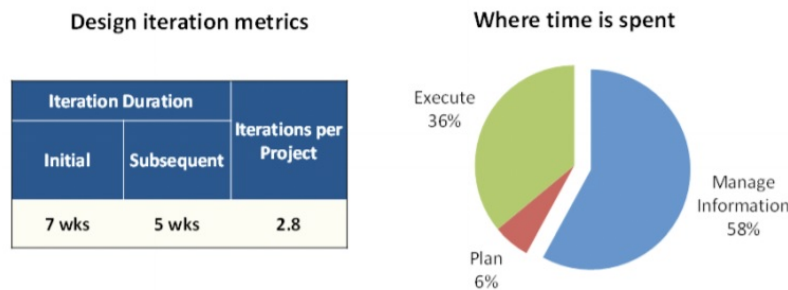


Figure 2.1: Only a few design alternatives are considered by AEC professionals using common decision-making methods due to significant time spent managing information [50].

These performance-based analysis methods are the most common method for estimating the performance of design alternatives. In these performance-based analysis methods, performance requirements are set, and each discipline focuses on its speciality to attain these requirements. The used method to reach these requirements is not described, and up to the specialist to determine. While having only in-depth knowledge regarding their discipline, each specialist optimizes the building, simultaneously and separately, according to his own speciality [12]. This method contributes to various issues:

- The coordination of desired design alterations from all experts is a very time-consuming process [100].
- The restriction of data exchanges and numerous interfaces increases the difficulty of the integration of data [55].

- The anticipated performance is not adequately considered, while this is starting to become more important for the decision-making in the earliest design stages [101].
- Preferences determine which design alternatives are assigned for a full evaluation. According to Koopman (2020), these preferences can be based on two things [92]. They are either preferences for certain materials or construction methods by the initiating party, or they are based on the knowledge concerning a certain building method by a contractor, which results in an automatism to choose for this building method [150].

It can be concluded that the performance-based methods that are commonly used for the determination of feasible design alternatives in the conceptual design phase do not provide a possibility for a change in this feedback loop. Thus, another decision-making method is required, for which this research proposes the Multidisciplinary Design Optimization (MDO) method.

2.1.2. Multidisciplinary Design Optimization method

This research proposes to use the Multidisciplinary Design Optimization (MDO) method for the determination of feasible design alternatives. This method is proposed to provide a rapid generation and evaluation of timber design alternatives in the conceptual design phase. This provides the opportunity to explore the design space.

Analysing design choices provides knowledge considering chosen building elements and their effects on costs and environmental impact. By creating a tool based on the MDO method the achievable performance of timber design can be identified. However, to accomplish this, the various design choices in timber design and their consequences must be analysed. Examples of design choices are the connections, stability system, floor type, and system integration. Lastly, the use of this tool in the conceptual design phase provides a possibility for comparison of the found timber design and its properties with a traditional building design, containing steel or concrete.

Optimization objectives

Multidisciplinary Design Optimization can give a possibility of an integral evaluation of the performances of several disciplines. When connected to parametric models, it can help generate, validate and optimize various design alternatives. As it is not possible to assess all of the disciplines in the AEC industry, only the disciplines which presumably have the biggest impact on design choices are assessed. As already mentioned, the main incentive of using timber instead of traditional building materials is often the smaller environmental impact of timber. However, timber buildings are frequently found to be more expensive than buildings constructed using traditional building materials. This difference in costs is often reported to be between 5 to 10%. According to Ahmed (2020), the construction cost for a hybrid timber building is 6.43% higher compared to a traditional concrete building. The considered hybrid timber building has 18 floors and consists of a timber superstructure with a concrete core [10]. So, in this research, the environmental impact is the incentive for creating timber design alternatives, while the costs are often the main obstacle. The structural and architectural disciplines together form the constraints according to which each model must be designed.

- **Structural - Constraint** Each building must be designed according to the constraints as determined in the Eurocode.
- **Architectural - Constraint** Each building must satisfy the architectural design requirements for acoustics, building height, and daylight entrance.
- **Environmental - Optimization objective** The environmental optimization objective is to minimize the shadow costs, which are determined according to the MPG methodology. The MPG methodology uses Life Cycle Analysis data to assess the embodied energy impact of structural materials. This embodied energy impact is expressed in shadow costs [22].
- **Economical - Optimization objective** The economical optimization objective is to minimize the construction costs.

MDO is used to indicate the building designs which show the most favourable results considering the optimization objectives. If the optimization objectives are conflicting, a Pareto front is expected to be found when performing an MDO [41]. This Pareto front consists of Pareto optimal building designs. These Pareto

optimal building designs show the most favourable combination of properties for shadow costs and construction costs. The competitiveness of a timber building compared to a concrete design alternative can be visualized using this Pareto front, see Figure 2.2.

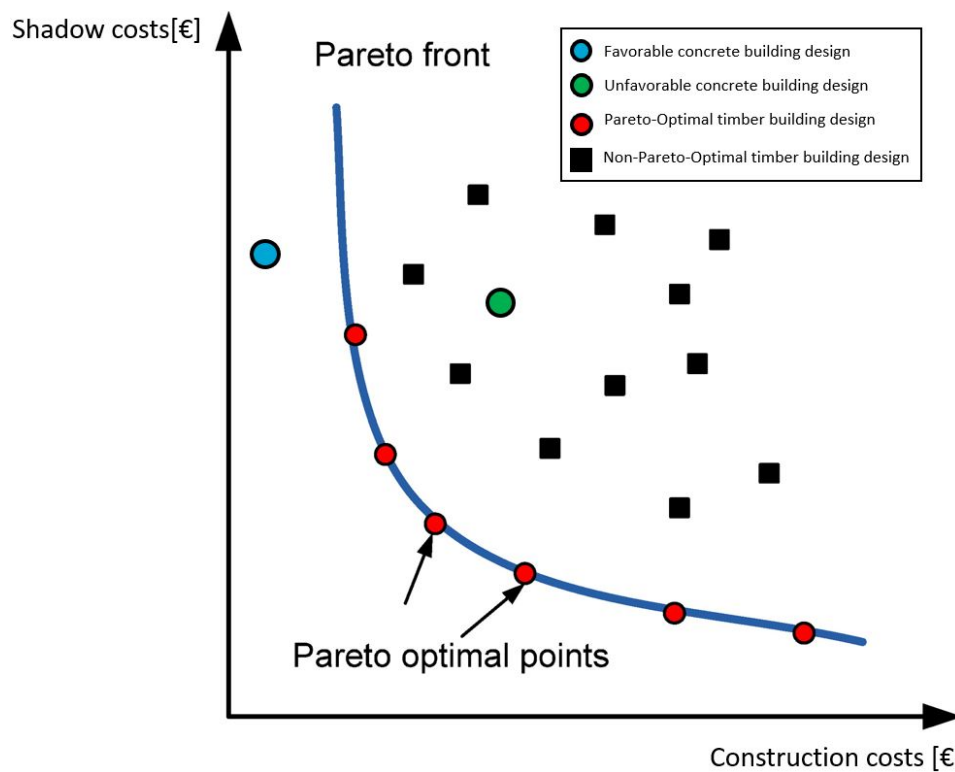


Figure 2.2: Pareto front of timber building designs compared to two concrete design alternatives.

Figure 2.2 shows the obtained timber building designs. The red circles indicate the Pareto optimal timber building designs. These building designs are compared to the concrete alternative present. There are two options, either the concrete building design is unfavourable compared to the timber building designs. This is the case when the green dot represents the concrete building design. In this design situation, timber building design is concluded to be competitive with the concrete design alternative. When the blue dot represents the concrete building design, the concrete design alternative is favourable over the Pareto optimal timber building designs. This implies the timber building designs are not competitive with the concrete alternative in this design situation.

2.2. Aim

This tool aims to identify in which design situation timber high-rise can be competitive to a concrete design alternative, considering the combination of properties for shadow costs and construction costs. To accomplish this comparison, the MDO method will be used. For timber building design, as opposed to concrete or steel building design, there is no standard building method. A wide variety of different design solutions is found when analysing various finished timber high-rise reference projects. This tool aims to display the achievable performance of timber high-rise design compared to concrete building design. A quick generation, optimization, and analysis is preferred to identify the possible timber high-rise designs. The foundation of this tool is created in this research. The hypothesis is that by identifying the design situations where timber high-rise can show a competitive combination of properties for shadow costs and construction costs compared to a concrete design alternative, timber design alternatives are evaluated in the following phase of the design process more frequently. This increases erection of timber buildings, which is expected to lead to a feedback loop that encourages the implementation of timber high-rise. Figure 2.3 shows a schematization of the proposed solution for the research problem.

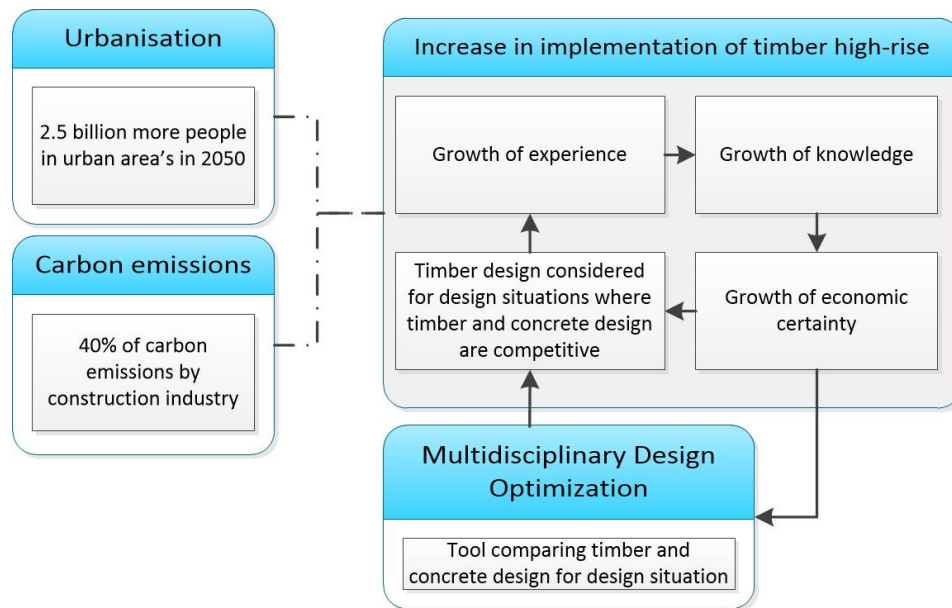


Figure 2.3: Representation of the proposed solution for the research problem.

3

Approach

3.1. Research question

The problem analysis in Chapter 2 leads to the following main research question:

"For which design situation can a timber braced tube system be economically and environmentally competitive with a concrete design alternative for a 50 to 70 meter tall building?"

3.1.1. Sub-questions

Answering of the following sub-questions provides knowledge, data, and conclusions. Conjointly, these sub-questions answer the main research question.

1. (a) How can the MDO method be applied to this design problem?
(b) What are the limitations of the use of MDO for this design problem?
(c) Which design considerations require thorough examination when designing a timber building?
(d) What type of structural system is appropriate for a 50 to 70 meter high fully timber building?
(e) How can the optimization goal of each discipline be defined and modelled?
2. (a) How can an integrated MDO tool be developed which provides accurate results for this design problem?
3. (a) Which assumptions and design choices affect the comparison between timber and concrete building design and how significant are the resulting differences?
(b) What design criteria are normative for timber building design?

3.2. Methodology

For this research, the engineering design process as defined by NASA is used [26]. This engineering design process is split into five parts in this research:

Part 1: Research Definition (Chapters 1,2 and 3) *Objective: Explain why and how this research is conducted.*
The introduction forms the basis of this research definition.

Part 2: Theoretical Framework (Chapter 4) The theoretical framework is the result of the literature study and unstructured interview. This provides the foundation for this research. All conducted interviews are summed in Annex F. It consists of three parts:

- **Multidisciplinary optimization.**
 - 1a) *How can MDO be applied to this design problem?*
 - 1b) *What are the limitations of the use of MDO for this design problem?*

The goal of this part is to report on the findings for the design of the tool, the used MDO architecture, and the implementation of the four layers in the tool. The MDO architecture as given in [86] is used as the main reference for the MDO architecture as used in this research. Different possibilities for implementation of the MDO architecture are researched.

- **Structural system**

- 1c) Which design considerations require thorough examination when designing a timber building?
- 1d) What type of structural system is appropriate for a 50 to 70 meter high full timber building?

This part starts with an analysis of the types of engineered timber, their properties, costs, and essential design considerations. Next, several stability systems are analysed by investigating five reference projects and several pieces of research to identify the most suitable stability system for this design problem. Based on the obtained information, the structural system can be defined. For implementation in the MDO tool, the structural system is split up into building elements.

- **Disciplines and their optimization goals.**

- 1e) How can the optimization goal of each discipline be defined and modelled?

This part discusses the modelling methodology and optimization goals per discipline. Furthermore, all structural and architectural design considerations are reported. This includes the loads, load combinations, and the constraints for structural design and the constraints for daylight and acoustics for architectural design.

Part 3: Multidisciplinary Design Optimization tool development (Chapter 5)

- 2a) How can an integrated MDO tool be developed which provides accurate results for this design problem?

Using the theoretical framework from Chapter 4, the MDO tool is created. First, every model is defined by its input parameters. The tool creates a building design that consist of the defined building elements and which satisfies all structural and architectural constraints. Based on this created building design, the optimization objectives are calculated. These optimization objectives provide a possibility for the definition of the optimal design. With the use of a Multi-Objective Genetic Algorithm, the building designs are optimized according to the defined optimization objectives. Lastly, the design space of timber buildings is visualised. This provides the possibility for comparison of a timber building design and a concrete building design. In this part, the created tool is also verified by recreating an existing building using the tool and comparing results between this modelled building and data from the actual building.

Part 4: Validation (Chapter 6)

- 3a) Which assumptions and design choices affect the comparison between timber and concrete building design and how significant are the resulting differences?
- 3b) What design criteria is normative for timber building designs?

By investigating two case studies, this part aims to gain insight into possibilities and design limitations for timber high-rise design.

Part 5: Final remarks (Chapters 7, 8 and 9)

- For what design situations can a 50 to 70 meter high timber building design in the conceptual design phase be competitive with a concrete design alternative?

In these chapters, first, the found results are discussed. Next, based on these found results, the sub-questions and main research question are answered. Finally, based on the gained knowledge, several recommendations are made.

Research Model The methodology is schematized in the research model. Figure 3.1 shows this research model.

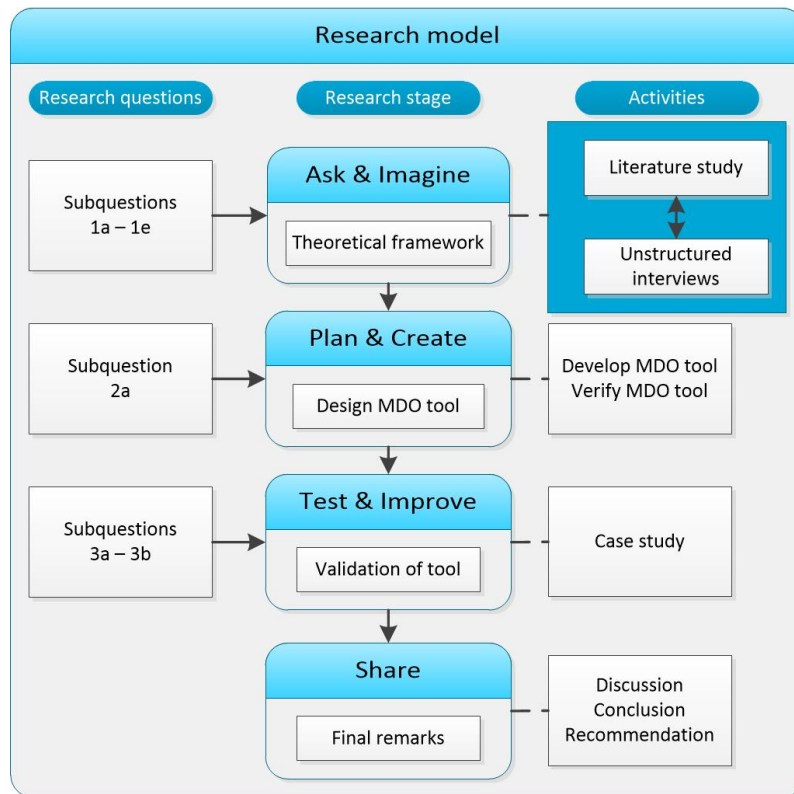


Figure 3.1: Research Model.

3.3. Scope

To be able to answer the research questions within the timeframe as set for a graduation thesis, scope limitations must be made.

- **Location:** The tool is based on a project located in the Netherlands. The Dutch annex of the Eurocode is used, and foundation assumptions are based on Dutch soil conditions.
- **Building geometry:** Only box-shaped building geometry is analysed.
- **Material:** Only fully timber buildings are considered.
- **Foundation:** The stiffness of the foundation is estimated in the calculation of the horizontal deflection of the building. The effect of a reduced building mass on the number of required foundation piles is analysed for the case study.
- **Acoustics:** The floors are designed to provide acoustic insulation for human-induced vibrations. The acoustic performances of connections are not analysed.
- **Loads:** The building is designed according to assumed normative load combinations, consisting of snow loads, rain loads, wind loads, dead loads, and floor loads. Earthquake loads are not considered.
- **Perforations:** Perforations in building elements are not considered in the calculations.
- **Environmental impact:** Only the impact of the embodied energy is analysed. The operational energy is not taken into account in this research.
- **Building elements:** This research focuses solely on the optimization of the structural system. Thus, other elements present in a building, such as vertical transport systems, façade design, and installations are not analysed.
- **Robustness:** The robustness of the building is not taken into account in the developed tool.

4

Theory

4.1. Multidisciplinary Design Optimization

The Multidisciplinary Design Optimization (MDO) method is widely applied in automotive engineering and aerospace. However, this method is rarely applied in the Architecture, Engineering and Construction (AEC) industry [50]. Nevertheless, over the past decade, this method started to be implemented more frequently in the AEC industry in order to improve the efficiency of the design process [38]. This chapter first introduces the MDO method by comparison to the common design process in Section 4.1.1. In Section 4.1.2, the used method for design optimization is elaborated on. Next, in Section 4.1.3, the MDO architecture is explained, which is split into four layers. Finally, the design choices for the implementation of MDO are discussed in Section 4.1.4.

4.1.1. Introduction

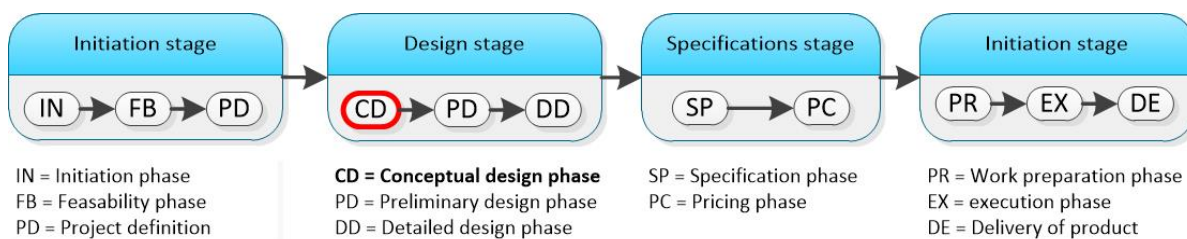


Figure 4.1: Design Process [151].

The conceptual design phase is the first phase in the design stage, see Figure 4.1. In the conceptual design phase, various design alternatives are produced and evaluated. This evaluation provides insight in the advantages and disadvantages of the various design alternatives. This evaluation is performed for multiple disciplines and thus contains multiple objectives for which the design can be optimized [151]. The decision-making in the conceptual design phase consists of two parts:

1. Decision making regarding the consideration of optimal trade-offs between various objectives.
2. Searching for solutions and their trade-offs between objectives.

The difference between the common decision-making process and the Multidisciplinary Design Optimization decision-making process is present in the sequence of execution of these two parts. This execution can be performed in two manners: [156], [108].

- **A priori preference articulation** (Decision → Search). First it is determined what is considered the optimal trade-off between disciplines. With this knowledge, a weighted sum function can be created. Then, the problem is optimized with the goal to minimize the weighted sum [164].

The common decision-making process is based on the a priori preference articulation. This methodology amounts to various disadvantages:

- The coordination of desired design alterations from all experts is a very time-consuming process [100].
 - The restriction of data exchanges and numerous interfaces increases the difficulty of integration of data [55].
 - The anticipated performance is not adequately considered, while this is starting to become more important for the decision making in the earliest design stages [101].
 - Decisions are influenced by preferences. According to Koopman (2020), [92], there are two main causes for these preferences. They are either preferences for certain materials or construction methods by the initiating party, or they are based on the knowledge concerning a certain building method by a contractor, which will result in an automatism to choose for this building method [150].
- **A posteriori preference articulation** (Search → Decision). First, the design space is fully explored. Then, using these obtained results, the optimal trade-off is determined. Using this optimal trade-off, it can be determined which designs in the design space is considered are optimal [164]. The MDO decision-making process is based on the a posteriori preference articulation. This process gives the best opportunities for discovering optimal building designs, since the complete set of trade-off characteristics between the various disciplines is determined [164].

Comparison

Figure 4.2 summarizes the differences between the common and the MDO decision-making process. It is clear that the a posteriori preference articulation (MDO approach) provides the possibility for finding more optimal designs since the design space is fully explored.

Process conceptual design phase		
	Common Process	MDO Process
Sequence	Decision → Search	Search → Decision
Method	Requirements are set, which every discipline tries to obtain separately with no prescribed method.	Optimization objectives are defined. An optimization algorithm aims to find optimal designs in the design space.
Connection disciplines	Uncoupled, optimization done separately per discipline.	Coupled, optimization done for the objective functions of all disciplines.
Design choice	Based on preferences [92], [150].	based on trade-offs between optimal designs.
Average amount of evaluated design alternatives	3 [50].	Thousands.

Figure 4.2: Difference between processes in the conceptual design phase

4.1.2. Design optimization

The goal of MDO is to "identify higher-performing designs through the exploration of both geometric and non-geometric variables according to established design objectives and constraints" [132], [40].

The complete set of trade-off characteristics between various disciplines is referred to as either the Pareto set or Pareto front.

- **Pareto set** Set of solutions in the variable decision space composed of all the Pareto optimal solutions [168].
- **Pareto front** Set of solutions in the objective function space. composed of all the Pareto optimal solutions [168].

Pareto dominance The Pareto front is defined as a non-dominated set of solutions, see Figure 4.3. The Pareto dominance can be described using the following definition [41].

- Solution A dominates solution B when solution A outperforms solution B in at least one objective function, and solution A outperforms or equals solution B in the other objective functions.
- Solution A does not dominate solution B when solution B outperforms solution A in at least one objective function.

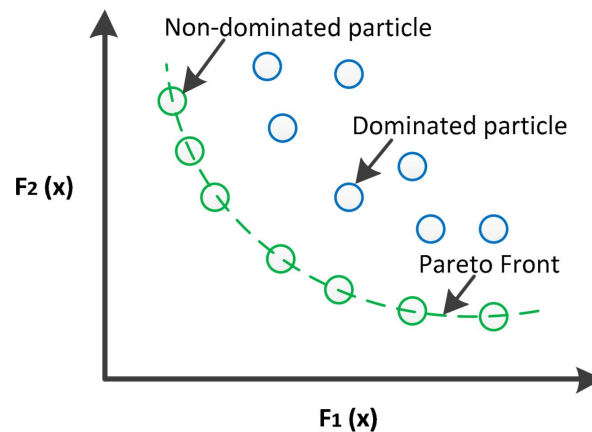


Figure 4.3: Pareto Dominance [99].

With an infinite design space, the Pareto front will consist of an infinite number of points. However, only a limited number of points is required to approximate the Pareto front. The goal of the multi-objective optimization is to approximate this Pareto front [168]. Zitzler et al. (2000) give three objectives of the multi-objective optimization to ensure this [170].

- A Pareto set containing well-distributed solutions is preferred.
- The obtained Pareto front should approach the Pareto front. Preferably, the obtained Pareto set is a subset of the optimal Pareto set.
- The range of the obtained Pareto front should be maximized. The non-dominated solutions must be covered by a broad range of values for each objective.

MDO can help generating and validating various design alternatives. It helps the managing of information and determining which design will result in the optimal trade-off between various disciplines [50]. Using Multi-Disciplinary Design Optimization will grant a possibility to explore the design space and improve the understanding of the possibilities of the design. Using the preferences and requirements of the design by the operator and the obtained Pareto front, the optimal design can be obtained. So, this optimal design is dependent on the chosen optimization objective.

4.1.3. MDO architecture

Jansen, 2014, proposes to use four separate layers to develop an MDO tool [86]. These layers are implemented in this research.

1. Modelling layer

Modelling software As already discussed, parametric design and modelling is a perfect framework for an MDO tool, since it can provide rapid design iteration [54]. In this research, two parametric design programs are considered: Dynamo and Grasshopper. These programs are both based on a visual programming language (Python) [106]. These programs are widely used in the AEC industry because of their low entry level. They are easier to use than conventional textual programming languages, because of the absence of syntax errors and other bugs [118]. These visual programming interfaces consist of a canvas, on which the nodes (Dynamo) or components (Grasshopper) can be placed. These nodes can be connected to each other using wires. A library gives the possibility to use precoded nodes, but custom nodes can also be created using C# or Python code [118]. So, the user can control the input data and all the desired modifications to this data, without needing to have in-depth programming knowledge.

Dynamo Dynamo is a visual programming platform, which can be connected to Revit using the Revit API. Dynamo is based on objects. Dynamo enables scripting in a visual workspace in which data can be created, customized, retrieved and documented from a Revit file. This data can feature both geometric and non-geometric information [118]. A big advantage of Dynamo is its direct connection to Autodesk, which provides possibilities for implementing the model in other Autodesk Software programs [106]. Revit is optimal for the delivering of drawings later in the design process. It uses objects with numerous properties, which is one of the causes for it to run slower than Grasshopper.

Grasshopper Grasshopper is an open-source visual programming language that was created by David Rutten at Robert McNeel & Associates in 2007. It runs within the Rhinoceros CAD application. Grasshopper is based on geometric data and features three types of components [144].

- **Linguistic components** These components represents nominal variables, for example the axis in the modelling space or the form of the geometry.
- **Numerical components** These components are quantitative data which specify dimensions and limitations of other parameters.
- **Graphical components** Using these components, geometry can be modified via manipulation of the graph.

Furthermore, data trees provide Grasshopper with an additional workability. A data tree provides the possibility of storing data in nested lists using a ranked order structure. Every branch of the tree contains sub-lists that have an index number. Such a data tree is helpful considering the creation of an optimisation tool, due to the improved data structuring. Grasshopper is mostly used in the earliest design stages, with the main goal of getting ideas and discovering possibilities. The software uses points, lines and elements for a quick manipulation of 3D-objects. Grasshopper is considered to be faster and less buggy compared to Dynamo. Furthermore Grasshopper is seen as more user-friendly, because of the wide community support. Lastly, more plug-ins are developed for Grasshopper. These plug-ins enable the possibility for fast analysis, with tools like Galapagos, Karamba3D and Octopus.

Conclusion Based on the literature study, Grasshopper is found to be favourable over Dynamo considering the design problem presented in this research. This is concluded since Grasshopper features more plug-ins, a wider community support and a faster and less buggy experience.

2. **Optimisation layer** There are various algorithms used for multidisciplinary design optimization. Especially the metaheuristics are becoming a favoured class of approximation algorithms for solving multi-objective optimization problems [66]. Within these metaheuristic algorithms, multi-objective genetic algorithms (MOGA's) are commonly used. MOGA's use genetic algorithms (GA's) on multi-objective

problems. These GA's are based on Darwinian principles and aim to find the optimal solution out of all possible solutions, without computing all possibilities.

The main advantage of a GA is its ability to find a near optimal solution in a short timespan. However, for complex optimization problems a GA requires hundreds evaluations of individuals fitness values [98].

Apart from using a GA, there are other possibilities like Artificial Neural Networks (ANN) [135]. The computational time of a MOGA is expected to decrease when the MOGA is combined with an ANN (Artificial Neural Network) [98].

Genetic algorithms According to Charles Darwin his evolution theory, a population evolves because the most fit parents in the population will bear offspring. This will create even better fitting offspring in the next generation. After multiple generation cycles, the population will be evolved as most-fitting or optimal in its environment.

Genetic Algorithms (GA's) work on the same principle. A GA can be divided in three stages: evaluation, selection and population. In the first stage, the population (a set of individual results) is evaluated based on the set of optimisation parameters or fitness functions. The second stage uses this information to select the results which fit the optimization objectives best. These individuals will produce new results (children) by a recombination of genes. Mutation is also a possibility in the selection stage. Based on the selected mutation parameter, a certain amount of genes will be randomly altered. This is done to ensure the GA finds a global optimum rather than a local optimum. The creation of this next generation of children is called the population stage. When this new population is created, one cycle or iteration is completed and a new iteration will automatically start. This cycle of creating new generations stops when the solution reaches the convergence criteria, or after a set amount of iterations, called the maximum iteration number [55]. The convergence criteria can be defined for a specific optimization process. A common convergence criteria is to stop the iterations when there are three generations that share nearly the same optimal result [164]. The workflow of a GA is shown in Figure 4.4.

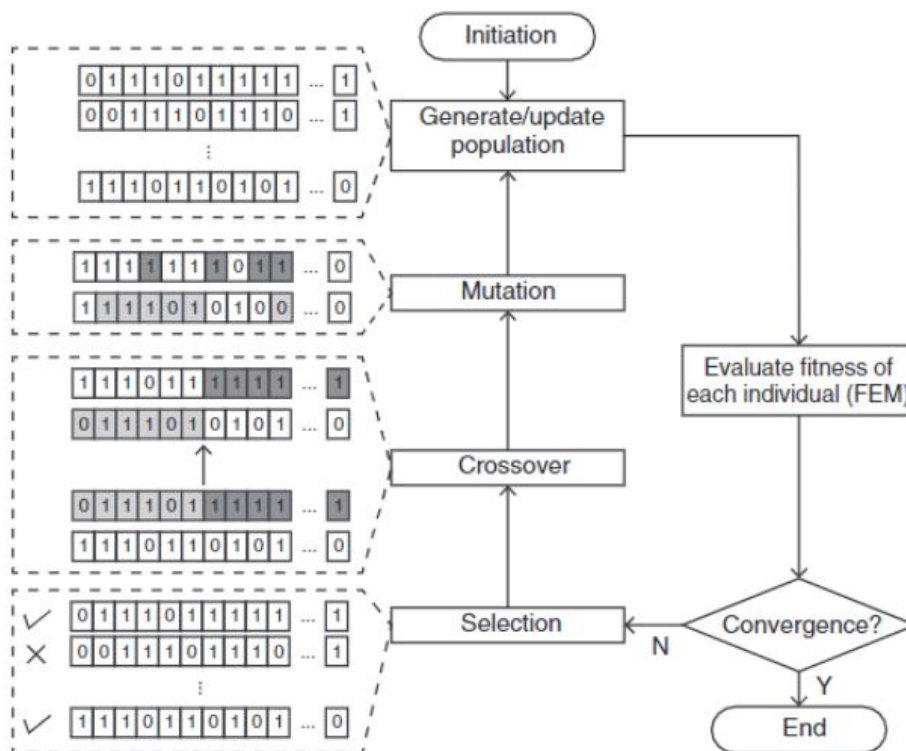


Figure 4.4: GA workflow [124].

Multi-Objective Genetic Algorithms There is a wide possibility of choice in MOGAs. The most used MOGAs nowadays in the AEC industry are: [168], [117]

- the Nondominated Sorting Genetic Algorithm-II (NSGA-II) proposed in [37] in 2002.
- the Strength Pareto Evolutionary Algorithm 2 (SPEA2) proposed in [171] in 2001.
- the Multi-Objective Evolutionary Algorithm based on Decomposition (MOEA/D) proposed in [169] in 2007.

Numerous researches have been conducted aiming to identifying the most accurate MOGA [63] [24] [168] [117]. However, the results are inconsistent. Since every building is different, every building will have its own optimal optimisation method. So, these researches identify varying MOGA's as the most accurate for the various analysed design problems.

3. **Generation layer** While the optimization layer produces the input for the parameters, the generation layers removes this data and generates the new designs as identified by the optimization layer.
4. **Visualisation layer** The visualisation layer provides constant feedback to the user, showing the found data and models. In the visualisation, the design space of timber buildings is visualised. Furthermore, the found data can provide insight in creating smart designs using timber.

4.1.4. Design choices

An optimization problem is always a trade-off between computational time and accuracy. More detailed models and analysis require more computational time, but will increase the accuracy of the result. The design choices influencing the accuracy of the results and the computational time are discussed below.

Design choices influencing accuracy of results

Every building is different. The location, type of stability system, used materials, client, subsurface, site dimensions and function(s) are an example of the set restrictions of a building. Since every building is different, every building will have its own optimal optimisation method. So, in order to develop an accurate tool, a building specific MDO is created. This is done by making specific design choices for this design problem to increase the accuracy of the tool. The following design choices influence the results:

- **Quantification** For MDO, it is necessary to be able to quantify the performance of the building for the considered disciplines. However, certain aspects are (nearly) impossible to quantify. For example, the architectural value of a building. For such aspects, simplifications are required to be able to quantify the performance.
- **Scale, offset and weighting performance** To find an optimal solutions, the performance of different aspects of the design are weighted. This weight, also referred to as trade-off, expresses the importance of aspects compared to one another. The possibility for comparison requires two aspects to be in the same range. This implies that the aspects need to be within the same scale and offset, see Figure 4.5 [33].

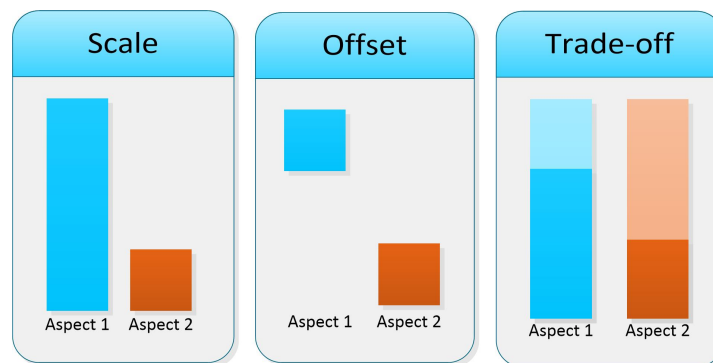


Figure 4.5: Scale, offset and trade-off performance [33].

Design choices influencing computational time

There are various design choices which can help reducing the computational time. The possibility for implementation is considered in this analysis. The following design choices are identified: [135], [167].

1. **Simplifying the models** The simplification of the model can be split into three parts.
 - (a) **Simplification of the building model.** The main risk is oversimplification of the building model. This can be prevented by using the right Level Of Development, LOD, as specified in Annex A.5. An LOD of 200 will be sufficient in this research. *Possibilities for implementation: An average connection in the stability system can be defined and implemented for all connections. The effects of perforations on strength and stiffness of building elements can be disregarded.*
 - (b) **Simplifying the building simulation models.** According to Sobieszczanski, the building analysis software can require over 90 percent of the total computational effort. With an increasing amount of design variables, this rate can grow quadratically to cubically [135]. This building analysis software can be replaced using surrogate models. This LF (Low Fidelity) analysis requires an occasional HF (High Fidelity) analysis to calibrate and confirm the LF analysis. So for example a full calculation in RFEM for the structural calculation. *Possibilities for implementation: Building cost simulation models can be recreated using analytical formula. The environmental calculation can be done by multiplying the used materials and the EPD data from the used materials. Simplified structural calculations following the Eurocode can be performed.*
 - (c) **Reducing design variables.** This can be done by linking subsystems in groups. Furthermore, when less design possibilities are available, the design space will be smaller and the Pareto front will be determined faster. *Possibilities for implementation: Certain input parameters can be simplified. For example the amount of possible stability system geometries, or the amount of possible connections. Also the grid can be simplified, if a certain grid size is preferred.*
2. **Improving the models** Or rather improving the used functions in the models.
 - (a) **Increasing the function linearity by using intervening variables.** By adding intervening variables, functions can be made linear which will decrease computational time of these functions.
 - (b) **Reducing the number of constraints.** This can be done by separating the well-satisfied constraints from the (close to) violated constraints. So for example: Only if constraint $X > 0,25$, then constraint Y needs to be checked.
3. **Simplifying the MOGA**
 - (a) **Smaller generation or population size** This decreases the amount of analysed building designs by the MOGA. The required generation and population size is dependent on the design problem.
 - (b) **Less strict convergence criteria.** This will create a less accurate Pareto front.
 - (c) **Conducting a preparation phase where the population is foreseeded.** This can be done using the PR GA algorithm. [63]
4. **Increasing computing power**
 - (a) **Parallelism, using multiple processors** The computational time will be approximately N times faster if N processors are used [167]. In Parallelised MOGAs, time-consuming simulation programs can run on a parallel processor. [98]

4.2. Timber

Throughout history, timber has been a conventional building material. Timber has provided humanity the possibility of building the first houses, tools and bridges. Apart from small timber houses, also bigger buildings were constructed using timber. For example the Pagoda of Fogong Temple, constructed in 1056, with a height of 67 meters, see Figure 4.6. These traditional timber construction methods are impressive. However, concrete and steel have become more popular over time because of their favourable properties and lower costs compared to traditional timber construction materials. Over the past decades however, with an increasing demand for environmental friendly buildings, timber is beginning to make its comeback. The advancement of processed timber building materials facilitates this comeback.



Figure 4.6: Pagoda of Fogong Temple [51].

4.2.1. Types of timber building materials

The building industry has a lot of preconceptions regarding timber, see Figure 4.7. These preconceptions are mostly based on the traditional timber construction methods. However, a major change in the possibilities of timber design occurred with the use of processed timber. These preconceptions are slowly changing as timber is successfully implemented in various construction projects. In this chapter, these preconceptions are discussed, with the goal of finding the main challenges and possibilities in the usage of timber as a building material.

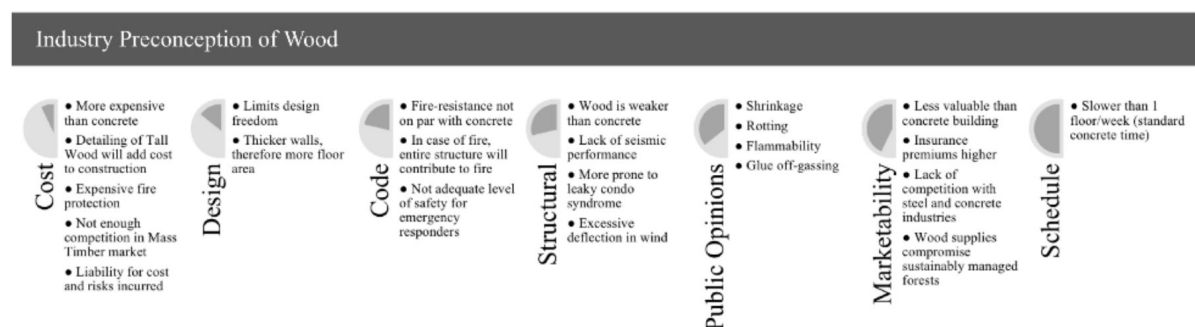


Figure 4.7: Industry preconception of timber [60].

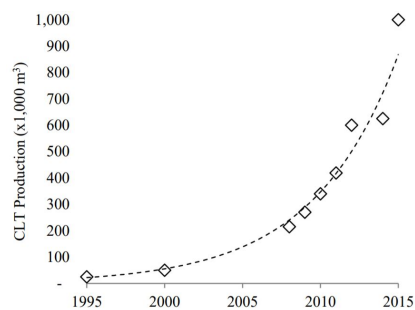
Traditional timber construction uses sawn timber or lumber. This unprocessed timber was sawn directly from the log of a tree. This gives the material various limitations in its ability to be used as a construction material. The main limitations of using unprocessed timber as a building material are:

- **Low durability.** The timber is prone to rotting and funghi attack
- **Limited dimensions** The maximum dimensions of the timber are determined by the size of the log.
- **Varying structural properties** Two reasons can be named for the varying structural properties. To start with, timber is anisotropic. This means that the properties of timber are not similar in all directions. Timber is relatively weak parallel to the grain. Secondly, the sawn timber contains imperfections, decreasing the structural properties locally.

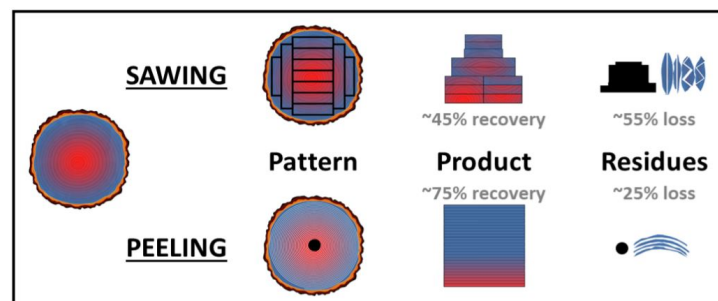
These limitations can be improved by processing of timber. The types of processed timber are mentioned below. Furthermore, the properties of these processed timber types are compared.

Glulam In glued laminated timber (glulam) various timber components, called lamellas, are glued together using an adhesive. These lamellas are all assembled parallel to the grain. The main advantages of using glulam are the possibility to create longer spans and the homogenisation of wood. There are two main reasons for this homogenisation of wood. To begin with, since the material properties of each lamellae differs, the end product will have the average material properties of all these materials. Secondly, the larger imperfections in the lamellae, such as knots or cracks, can be removed. The maximum length of a glulam element is limited by transport possibilities. Various wood species can be used for the creation of glulam. However, spruce is used up to 95 % in Germany [21]. Glulam can be used in beams and columns.

CLT In Cross Laminated Timber (CLT), logs are converted into board layers, also know as lamellas, in a process called sawmilling. These lamellas are glued together using adhesive with a 90 degree inclination between the various layers. This creates a material that is approximately isotropic in plane [21]. Typically, these lamellas are made using Spruce with a strength class C24. The maximum CLT plate length is determined by handling of panels and transporting limitations. CLT is a relatively new material, which popularity is increasing rapidly, see Figure 4.8a.



(a) Global CLT production from 1995 to 2015 [45].



(b) Comparison between sawmilling and rotary peeling regarding product recovery [104].

Figure 4.8

In general, softwood is used for the production of CLT. When CLT is used for flooring, it has two-way spanning capabilities. Since CLT is kiln dried, Kiln dried shrinking and swelling is prevented. It does not distort with changing moisture content [4].

LVL Laminated Veneer Lumber is a variant of plywood where veneers are orientated in one direction. Adhesives are applied to these veneers, and they are assembled under a high temperature and pressure. A big advantage of LVL compared to CLT is the ability to take a bigger bending stress of around 30 N/mm^2 . This building material can be used as columns, beams, walls and floors. The building material is gaining popularity in North-America, New Zealand and Australia. In Europe, LVL is still rarely used. However, the knowledge regarding this building material is gaining quickly. For example *Metsäwood* published a European LVL handbook in September 2019, which provides information considering the correct calculation and usage of this material.

For the production of plywood panels, rotary peeling methods can be used. Rotary peeling provides two main advantages compared to saw milling. To begin with, a higher proportion of log volume can be recovered [104]. See Figure 4.8b. Furthermore, each LVL panel will contain reasonably consistent wood properties, as depicted with the same color in Figure 4.8b. In Figure 4.8b the juvenile wood (red) and the higher quality outer wood (blue) are clearly depicted.

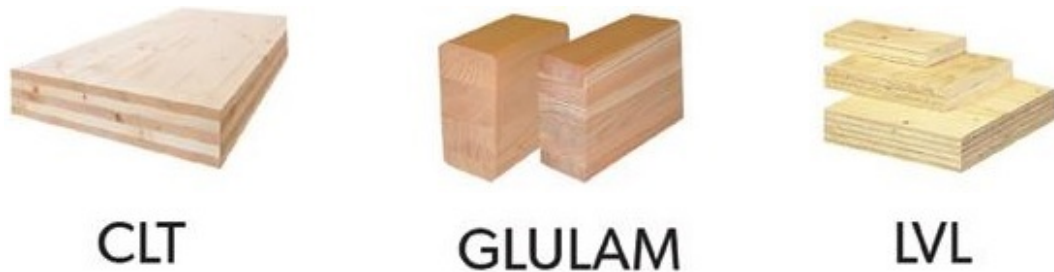


Figure 4.9: CLT glulam and LVL [163].

Comparison timber types CLT, glulam, and LVL all show potential for implementation in timber high-rise. Figure 4.10 shows the possible implementation of the different processed timber types. For exterior walls, CLT is favourable over LVL, since it does not distort with changing moisture content.

Implementation timber types				
Timber type	Column	Beam	Wall	Floor
Glulam	X	X		
CLT			X	X
LVL	X	X	X	X

Figure 4.10: Possible implementation of the considered timber types.

4.2.2. Properties and costs

This section provides insight in the properties of timber as a building material, and the resulting design considerations. These properties are not similar for every timber product. Because of a wide range of wood types, processing methods and coatings the properties of different timber products can vary substantially. With the introduction of processed timber, the possibilities for application of timber as a building material have increased. However, there are still various incorrect preconceptions regarding timber. Annex A.1 provides a full description of the properties of timber. The following conclusions can be made regarding various properties and the costs of processed timber.

- **Structural** When the structural properties of timber are normalized by density they are comparable to steel and concrete. Furthermore, timber requires extra attention during structural design since it is an anisotropic material.
- **Sustainability** Various research has been performed regarding the sustainability of timber. Since research is often influenced by either the concrete industry or the timber industry, the results vary greatly. So, the results from an autonomous source, the European Commission (2018), are adopted [138]. An average reduction of 2.1 tons of CO_2 emissions per ton of used timber compared to non-wood products is found, assuming timber from a sustainably managed forest.
- **Durability** With the correct design and coatings, the same lifespan can be achieved for timber as for traditional building materials [120], [125].
- **Fire safety** Due to the charring process of timber, the inner part of the timber element is separated from the fire. This helps maintaining the structural requirements in a fire situation.
- **Acoustics** Due to the low self-weight of timber, acoustics is one of the biggest issues in design. However, various possibilities of improvement of acoustic properties of floors have been researched and implemented.

- **Costs** The construction costs for timber design are often assumed to be between 5% to 10% higher than building design using traditional building materials. However, with increasing knowledge and usage of timber these costs are expected to drop. Furthermore, a carbon tax or adaptations of the Eurocode 5 could help lower the costs even further.
- **Well being** Several studies have shown exposed timber has several health benefits for occupants, such as reduced heart rate, blood pressure and stress levels. Furthermore, it improves the emotional state and level of self-expression of inhabitants [14].

4.3. High-Rise

In this research, the term timber high-rise is used for a building between 50 and 70 meters high, where timber is used for the majority of the engineered parts of the superstructure. Since the Dutch building regulations (Bouwbesluit) only provide design rules for high-rise buildings up to 70 meters, this is used as the maximum height of the building.

Building up to 70 meters high using timber is a major challenge. However, the tallest tree on earth is measuring 115.6 meters, see Figure 4.11, which shows timber's potential to reach great heights.

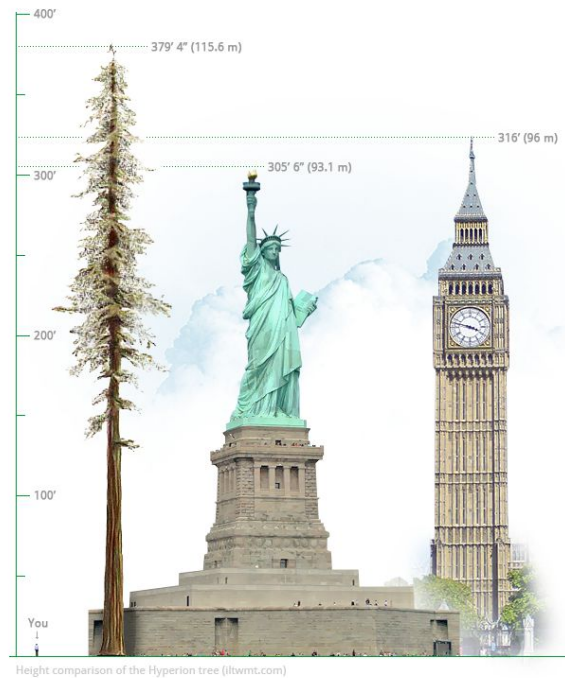


Figure 4.11: Tallest tree height comparison [1].

4.3.1. Reference projects

In this section, five reference projects and their stability systems are compared. Additional information regarding these reference projects can be found in Annex A.2. Figure A.17 shows the comparison between these five buildings.

Building Comparison						
Comparison criterion	unity	25 King	Treet	Murray Grove	Mjøstårnet	Brock Commons
Stability system	-	Tube	Tube	Shear walls	Tube	Core
Use of wood	m^3/m^2	-	0.16	0.31	0.25	0.15
Height of building	m	47	52.8	26	85.4	54
Number of floors	<i>number</i>	10	14	9	18	18
Building cost	$Euro/m^2$	4300	3774	1546	4087	2045
Construction time	<i>days / floor</i>	-	15	7	12	12
Reduced CO2 emissions	<i>tonnes of CO2</i>	-	2000	310	1577	2432
Use of Energy	$kW/m^2/year$	-	84	144	102	135

Figure 4.12: Building comparison [85], [145].

4.3.2. Lateral stability systems

As the height of a building increases, the lateral loads become more crucial, opposed to the gravitational loads. Thus, providing lateral stability is one of the main challenges in the construction of a high-rise building. The five most common stability systems are considered in this research. These consists of a rigid frame, a shear core, an outrigger, a tube and a diagrid system, see Figure 4.13. In this Section, these five lateral stability systems are discussed.

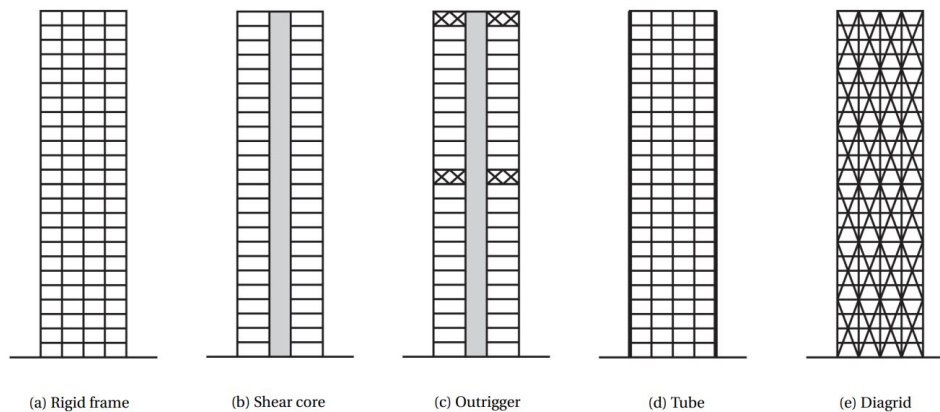


Figure 4.13: Lateral stability systems [155].

Rigid frame

A rigid frame stability system consists of beams and columns that are rigidly connected. Rigid timber frames are commonly used for low-rise housing. However, creating a rigid frame using timber is impractical regarding the required stiffness of the connections and dimensions of timber elements.

Shear walls

When CLT plates are used as bearing and shear walls, sufficient lateral stability of the building can be achieved. Murray Grove, see subsection A.2.4 is a timber building where this stability system is implemented. It reaches a height of approximately 30 meters. This stability system is used in residential buildings, as the CLT plates also divide different rooms and apartments. This stability system is not desired for offices, as an open floor plan is favoured.

Stability core

In this structural system, a stiff core is created using either concrete or CLT plates. Subsequently, the frame of the building is connected to this core using beams and columns or CLT plates as shear walls.

CLT core Van Rhijn (2020) argues a the usage of a CLT stability core ($t=495$ mm) is the most efficient stability system for high-rise buildings up to 70 meters [155]. De Jong (2017) researched a 102 meter tall timber building with a CLT core ($t=500$ mm) and a timber frame structure. This building was found to comply with all unity checks, except the lateral displacement limits, where a unity check of 1.02 was found [36]. van Rhijn assumes fully rigid connections using glued in rods and de Jong creates almost fully rigid connections between the CLT elements using HSK connectors.

However, the creation of such rigid connections is questionable. As Znabei (2020) shows in her research, the stiffness of the connections has a huge impact on the total displacement of the structure. Znabei argues four displacement modes are present on a laterally loaded CLT core. These four displacement modes are shown in Figure 4.14a.

So, the total deformation of the building is:

$$u_{TOTAL} = u_{EI} + u_{GA} + u_{\phi} + u_s \quad (4.1)$$

Figure 4.14b shows the influence of the sliding and rocking effect on a building stabilized with a CLT core ($t=240$ mm) for varying height. Based on this big influence of the uplift and sliding force, Znabei (2020) proposes to use pre-tensioning in the CLT core to minimize these effects. By minimizing the sliding and uplift

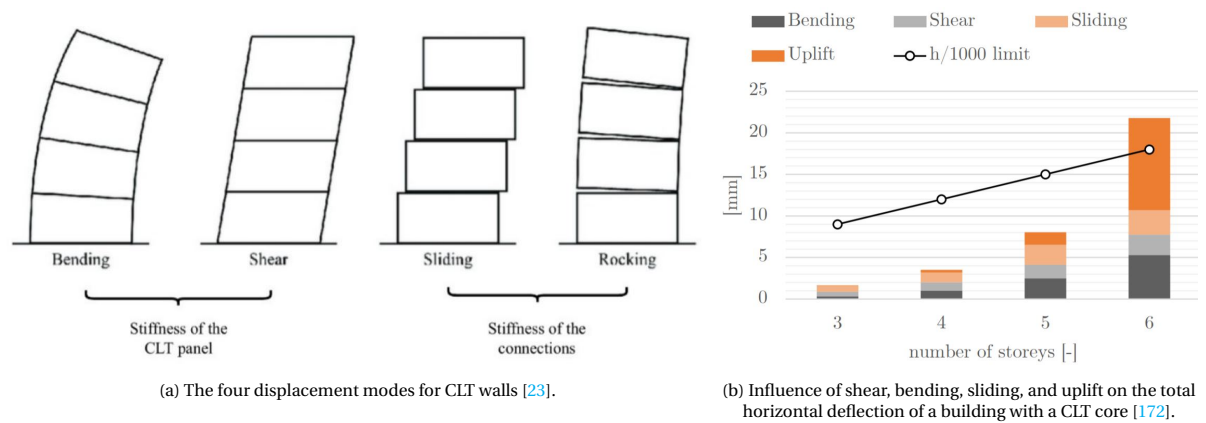


Figure 4.14: Design considerations for CLT core.

forces, a building up to 24 meters high can be created. For higher buildings, two limiting factors are present: the deflection of the building and the compression toe stress in the CLT core. Two reasons are identified causing this big influence of the uplift and sliding force on the CLT core. At first, a timber building has a lower self-weight, which leads to smaller compression in the core. When the compression of the core increases, the sliding and rocking effect of the core decreases. Secondly, the creation of stiff connections in timber is a major challenge.

It can be concluded that the assumption of a fully rigid and a near rigid connection between CLT core elements by Van Rhijn and De Jong is questionable. These assumptions have a big impact on the total structural behaviour.

Moudgil (2017) found that using a CLT core instead of a concrete core in the Brock Commons Building provides some challenges. Using a CLT core leads to torsional behaviour in the fundamental mode and higher storey drift. These challenges can be dealt with by increasing the thickness of the CLT core, or adding additional CLT shear walls to meet the seismic performance criteria [110]. Chapman (2012) found that a 30 storey building with a CLT core met the interstorey deflections limits. In this research, the lack of damping was determined to be the biggest challenge, as the dynamic properties of the building were insufficient [30].

Concrete core Haut is a 73 meter tall timber building in Amsterdam. During its construction, it was concluded that the usage of a CLT core, would increase the required amount of steel in the connections so much, that a concrete core would be favourable considering environmental impact [34]. So, it can be concluded that a CLT core is not necessarily a more environmental friendly solution than a concrete core. The main challenge when constructing a building using a concrete core and timber columns is the differential vertical shortening. The difference in relative vertical shortening between two vertical load bearing elements have a negative effect on secondary building elements [162]. Mostly on the vertical mechanical services and elevation tolerances between the core and timber frame. Fast et al. (2016) researched the Brock Commons Building and found that when the differential vertical shortening is not sufficiently considered in the design, this can create an extra 50 mm deflection at the top of the building [48].

Diagrid

The diagrid stability system is based on the workings of a lattice girder. Elements are placed diagonally, often in the façade of the building, to provide the lateral stability of the building. This stability system has not been implemented in a timber high-rise building yet. However, the River Beech Tower is a proposal of a timber high-rise building where a diagrid system is implemented.

Outrigger

An outrigger stability system creates a stiff connection between the core and the outer columns of a building. This way, tension and compression forces can be induced in the outer columns of the building. These tension and compression forces reduce the moment in the core, generated by the wind forces. An example of a timber high-rise building using the outrigger stability system is the Treet building, see subsection A.2.3.

Tube

In the tube stability system, the façade is created as a stiff structure. This façade consists of elements that are joined together to create a stiff tube around the building. In concrete buildings this tube is often created by the outer concrete walls working as a large diaphragm. However, creating a stiff tube using CLT panels containing holes for windows is ambitious considering the four displacement modes of CLT panels causing deformations, see Figure 4.14a. Using a timber frame containing diagonals in the façade to provide lateral stability is a more suitable approach for creating a timber tube structure. This is called a braced tube system and this approach is used in Mjøstårnet, see Annex A.2.5. A braced tube system has several advantages compared to a core system:

- The moment of inertia is maximal. This results in lower stresses in the elements.
- There are no eccentricities, thus no torsion is present.
- Forces are spread over a bigger area and are thus easier to transfer to the foundation.
- Full floor plate flexibility: The architectural firm Sidewalk labs (2020) researched the possible stability systems and the estimated square feet (1 square foot = 0.092 m²) of floor loss per storey for a 35 storey high building. This floor loss was found to be 56 m² for a CLT core system. A concrete core results in 13 m² of floor loss, while in a tube system, no floor loss is present, see Figure 4.15.

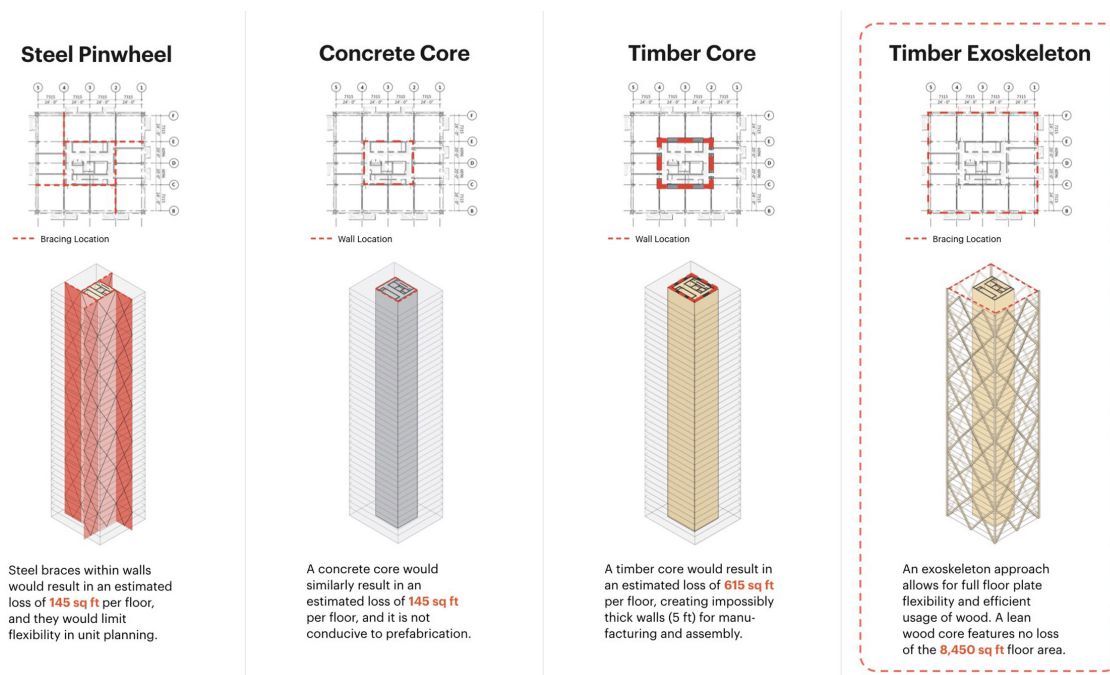


Figure 4.15: Comparison of stability systems by Sidewalk Labs [6].

Conclusion

The aim of this research is to create a full timber building. The use of a CLT core is questionable because of the thick CLT panels and rigid connections which are required. When considering the reference projects, there are three full timber buildings which reach a height over 45 meter: Treet, Mjøstårnet and 25 King, see Figure 4.12. These three buildings still contain non-timber parts in the connections. Furthermore, 25 King has a concrete ground floor and Mjøstårnet contains six concrete floors. All these reference projects use diagonal elements in the façade to create lateral stability. These systems are referred to as braced tube systems.

Although a braced tube system is used to provide lateral stability, a core is required to function as a fire escape and for vertical transport. For this, a CLT core is used. The lateral stability of such a CLT core compared to a braced tube system for buildings over 50 meters tall is negligible. Thus, the CLT core system does not provide sufficient lateral stability to a 50 meter tall the building.

4.4. Building Elements

This section covers all building elements that are used in the MDO tool. For every building element, the options are discussed, and the consequences of each option are reported. Annex B elaborates on all executed calculations for these building elements in the tool.

4.4.1. Connections

In the design of timber structures, the connections have a considerable influence. Not only does the capacity of the connection determine the capacity of the structure, but the stiffness of the connection also greatly influences the overall displacements of the structure [131]. First, the techniques of creating timber connections are mentioned. Thereafter, the main considerations in timber connection design are mentioned. Next, the considered types of connections in this research are mentioned. Finally, the required types of connections are specified.

Connection technique

There are three main techniques to create a strong timber connection [147].

1. **Direct contact between timber members.** Also called carpentry connections. This type of connection has two advantages: A lack of need for steel or glue, and possibilities for re-use. Since a timber element is weaker parallel to the grain, the transfer of forces between two timber elements can create issues. Thus, slip and shear create the main challenges in the usage of this type of connection.
2. **Adhesive bonding** Adhesive bonding can prevent slip and shear almost completely, resulting in a high interaction, resulting in a stiffer connection and thus a rigid structure [29]. Creating adhesive bonded connections is a labour intensive process, increasing the costs of the project.
3. **Mechanical fasteners** Using mechanical fasteners provide a greater opportunity for re-use of the elements. Kuijpers (2020) mentioned that mechanical fasteners in connections will only achieve around 20% to 30% of the efficiency which adhesive bonding can achieve. This is mostly due to issues in slip and shear resistance [93].

Design considerations

Some factors must be thoroughly examined in timber connection design.

1. **Changes in moisture content.** Structural timber is often regarded as a living material. In a way this is a legitimate claim since the changes in moisture content cause the timber to shrink and swell. The shrinkage perpendicular to the grain is significantly greater than parallel to the grain. In connection design, this must be considered to prevent splitting of timber, see Figure 4.16a [113].
2. **Shear strength** The shear strength is around 10% of the total bending strength. Thus, eccentricities in connections can cause problems, see Figure 4.16b [113].
3. **Tensile strength perpendicular to the grain** Tensile strength perpendicular to the grain is between 30 to 50 times smaller than the tensile strength parallel to the grain. This might lead to cleaving of timber, see Figure 4.16c [113].
4. **Fire design** Concealing the timber connection is often the solution. Intumescent fire strips in gaps and slots of connections can provide this concealment.
5. **Costs** The design of the connection has a huge influence on the construction costs since connections require special attention through the design and production process. For high-rise complex glued connections are required. These connections require extra assembly work, quality and environmental controls and delays due to curing of the glue [61].

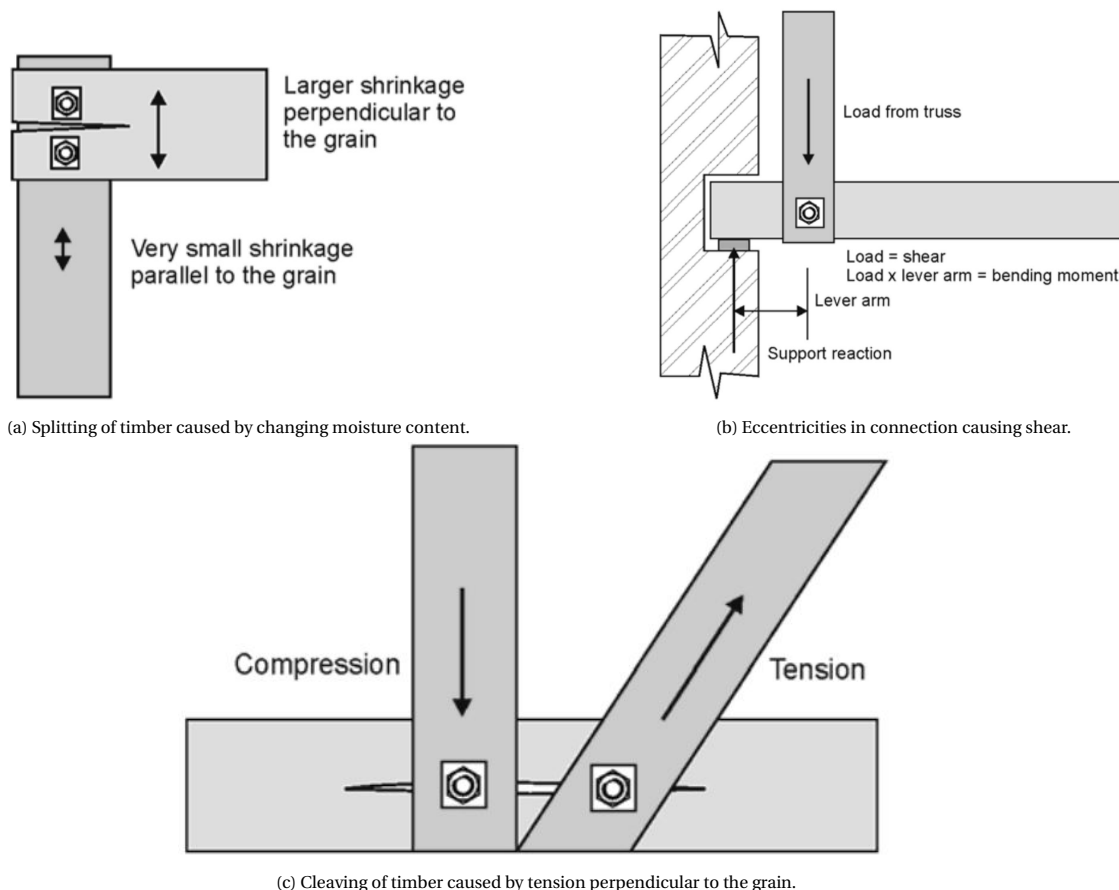


Figure 4.16: Timber connection design considerations [113]

Considered connections

In this research, three different types of connections are used for connection design.

1. Steel plate and dowels
2. Screws (combined with metal brackets, or carpentry connections)
3. Knapp connectors

The distancing, strength, and stiffness calculations are mentioned in Annex A.3 for the steel plate and dowel connection.

Required connections

Connections for a number of different situations must be realised for the construction of a timber building. These situations differ based on a number of factors, for example: material type, type of loading, magnitude of loading, and workability. In this research, all connections are grouped into nine categories:

1. **Braced tube system connection** Steel plate and dowel connections are used to connect the glulam elements in the façade.
2. **Floor-beam connection** The top plate of the Kerto-Ripa floor elements is placed on the beams. Subsequently, these elements are screwed to the beams.
3. **Floor-floor connection** The floor plates transfer the wind loads to the stability system. This results in shear forces between floor elements. These forces are assumed normative in the floor-floor connection. Screws are used to transfer these shear forces between floor elements.

4. **Core-core connection** Since the core is not part of the lateral stability system, the only horizontal forces consist of the internal wind pressure forces. These forces are relatively small compared to the gravitational loads. Thus, the connections between core elements are mainly designed to provide sufficient compression resistance. Angle brackets are used for the connection between the CLT plates that make up the core.
5. **Core-beam connection** Knapp connectors are used to create the core-beam connection. These connectors consist of a steel plate, attached to both elements using screws. These two steel plates can be slid into each other to create the connection. The main advantage of these connectors is the possibility to attach the steel plates to the timber elements at the factory. On-site these two parts can simply be slid into place to create a stiff connection.
6. **Core-foundation connection** Since the core is not part of the lateral stability system, the only horizontal forces consist of the internal wind pressure forces. These forces are relatively small compared to the gravitational loads, thus no tension forces are assumed to be present in the bottom of the core. So, a hold-down connection is not required to connect the core to the foundation. Metal brackets and screws are used to connect the CLT plates in the core to the concrete foundation.
7. **Column-column connection** This connection concerns the columns which are not located in the facade. For these columns, the gravitational loads are normative. So, the column-column connection is realized using a carpentry connection and screws, similar to the columns in the 25 King reference project, see Figure A.7c. An average of 24 screws per column-column connection is assumed to ensure a safe connection.
8. **Column-beam connection** Knapp connectors are also used to create the column-beam connection.
9. **Column-foundation connection** For the column-foundation connection, steel plates and dowels are used. The column to foundation connection is considered to be an infinitely stiff connection. To take into account the extra rotation caused by the foundation, the deformation at the top of the building is considered to be a maximum of $H/750$.

Below, the connections are visualized. Figure 4.17 gives a summary of the applied connection types in the model.

Required connection types	
Connection category	Connection type
Braced tube system connection	Steel plates and dowels
Floor-beam connection	Screws
Floor-floor connection	Screws
Core-core connection	Angle brackets and screws
Core-beam connection	Knapp connectors
Core-foundation connection	Metal brackets and screws
Column-column connection	Carpentry connection and screws
Column-beam connection	Knapp connectors
Column-foundation connection	Steel plates and dowels

Figure 4.17: Required connection types in the model.

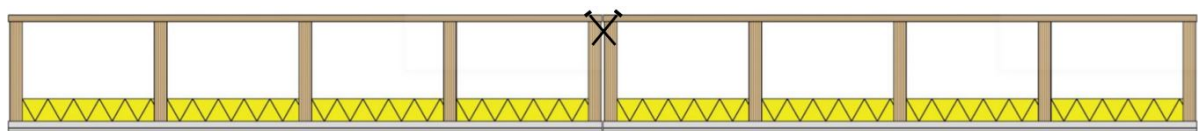
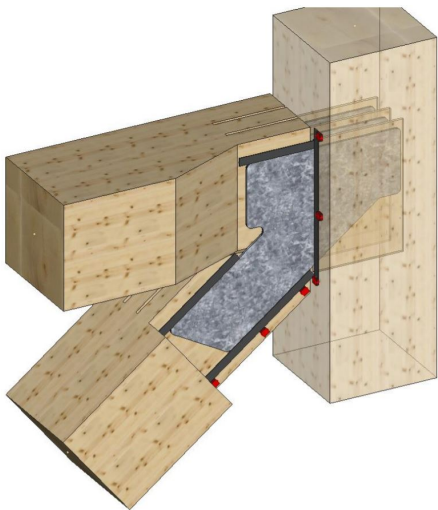


Figure 4.18: Floor-floor connection.



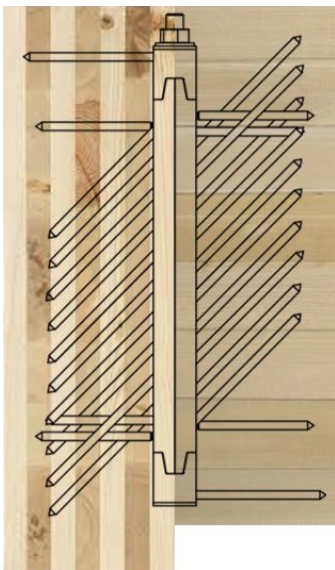
(a) Braced tube system connection [8].



(b) Floor-beam connection [109].



(c) Core-core connection [126].



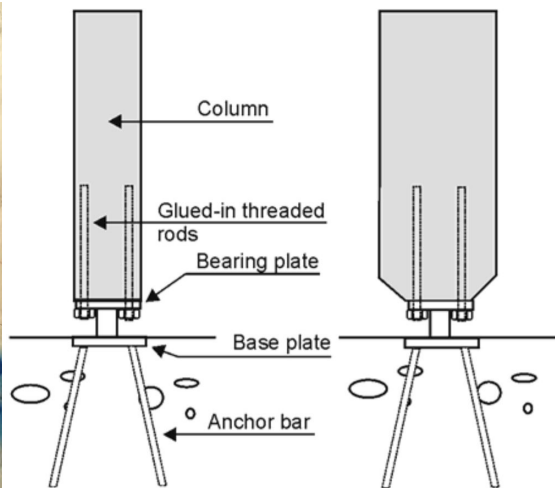
(d) Core-beam and column-beam connection



(e) Core-foundation connection [126].



(f) Column-column connection [85].



(g) Column-foundation connection [113].

Figure 4.19: Visualization of used connections.

4.4.2. Floor

For the design of the floors, there are several requirements. These requirements are based on acoustics, fire safety, comfort, and deflection. Normally, the stiffness or strength of a floor is normative. However, for light floors such as timber floors, the human-induced floor vibrations are often normative. For the design of the floors, three different timber floor types are considered. The manufacturer's data is used to obtain the properties of the floors.

Kerto-Ripa floor

In Mjøstårnet, a system based on the Metsä Woods RIPA deck system is used. This floor system is an LVL floor system, consisting of ribs, connected to a top flange. The spaces between the ribs can be used for pipes or ducts, or for adding acoustic insulation or thermal insulation. In Mjøstårnet, Rockwool is used to obtain the required 90 minutes of fire resistance. Floor spans up to 16 meters can be reached with this system. The carbon footprint is $65 \text{ kg CO}_2/\text{m}^2$. The system can be used with steel or glulam trusses, CLT shear walls or stabilizing concrete cores [8]. The weight is approximately $30 \text{ kg}/\text{m}^2$.

KLH floor

KLH Massivholz floors are applied in the Murray Grove StadtHaus. These floors consist of CLT panels combined with either a wet or dry screed. A minimum thickness of 6 cm of wet screed is required to meet the acoustic requirements. The maximum span is 20 meters. Sufficient thickness of the CLT panels results in an acceptable fire resistance. An advantage of using CLT panels is their two-way spanning capabilities. The weight is at least $60 \text{ kg}/\text{m}^2$.

Lignatur floor

This floor is considered to be the timber equivalent of a hollow core slab. The Lignatur LF floor element consists of timber beams that are connected using glue to form boxes. These boxes have a width of 200 mm. Four boxes form one LF floor element. These elements are either 514 mm or 1000 mm wide. This floor can span up to 15 meters. The boxes can be used for adding pipes or ducts, or for adding acoustic insulation or thermal insulation. A fire resistance up to 90 minutes is possible by adding a protective layer or increasing the thickness of the bottom panel. The weight is $34\text{-}48 \text{ kg}/\text{m}^2$.

Comparison

Each floor type has their own advantages and drawbacks. The floors are scored on seven categories which is shown in Figure 4.20. The KLH floor is considered the least applicable, because of its higher weight and lack of possibility of integration of ducts. The Kerto-Ripa floor and Lignatur floor show similar results. The Kerto-Ripa floor is chosen because of the easier possibility of integration of ducts and insulation in the floor. Furthermore, the Kerto-Ripa floor has already proved its qualities in Mjøstårnet. Based on the found results, the Kerto-Ripa floor is used in the model.

Characteristics of the floor types			
Characteristic	Kerto-Ripa	KLH	Lignatur
Available dimensions	+	++	0
Mass	++	-	+
Fire resistance	0	++	0
Sound insulation	-	0	+
Ducts	++	-	++
Workability	++	0	++
Floor Thickness	+	-	0

Figure 4.20: Characteristics of the floor types.

4.4.3. Beam

The glulam beams in the structure provide two main functions. Firstly, the beams help with transferring of wind forces to the stability system. Secondly, the beams support the floors. For the Kerto-Ripa floor system, supporting beams in one direction are required. The sizes of the beams are dependent on the weight of the floor, the function of the building, the used connections and the grid sizes. To minimize the total height of a floor, it is helpful to integrate the beams and the floor system. The Kerto-Ripa floor system provides this possibility, since the top plate of the floor system can be connected to the beams.

The total floor height can also be minimized by creating a service penetration of the beams to distribute services, see Figure 4.21a. Often, LVL is added to the beams to provide the possibility to create these openings, see Figure 4.21b.



(a) Penetration of beams for service distribution in the International House in Sydney [27].

(b) LVL elements in the beams [85].

Figure 4.21: Beam penetration

4.4.4. Column

In a building stabilized using a braced tube system, two types of columns can be distinguished. The columns in the braced tube, and the inner columns. Since the braced tube system transfers the horizontal forces, the main contributor of force on the inner columns are the gravitational loads.

4.4.5. Diagonals

For the diagonal elements in the façade, various angles provide different results. In this research, the optimal diagonal angle was aimed to be obtained using three methods. Firstly, a simplified calculation was performed, with the aim of maximizing the shear rigidity of the structural system. At an angle of 35° , the maximum shear rigidity was found, see Annex B.6. Secondly, Panchal et al. (2014) researched the optimal angle for steel diagonals in a megabrace system. The displacement, inter-storey drift, shear force and material usage were checked. An angle of the diagonal between 65° and 75° was found to show the most favourable results. Lastly, when calculating the diagonals Mjøstårnet, an angle of 27.4° and 45.8° is found. So, different optimal diagonal angles were obtained in these three analyses. So, no clear statement on an optimal angle can be made based on this information.

4.4.6. Core

A core has multiple functions. Firstly, it provides a possibility for vertical transport of people, with stairs and elevators. The core is often created as a fire compartment, to be able to function as a fire escape. Furthermore, pipes and ducts are integrated in the core. Lastly, the core can help to provide lateral stability to the building. In this research, the required core size is set by the user of the tool.

4.5. Disciplines

Various disciplines are involved in high-rise building design, for example HVAC engineering, electrical engineering, wind engineering, geotechnical engineering, vertical transport design, façade engineering, cost estimation, environmental engineering, structural engineering, and architecture. Since all disciplines have their own goals, a way of collaborative design is required to obtain an integral design. The possibility for collaborative design in the AEC industry is increasing with the increasing use of building information modelling (BIM) tools. These tools provide the possibility of integrating different software into one integrated model. All disciplines can use this model to analyse and improve the design. However, the changes made by one discipline can affect other disciplines significantly. If the trade-off between disciplines is not clearly established, an assumed improvement by one discipline can reduce the value of the overall design. If these trade-offs are clearly established, the consequences of design changes become comprehensible.

In this research, four disciplines are considered. This chapter gives some background per discipline, mention the modelling choices for analysis and the optimization objective. In short, each discipline has objectives conflicting with the objectives of the other disciplines:

- **Structural Constraint:** The building must meet all regulations defined in the Eurocode, see section 4.6.
- **Architectural Constraint:** The building must satisfy the architectural design requirements for acoustics, building height, and daylight entrance. see section 4.7.
- **Environmental Objective:** Minimizing the shadow costs.
- **Economical Objective:** Minimizing the construction costs.

4.5.1. Structural

Introduction

The timber structure must be designed according to the constraints for structural systems in timber, as given in Section 4.6. Section 4.3.2 concluded a braced tube system is most appropriate for a timber building between 50 and 70 meters.

Modelling

All structural calculations are shown in Figure 5.2. These calculations are performed using custom nodes and the parametric engineering plug-in Karamba3D in Grasshopper. All calculations are performed for the assumed normative ULS and SLS load combination, see Section 4.6.1.

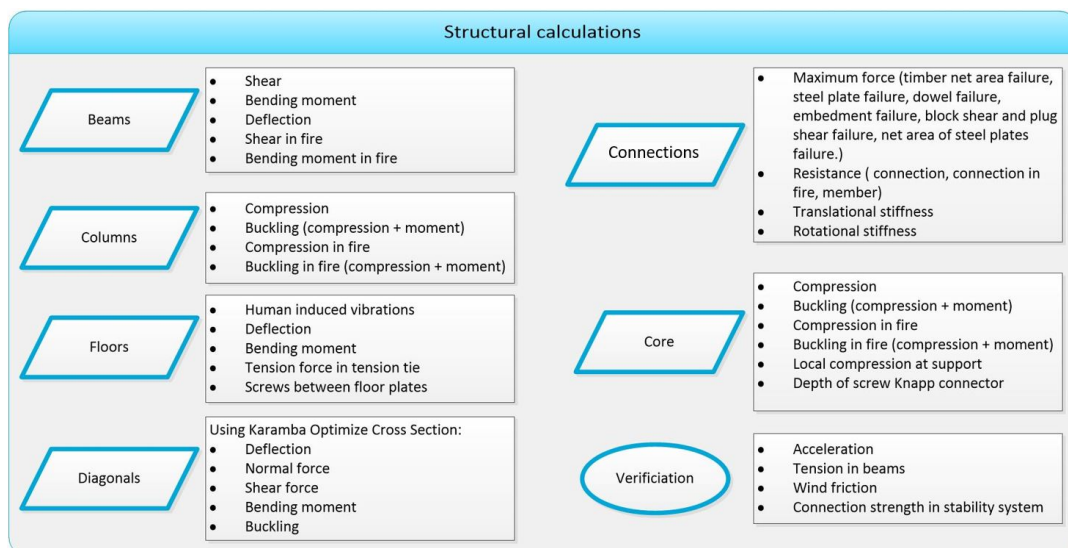


Figure 4.22: Structural calculations performed in Grasshopper. Full calculations can be found in Annex B.

In order to simplify the calculation of the 3D stability system, it is analysed in 2D. So, two 2-dimensional calculations of the lateral stability system are performed, see Figure 5.16. For these calculations, the Karamba3D

component Optimize Cross Section is used, which obtains the optimal dimensions of elements in the façade. This component is verified in Annex A.6.1. After all timber elements and all connections are dimensioned and determined, some verification calculations are performed.

Optimization constraint

Each model must be designed according to the constraints for structural systems in timber, as given in Section 4.6.

4.5.2. Architectural

Introduction

A high architectural performance of a building increases the marketability of a building. Quantification of the architectural performance of a building has been attempted in various research. However, these results are controversial and methods are not applicable in this research. So, in this research the architectural discipline is included solely by architectural constraints for acoustics, daylight, and storey height.

Modelling

To satisfy the architectural constraints for acoustics, the required thickness of floor elements for human-induced vibrations is determined. For this calculation, the European standard EN 1995-1-1 combined with the Dutch national annex [74] will not provide an accurate result. So, the calculations are based on two alternative guidelines that provide more accurate calculations: the Austrian standard Önorm B 1995-1-1 [71], and the HIVOSS design guidelines for calculation of floor vibrations [67]. This calculation will provide the minimal required height of the ribs of the kerto-ripa plate that satisfy both the Austrian standard Önorm B 1995-1-1 and the HIVOSS design guidelines for calculation of floor vibrations, see Figure 5.11. To maximize the amount of daylight entry, the core in the timber building designs, as generated in the tool, is placed such that the amount of area close to a window is maximized. Lastly, the Dutch Building Code mentions a minimum floor-to-ceiling height of 2.6 meters. For all optimizations, a floor-to-ceiling height of 3.0 meters is used.

Optimization constraints

Each model must be designed according to the constraints as given in Section 4.7.

4.5.3. Environmental

Introduction

The environmental impact of a design choice is often quantified using carbon emissions, which are related to the energy use. The embodied and the operational energy consist of approximately 30% and 70% respectively of the total energy consumption during the lifetime of a building, see Figure 4.23.

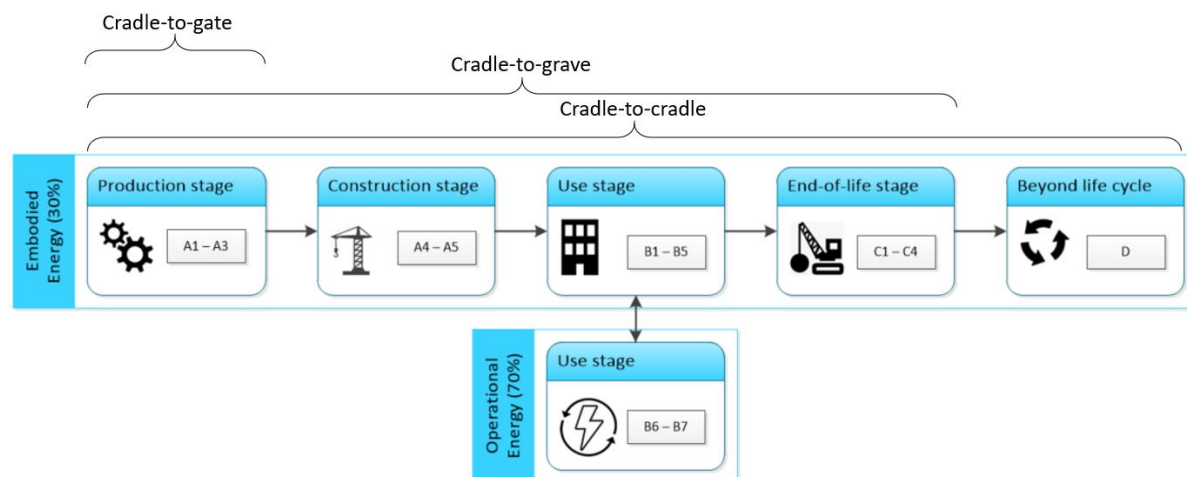


Figure 4.23: Embodied and Operational Energy.

This figure shows which design stages these factors impact. The implementation of a timber structure impacts the embodied energy but does not affect the operational energy.

Embodied energy The embodied energy consists of the energy required in the entire process of building construction. This embodied energy also consists of transportation. Transportation can have a huge influence on the total energy consumption if no reputable timber manufacturers are present near the building site. Furthermore, the used timber in this research is assumed to originate from a sustainably managed forest. Certain certifications such as the FSC certification provide the guarantee that the used timber finds its origin in a sustainably managed forest. The embodied energy also consists of the recycling potential. The recycling potential of building materials is estimated to be 37 to 42 percent of the embodied energy, assuming a 50-year lifetime [140]. Only limited documentation is found on the recycling potential of timber buildings. However, Richardson found in 2013 that the embodied CO_2 savings for timber joists and beams is approximately 0.5 kg CO_2 /kg [123].

Operational energy The operational energy consists of the energy consumed during the operational phase of the building. Four design choices which have the biggest impact on the operational energy are:

- Overhang
- Shape
- Orientation
- window-wall ratio of façade

So, the used building material for the structure does not affect the operational energy.

Total energy Recently, considerable improvements have been made in the reduction of operational energy of buildings. More insulating materials, energy-efficient windows and high-efficiency HVAC systems are used to reduce this operational energy [31]. A recent study on Dutch residential construction shows the results of these changes. It reports that for standard homes, the operational energy accounts for 78 to 80 percent of the total lifetime energy consumed. However, for advanced new homes, the operational energy only accounts for 54 to 69 percent of the total lifetime energy consumed [91].

The increase of the impact of the embodied energy compared to the operational energy shows that the use of sustainable materials is becoming increasingly more important in the future. Since we are moving toward energy-neutral buildings, the part of the total impact caused by embodied energy is increasing.

The energy use as shown in Figure 4.23 consists of several phases. These phases and what parts are dismissed in this research are mentioned below.

- **Production stage [A1-A3]** The production stage consists of consecutively, tree growth and felling, transportation to factory, and industrial processing, see Figure 4.24. This industrial processing differs per required timber product.
- **Construction stage [A4-A5]** Since the environmental impact caused by transport is dependent on the project, it is excluded from analysis in this research. Furthermore, Stage A5, the construction installation process, is excluded from the EPD calculation.
- **Use stage [B1-B7]** The potential environmental impact caused by replacement or maintenance is excluded from analysis in this research.
- **End of life scenarios [C1-C4, D]** Here C1-C4 consists of the demolition and processing phase, while stage D analyses the environmental charges and benefits beyond the system boundary of the building. In models calculating the environmental impact of a timber building, the correct consideration of the carbon sequestration has major effects.

There are three analysis methods which are commonly used to determine the environmental impact of a material, see Figure 4.23:

- **Cradle-to-gate** Which analyses stages A1-A3.
- **Cradle-to-grave** Which analyses stages A, and C.
- **Cradle-to-cradle** Which analyses stages A, C and D.

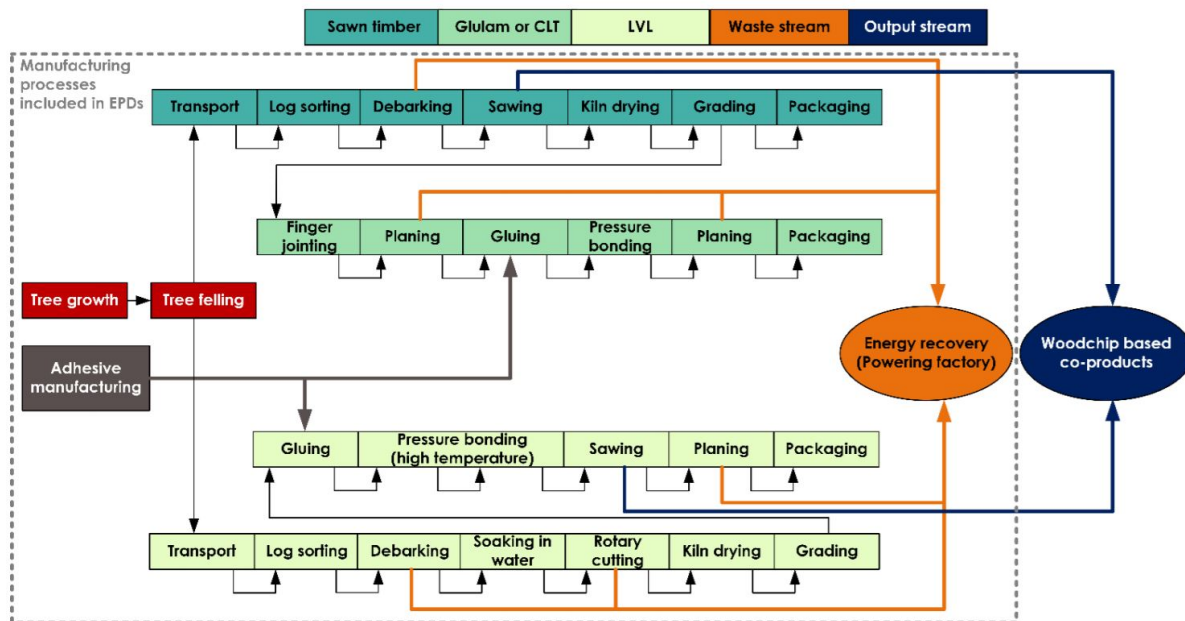


Figure 4.24: Production stage [157].

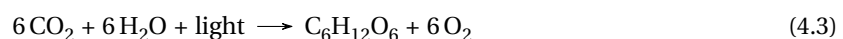
Modelling

Shadow cost calculation To get a better understanding regarding the differences in sustainability between building materials, various factors must be taken into account. A Life Cycle Assessment (LCA) provides a clear overview of these factors. An exact LCA should follow the ISO 14040 Guidelines [114]. Environmental Product Declarations (EPD's) are used in this research to determine the LCA data of building elements. These EPD's are often provided by manufacturers of building elements. Based on this LCA data from EPD's, the shadow costs of a building can be determined. This is done using the Milieuprestatie Gebouwen (MPG) methodology. This methodology uses the LCA data to record the material-related environmental performance in several phases of the design process [22]. To accomplish this, eleven environmental cost indicators (MKI's) are defined. These environmental cost indicators consist of a shadow price per unit. By multiplying the quantity of the unit of an impact category with the shadow price per unit, the environmental performance is determined, see Equation 4.2.

$$\text{Environmental Performance} = \sum_{i=1}^n \text{Quantity of building element} \cdot \text{EPD data of building element} \cdot \text{MKI} \quad (4.2)$$

Calculation of the environmental performance is affected greatly by the used EPD data. Two factors influence the EPD data enormously. Firstly, EPD data provided by manufacturers can vary greatly for the same material. Therefore, it is crucial to assess this data thoroughly, and use EPD data which is independently researched. For timber elements, this research uses the EPD data as obtained by Van Wijnen (2020) [157]. Van Wijnen researched EPD data from various manufacturers is for use in the Netherlands, according to the rules as defined for a MPG calculation. All used EPD data is mentioned in Annex C.1. Secondly, the EPD data of a building element is greatly affected by the used methodology considering carbon sequestration. An introduction regarding carbon sequestration and the assessment methods used in this research are elaborated below.

Carbon sequestration The growth of a tree results in the storage of carbon dioxide outside of the atmosphere during its lifetime. During the forming of the biomass, a process called photosynthesis takes place, see Formula 4.3. During this process carbon dioxide, water and light are turned into $C_6H_{12}O_6$, a simple sugar, and oxygen. The carbon is stored in the form of $C_6H_{12}O_6$ in the biomass, while the oxygen is emitted. Only when the biomass is burned or rots, this carbon dioxide will be released into the atmosphere [21].



Additional information regarding carbon sequestration is found in Annex A.1.2.

Figure 4.25 shows a comparison between carbon storage in a commercially managed and an unmanaged forest. An unmanaged forest eventually reaches a steady-state, while the carbon storage of a commercially managed forest is a cyclic process which is harvested before reaching the steady-state. So, the depletion of carbon storage in a commercially managed forest during harvesting will not affect the carbon storage potential of the forest. With the accumulation of timber products from a commercially managed forest, the carbon sequestration for a commercially managed forest becomes greater than that of an unmanaged forest.

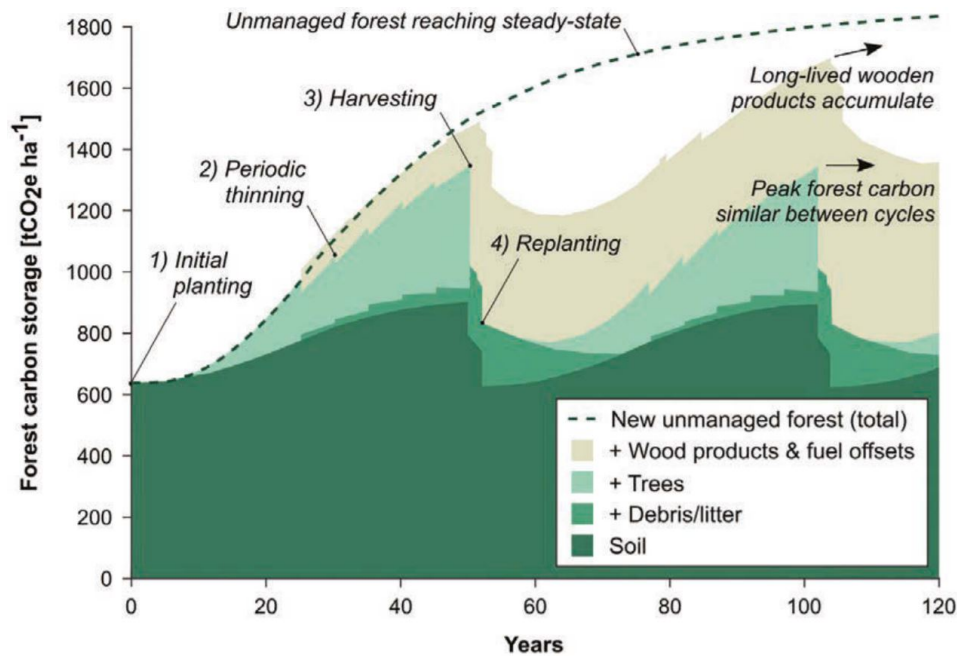


Figure 4.25: Changes in carbon storage between commercially managed and unmanaged forest [65].

Based on Figure 4.25, three different assessment methods for the inclusion of carbon sequestration are defined, which will be used in this research, see Figure 4.26.

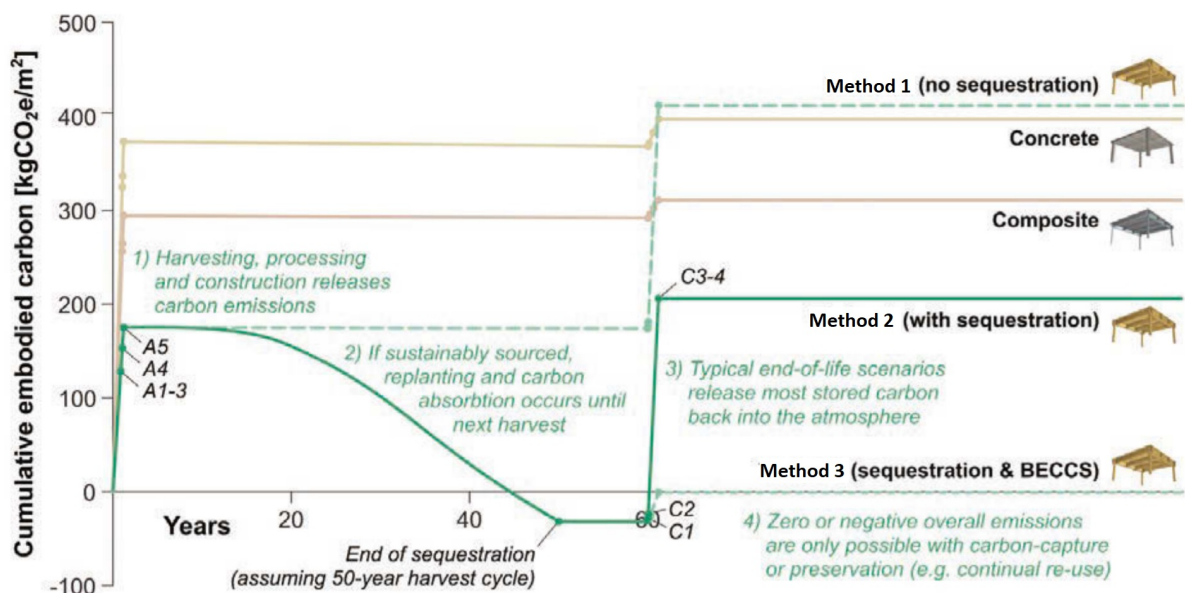


Figure 4.26: The cumulative embodied carbon emissions for a concrete, steel, and timber building. Showing three calculation methods for timber buildings [65].

1. **Method 1: Exclusion of carbon sequestration** In the Netherlands, the environmental impact is determined using the NEN-EN 15804 norm. In this norm, the process of carbon sequestration is excluded. This can even lead to timber buildings being unfavourable over concrete buildings considering the cumulative embodied carbon, see Figure 4.26.
2. **Method 2: Inclusion of carbon sequestration with re-emitting** [65] Hawkins, 2021, argues in the IStructE guide, that simply adding the carbon sequestration as a negative emission would be an oversimplified approach. Hawkins advises to include end-of-life values since typically most of the stored carbon is re-emitted. By decreasing the re-emittance of stored carbon, the carbon emissions can be decreased. The aim for circularity and recycling can help with this since it influences the amount of used timber building elements being re-used, and thus still sequestering carbon. Smart building design, by for example using dry connections creates a possibility for re-use. Recycling could be done by chipping the wood to create chipboards or other materials. So, A cradle-to-grave analysis is performed which assumes a life-span of 50 years and a harvesting cycle of 50 years. Here, the carbon sequestration is subtracted from the found cradle-to-grave EPD values. The end-of-life scenario greatly affects carbon sequestration. There are several ways of modelling the carbon sequestration and the release of carbon at the end-of-life scenario in the EPD. However, often EPDs only include carbon sequestration with no release of carbon at the end-of-life scenario.
3. **Method 3: Inclusion of carbon sequestration with BECCS.** BECCS (Bioenergy with carbon capture and storage) is a process where the carbon from biomass is captured and stored. This process ensures carbon sequestration in the end-of-life stage of a building. Stark (2019) argues that BECCS can potentially capture up to 90% of combustion emissions [136].

Optimization objective

The environmental optimization objective is to minimize the environmental performance, expressed in shadow costs which are determined according to the MPG methodology. The three carbon sequestration calculation methods discussed above are used to determine the environmental performance.

4.5.4. Economical

Introduction

Van Oss (2007) and Ajouz (2018) argue that the total investment costs of a building can be divided as shown in Figure 4.27 Van Oss states that the construction costs make up around 58% of the total costs of a building [154], [13].

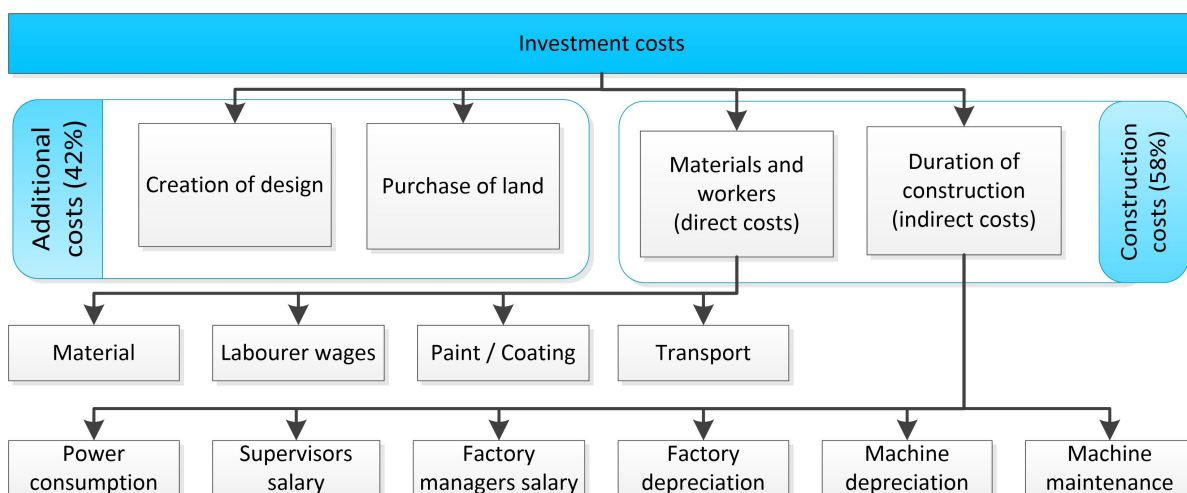


Figure 4.27: Investment costs according to Van Oss and Ajouz [154], [13].

These construction costs can be grouped into various categories. Watts (2010) researched the direct and indirect construction costs of high-rise office buildings in London [161], see Figure 4.28a. Van Oss (2007) researched the direct and indirect construction costs of several concrete and steel high-rise buildings in the Netherlands [154], see Figure 4.28b.

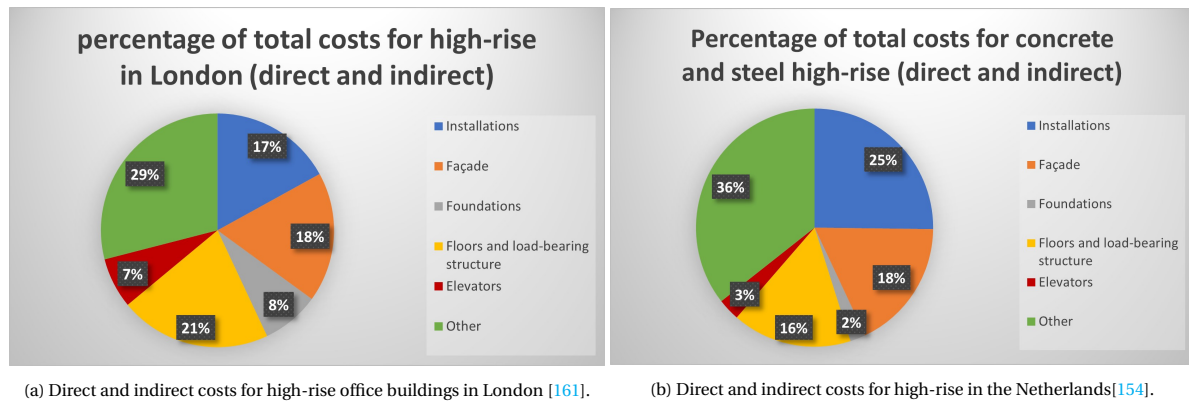


Figure 4.28: Direct and indirect costs for high-rise

Cost influencers Some additional factors influence the construction costs which are not included in the tool:

- **Market** The market is dependent on competition, supply, and demand.
- **Construction time** A faster construction time results in a reduction of construction costs. Because of the high running costs of construction, and since the building can be rented out earlier [47].
- **Number of repetitions** It should be aimed to use as many identical building elements as possible since fewer errors are made by factory workers for repetitive tasks [59].
- **Bulk** Average prices drop when a greater quantity is bought.
- **Availability** The availability of sustainably harvested engineered timber fluctuates, which impacts the costs.

Modelling

For the determination of the Economical performance, the MAMO (Materiaal, Arbied, Materieel, Onderaanneming) rules for budgeting are used. These rules divide all direct and indirect costs into four groups:

1. Materials
2. Labor
3. Equipment
4. Subcontracting

In this design problem, there are no subcontracting costs. Following these rules, the economical performance of the timber elements and connections is determined separately and subsequently summed to find the total economical performance of the building model.

4.6. Structural design considerations

For the structural design of buildings, the Eurocode is used. Although the Eurocode is universally used in Europe, each country has its own national annex. The NEN publishes this Eurocode in Dutch including the national annex. These design requirements apply to high-rise buildings up to 70 meters. These structural requirements can be grouped into two groups.

- **Usability** This includes the Serviceability Limit State (SLS).
- **Safety** This includes both the Ultimate Limit State (ULS) and the fire safety.

4.6.1. General

Safety factors

The structure should provide enough structural resistance to withstand the loads. But, for every structure the structural resistance and the loads are approximations. So this structural resistance and loads (actions) are normal distributions, see Figure 4.29. To ensure an acceptable resistance, partial safety factors (γ_G , γ_Q and γ_M) and the k_{mod} factor are used. These factors transform the characteristic values to design values. These design values are used for calculation. These factors increase the distance between both normal distributions. This way, the probability of failure is reduced, see Figure 4.29.

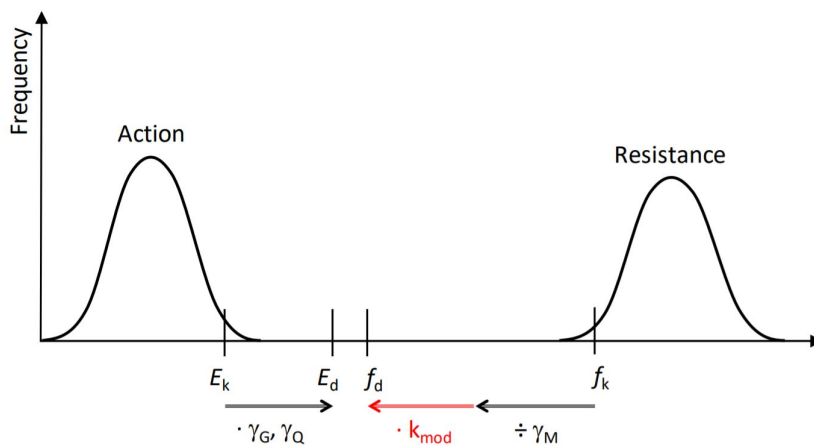


Figure 4.29: Reducing the probability of failure using partial safety factors and the k_{mod} factor [21].

These design values are calculated using

$$X_d = k_{mod} \cdot \frac{X_k}{\gamma_M} \quad (4.4)$$

γ_M = partial safety factor

SLS For SLS, the partial safety factors γ_M , γ_G and γ_Q are assumed to be equal to 1.0.

ULS For ULS, the partial safety factors γ_G and γ_Q are included in the load combinations, see Figure 4.31. Furthermore, $\gamma_M = 1.25$ is used for punched metal plate fasteners. For all other connections and wood products, $\gamma_M = 1.3$ is used. The k_{mod} factor is used for both the determination of the ULS and SLS. The k_{mod} factor is used to consider both the load duration and the moisture content of the material. The k_{mod} factor can be determined using Figure 4.30.

Consequence class

NEN-EN-1990-1-1 gives the consequence class of the building [80]. Consequence class 2 (CC2) is assigned to residential and office buildings. The loss of human life, economic, social, or environmental consequences are considered to be medium. For buildings above 70 meters, consequence class 3 (CC3) must be used.

k_{mod} factor for solid timber and glulam				
Load-duration class	Duration	Examples for loads	k_{mod} for service class	
			1 and 2	3
Permanent	More than 10 years	Self-weight	0.60	0.50
Long-term	From 6 months to 10 years	Storage	0.70	0.55
Medium-term	From 1 week to 6 months	Imposed floor load	0.80	0.65
Short-term	Less than one week	Snow, wind	0.90	0.70
Instantaneous	Accidental load	Explosion	1.10	0.90

Figure 4.30: the k_{mod} factor for solid timber and glulam [21].

Loads

There are five loads that are considered in the structural analysis of the structure.

- Dead load
- Live load
- Wind load
- Snow load
- Rain load

The calculations of these loads are given in Annex A.4.1.

Load combinations

All these different loads are combined using load combinations as given in NEN-EN-1990-1-1 to find the normative load situation for both the ULS and SLS [80]. The load combinations for consequence class 2 are used. Furthermore, an office building is considered, so the factors $\psi_0 = 0.5$, $\psi_1 = 0.5$ and $\psi_2 = 0.3$ are used for floor loads. For snow and wind loads, the factors $\psi_0 = 0$, $\psi_1 = 0.2$ and $\psi_2 = 0$ are used.

As specified in NEN-EN 1991-1-1, when the leading variable action is the imposed load, which acts on the columns or walls. The full imposed load can be applied to the two top floors of the building, while the imposed load on the other floors is reduced by multiplying with the reduction factor ψ_0 . A reduction factor α_n can be used to calculate the remaining total load, see Equation 4.5 [72].

$$\alpha_n = \frac{2 + (n - 2) \cdot \psi_0}{n} \quad (4.5)$$

α_n = reduction factor

n = amount of floors above the position of the considered element

ψ_0 = factor for combination value of a variable action

Serviceability Limit State In the Serviceability Limit State (SLS), the partial factors for action γ_G and γ_G are equal to 1.0. The load combinations for SLS are determined using one of the three equations given below, depending on the load duration. For irreversible limit states, Equation 4.6 is used. For reversible limit states, Equation 4.7 is used. For long-term effects, the quasi-permanent combination given in Equation 4.8 is used.

$$E_d = \sum_{j \geq 1} G_{k,j} + Q_{k,1} + \sum_{i \geq 1} \psi_{0,i} \cdot Q_{k,i} \quad (4.6)$$

$$E_d = \sum_{j \geq 1} G_{k,j} + \psi_{1,1} \cdot Q_{k,1} + \sum_{i \geq 1} \psi_{2,i} \cdot Q_{k,i} \quad (4.7)$$

$$E_d = \sum_{j \geq 1} G_{k,j} + \sum_{i \geq 1} \psi_{2,i} \cdot Q_{k,i} \quad (4.8)$$

- γ_G = partial factor for permanent actions
 γ_Q = partial factor for variable actions
 ψ_0 = factor for combination value of a variable action
 ξ = reduction factor
 G_k = characteristic value of a permanent action
 $G_{k,j}$ = characteristic value of permanent action j
 Q_k = characteristic value of a single variable action
 $Q_{k,1}$ = characteristic value of the leading variable action 1

Ultimate Limit State The load combinations for Ultimate Limit State are determined for limit states for static equilibrium, see Equation 4.9 and limit states of failures, see Equations 4.10 and 4.11.

$$E_d = \sum_{j \geq 1} \gamma_{G,j} \cdot G_{k,j} + \gamma_{Q,1} \cdot Q_{k,1} + \sum_{i \geq 1} \gamma_{Q,i} \cdot \psi_{0,i} \cdot Q_{k,i} \quad (4.9)$$

$$E_d = \sum_{j \geq 1} \gamma_{G,j} \cdot G_{k,j} + \gamma_{Q,1} \cdot \psi_{0,1} \cdot Q_{k,1} + \sum_{i \geq 1} \gamma_{Q,i} \cdot \psi_{0,i} \cdot Q_{k,i} \quad (4.10)$$

$$E_d = \sum_{j \geq 1} \xi_j \cdot \gamma_{G,j} \cdot G_{k,j} + \gamma_{Q,1} \cdot Q_{k,1} + \sum_{i \geq 1} \gamma_{Q,i} \cdot \psi_{0,i} \cdot Q_{k,i} \quad (4.11)$$

- γ_G = partial factor for permanent actions
 γ_Q = partial factor for variable actions
 ψ_0 = factor for combination value of a variable action
 ξ = reduction factor
 G_k = characteristic value of a permanent action
 $G_{k,j}$ = characteristic value of permanent action j
 Q_k = characteristic value of a single variable action
 $Q_{k,1}$ = characteristic value of the leading variable action 1

Using the equations as given above, the normative load combinations for ULS and SLS are assumed, see Figure 4.31. For all building elements, two or more load combinations are used for calculation in the tool. These load combinations are assumed to be normative for the considered building element. It is assumed that by using these load combinations in the tool, a structurally safe building is created.

Load combinations for ULS and SLS		
	Load combination	Application
ULS1	$0.9 \cdot \mathbf{G} + 1.5 \cdot \mathbf{Q}_{wind}$	Tension in foundation
ULS2	$1.2 \cdot \mathbf{G} + 1.5 \cdot \mathbf{Q}_{imposed}$	Beams, Floors
ULS3	$1.2 \cdot \mathbf{G} + 1.5 \cdot \mathbf{Q}_{wind} + 1.5 \cdot 0.5 \cdot \alpha_n \cdot \mathbf{Q}_{imposed}$	Stability system, Core
ULS4	$1.2 \cdot \mathbf{G} + 1.5 \cdot \alpha_n \cdot \mathbf{Q}_{imposed}$	Columns, Core
ULS5fire	$1.0 \cdot \mathbf{G} + 1.0 \cdot 0.2 \cdot \mathbf{Q}_{wind} + 1.0 \cdot 0.3 \cdot \mathbf{Q}_{imposed}$	Gravitational system
ULS6fire	$1.0 \cdot \mathbf{G} + 1.0 \cdot 0.5 \cdot \mathbf{Q}_{imposed}$	Beams, Floor
ULS7fire	$1.0 \cdot \mathbf{G} + 1.0 \cdot 0.5 \cdot \alpha_n \cdot \mathbf{Q}_{imposed}$	Columns, Core
ULS8fire	$1.0 \cdot \mathbf{G} + 1.0 \cdot 0.2 \cdot \mathbf{Q}_{wind} + 1.0 \cdot 0.3 \cdot \alpha_n \cdot \mathbf{Q}_{imposed}$	Core
SLS1	$1.0 \cdot \mathbf{G} + 1.0 \cdot \mathbf{Q}_{wind} + 1.0 \cdot 0.5 \cdot \mathbf{Q}_{imposed}$	Stability system
SLS2	$1.0 \cdot \mathbf{G} + 1.0 \cdot \mathbf{Q}_{imposed}$	Beams, Floors

Figure 4.31: Load combinations for ULS and SLS

4.6.2. Serviceability Limit State

When a structure satisfies the serviceability limit state, it is ensured the structure is serviceable and performs its intended function throughout its lifetime. The following calculations are performed to cover the aspects the structure must satisfy to ensure its serviceability.

- Horizontal deformation
- Vertical deformation
- Acceleration
- Inter-storey drift

The full calculation as defined in the Eurocode are given in Annex [A.4.2](#)

4.6.3. Ultimate Limit State

When a structure satisfies the serviceability limit state, it is ensured the structure can withstand all possible load situations throughout its lifetime. The following calculations are performed to cover the aspects the structure must satisfy to ensure its structural safety:

- Normal force
- Shear
- Bending moment
- Second order effect
- Global initial sway imperfections
- Buckling
- Robustness
- Internal wind pressure

The full calculation as defined in the Eurocode are given out in Annex [A.4.3](#)

4.6.4. Fire safety

Two fire safety strategies are mentioned, see Annex [A.4.4](#)

- Exposed fire safety strategy
- Gypsum encapsulated strategy

4.6.5. Scope

The following structural design considerations are out of the scope of this research, and thus not included in the tool development.

- Torsional and cross-wind acceleration
- Earthquake resistance
- Deflection of the façade
- Wind suction on the façade
- Robustness.

4.7. Architectural design considerations

4.7.1. Acoustics

The Netherlands does not have sound insulation requirements for offices [121]. However, sound insulation requirements for residential buildings are present. There are two main considerations when determining the acoustic performance of a building: the Sound Transmission Class (STC) and the Impact Insulation Class (IIC).

Sound Transmission Class The STC concerns how well a partition can absorb the sound waves hitting it on one side, preventing vibrations on the other side. For residential buildings, NEN 5077 mentions a minimum characteristic airborne sound level difference of 52 dB [82]. Green (2012) found that with a doubling of the mass of a partition, the STC will increase by roughly 5 dB [60]. This clearly shows the challenge of sound insulation for lightweight materials.

Impact Insulation Class The IIS concerns how well a partition can absorb the direct contact or impact on a floor or wall on one side, preventing vibrations on the other side. NEN 5077 mentions a maximum difference in sound pressure level for a residential building of 54 dB for wooden floors [82].

Kerto-Ripa insulation Acoustical tests performed by Metsa Wood on Kerto-Ripa floors indicated airborne sound insulation between 59 and 67 dB, and an impact sound insulation between 47 and 55 dB [105]. For residential buildings, this airborne sound insulation is sufficient, while the impact sound insulation might not be sufficient. Thus, the Kerto-Ripa floor elements are dimensioned for each building design in the tool according to the impact sound insulation requirements.

4.7.2. Storey height

The Dutch Building Code mentions a minimum floor-to-ceiling height of 2.6 meters. For all optimizations, a floor-to-ceiling height of 3.0 meters is used.

4.7.3. Daylight

The amount of daylight entry in a space within a building is dependent on the floor-to-window area ratio and the maximal floor depth. The Dutch Building Code states that for an office function the minimum floor-to-window area ratio is 2.5% with a minimum of 0.5 m^2 of window area. However, the Dutch health and safety regulations for workspaces named the "ARBO", determined that the window area has to be at least 5% of the floor area. The core in the timber building designs, as generated in the tool, is placed such that the amount of area close to a window is maximized.

5

Development of Multidisciplinary Design Optimization Tool

5.1. Introduction

Chapter 1 to 3 outlines the design problem, while chapter 4 discusses the theoretical framework of the MDO tool. Based on this information, the design problem is translated into logic, which is done in this Chapter. To accomplish this, a relation between the determined parameters must be set. Next, the tool finds a certain result based on these parameters. In this case this result consists of two optimization objectives: the environmental performance and the economical performance. When the boundaries of the parameters are set, the design space can be explored. This exploration is done using a Multi-Objective Genetic Algorithm (MOGA). This MOGA optimizes the building design for the two optimization objectives. So, to accurately develop an MDO tool, first the design problem must be clearly stated, with all assumptions. Next, based on this design problem and the theoretical framework the tool can be developed.

5.1.1. Design problem

This tool aims to identify in which design situation timber high-rise can be competitive to a concrete design alternative, considering the combination of properties for shadow costs and construction costs. The created designs must satisfy all architectural and structural boundary conditions. So, the structural model and all its separate building elements must be known thoroughly to be able to translate this logic correctly in the tool.

Structural model Figure 5.1a shows the structural system. This structural system is split into three separate systems in the structural calculations in the tool. The gravitational system, shown in Figure 5.1b transfers the gravitational and floor loads. It consists of floor plates, columns, beams, and a core. The floor system is shown in Figure 5.1c. This floor system transfers the wind loads to the stability system through the floor plates and the beams. The stability system provides lateral stability to the building using a braced tube system, see Figure 5.1d. It carries both gravitational and lateral loads. All connections between elements in the braced tube system are created using steel plate and dowel connections.

To provide maximum daylight in the used spaces and minimize the number of required beams, the tool is developed such that the core is always placed between two beams in the center of the building. Custom nodes are used to perform the required structural calculations of the building elements, these calculations are elaborated on in Annex B. Figure 5.2 shows which calculations are performed per building element. The floor plates span in one direction. The loads on the floor plates are transferred to the beams, using a screwed connection. The beams transfer the loads to the core, or the columns using Knapp connectors. Lastly, the wind forces are transferred through the columns, beams, and diagonals in the façade to the foundation. Steel plates and dowel connections are used to connect these elements in the stability system.

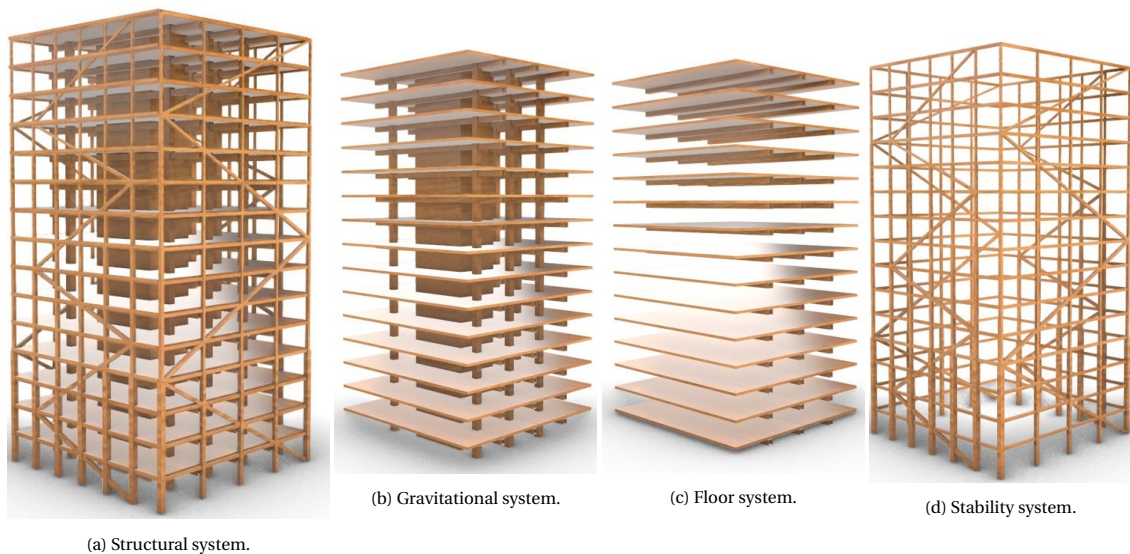


Figure 5.1

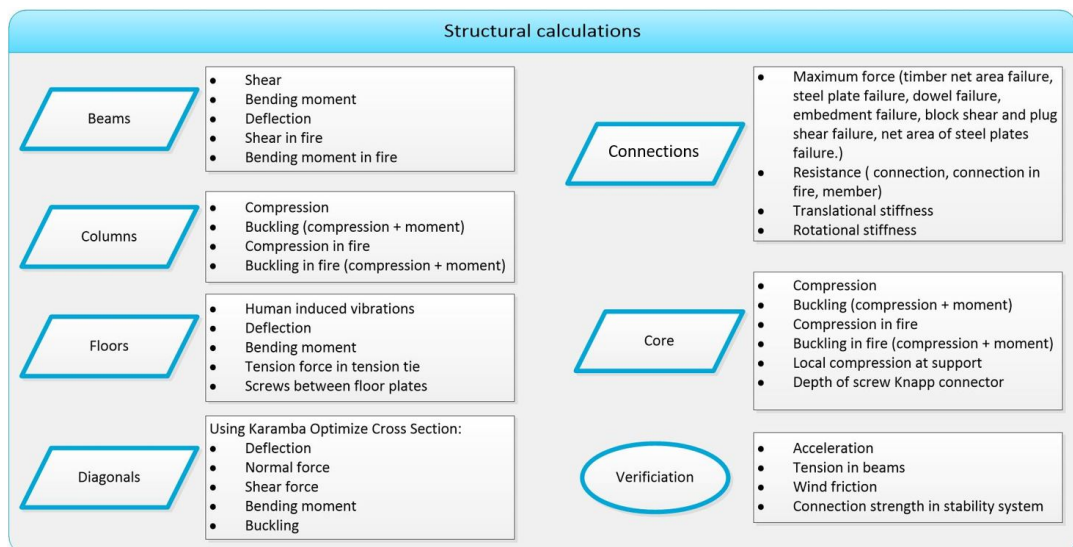


Figure 5.2: Structural calculations performed in Grasshopper. Full calculations can be found in Annex B.

Building sequence The building sequence influences the structural and economical performance. Below, a possible scenario for this building sequence is described.

- Using cranes, the CLT plates are hoisted in place. Metal brackets and angle brackets are used for the connection between CLT plates. Knapp connectors are used to mount the CLT plates to the beams.
- Meanwhile, the columns, diagonals, and beams making up the braced tube system are installed using steel plate and dowel connections. For the placement of the elements, a crane is used. Using a cherry picker, the dowels are put into place to complete the connections.
- The inner columns are placed on the columns below, the carpentry connections and screws ensure the stability of these columns. The Knapp connectors have been connected to the inner beams and columns in the factory. These beams are connected to the columns and core elements by hoisting and sliding the Knapp connectors together.
- The top parts of the floor plates are placed on the beams. Subsequently, the floor plates are connected to floor plates and beams using screws.

Assumptions

- The load combinations, as specified in Section 4.6.1 are assumed to be normative. It is assumed that by using these load combinations, a building will be created which satisfies all load combinations. This is a reasonable assumption since simple calculations indicate these normative load combinations are never smaller than the non-regarded load combinations in this design problem.
- The CLT core hardly provides any possibility for transfer of horizontal forces. This is the result of the lack of stiffness in the connections between the CLT plates in the core. So, it is assumed the braced tube system provides all lateral stability. Horizontal forces are presented on the CLT core, caused by internal wind loads. The floor system is assumed to transfer wind forces to this stability system through diaphragm action.
- As mentioned in Section A.4.2, it is expected either an along-wind response, or the cross-wind response will provide a critical acceleration of the building. So, the torsional response is not included in the calculations, since this response is not assumed to be normative.
- An additional 10% of deflection is used to account for second-order effects. This is added in the SLS calculation of the stability system. This 10% is according to the research on second-order effects of timber high-rise structures as found by Slooten (2018) and Gijzen (2017) [57], [134].

5.1.2. Design choices

- The steel plate length input parameter determines the stiffness and strength of the steel plate and dowel connections. The calculations performed to determine the stiffness and strength based on the steel plate length are given in Annex B.1. The stiffness of these connections affects the required strength of the connections in the braced tube system. To be able to obtain the optimal steel plate and dowel connections in a building model, the strength and stiffness properties must be determined in an iterative process. Such an analysis provides an overly detailed result, which is not required in the conceptual design phase as such an iterative process increases the computational time significantly. So, it is chosen to not perform this iteration for each building model but to perform this iteration in the Multi-Objective Genetic Algorithm. This is done by defining a maximum percentage of all connections which may fail on strength, and a steel plate length for all steel plate and dowel connections. Since only one universal connection is calculated, a significant part of the connections is over-dimensioned or under-dimensioned. The defined maximum percentage of all connections which may fail on strength accounts for this. Accordingly, it is aimed to obtain a structure that is neither over-dimensioned nor under-dimensioned.
- Except for the corner columns, only square cross sections are used for optimization of the columns and diagonals in the stability system. This will provide an accurate calculation compared to complete freedom in cross section dimensioning. This seems like a reasonable assumption because in Mjøstårnet, the dimensions of these elements in the stability system are approximately square.
- The Optimize Cross Section component of the Karamba3D plug-in is used to dimension the columns and diagonals in the stability system. This component is verified in Annex A.6. Although the Optimize Cross Section component provides accurate results overall, there are two disadvantages regarding using this tool in timber building design. Firstly, the tool uses the requirements as specified in Eurocode 3 for steel structures for the determination of buckling. Secondly, this component is based on materials for which the compressive and tensile design strength are similar. But, for engineered timber, the maximum tension design strength of the material is roughly 80% of the maximum compression design strength in the strong direction. To create a structurally safe structure, the compressive design strength is set equal to the tensile design strength. This way, the compression design strength is smaller than in reality, but this conservative assumption might be required since buckling is not accurately regarded.
- In Mjøstårnet, the inner beams and the beams in the façade have similar dimensions. Thus, it is assumed an optimal stability structure can be created by assuming the same dimensions for inner beams and beams located in the façade.
- The steel plate and dowel connection is dimensioned assuming a straight transfer of forces. However, some steel plate and dowel connections transfer forces under an angle. The effect of this is not considered in the tool

- Three simplifications are made in the structural model. Since the effect of these simplifications is small, they are regarded as reasonable simplifications. Firstly, the concrete ground floor is not considered in the tool. Secondly, Kerto-Ripa floor elements are used for the roof structure. Lastly, the uplift forces caused by wind loads on the floors are not considered.
- For simplification reasons and due to their low impact, the column-foundation and core-foundation connections are not regarded in the model.
- The core-core connections are included in the construction cost estimation of the CLT elements. For the shadow cost calculation of these connectors, an estimated 1 kg of steel per m^2 of CLT is used.

5.2. Overview of modelling

Figure 5.3 shows a simplified schematization of the framework, the numbers reference the sections in this chapter that elaborate on the corresponding part. Figure 5.4 shows a schematization of the framework of the MDO tool, which follows the layout of the script in Grasshopper. The layout of the script in Grasshopper is shown in Annex E.3.

- **5.3:** The input is determined. Part of this input is set based on the design situation and part of this input is what the tool optimizes for.
- **5.4:** Using this input, and a minor structural calculation, the geometry of the building is obtained. This geometry indicates the location of building elements and connections.
- **5.5, 5.6, 5.7:** The cross section sizes of the elements in the structural system are determined using custom node calculations and Karamba's Optimize Cross Section component to determine the minimum required cross sections and connections that fulfil the defined ULS and SLS requirements. Now, a database with all required timber elements and connections is obtained.
- **5.8, 5.9:** Using this database the economical and environmental performance can be determined.
- **5.10:** A verification is executed which checks the structural system on acceleration, connection strength, tension forces in the tension ties and wind friction. If the structural system is within the set constraints of the verifications, the obtained results for economical and environmental performance are transferred to the optimization component.
- **5.11:** Based on the optimization objectives, the optimization component determines the input of the next generation of building elements, starting a new loop.

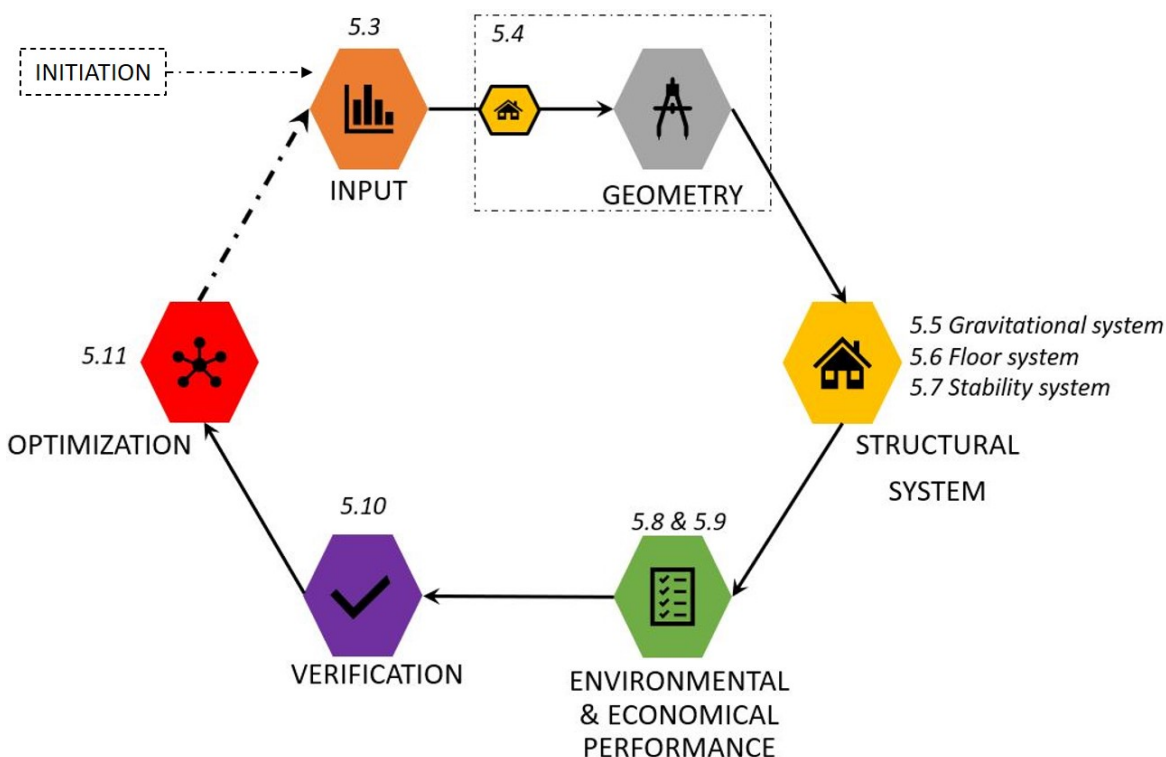


Figure 5.3: Simplified schematization of the framework

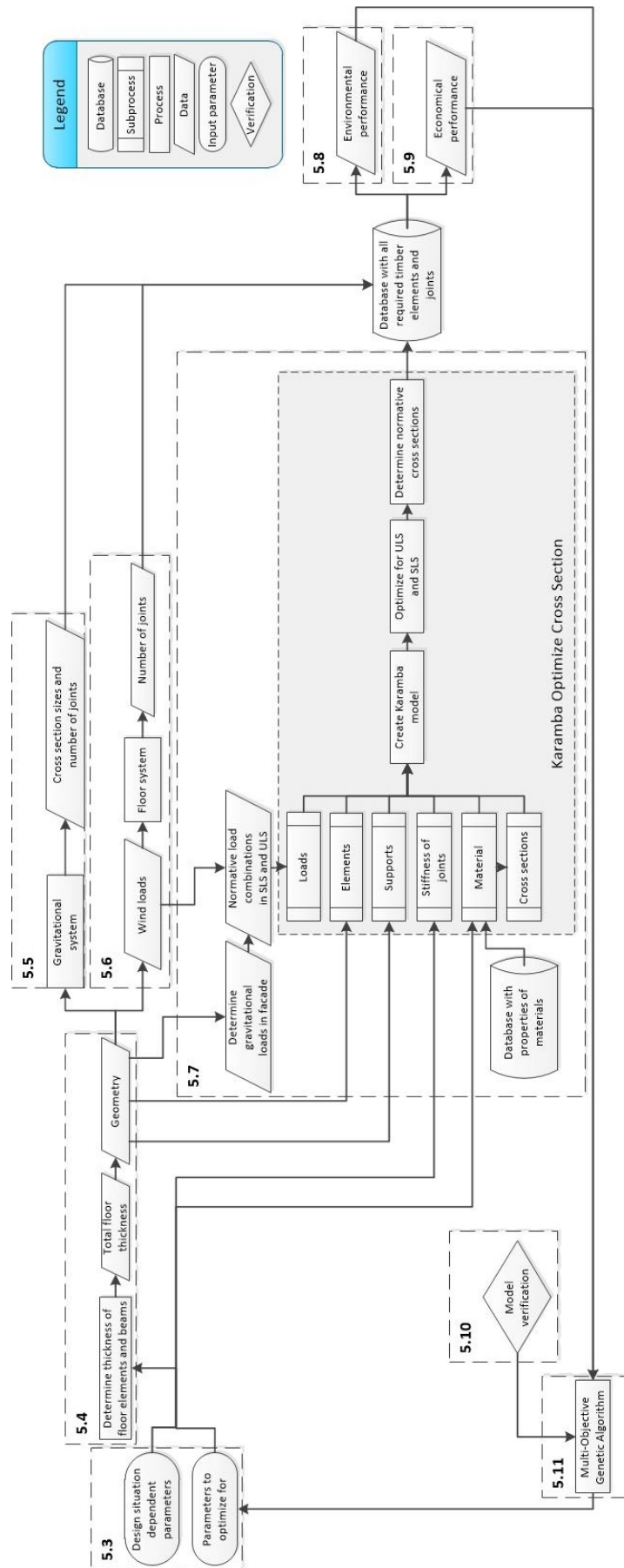


Figure 5.4: Schematization of the framework

5.3. Input parameters

The model consists of fixed input parameters, design situation dependent input parameters and optimization parameters. The parameters to optimize for are shown in Figure 5.5. The tool aims to find the optimal values for these parameters concerning all considered disciplines. The possible quantities per parameter might be slightly altered based on the design situation. The design situation dependent input consists of a fixed and an adaptable part, see Figure 5.6b. The fixed part is the direct translation of the design situation. The adaptable part is the interpretation of the design situation by the operator. For the fixed design situation input some assumptions are made. One of these assumptions is an additional floor mass of 160 kg/m^2 . This additional floor mass consists of:

- 40 mm dry screed: 48 kg/m^2
- Installations: 5 kg/m^2
- 2 gypsum boards: 15 kg/m^2
- Variable load · combination value: $3 \cdot 0.3 = 0.9 \text{ kN/m}^2$: 92 kg/m^2

When this input is not specified in this research, the assumed values are used. The fixed model input parameters are summarized in Annex E.1.

Parameters to optimize for						
Parameter	Unity	Quantity				
Grid X	m	Dependent on building dimensions				
Grid Y	m	Dependent on building dimensions				
N diagonals X	Amount	1	2	3		
N diagonals Y	Amount	1	2	3		
Diagonals X placement	-	0	1			
Diagonals Y placement	-	0	1			
length steel plate in steel plate and dowel connection in X	Length	600	800	1000	1200	1400
length steel plate in steel plate and dowel connection in Y	Length	600	800	1000	1200	1400

Figure 5.5: Parameters to optimize for.

Fixed design situation dependent input		
Parameter	Unity	Assumption
BuildingSizeX	m	-
BuildingSizeY	m	-
Minimum required floor area	m^2	-
Floor-to-ceiling height	m	3.0
Terrain category	-	3
Wind zone	-	1
Additional floor height	m	0.4
Additional floor mass	kg/m^2	160
Imposed floor load	kN/m^2	3
Dead load façade	kN/m^2	2

(a) Fixed design situation dependent parameters

Adaptable design situation dependent input	
Parameter	Unity
Maximum percentage of failure of steel plate and dowel connection	%
Maximum unity check	-
Floor type	-
Core size ratio	%
Carbon sequestration calculation method	-

(b) Adaptable design situation dependent parameters

Figure 5.6: Design situation dependent input parameters

Figures 5.7 and 5.8 explain the meaning of the input parameters. The exact position of the diagonals in the façade is dependent on two input parameters: the "N diagonals parameter" and the "Diagonals placement parameter". The "N diagonals parameter" determines the number of times the diagonal crosses the full width of the façade back and forth. The "Diagonals placement parameter" determines if the diagonal crosses the full width of the façade, or if it crosses the façade starting at the second columns up to the second last column.

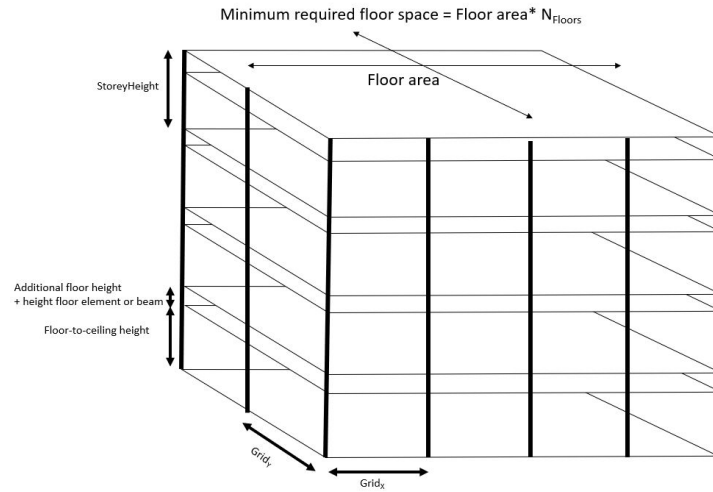


Figure 5.7: General input parameters

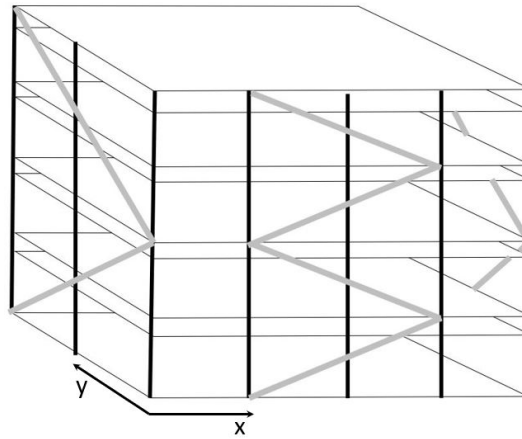


Figure 5.8: Input parameters of diagonals

In Figure 5.8, the "N diagonals parameter" and the "Diagonals placement parameter" are:

- N diagonals X = 2
- N diagonals Y = 1
- Diagonals X placement = 1
- Diagonals Y placement = 0

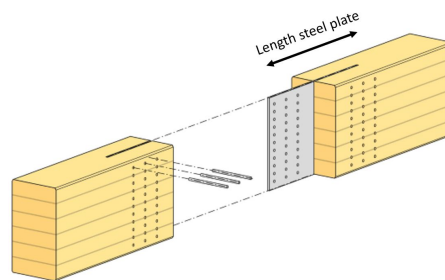


Figure 5.9: Input parameters of length of steel plate

5.4. Building geometry

The building geometry is determined in two steps. First the required total storey height is determined. Using the obtained storey height and several input parameters, the building geometry is found.

5.4.1. Storey height

The total storey height is found by determining the required thickness of floor elements and beams. To accomplish this, two custom components are used. Figure 5.10a shows the placement of floor elements on the beam.

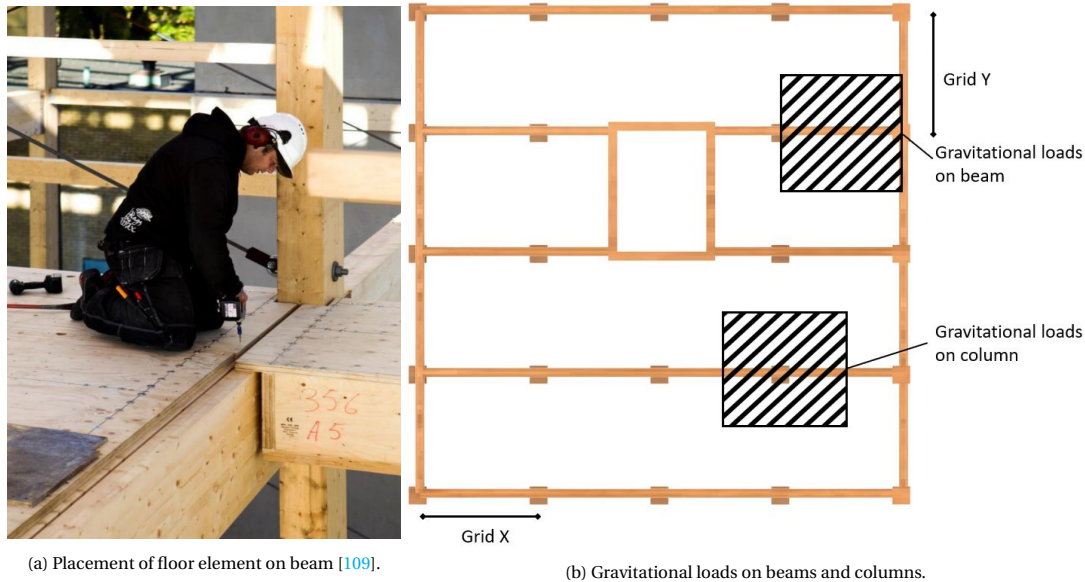


Figure 5.10

So, either the thickness of the floor element or the height of the beam is normative in determination of the floor thickness.

1. **Determination of floor thickness.** The required thickness of the Kerto-Ripa floor elements are determined by calculating the required thickness to satisfy the deflection, bending moment and human-induced vibration requirements, see Annex B.3. The used design guidelines for determination of the human-induced vibration are given in Annex B.3.1. For this calculation, the European standard EN 1995-1-1 combined with the Dutch national annex [74] will not provide an accurate result. So, the calculations are based on two alternative guidelines that provide more accurate calculations: the Austrian standard Önorm B 1995-1-1 [71], and the HIVOSS design guidelines for calculation of floor vibrations [67]. This calculation will provide the minimal required height of the ribs of the kerto-ripa plate that satisfy both the Austrian standard Önorm B 1995-1-1 and the HIVOSS design guidelines for calculation of floor vibrations, see Figure 5.11.

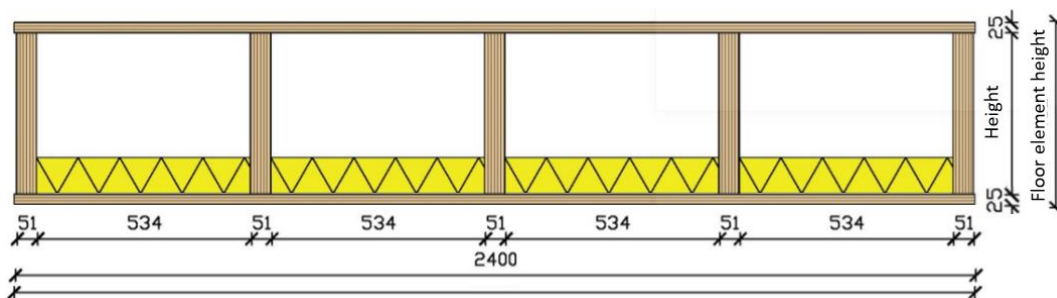


Figure 5.11: Determination of height of floor element.

2. **Determination of unprotected beam dimensions.** Using the found live and dead loads and the grid sizes in X- and Y-direction, the beam dimensions are determined, see Figure 5.10b. This calculation is elaborated in Annex B.4. The beams are not fire protected and have the same dimensions. The bending moment and shear resistance are determined in a standard and in a fire situation. Furthermore the deformation is determined. This is done according to NEN-EN 1995-1-1 [74].

Now that the height of the floor elements and the height of the beam is found, the storey height can be determined, see Equation 5.1.

$$\text{Storey height} = \max(\text{Height floor element, Height beam}) + \text{Additional floor height} + \text{Free floor height} \quad (5.1)$$

Storey height = total height of a single storey in the building.

Additional floor height = additional height of the floor as a result of gypsum plates, structural screed and installations.

Free floor height = desired height between floor and ceiling.

5.4.2. Geometry

The building geometry consists of the dimensioning of the building and the positioning of the structural elements in the building.

Dimensions of building

The height, width, and length dimension of the building depends on the total storey height, minimum required floor area, and building size in X- and Y-direction. The amount of floors is calculated using Equation 5.2, see Figure 5.12. The roof is not included in the N_{floors} - parameter.

$$\text{Actual created floor area} = S_X \cdot S_Y \cdot N_{floors} \geq \text{Minimum required floor area} \quad (5.2)$$

S_X = building size in X-direction in m. Where $S_X = (N_X - 1) \cdot Grid_X$

N_X = amount of columns in X-direction

$Grid_X$ = grid size in X-direction

S_Y = building size in Y-direction in m. Where $S_Y = (N_Y - 1) \cdot Grid_Y$

N_Y = amount of columns in Y-direction

$Grid_Y$ = grid size in Y-direction

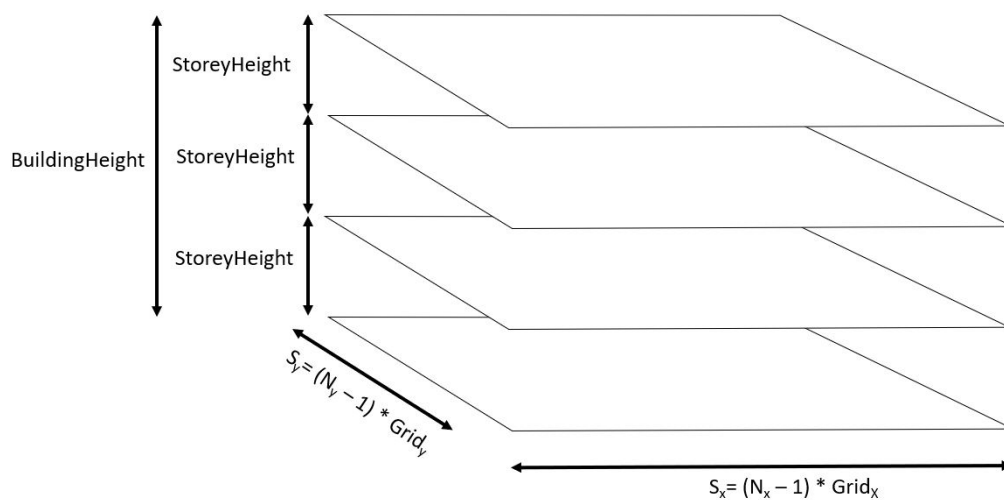


Figure 5.12: Determination of the building geometry.

Positioning of elements

The building geometry also determines the position of the following structural elements.

1. **Determination of position of columns and beams** The position of all columns and beams is determined based on the grid sizes and amount of columns in X- and Y-direction.
2. **Determination of position of core** To provide maximum daylight in the used spaces and minimize the number of required beams, the tool is created such that the core is always placed between two beams in the center of the building. Figure 5.13 shows a top view of the position of the core for all combinations of even and uneven number of columns in X- and Y-direction.

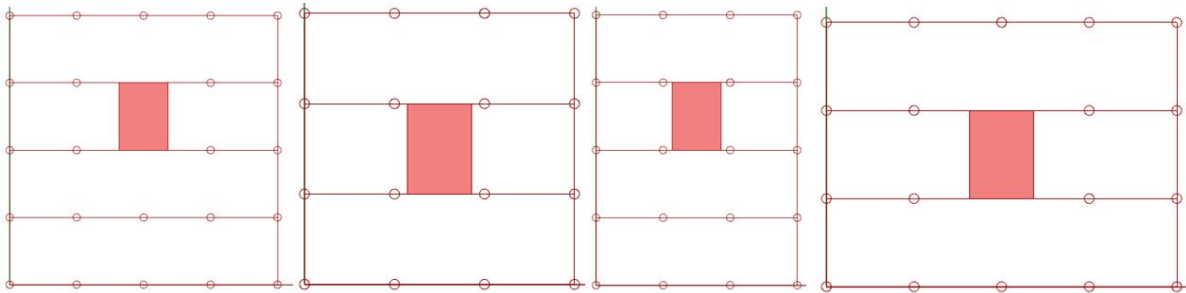


Figure 5.13: Position of core for various building layouts.

3. **Determination of position of diagonals in façade** The exact position of the diagonals in the façade is dependent on two input parameters: the "N diagonals parameter" and the "Diagonals placement parameter". The "N diagonals parameter" determines the amount of times the diagonal crosses the full width of the façade back and forth. The "Diagonals placement parameter" determines if the diagonal crosses the full width of the façade, or if it crosses the façade starting at the second columns up to the second last column. Together these two parameters determine the diagonal layout.

5.5. Gravitational system

Using the input parameters, the building geometry, and the load combinations for ULS and SLS as defined in Section 4.6.1, the gravitational system can be dimensioned. To accomplish this, the following steps are taken.

1. **Determining required core-beam connections** The connection between the core and beams is realized using Knapp connectors. By calculating the forces acting on the beams, the required Knapp connector is found, this process is elaborated in Annex B.2. In the determination of the required Knapp connector, only the 150 mm wide Knapp connectors are analysed.
2. **Determining core dimensions and thickness.** The core dimensions are determined using the formulas given in Section 4.4.6. Next, the thickness of the CLT core elements is determined. To accomplish this, the compression and buckling resistance is determined in a standard and in a fire situation. Furthermore, the local compression stress at the support location, and the required thickness to insert the screws is checked. Since the required Knapp connector is found, the compression forces in the supports can be determined. The full calculation of the core thickness is clarified in Annex B.7.
3. **Determining initial sway imperfections.** This is done according to NEN-EN 1993-1-1 [83], see Formula A.53. The initial sway imperfections will provide additional horizontal forces on the structure. These horizontal forces are multiplied with the height of a column, to find the bending moment which will act on the columns. It is assumed the effect of these bending moments on the columns in the stability system is negligible. So, these bending moments are only applied to the calculations of the inner columns.
4. **Determining unprotected inner column dimensions.** Using the found live loads and dead loads, see Figure 5.10b, and the bending moment created by the initial sway imperfections, the column dimensions can be determined. The calculations implemented in the tool are elaborated on in Annex B.5. The columns are not fire protected. Since the loads acting on a column differs over the height of the

building, the columns are divided into four groups. The normative column sizes for each group is determined. To accomplish this, the compression, bending moment and buckling resistance are determined in a standard and in a fire situation. This is done according to NEN-EN 1995-1-1 [74].

5. **Determining required column-beam connections.** The connection between the columns and beams is realized using Knapp connectors. By calculating the forces acting on the beams, the required Knapp connector is found, see Annex B.2.
6. **Determining required column-column connections.** The column-column connection is realized using a carpentry connection and screws, similar to the columns in the 25 King reference project, see Figure A.7c. An average of 24 screws per column-column connection is assumed to ensure a safe connection.

To execute these calculations, the "GHPython Script" component is used. This custom node is created using python code. The output of these calculations consists of a list of cross section sizes and a number of required connections. The custom node calculations are fully explained in Annex B.

5.6. Floor system

The wind loads on the model are calculated according to NEN-EN 1991-1-4 [73]. These calculations are elaborated in Annex B.3.2. The floor system transfers these wind loads to the lateral stability system in the façade, see Figure 5.14.

For the transfer of forces in the floor system, the gravitational forces have no effect. So, $1.5 \cdot Q_{wind}$ is assumed to indicate the normative load combination.

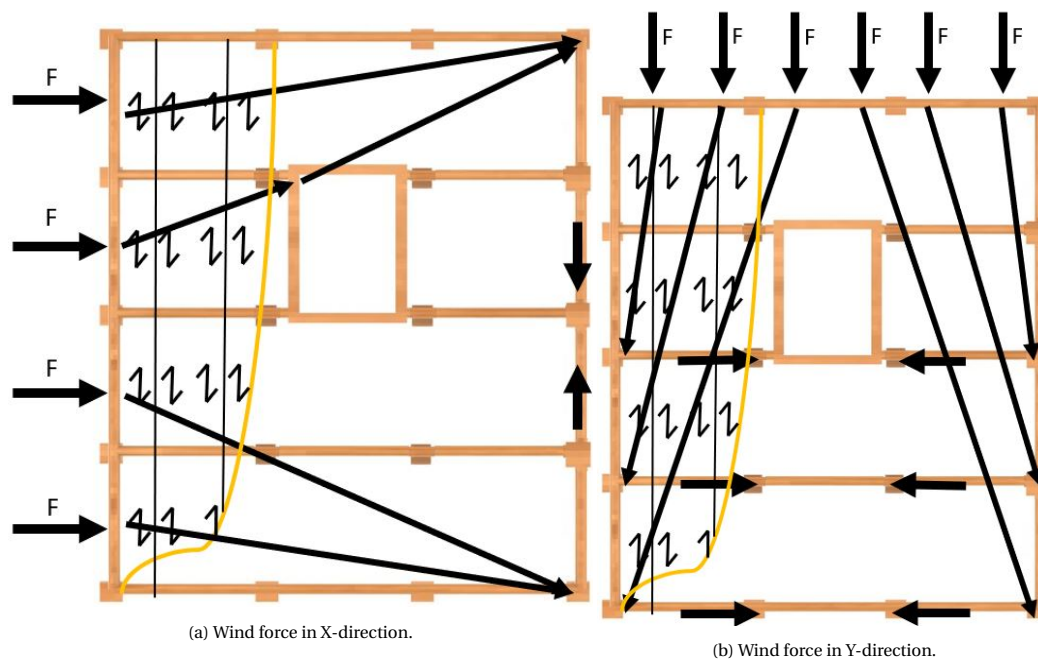


Figure 5.14

Now the floor system can be dimensioned. This consists of four steps, which are performed by creating custom nodes.

1. **Determining the wind load on the building in X and Y direction.** This is done according to NEN-EN 1991-1-4 [73]. The evenly distributed load on the façade of the building is obtained.
2. **Determining the required amount of floor plates.** Kerto-Ripa plates are produced with a 1.8 and 2.4 meter width. The grid is sized such that it can always be covered using these two plate types. For simplicity reasons, it is assumed that all floor area's can be covered using 2.4 meter wide floor plates only.

3. **Determining the force in the tension ties and the shear between floor plates.** Using the wind force in X and Y direction and the floor layout, these forces can be calculated. If the beams are able to transfer these tension forces is determined in the post optimization verification, see Section 5.10
4. **Determining the amount of required screws between floor plates.** Using the found shear forces between floor plates, the amount of required screws can be calculated. The full calculation is found in Annex B.3.2.

5.7. Stability system

Lastly, the required elements in the stability system are calculated using the Karamba3D plug-in. The Karamba3D Optimize Cross Section component is used for cross section optimization of the stability system. This component provides a rapid evaluation of optimal cross sections in the structure. This accuracy of this optimization is analysed using hand calculations. Based on this analysis it was concluded that the Optimize Cross Section component works excellent for implementation in the conceptual design phase, see Annex A.6.1.

A wind force perpendicular to the façade is assumed to give the normative design situation. Since the structure is not symmetrical in X-direction nor Y-direction, four wind directions can result in the normative design situation. For these four wind directions, the stability system is checked on both SLS and ULS, see Section 4.6.1. In the SLS calculation, the maximum horizontal deformation of $\frac{h}{825}$ is used, see Annex A.4.3. In the ULS calculation, all elements are checked on bending moment, shear force, normal force and bending. The Karamba3D plug-in requires the following input:

- **Loads** Gravitational loads and wind loads in X- and Y-direction are used. Figure 5.15 depicts the area on which the floor loads and façade loads are summed to find the gravitational loads.
- **Elements** Here, the beams, columns, and diagonals are grouped. The cross sections of the columns and diagonals are optimized. The cross sections of the beams in the stability system are set according to the beam cross sections as found in the calculations of the gravitational system.
- **Stiffness of connections** Here, the translational and rotational stiffness of the steel plate and dowels connection are used. The used calculations to obtain the translational and rotational stiffness of the steel plate and dowel connection is elaborated on in Annex A.3.1.
- **Material** Concerning the material, CLT made using C24 lamellas and glulam GL30c are used. The used properties of these materials are found in Appendix E.1.
- **Cross sections** Here, a list of available cross sections for which the stability system is optimized is given.
- **Supports** For all supports, fixed supports are assumed in the tool.

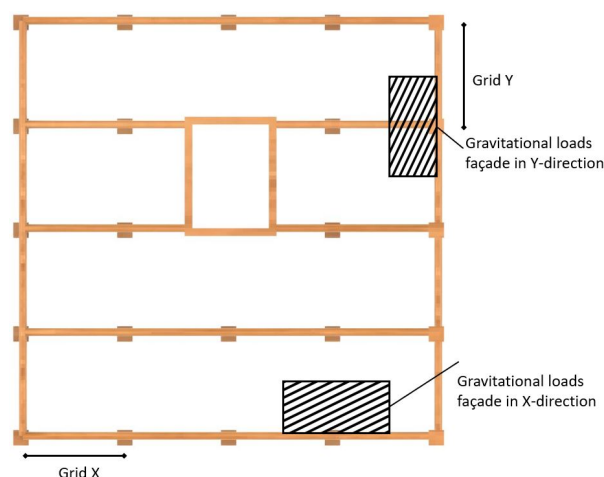


Figure 5.15: Gravitational facade loads.

Figure 5.16 shows the set-up of a model in Karamba3D including the loads, elements, stiffness of connections, material and supports. Furthermore the figure shows the obtained structure including the cross section sizes for these two load situation.

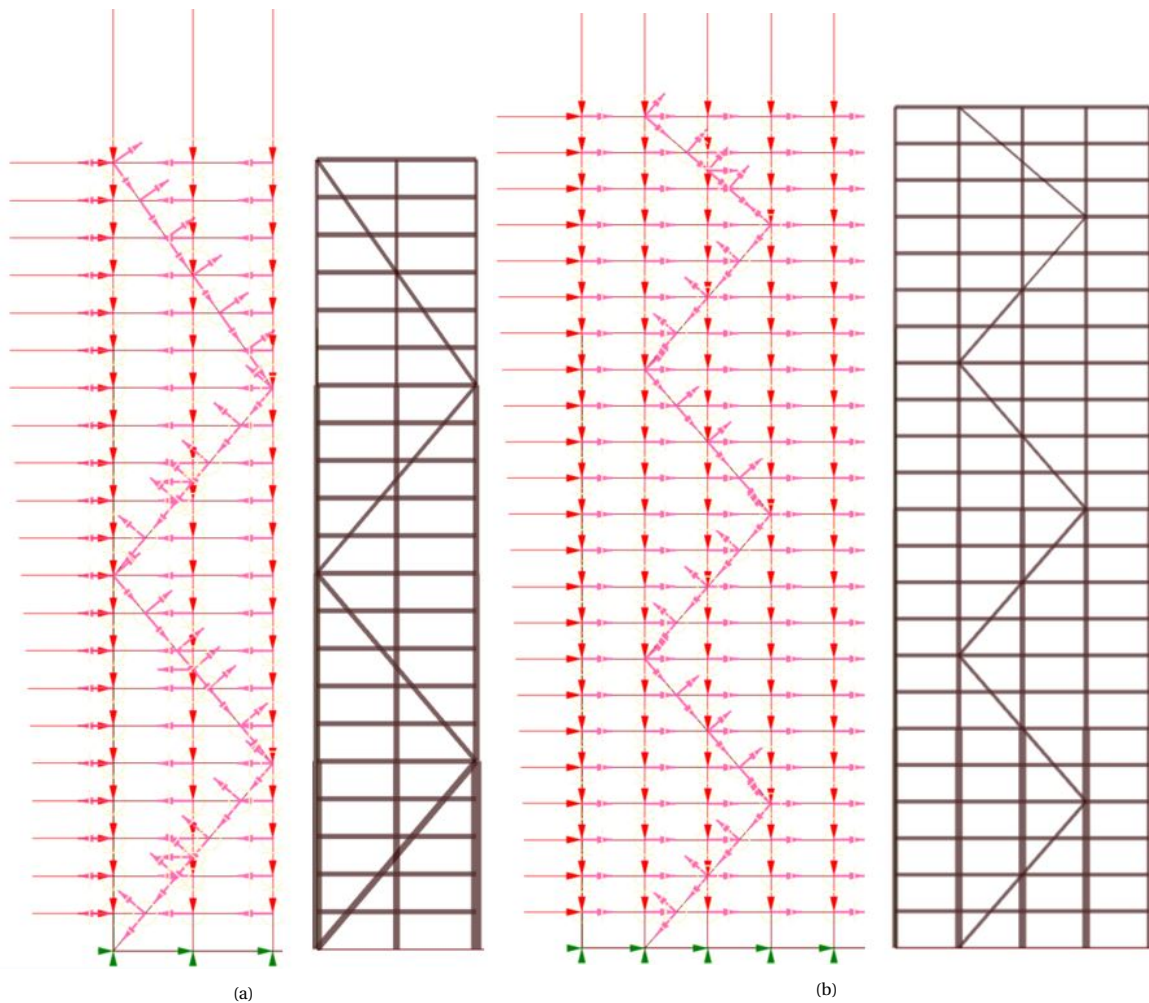


Figure 5.16: Stability system calculation

5.7.1. Grouping of members

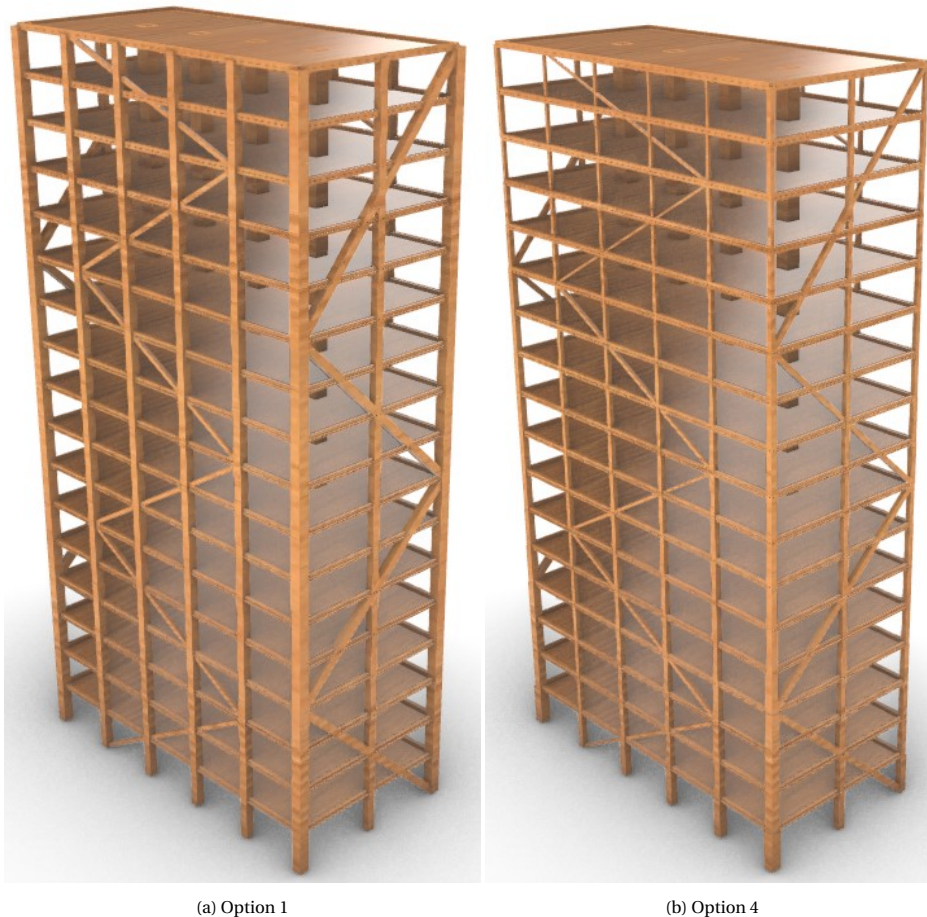
In structural design, it is preferred to use as much identical cross sections as possible since costs of elements are reduced when ordered in bulk. Furthermore, the design of connections is a repetitive process for identical cross sections which reduces costs. However, grouping of elements will result in the over-dimensioning of elements, which results in increasing costs. So, for the grouping of elements a balance between these aspects must be found. The over-dimensioning of elements must be minimized, while the advantage of having identical cross sections is still present.

The grouping of elements is done based on two observations:

1. The geometry of the structure results in large forces and moments in the corner columns (referred to as the outer columns) under wind loads. So, the outer columns are grouped and the inner columns are grouped.
2. Because of the increasing moment due to wind force and the higher gravitational loads, the columns positioned at a lower level in the building require a bigger cross section compared to columns at a higher level.

Four calculations for the grouping of members are performed using Mjøstårnet as a case study, see Figures 5.17 and 5.18. Mjøstårnet is modelled using the input as defined in Annex E.2. There are inner, and outer columns, beams and diagonals which can be grouped in four sub-groups or be analysed as a whole group. In option 1, all elements are analysed as a whole group. In option 2, the inner and outer columns are both grouped into a sub-group, while the diagonals and beams are analysed as a whole group. In option 3, the inner and outer columns and the diagonals are grouped into a sub-group and the beams are analysed as a whole

group. In option 4, all elements are optimized individually. According to Figure 5.18, the amount of required timber is more than halved for option 4, compared to option 1. Meanwhile, the total amount of different glulam cross sections more than doubles, from seven to sixteen different cross sections. An optimal balance for grouping of elements is found between these two extremes. Option 3, the inner and outer columns and the diagonals are grouped into a sub-group results a reduction of 59% of total volume of timber required compared to option 1. Furthermore, it requires 11 different glulam cross sections. It is concluded that option 3 is the most favourable approach for grouping of elements and will be used in the developed tool.



(a) Option 1

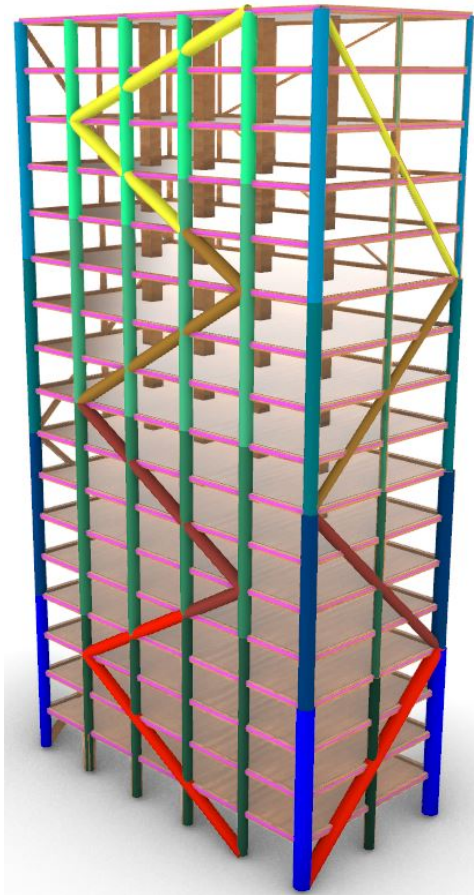
(b) Option 4

Figure 5.17: Two analysed options for grouping of elements.

Implementation timber types				
	Option 1	Option 2	Option 3	Option 4
Amount of groups	4	10	13	All
Columns grouped		X	X	All individual
Diagonals grouped			X	All individual
Volume of diagonals and inner columns in facades in X-direction [m3]	206.9	183.0	144.3	125.4
Volume of diagonals and inner columns in facades in Y-direction [m3]	540.8	340.4	316.9	242.4
Volume of corner columns in facade in X-direction [m3]	234.1	115.6	121.6	107.0
Total volume [m3]	981.8	639.0	582.9	474.8
Percentage compared to 4 Groups of elements	100	65	59	48
Amount of different glulam elements	7	10	11	16

Figure 5.18: Effect of grouping of members on total volume of timber based on Mjøstårnet geometry.

Figure 5.19 shows the result for this approach to the grouping of members. The cross section of the beams are dimensioned according to the beam cross sections as found in the calculations of the gravitational system.



(a) Visualization of element groups.

Element group	Color
ColumnsOut1	Dark Blue
ColumnsOut2	Blue
ColumnsOut3	Teal
ColumnsOut4	Light Blue
ColumnsIn5	Dark Green
ColumnsIn6	Green
ColumnsIn7	Light Green
ColumnsIn8	Lightest Green
Diagonals9	Yellow
Diagonals10	Orange
Diagonals11	Red-Orange
Diagonals12	Red
Beams	Pink

(b) Element groups and color indicator

Figure 5.19: Visualization of grouping of elements

5.8. Economical performance

For the determination of the economical performance, the MAMO (Materiaal, Arbied, Materieel, Onderaanneming) rules for budgeting were recommended by Frehe, a cost expert at Arcadis, during an interview in 2021 [53]. According to these rules, the direct and indirect costs can be divided into four groups:

1. Materials
2. Labor
3. Equipment
4. Subcontracting

In this design problem, there are no subcontracting costs. Following these rules, the economical performance of the timber elements and connections is determined separately and subsequently summed to find the total economical performance of the building design. All cost estimations have been discussed with Frehe during unstructured interviews [53].

Timber elements

- **Materials** For all timber elements, the dimensions are known. Based on these dimensions, the costs of the materials are estimated. Based on an interview with Heko Spanten, CLT elements are estimated to cost 1000 €/m³ including connections [141]. The costs for various glulam elements are based on an interview conducted with de Groot Vroomshop and are mentioned in Annex C.2.1 [160]. The assumed costs for Kerto-Ripa floor plates with different thicknesses are determined using an Arcadis datasheet that provides the production costs. These calculations are given in Annex C.2.1.
- **Labor** The labor required for the installation of an element differs. Floor panels require five labor hours, CLT panels require four labor hours, and columns and beams require two labor hours for installation. An hourly wage of €44 is assumed, as mentioned by the "Bouwen met Staal" organization [116]. The glulam elements must be prepared for connection. Sawing is required for installation of the steel plates.
- **Equipment** Every element is assumed to require 15 minute of crane usage. A crane with a capacity of 30 tons is estimated to cost €200 per hour. For the floor elements, concrete pumps are required for the structural screed.

Connections

- **Material** To determine the material costs, the total amount of required steel in the steel plate and dowel connections is multiplied by the steel price. These material costs are multiplied by 2.5 to account for the costs for glue, fire strips, and preparation of the steel (cutting, drilling). For the Knapp connectors, the prices specified on the Knapp website are used, see Annex B.2. [5]. For the screws, a price of 10 cents per screw is assumed. Installation of a Knapp connector is assumed to require 1 labor hour.
- **Labor** The indirect costs are determined by estimating the required time for manufacturing and installation of the connection. Then, this time is multiplied with the estimated hourly wage. The preparation of the steel plates requires one labor hour. Furthermore, the installation of the steel plates, requires another labor hour per connection. Per dowel, 108 seconds are required for installation. This is according to the estimates by Johnsson (2001) [89]. The installation of a screw is estimated to require 36 seconds [89]. Lastly, the installation of a Knapp connector is estimated to require one hour. Again, an hourly wage of €44 is assumed [116].
- **Equipment** Using the Knapp connectors, a connection is made by sliding both parts of the connection into each other. This comes with the benefit that the connectors can be installed in the factory. So no hoisting is required. Also for the screwed connections in the columns and floor elements, no hoisting is required. For the steel plates and dowel connections, a cherry picker is required for installation, see Figure A.12b

Annex C.2.2 provides an example of the budgeting as performed in the tool following the MAMO rules. A worked-out calculation for Mjöstårnet is shown in Figure 5.24.

5.9. Environmental performance

Figure 5.20 shows the determination of the environmental performance. The database containing all required timber elements and connections is the input of this calculation. The environmental performance of the timber elements and connections is determined separately and subsequently summed in order to obtain the total environmental performance. As is explained in Section 4.5.3, which provided Equation 8.1 for calculation of the environmental performance.

$$\text{Environmental Performance} = \sum_{i=1}^n \text{Quantity of building element} \cdot \text{EPD data of building element} \cdot \text{MKI} \quad (5.3)$$

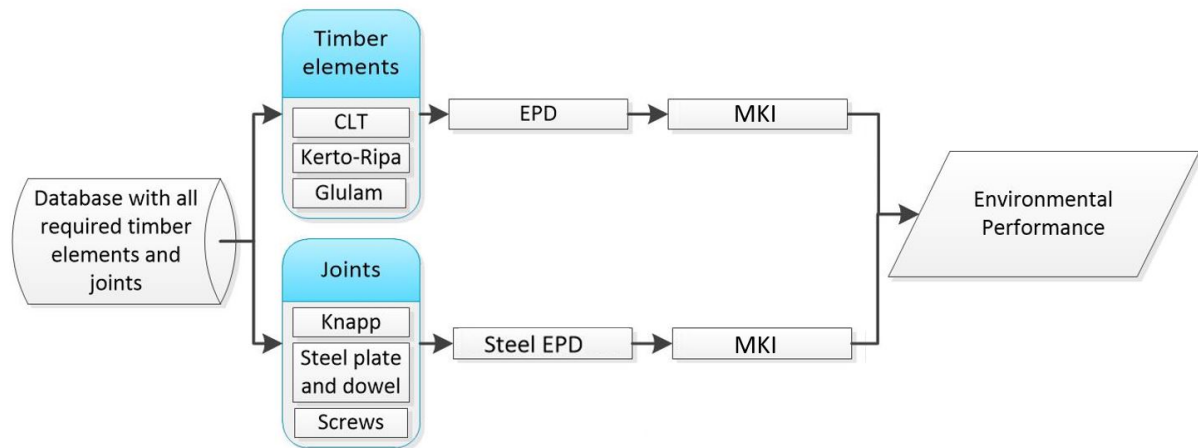


Figure 5.20: Determination of environmental performance.

Timber elements A database is created containing the Environmental Product Declarations (EPD) of all timber elements. These EPD's contain the impact of the product regarding eleven impact categories. Next, these impact categories are multiplied with the Environmental Costs Indicators (MKI). The sum of the found result is the total shadow cost of the building. Which is the environmental performance of the building.

Connections To determine the environmental impact of the connections, the amount of steel in the connection is determined. For this steel, the environmental impact regarding the eleven impact categories is found. The found environmental impact is multiplied with a factor to account for the fire strips or glue depending on the considered connection.

Carbon sequestration An interesting point for discussion is the assessment of the carbon sequestration in the determination of the environmental impact. Three different assessment methods for the consideration of carbon sequestration on the environmental performance are evaluated in this research, these methods are elaborated on in Section 4.5.3.

5.10. Post optimization verification

After calculation, each building design is verified based on four verification criteria.

- **Acceleration limits** The acceleration limits check is performed according to Section A.4.2.
- **Tension forces in beams** The beams work as tension ties in the transfer of wind forces to the stability system in the façade. The unity check is calculated for these tension forces in the beams.
- **Assumption of wind friction neglect.** As mentioned in Section A.4.1, the wind friction can be neglected if the total area of all surfaces parallel to the wind force direction is smaller than four times the total area of all surfaces perpendicular to the wind force direction. This gives the following Equation, see Figure 5.21.

$$d \leq \frac{400b}{100 + b} \quad (5.4)$$

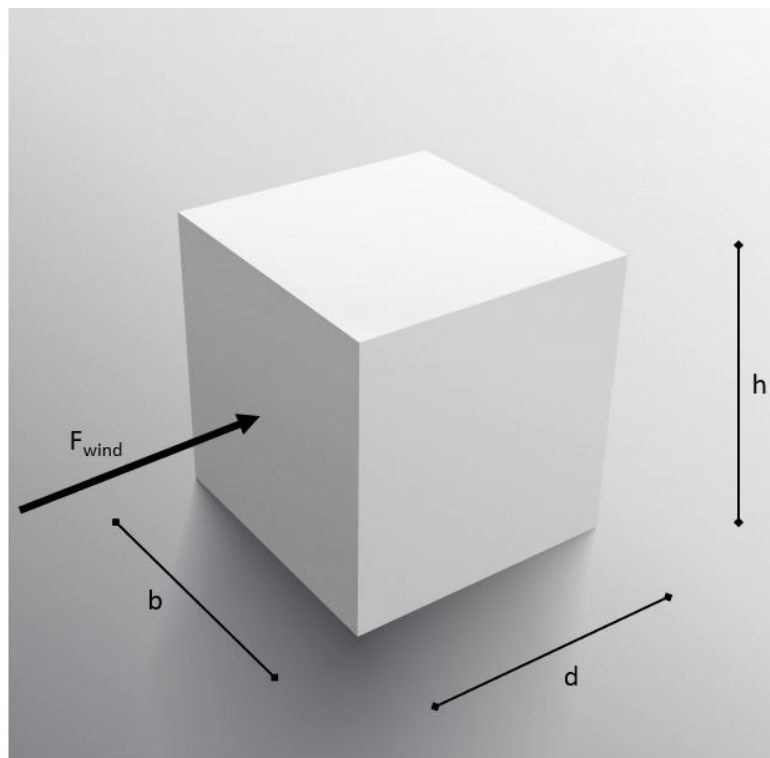


Figure 5.21: Wind Friction.

- **Steel plate and dowel connection strength** In both X- and Y-direction, only one universal steel plate and dowel connection is created, see the first bullet point in Section 5.1.2. This verification determines if the percentage of steel plate and dowel connections which fail on strength is smaller than the maximum percentage of failure of steel plate and dowel connection.

5.11. Multidisciplinary Design Optimization

The Octopus plug-in is used to perform the multi-objective optimization. This plug-in is able to perform an optimization for multiple objective functions, producing trade-off solutions between the extremes of these objectives. The user interface is based on Galapagos, creating a user-friendly plug-in.

The Octopus plug-in requires genes and objectives. These genes are the input parameters for which the model is optimized, see Section 5.3. The objectives contain the optimization objectives, see Section 5.8 and 5.9.

Furthermore, Octopus provides the possibility for hard constraints by choosing a boolean value as one of the objectives. This provides the possibility to exclude all models which do not fulfil the verification checks as mentioned in Section 5.10.

The multi-objective genetic algorithm in the Octopus tool is a mix of two algorithms SPEA-2 and HypE from ETH Zürich [158]. SPEA-2 was proposed by Zitzler et al in 2001. It is the successor of SPEA (Strength Pareto Evolutionary Algorithm). SPEA applies the elitism principles. It guarantees a handful of most fit individuals to be placed in the next generation. SPEA follows five steps in each cycle [171]:

1. **Update operation** In this step, All non-dominated individuals are copied to an archive while all dominated members of the population are removed from this archive.
2. **Deleting elements from archive** Optionally, when the size of the archive surpasses a set limit, a clustering technique is performed to delete individuals which do not contain characteristics of the non-dominated front.
3. **Assigning fitness values** Next, fitness values are assigned to the population members and the archive in the following manner:
 - For each individual in the archive the strength value is determined. This strength value or fitness depends on the number of population members which are dominated by the considered individual.
 - A fitness value is determined for each individual in the population by summing all strength values of the archive members which dominate the considered individual, adding one to the end.
4. **Mating selection phase** Using binary tournaments, individuals from the population and archive are selected. Individuals from the archive have a greater chance to be selected than individuals from the population. The selected individuals produce an offspring population.
5. **Replacement of population** in this step, the offspring population replaces the old population.

Since SPEA shows several weaknesses, an improved version was made: SPEA-2.

HypE is a hypervolume estimation algorithm which was created by Bader and Zitzler in 2008. This algorithm is able to measure the set quality of a Pareto set approximation. Compared to other Multi-Objective Genetic Algorithms, the HypE is considered highly effective for multi-objective problems [18].

5.12. Tool verification

The tool is verified by analysing the comparison between Mjøstårnet and a modelled version of this building which was created using the developed tool. For this modelled version, the input is chosen similarly to the actual building. This used input is summed in Annex E.2. The structural system of the actual building and of the modelled building are shown in Figure 5.22, which show a clear resemblance.



Figure 5.22: Mjøstårnet

There are three main differences between the modelled building and the actual building.

- **Different positioning of the core** Since the core does not provide lateral stability, this is assumed to only create a significant difference in daylight entrance of the building.
- **Mjøstårnet contains seven concrete floors and an architectural top.** In Mjøstårnet, floors 12 to 18 are constructed using 300 mm thick concrete, cast in place. To account for the concrete floors, an additional load is added to the gravitational loads. According to the model, the selfweight of the Kerto-Ripa floor is 2.28 kN/m^2 . The selfweight for a 300 mm thick concrete floor is $23.5 \text{ kN/m}^3 \cdot 0.3 \text{ m} = 7.05 \text{ kN/m}^2$. So, an extra dead load of $7.05 - 2.28 = 4.77 \text{ kN/m}^2$ is acting on floors 12 to 18. So, an additional load of $4.77 \cdot 7 \cdot 18 \cdot 36 = 21636 \text{ kN}$ is added in the calculations.
- **The architectural top is not modelled.** So, the wind force calculation is based on a 72 meter tall building. To account for the weight of the architectural top, it is assumed it consists of roughly 250 m of 300x300 glulam elements. The mean selfweight of a glulam element is $480 \text{ kg/m}^3 = 4.7 \text{ kN/m}^3$. So, the total selfweight of the architectural top is $4.7 \text{ kN/m}^3 \cdot 250 \cdot 0.3 \cdot 0.3 = 105.75 \text{ kN}$.

So, the addition of a load of $21636 + 105.75 = 21742$ kN on the building accounts for these differences in loads. Using this modelled building, a verification is performed. This verification consists of three parts. The structural, economical, and environmental verification.

5.12.1. Structural

For the structural verifications, several comparisons are made. Figure 5.23 shows eleven properties for which the results obtained using the model created in the tool are compared with the found values for Mjøstårnet. These found values consist of the values mentioned for Mjøstårnet by Abrahamsen (2017), Madsen (2019), and Tupenaite (2019) [8], [97], [145]. The accuracy is expressed in a percentage in which the obtained results and given values differ. For the cross section dimensions, the total area of the cross section is used to calculate the difference.

Structural comparison model and Mjøstårnet				
Property	Mjøstårnet	model	Normative load combination	Difference [%]
Maximum tension force [kN]	5500	5463	ULS1	1
Maximum compression force [kN]	11.500	12.152	ULS3	5
Beam dimensions under timber floor	395x585	383x574	ULS2, ULS6fire, SLS2	5
Column dimensions	625x630	658x658	ULS4, ULS7fire	9
Corner column dimensions	625x1485	750x1100	ULS3, SLS1	13
Facade column dimensions	728x810	850x850	ULS3, SLS1	18
Diagonal dimensions	625x900	750x750	ULS3, SLS1	0
Amount of steel [kg]	106916	102031	-	2
Amount of glulam [m^3]	1329	1358	-	2
Amount of CLT [m^2]	5069	4604	-	10
Amount of total timber [m^3/m^2]	0.250	0.261	-	4

Figure 5.23: Structural comparison model and Mjøstårnet

Furthermore, two other verifications are performed:

- Acceleration check: with the damping coefficient of 0.019 as reported by Abrahamsen (2017), the building satisfies the acceleration limits for an office building [8].
- 33.3 % of steel plate and dowel connections fail on compression. The tool only creates one average steel plate and dowel connection in X- and Y-direction, see the first bullet point in Section 5.1.2. Thus, it is expected that a certain percentage of connections will be overdimensioned and underdimensioned. An underdimensioning of 33% of all connections, and thus an overdimensioning of 67 % of all connections is a reasonable result.

Based on these verifications and the accuracy as found in Figure 5.23, it can be concluded that the model simulates the actual building as accurately as required in the conceptual design phase.

5.12.2. Economical

Tupenaite (2019) reported a total costs of Mjøstårnet of $4087 \text{ €}/m^2$. The Gross Floor Area (GFA) of Mjøstårnet is $37 \cdot 17 \cdot 18 = 11322 \text{ m}^2$. So, the total investment cost of Mjøstårnet is $€46.3$ million [145]. Figure 4.27 shows 58% of the investment costs consist of construction costs. Furthermore, Van Oss (2007) reports the structural system averagely amounts to 15.6% of the total construction costs in 74 meter high concrete and steel high-rise [154]. This percentage is used for estimation of the costs for timber high-rise. So, the construction costs for the timber structural system are expected to be roughly $€46.3 \text{ million} \cdot 58\% \cdot 15.6\% = €4.19 \text{ million}$. Lastly, timber is reported to costs 5-10% more than concrete. So, the construction costs for the timber structural system for Mjøstårnet are expected to be between $€4.4$ and $€4.61$ million.

MAMO Calculation Mjøstårnet		Item	Quantity	Unit	Material	Labor	Equipment	Subcontracting	Unit Costs	Subtotal			
						Hour	Hour	Material	Hour	Material			
						Hourly wage	Hour	Subcontracting					
Connections	Steel plate and dowel connection	Steel price per connection	389,8	kg per connection		2,5				€ 974,50			
		Fire strips and glue			10					€ 10,00			
		Steel preparation (sawing, cutting, drilling of steel)				1	44			€ 44,00			
		Installation of steel plates				1	44			€ 44,00			
		Installation of steel dowels	350	Amount of dowels per connection		0,03	44			€ 462,00			
		Cherry picker (hoogwerker)						1	100	€ 100,00			
		TOTAL								€ 1.594,50	€ 315,459		
		Screw price				0,1				€ 0,10	€ 0,44		
		Installation of screws					0,01	44		€ 0,34	€ 5,509		
		TOTAL								€ 296,30			
Floor	Knapp	Price per Knapp connector	10201	Amount of screws					€ 0,54	€ 5,509			
		Installation of Knapp connector				1	44		€ 44,00				
		TOTAL							€ 340,30	€ 159,941			
		Price per floor element	470	Amount of Knapp connectors						€ 1,877,45			
		Installation of floor element				5	44			€ 220,00			
		Finishing layer (50mm of concrete)	17,28	m ² per floor element		0,15				€ 12,96			
		Concrete pump	17,28	m ² per floor element			1	0,3		€ 5,18			
		Crane 30 tons						0,25	200	€ 50,00			
		Plate clamp						0,002	112,5	€ 0,23			
		TOTAL								€ 2.168,82	€ 1.380,710		
Building elements	CLT	CLT price per m ³ (including connections)	1,3	m ³ per CLT element					€ 1.300,00				
		Gypsum boards	10	m ² per CLT element		20			€ 200,00				
		Installation of CLT element				4	44		€ 176,00				
		Crane 30 tons						0,25	200	€ 50,00			
		TOTAL							€ 1.726,00	€ 793,960			
		Glulam	Glulam	460	Amount of CLT elements								
				Glulam price per element								€ 2.268,25	
				Preparation for connection (cutting)				1,5	44			€ 66,00	
				Installation of glulam element				2	44			€ 88,00	
				Crane 30 tons						0,25	200	€ 50,00	
TOTAL										€ 2.472,25	€ 1.878,910		
760 Amount of glulam elements													
TOTAL									€ 4.534,488				
m ² GFO									€ 11,016				
€/m ² GFO									€ 412				

Figure 5.24: MAMO calculation of Mjøstårnet model.

According to the MAMO calculation, the total construction costs of the structural system in Mjøstårnet is €4.53 million, see Figure 5.24. This result is in line with expectations, as the construction costs of the timber structural system is estimated to cost between €4.4 and €4.6 million. Furthermore, the construction costs of the structural system amount to $\frac{€4.53\text{million}}{€46.3\text{million}} = 9.8\%$ of the total investment costs.

5.12.3. Environmental

Madsen et al. (2019) performed an LCA analysis regarding the environmental impact of Mjøstårnet citemadsen2019miljovurdering. Figure 5.25 shows three properties for which the results obtained using the model created in the tool are compared with the found values by Madsen et al. for Mjøstårnet. The accuracy is expressed in a percentage in which the obtained results and given values differ.

Environmental comparison model and Mjøstårnet			
Property	Mjøstårnet	model	Difference [%]
tonnes of CO_2 emissions excluding carbon sequestration	3393.8	3412.5	0
GWP including carbon sequestration [10^{-6} kg CO_2 eq]	-1.83	-1.476	24
ODP [kg CFK-11 eq]	0.0333	0.02582	29

Figure 5.25: Environmental comparison model and Mjøstårnet

*GWP and ODP both are environmental costs indicators (MKI's) GWP considers the Global Warming Potential. ODP concerns the Stratospheric Ozone Depletion Potential.

Since an LCA analysis and chosen EPD values are based on a lot of assumptions, a deviation in results is anticipated. Thus, the comparison above shows that the order size of the performance calculation is within reasonable boundaries.

6

Case Studies

In this chapter, the tool is analysed and tested through two case-studies. This will provide insight in both the tool and timber high-rise. Both case-studies are concrete buildings, for which the tool aims to find competitive timber alternatives, considering the construction costs and shadow costs. First, the case studies are introduced and the methodology for finding competitive timber building designs is elaborated, in Section 6.1. To gain more insight, the genetic algorithm, the stability system and the timber high-rise is analysed in Sections 6.2, 6.3 and 6.4 respectively. These analysis are done to gain more insights regarding improvements of the performance of timber buildings. Finally, using all data gathered in this analysis, in Section 6.5 a thorough analysis is done where for both concrete case-studies, timber building design alternatives are created.

6.1. Introduction

6.1.1. Case studies

The case-studies are based on a current Arcadis project where several high-rise office buildings are created above and next to the Amsterdam Sloterdijk train tracks, see Figure 6.1. A concrete core is used as the stability system. One of these buildings is 28.8 meters long and wide and 60 meters high. This high-rise building is referred in this research as "The Square", referring to its square floor plan.

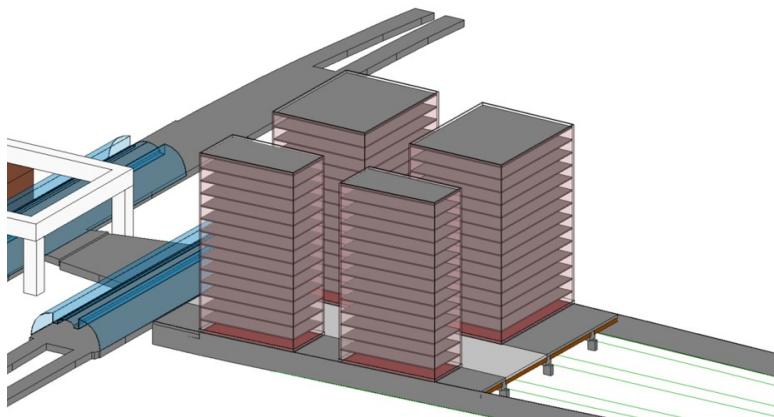


Figure 6.1: Visualisation of the high-rise buildings above the traintracks [Courtesy of Arcadis].

The second design situation which is analysed is based on the high-rise building referred to as "The Rectangle". This building has a length of 43.2 meter, a width of 21.6 meters and a height of 50 meters. The design is based on the design of "The Square". With the knowledge of Tom Borst, a senior structural engineer working at Arcadis, a realistic building design was created. For both buildings, the construction costs are based on the calculation as performed by cost-experts from Arcadis. The shadow costs are calculated using MPG calc 1.2 [3]. The construction cost calculations are expanded on in Annex D.1. The shadow costs calculations are elaborated on in Annex D.2.

Figure 6.2 provides additional information regarding the concrete buildings.

Properties of The Square and The Rectangle* **		
Property	The Square	The Rectangle
Dimensions	28.8x28.8x60	21.6x43.2x50
Gross floor area [m^2]	12442	12131
Nett floor area [m^2]	10575	10311
Construction costs including foundation [million €]	4.05	3.92
Construction costs excluding foundation [million €]	3.47	3.28
Construction costs excluding foundation per GFA [€/ m^2]	278.9	270.4
Shadow costs including foundation [€]	143.654	139.837
Shadow costs excluding foundation [€]	120.123	114.693
Shadow costs excluding foundation per GFA [€/ m^2]	9.7	9.5

Figure 6.2: Properties of concrete case studies.

*The ground floor is considered as part of the foundation in both the calculation of the concrete and timber buildings. **The construction and shadow costs only concern the structural system.

The construction of a timber building might be extra beneficial in this design situation because of the low self-weight. When building above traintracks, as presented by this case-study, the foundation becomes expensive, since loads have to be transferred to the foundation which can not be positioned below the buildings where the traintracks are situated. Therefore, a lighter building has a big impact on decreasing of construction costs for the foundation. However, a critical note must be made regarding the vibration caused by the trains as this can provide issues regarding the acceleration of a timber building. Therefore, it is chosen to focus on the buildings which are not positioned above the traintracks.

Timber building designs

The developed tool generates timber building designs based on the concrete case study buildings. In this research, Building A3 represents 'The Square' and Building B3 represents "The Rectangle". The dimension of the floor plan and the amount of floors is set for the building designs. One of the parameters for which the timber building design is optimized concerns the grid size in X- and Y-direction.

In the 25King reference project, a 6 by 8 meter grid was implemented [85]. Metsa Wood mentioned in 2012 that a clear span of up to 9 meters is feasible using Kerto-Ripa floor panels [107]. To get the most information out of the tool, a wide range of possible grid sizes is set, ranging from 4.32 meters to 9.6 meters, see Figure 6.27.

Possible case study grid sizes							
Building A3 [28.8x28.8]				Building B3 [43.2x21.6]			
Grid X[m]	NColumnsX	Grid Y[m]	NColumnsY	Grid X[m]	NColumnsX	Grid Y[m]	NColumnsY
4.8	7	4.8	7	4.32	11	4.32	6
5.76	6	5.76	6	4.8	10	5.4	5
7.2	5	7.2	5	5.4	9	7.2	4
9.6	4	9.6	4	7.2	7	X	X
X	X	X	X	8.64	6	X	X

Figure 6.3: Grid sizes Building A3 and B3.

Additionally, the timber building designs are created and optimized based on the materials, connections, stability system, floor elements, structural and architectural restrictions as discussed in Chapter 4.

Input parameters which are used in the tool and influence the timber design are summed in Annex E.1.

6.1.2. Tool guideline

The developed tool generates timber building designs and use a genetic algorithm to obtain the most competitive timber building design compared to the concrete case study buildings. A more exact description of this process can be described in five steps:

1. The design situation dependent parameters in the tool are set such that they match the considered design situation. These parameters can be split in a fixed and an adaptable part. The fixed part is the direct translation of the design situation. The adaptable part is the interpretation of the design situation by the operator. For the two case studies, The design situation dependent parameters used for the two case studies are depicted in Figure 6.4b.

Fixed design situation dependent parameters	
Parameter	Unity
Building dimension in X-direction [m]	X
Building dimension in Y-direction [m]	X
Minimum required floor area [m^2]	12000
Floor-to-ceiling height [m]	3
Terrain category	3
Wind zone	1
Additional floor height [m]	0.4
Additional floor mass [kg/m^2]	160
Imposed floor load [kN/m^2]	3
Dead load facade [kN/m^2]	2

(a) Fixed design situation dependent parameters

Adaptable design situation dependent parameters	
Parameter	Unity
Maximum unity check	1.0
Maximum percentage of failure of steel plate and dowel connection [%]	0.333
Floor type	Box floor
Core size ratio [%]	0.15

(b) Adaptable design situation dependent parameters

Figure 6.4: Design situation dependent parameters

2. The possible grid sizes are defined in the Grasshopper script.
3. The input values regarding the genetic algorithm in the Octopus plugin are defined.
4. The optimization is run in Octopus.
5. When the optimization is completed, the Pareto front is obtained. Using this Pareto front, and the data from the concrete building, it can be decided whether a timber building can be a competitive alternative. Based on this result, it is determined if a timber building alternative is considered in the following design stages.

6.1.3. Methodology

The methodology of this research can be divided into four steps, where steps 1 to 3 gather information and step 4 implements this information in an optimization for the case studies. This last step provides results which answer the main research question.

1. In Section 6.2 the genetic algorithm is analysed. Here, the effect of input values in the genetic algorithm on the computational time and on the accuracy of the results is analysed.
2. The stability system and the effect of its input is analysed in Section 6.3.
3. The timber buildings are analysed in Section 6.4. This is done by optimizing several timber building designs with a different amount of floors and thus a different building height. Next, the effect of several set building heights on the timber buildings is studied. This effect is analysed by considering unity checks, comparing to reference projects, comparing to the two concrete case-studies and by checking the effects of the individual building elements.
4. Using all data gathered in this analysis, in Section 6.5 a thorough analysis is done comparing the concrete case study buildings and the timber alternatives.

This full methodology is depicted in Figure 6.5.

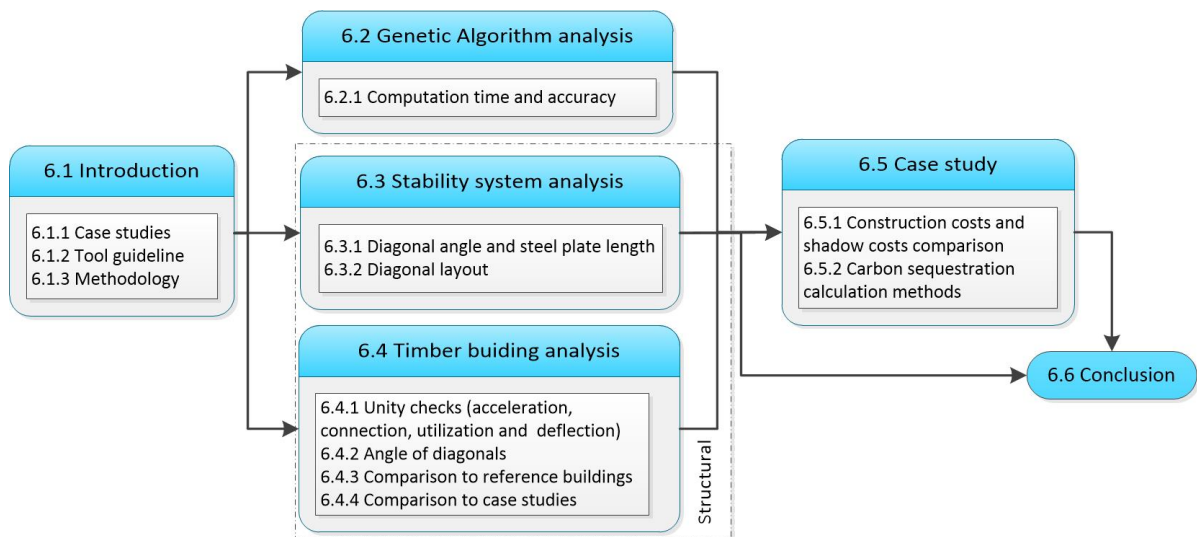


Figure 6.5: Methodology

In the last step of the methodology, the optimization as defined in the tool guideline, see Section 6.1.2, is performed for both case studies using three carbon sequestration calculation methods.

6.2. Genetic Algorithm analysis

6.2.1. Computational time and accuracy

Input parameters The Octopus plug-in is used to perform the multi-objective optimization. The mechanism of this tool is explained in Section 5.11. Several input values can be altered in the Multi-Objective Genetic Algorithm in the Octopus plugin. In this research, only the population and generation size are evaluated. The other input values are set as defined below in all optimizations in the research:

- Elitism: 0.5
- Mutation probability: 0.4
- Mutation rate: 0.9
- Crossover rate: 0.8
- Reduction: SPEA-2
- Mutation: HypE

When using a multi-objective genetic algorithm, there is a choice regarding the trade-off between computational time and accuracy of the results. A longer computational time implies more results are analysed, thus increasing the accuracy of the obtained results. This accuracy can be measured by defining the amount of results which are Pareto optimal. In this research, this trade-off between computational time and accuracy of the results is analysed by evaluating the population and generation size. This is regarded as a suitable assessment method since the amount of evaluated verified building equals the population size times the generation size.

The theoretical design space can be found by multiplying the number of possible input values per parameter. For building A3, the theoretical design space is:

$$4 \cdot 4 \cdot 3 \cdot 3 \cdot 2 \cdot 2 \cdot 5 \cdot 5 = 14400 \text{ building designs} \quad (6.1)$$

For building B3, the theoretical design space is:

$$5 \cdot 3 \cdot 3 \cdot 3 \cdot 2 \cdot 2 \cdot 5 \cdot 5 = 13500 \text{ building designs} \quad (6.2)$$

However, this number includes all building designs, the actual design space is considerably smaller depending on the design situation since buildings may not pass the verification requirements.

Analysis Building B3, with carbon sequestration calculation method 3, is used to determine the effect of population and generation size. This design situation is chosen since it results in a multitude of Pareto optimal points. An average evaluation time of 1.22 seconds per timber building design is found for the analysed design situation using a computer with a 2.4 GHz processor.

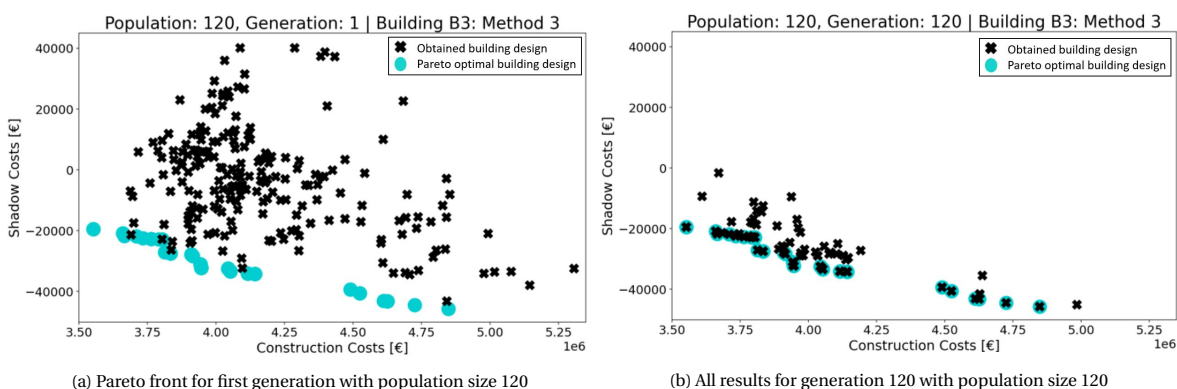


Figure 6.6

First, the Pareto front is obtained by evaluating all 14400 buildings. This requires a population and generation size of 120, see Figure 6.6b. Figure 6.6a shows the results of the 1st generation. From the first 120 random

generated individuals, one result which is Pareto optimal is found, so it is clear that the genetic algorithm moves closer to the Pareto front every generation.

In theory, the Pareto front contains an infinite amount of Pareto optimal points. However, due to the discrete and finite amount of input parameters in this tool, a finite amount of Pareto optimal points is found. It is assumed that Figure 6.6b shows all Pareto optimal building designs. So, for Building B3 and carbon sequestration calculation method 3, there are 24 Pareto optimal points. Based on this assumption, the accuracy of evaluations with smaller population and generation sizes can be evaluated. On average, every 1.22 seconds, a building design which meets the verification requirements is evaluated for this design situation.

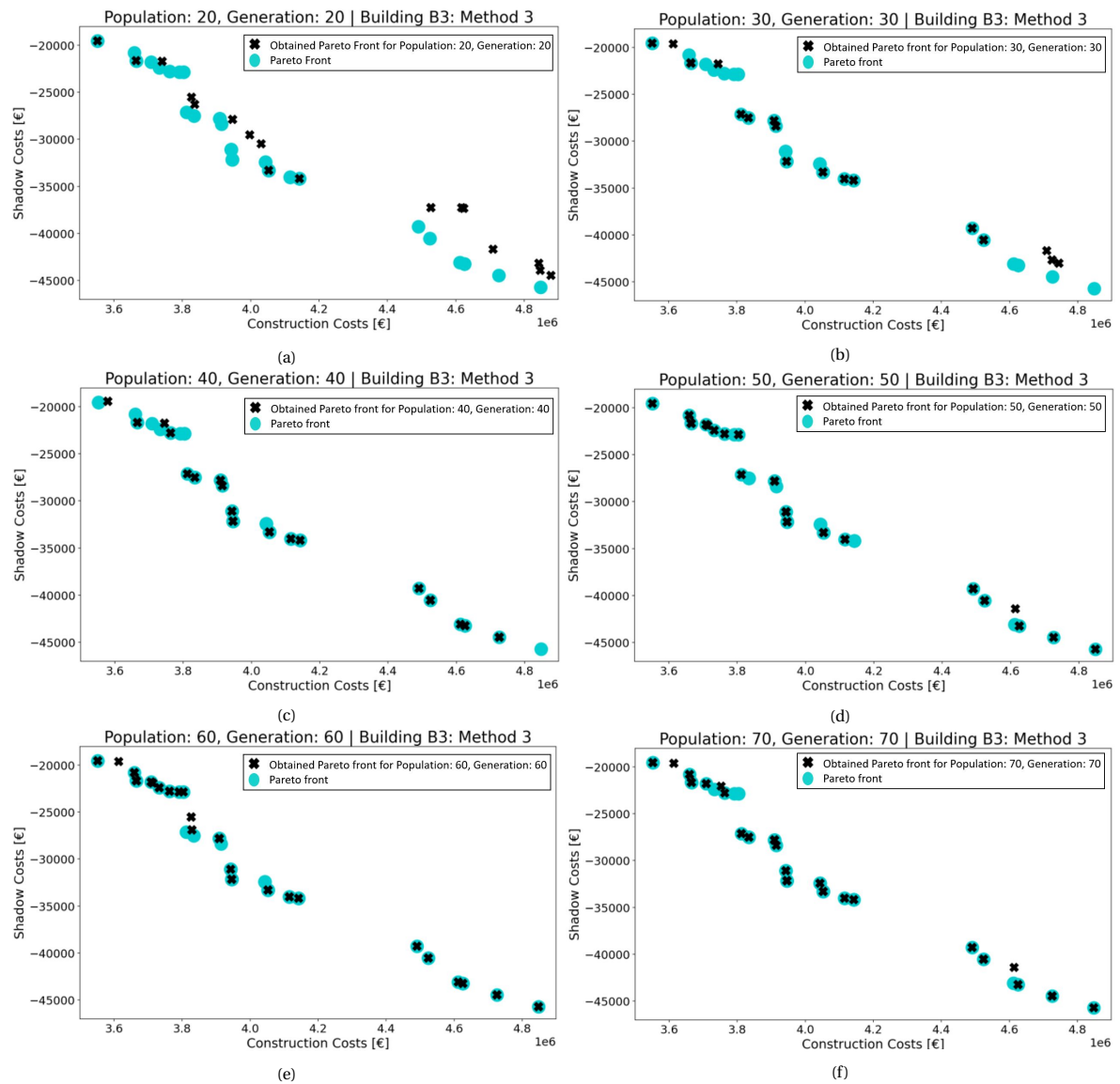


Figure 6.7: Found Pareto front for various generation and population sizes.

Figure 6.7 visualizes the obtained Pareto fronts for varying population and generation sizes. For every analysed population and generation size, the computational time is obtained, and the amount of Pareto optimal building designs is calculated. These results are summarized in Figure 6.8.

Accuracy vs. computational time						
	G20P20	G30P30	G40P40	G50P50	G60P60	G70P70
Generation size	20	30	40	50	60	70
Population size	20	30	40	50	60	70
Minimum evaluated building designs	400	900	1600	2500	3600	4900
computational time [minutes]	8	18	32	50	72	98
Amount of Pareto optimal building designs found	4	12	16	18	20	20
Percentage of Pareto optimal building designs [%]	16.7	50	66.7	75	83.3	83.3

Figure 6.8: Accuracy vs. computational time

To gain more insight in trade-off between computational time and accuracy of the results, the found results are plotted in Figure 6.9. This figure shows a clear relation between computational time and accuracy of the results. The genetic algorithm tends to find Pareto optimal building designs faster at the start of the optimization than when the optimization has been running for some time.

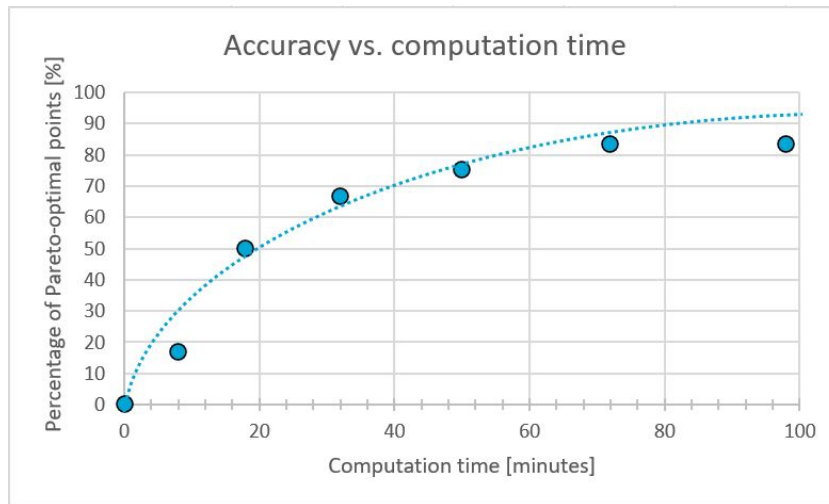


Figure 6.9: Relation between accuracy and computational time

Conclusion Based on Figure 6.9 it can be concluded that there is a clear relation between computational time and accuracy of the results. The Multi-Objective Genetic Algorithm is able to quickly identify Pareto optimal building designs. When only 6.25% of all possible building designs have been analysed, half of the Pareto optimal building designs are found. Two critical notes must be made based on this analysis.

- The Octopus plug-in is based on the assumption of continuous input, not discrete input. Thus another plug-in might provide accurate results more rapidly.
- The amount of possible building designs in a design situation depends on the verification criteria. Thus, the design situation can have a big effect on the computational time, since more time is required to obtain verified building designs.

It is found that for a generation and population size of 80, roughly 95% of the Pareto optimal points are obtained. This generation and population size is used in the performed optimization in Section 6.5 where timber building designs are created based on the two case studies.

6.3. Stability system analysis

The goal of this chapter is to gain insight in the timber stability system through the exploration of stability system sensitivities. A 150 meter tall building is chosen since it provides the possibility for analysis of ten different diagonal layouts. However, for this height and forces, the defined steel plate and dowel connection with the set input in this model is not a feasible choice. Thus, the structure will fail for all analysed steel plate and dowel connections. Still, even though it fails for all analysed connections, the unity checks found for these connections can improve understanding.

6.3.1. 150 meter tall building

To gain more insight in the effect of the diagonal placement and steel plate length in the stability systems, a 150 meter tall stability system is created. This stability system has a width of 43.2 meters and a grid size of 8.64 meters. It is similar to the stability system that is present in the façade in the timber building designs. 60 different stability systems are created with various steel plate length, number of diagonals and placement of diagonals.

The "Ndiag" parameter determines the amount of times the diagonal crosses the full width of the façade back and forth. The "Pdiag" parameter refers to the placement of the diagonals. If it is set to zero, the diagonal crosses the full width of the façade. If it is set to one, it crosses the façade starting at the second columns up to the second last column, Figure 5.8 visualizes the layout of diagonals for these two parameters.

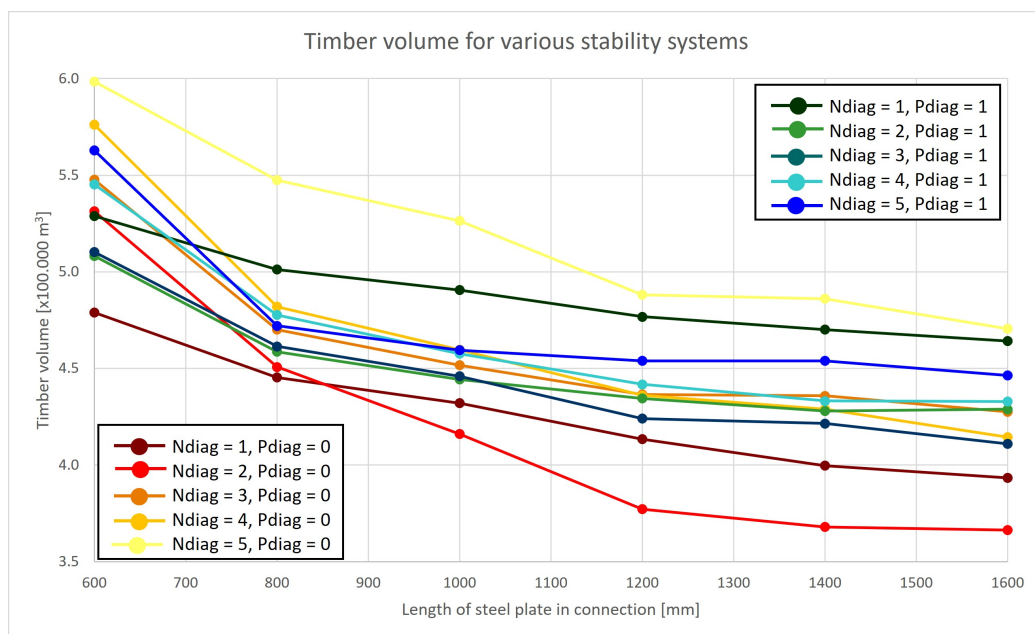


Figure 6.10: Timber volume for different stability system structures for a 150 meter high building.

Timber volume Figure 6.10 shows a decrease in timber volume in the stability system for an increasing length of the steel plate in the connection. A longer steel plate in the connection results in a stiffer connection. This stiffer connection results in a stiffer structure. The stability system will act more as a moment frame rather than a truss. This results in a decrease in cross section sizes of the timber elements, which decreases the timber volume of the stability system. Furthermore, the Figure indicates that the length of the steel plate has an effect on the preference of a stability system.

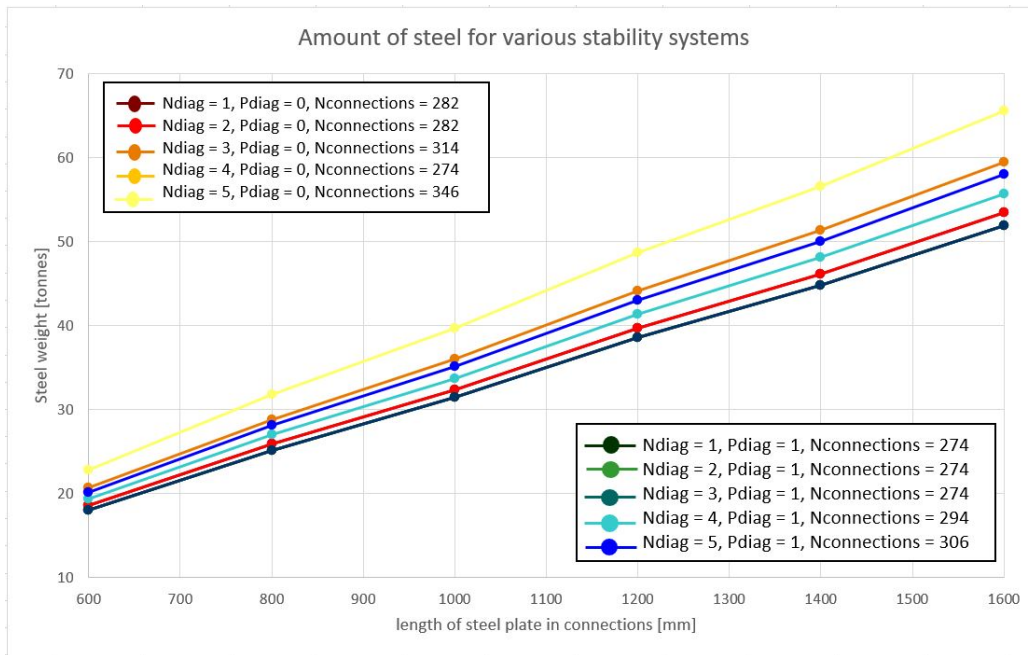


Figure 6.11: Amount of steel for different stability system structures for a 150 meter high building.

Steel weight Figure 6.11 shows a linear increase in steel mass in the stability system for an increasing length of the steel plate in the connection. The amount of steel is dependent on the amount of connections present in the façade. This amount of connections depends on the positioning of the diagonals. If a diagonal intersects with a column and beam, only one connection is required. When a diagonal intersects with a column and a beam separately, two connections are required. So, an intersection of the diagonal with a column and a beam is preferred since this reduces the total amount of required connections. Also, this can lead to a more efficient transfer of forces. However, the connection design is more complex. The definition of placement of diagonals as defined in the tool does not allow for adaptation of the layout of diagonals.

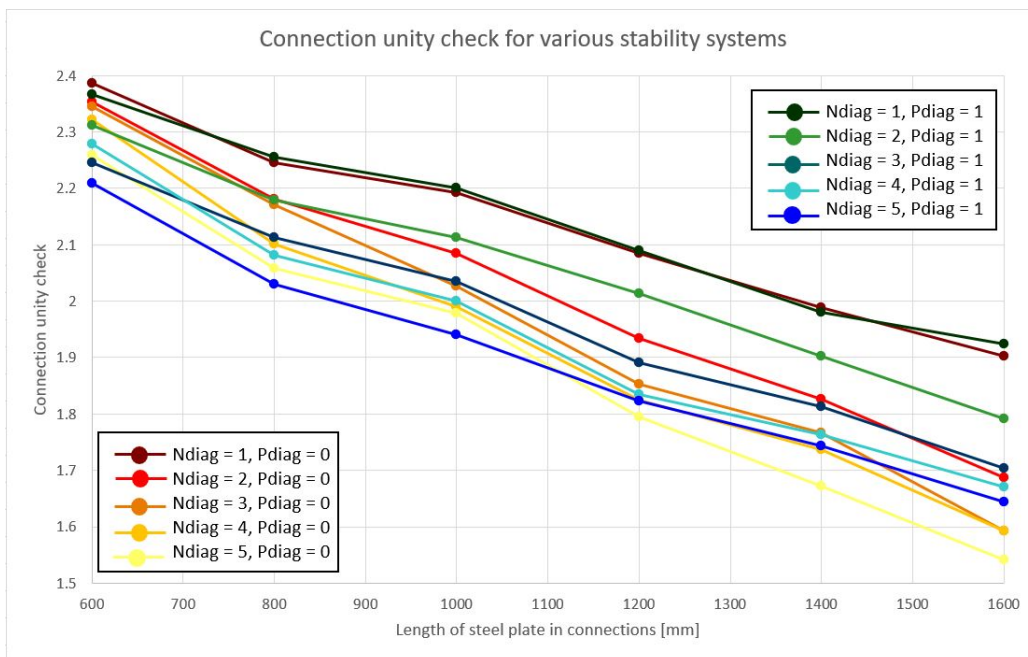


Figure 6.12: Connection unity check for different stability system structures for a 150 meter high building.

Connection unity check Figure 6.12 shows a linear decrease for the connection unity check for increasing steel plate lengths.

The steel plate length in the connections is defined as the average steel plate length in the model, see the first bullet point in Section 5.1.2. A certain percentage of the connections present may fail on strength for this steel plate length. This percentage is set to 33%, as was observed for Mjøstårnet in Section 5.12.1.

However, for this height and forces, the defined steel plate and dowel connection with the set input in this model is not a feasible choice. Thus, the structure will fail for all analysed steel plate and dowel connections. Still, even though it fails for all analysed connections, the unity checks found for these connections can improve understanding.

Deflection unity check Each building is designed based on the SLS and ULS requirements. The ULS check assures all elements are dimensioned such that they can transfer all present forces and moments. This is done by defining an utilization factor of 1.0. The SLS check is based on the maximum horizontal deflection of the building. To gain insight into which unity check is normative, the 'deflection unity check' is introduced. First, the stability system is optimized based on the ULS requirements. Next, the horizontal deflection of this stability is determined and using the maximum horizontal deflection of $\frac{h}{825}$ as specified in Annex A.4.3, the 'deflection unity check' is determined.

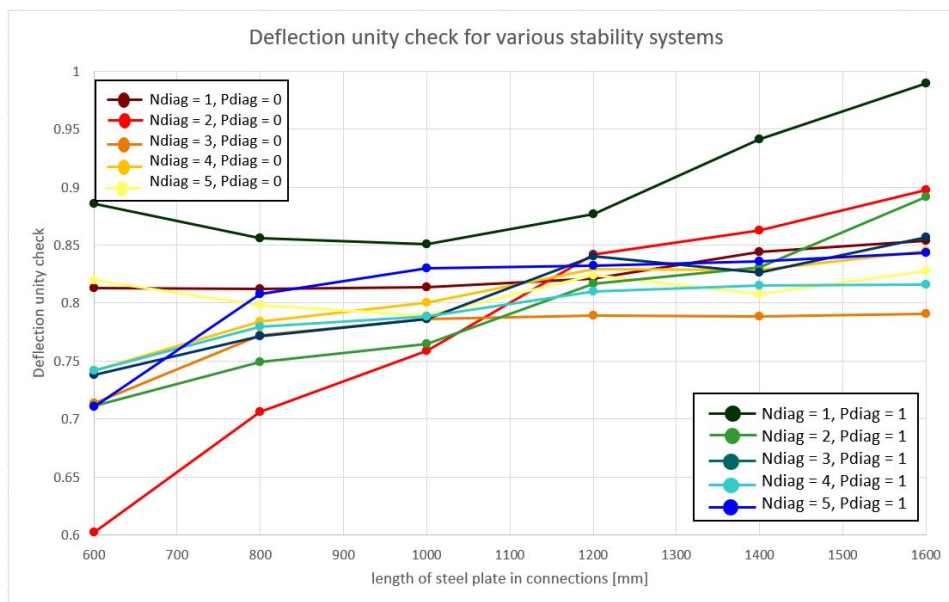
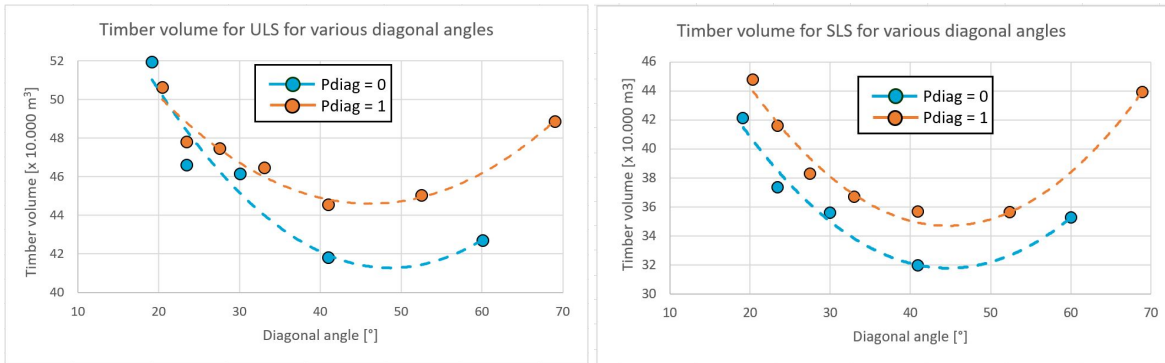


Figure 6.13: Deflection unity check for different stability system structures for a 150 meter high building.

Figure 6.13 shows the deflection unity check for increasing steel plate lengths. Two statements can be made based on this graph. Firstly, for all 60 defined stability systems, the deflection is not normative, with a deflection unity check of roughly 0.8. Secondly, a slight increase in the deflection unity check is observed. The deflection unity check indicates the unity check for the deflection regarding the stability system which is optimized based on the ULS requirements. This increase in deflection unity check, is expected to be caused due to the fact that the stability system which is optimized based on the ULS requirements requires smaller elements for longer steel plate lengths. These smaller elements are assumed to effect the deflection of the stability system.

Diagonal angle Although these lines provide some insights regarding various stability systems, it is not clear what parameter causes the most efficient design. It is expected the diagonal angle is the most important parameter which influences the efficiency of a design. For the analysis of this statement, an average score is calculated for the timber volume in ULS and SLS, the connection unity check and the deflection unity check for all stability systems. This was done by calculating the average value found for all analysed steel plate lengths per stability system. Subsequently, the diagonal angle is calculated and plotted with the obtained average scores, see Figures 6.14 and 6.15. Also, two stability systems are added to increase the accuracy of this analysis. The chosen parameters for these stability systems are: Ndiag=6, Pdiag=1 and Ndiag=7, Pdiag=1.

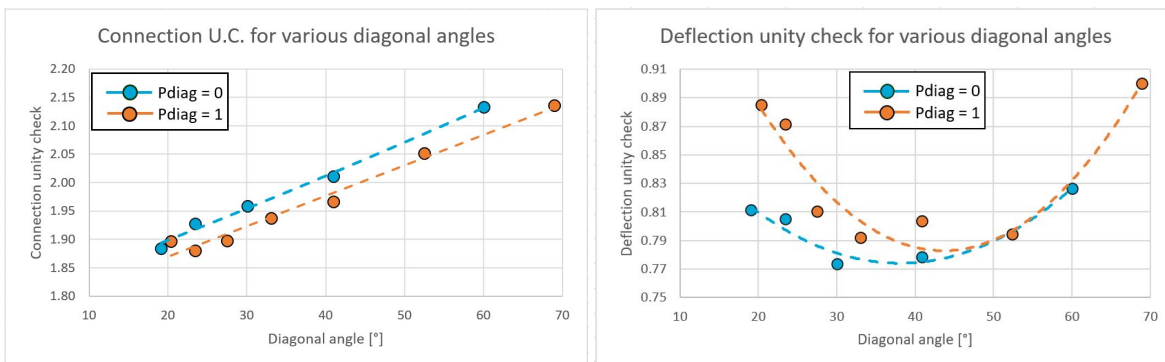


(a) Timber volume for ULS design for different diagonal angles for a 150 meter high building

(b) Timber volume for SLS design for different diagonal angles for a 150 meter high building

Figure 6.14

Figure 6.14 shows the timber volume the stability systems contain for a ULS and a SLS check. Two conclusions can be drawn based on this Figure. Firstly, for the analysed stability system, a diagonal angle of roughly 45° will result in a structure with the smallest timber volume. Secondly, for this set geometry, diagonals which cross the full width of the stability system are favourable over diagonals which cross the stability system between the second and second-to-last column.



(a) Unity check of connection for different diagonal angles for a 150 meter high building

(b) Unity check of deflection for different diagonal angles for a 150 meter high building

Figure 6.15

Figure 6.15 shows the connection and deflection unity checks for the analysed stability systems.

Figure 6.15a shows a linear relation between diagonal angle and unity check of the connections. This is expected to be caused due to the fact that diagonals with a smaller diagonal angle have a better ability to transfer the wind forces to the foundation, since the forces in the diagonals are smaller.

Figure 6.15b shows the unity check for deflection for the analysed stability systems. As expected, when Pdiag=1, so when the diagonals cross the stability system between the second and second-to-last column, the unity check for deflection is higher. Since the diagonals cross less width, the structure has a bigger tendency to deflect. Since the timber volume in the stability system was found to be the smallest for a diagonal angle of 45°, see Figure 6.14, it is expected that optimal buildings will have a deflection unity check between 0.75 and 0.8.

6.3.2. Diagonal layout

The layout of the diagonals has an effect on the forces and moments in the elements and thus on the dimensions of the cross section. Depending on the set input parameters, a diagonal may intersect with a column and a beam in the same point, which reduces the total amount of required connections and may lead to a more efficient transfer of forces. The effect of a different layout of diagonals is analysed by creating two stability systems with a different layout:

- **Diagonal layout 1:** In this stability system, all diagonals cross all columns and beams in the same point, see Figure 6.16c.
- **Diagonal layout 2:** In this stability system, the diagonals rarely cross the columns and beams in the same point, see Figure 6.16d.

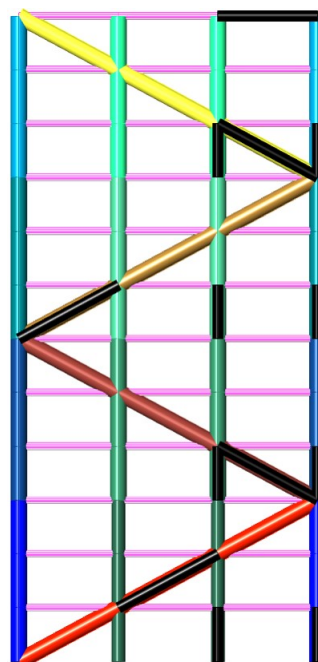
The analysis is performed for a 50 meter high, 30 meter wide stability system. The loads consist of gravitational loads and wind loads, as obtained using the tool. The wind loads are determined according to the Eurocode, see Figure A.23. This results in a uniform wind load of approximately 35 kN/m.

Normal force, shear force, bending moment and cross section in normative element per element group for diagonal layout 1					
Element group	Color	N [kN]	V [kN]	M [kNm]	Cross section [mm]
ColumnsYOut1		-4051	0	1	600x600
ColumnsYOut2		-1857	4	16	450x450
ColumnsYOut3		-1460	1	3	400x400
ColumnsYOut4		-398	1	2	250x250
ColumnsYIn5		-1594	0	1	400x400
ColumnsYIn6		-1102	0	2	350x350
ColumnsYIn7		-798	1	2	300x300
ColumnsYIn8		-304	0	1	250x250
DiagonalsY9		-600	0	3	350x350
DiagonalsY10		1188	1	5	350x350
DiagonalsY11		-1788	2	17	500x500
DiagonalsY12		2378	3	26	500x500
BeamsY		178	0	0	-

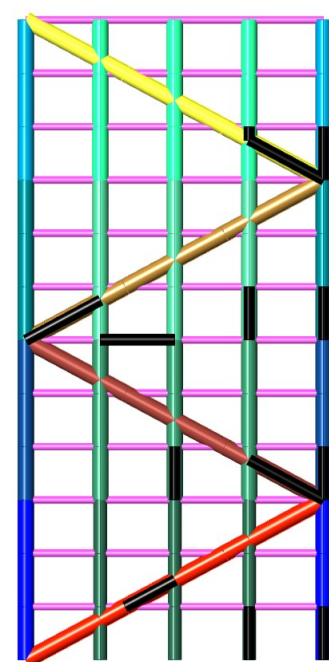
(a) N, V, M and cross section for normative element

Normal force, shear force, bending moment and cross section in normative element per element group for diagonal layout 2					
Element group	Color	N [kN]	V [kN]	M [kNm]	Cross section [mm]
ColumnsYOut1		-3571	1	5	600x600
ColumnsYOut2		-1521	27	100	500x500
ColumnsYOut3		-1230	5	11	400x400
ColumnsYOut4		-291	8	26	300x300
ColumnsYIn5		-1162	4	14	400x400
ColumnsYIn6		-821	6	14	350x350
ColumnsYIn7		-584	4	10	350x350
ColumnsYIn8		-291	38	19	300x300
DiagonalsY9		-577	6	21	350x350
DiagonalsY10		1154	8	32	400x400
DiagonalsY11		-1736	18	91	550x550
DiagonalsY12		2326	25	128	550x550
BeamsY		203	0	0	-

(b) N, V, M and cross section for normative element



(c) Visualization of element groups



(d) Visualization of element groups

Figure 6.16: Effect of diagonal layout with wind force from the left.

The elements in these stability systems are grouped using Karamba3D's Optimize Cross Section component. All elements in an element group have the same dimensions of the cross sections. In the visualizations of the stability systems, and in the Tables shown below, various colours are used to indicate the element groups. Furthermore, a black line indicates the normative element in the visualization of a stability system.

Both stability systems are checked for a normative wind force from the left, see Figure 6.16 and the right, see Figure 6.17. The two stability systems are analysed regarding normal force, shear force, moments, cross section dimensions and the position of normative element per element group.

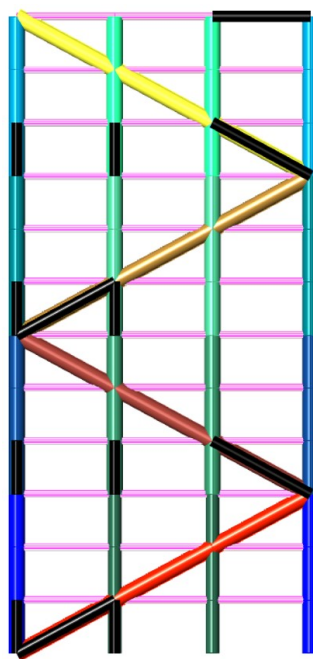
For diagonal layout 1, the bending moments are significantly smaller than the bending moment in diagonal layout 2. This is since an intersection of diagonals, beams and columns result in a more efficient transfer of forces. Forces can be transferred mostly through normal forces, little bending moments are required to transfer forces. These smaller bending moments result in smaller required cross sections per element group. This reduction in timber volume is dependent on the analysed stability system and wind direction. For a wind force from the left, as shown in Figure 6.16, the required timber volume is reduced with 14%. When the wind force acts on the right side of the stability system, as is depicted in Figure 6.17, the timber volume is reduced with 5%.

Normal force, shear force, bending moment and cross section in normative element per element group for diagonal layout 1					
Element group	Color	N [kN]	V [kN]	M [kNm]	Cross section [mm]
ColumnsYOut1	Dark Blue	-2919	2	18	550x550
ColumnsYOut2	Blue	-2520	6	14	500x500
ColumnsYOut3	Light Blue	-892	0	2	350x350
ColumnsYOut4	Teal	-494	3	8	300x300
ColumnsYIn5	Dark Green	-1610	2	7	400x400
ColumnsYIn6	Green	-1302	4	9	400x400
ColumnsYIn7	Light Green	-804	0	6	350x350
ColumnsYIn8	Yellow-Green	-496	3	8	300x300
DiagonalsY9	Yellow	584	0	1	250x250
DiagonalsY10	Orange	-1199	2	15	450x450
DiagonalsY11	Red-Orange	1765	0	3	400x400
DiagonalsY12	Red	-2381	2	18	550x550
BeamsY	Pink	-179	0	0	-

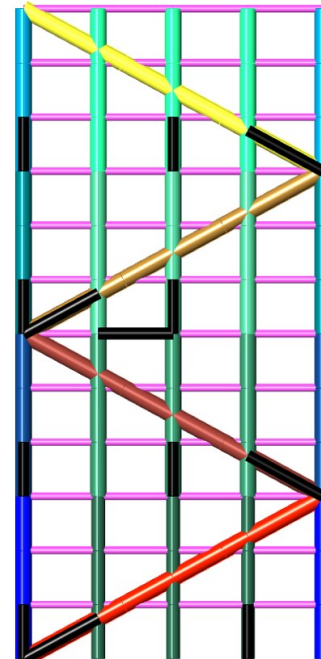
(a) N, V, M and cross section for normative element

Normal force, shear force, bending moment and cross section in normative element per element group for diagonal layout 2					
Element group	Color	N [kN]	V [kN]	M [kNm]	Cross section [mm]
ColumnsYOut1	Dark Blue	-2480	10	41	550x550
ColumnsYOut2	Blue	-2189	13	35	500x500
ColumnsYOut3	Light Blue	-678	7	21	350x350
ColumnsYOut4	Teal	-387	8	20	300x300
ColumnsYIn5	Dark Green	-1176	2	8	400x400
ColumnsYIn6	Green	-927	8	24	400x400
ColumnsYIn7	Light Green	-588	5	14	350x350
ColumnsYIn8	Yellow-Green	-350	10	21	300x300
DiagonalsY9	Yellow	561	1	8	350x350
DiagonalsY10	Orange	-1167	3	10	450x450
DiagonalsY11	Red-Orange	1721	1	7	450x450
DiagonalsY12	Red	-2354	8	41	550x550
BeamsY	Pink	-221	0	0	-

(b) N, V, M and cross section for normative element



(c) Visualization of element groups



(d) Visualization of element groups

Figure 6.17: Effect of diagonal layout with wind force from the right.

The position of the normative elements per element group for diagonal layout 1 are systematic for both wind directions, see Figures 6.16c and 6.17c. For diagonal layout 2, The position of the normative elements per element group show more randomness for both wind directions, see Figures 6.16d and 6.17d. This is expected to be caused since the diagonal layout may lead to suboptimal transfer of forces and thus unnecessary big moments and forces in some elements. This is according to expectations, see Annex B.8.

Utilization factor For each group, one element is normative and has an utilization factor close to 1.0, see Figure 6.18. The dimensions of the other elements in the group are similar to the normative element. These elements are often over-dimensioned which is clear when regarding the average utilization factor per group, see Figure 6.19. This average utilization factor is roughly 0.6.

Normative utilization factor per element group						Normative utilization factor per element group					
Diagonal layout 1			Utilization factor			Diagonal layout 2			Utilization factor		
Element group	Color	N	V	M	Total	Element group	Color	N	V	M	Total
ColumnsYOut1	Dark Blue	0.94	0.03	0.06	0.94	ColumnsYOut1	Dark Blue	0.83	0.02	0.29	0.84
ColumnsYOut2	Blue	0.80	0.00	0.10	0.90	ColumnsYOut2	Blue	0.52	0.02	0.42	0.94
ColumnsYOut3	Light Blue	0.82	0.00	0.08	0.85	ColumnsYOut3	Light Blue	0.69	0.01	0.36	0.79
ColumnsYOut4	Teal	0.68	0.00	0.07	0.75	ColumnsYOut4	Teal	0.32	0.02	0.50	0.82
ColumnsYIn5	Dark Green	0.90	0.00	0.13	0.90	ColumnsYIn5	Dark Green	0.65	0.05	0.26	0.78
ColumnsYIn6	Green	0.84	0.00	0.13	0.93	ColumnsYIn6	Green	0.62	0.06	0.29	0.81
ColumnsYIn7	Light Green	0.87	0.00	0.07	0.93	ColumnsYIn7	Light Green	0.44	0.06	0.36	0.67
ColumnsYIn8	Yellow-Green	0.52	0.00	0.08	0.55	ColumnsYIn8	Yellow-Green	0.26	0.09	0.51	0.60
DiagonalsY9	Yellow	0.73	0.00	0.04	0.76	DiagonalsY9	Yellow	0.54	0.04	0.41	0.81
DiagonalsY10	Orange	0.78	0.00	0.06	0.83	DiagonalsY10	Orange	0.58	0.03	0.24	0.80
DiagonalsY11	Red-Orange	0.79	0.00	0.08	0.87	DiagonalsY11	Red-Orange	0.54	0.02	0.27	0.81
DiagonalsY12	Red	0.76	0.00	0.09	0.85	DiagonalsY12	Red	0.62	0.02	0.33	0.95
BeamsY	Pink	0.10	0.00	0.00	0.10	BeamsY	Pink	0.14	0.00	0.00	0.14

(a) Normative utilization for diagonal layout 1

(b) Normative utilization for diagonal layout 2

Figure 6.18: Normative utilization factor with wind force from the left

Figures 6.18 and 6.19 indicate that for diagonal layout 2, a large part of the utilization factor is present in the bending moment. This is most true for the elements positioned higher in the building. Elements higher in the building transfer bigger wind loads and smaller gravitational loads. These wind loads are horizontal

Average utilization factor per element group					Average utilization factor per element group						
Diagonal layout 1		Utilization factor			Diagonal layout 2		Utilization factor				
Element group	Color	N	V	M	Total	Element group	Color	N	V	M	Total
ColumnsYOut1		0.47	0.00	0.01	0.48	ColumnsYOut1		0.43	0.00	0.06	0.49
ColumnsYOut2		0.43	0.00	0.03	0.45	ColumnsYOut2		0.33	0.00	0.10	0.42
ColumnsYOut3		0.53	0.00	0.03	0.56	ColumnsYOut3		0.43	0.00	0.12	0.55
ColumnsYOut4		0.42	0.00	0.05	0.47	ColumnsYOut4		0.17	0.01	0.17	0.35
ColumnsYIn5		0.79	0.00	0.05	0.84	ColumnsYIn5		0.55	0.01	0.16	0.71
ColumnsYIn6		0.77	0.00	0.06	0.83	ColumnsYIn6		0.53	0.02	0.21	0.75
ColumnsYIn7		0.67	0.00	0.05	0.72	ColumnsYIn7		0.32	0.02	0.23	0.55
ColumnsYIn8		0.37	0.00	0.05	0.42	ColumnsYIn8		0.16	0.03	0.33	0.50
DiagonalsY9		0.49	0.00	0.03	0.52	DiagonalsY9		0.31	0.02	0.35	0.66
DiagonalsY10		0.65	0.00	0.05	0.70	DiagonalsY10		0.49	0.02	0.21	0.70
DiagonalsY11		0.70	0.00	0.05	0.75	DiagonalsY11		0.45	0.01	0.12	0.56
DiagonalsY12		0.70	0.00	0.06	0.76	DiagonalsY12		0.57	0.01	0.12	0.69
BeamsY		0.05	0.00	0.00	0.05	BeamsY		0.06	0.00	0.00	0.06

(a) Average utilization for diagonal layout 1

(b) Average utilization for diagonal layout 2

Figure 6.19: Average utilization factor with wind force from the left

and must be transferred in vertical direction to the foundation. For diagonal layout 2, this transfer is done partly through bending moments, increasing their impact in the utilization factor.

As mentioned before, the sizes of the beams are similar in the stability system as in the gravitational system. In the stability system, these beams are overdimensioned as can be seen when regarding their utilization factor.

6.4. Timber buildings analysis

In this section, the effect of the height of a timber building on the obtained results is analysed. To accomplish this, the tool is used to obtain the optimal building designs for various amount of floors, each representing a design situation. The analysed buildings are based on building A3 and building B3, with the design situation dependent parameters as defined in Figure 5.6b. For both buildings, other design situations are created containing less or more number of floors. A generation and population size of 30 is used in the optimization. According to Section 6.2.1, this implies approximately half of the Pareto optimal building designs are found

In this analysis it was chosen to select the Pareto optimal design with the lowest construction costs for each design situation. This way, a fair comparison can be made. The Pareto optimal design with the lowest construction costs was chosen, since the construction costs are identified as the biggest obstacle in timber building design. All these buildings are thoroughly analysed in order to gain more insight in dependencies between the regarded property and the building height.

Building types A

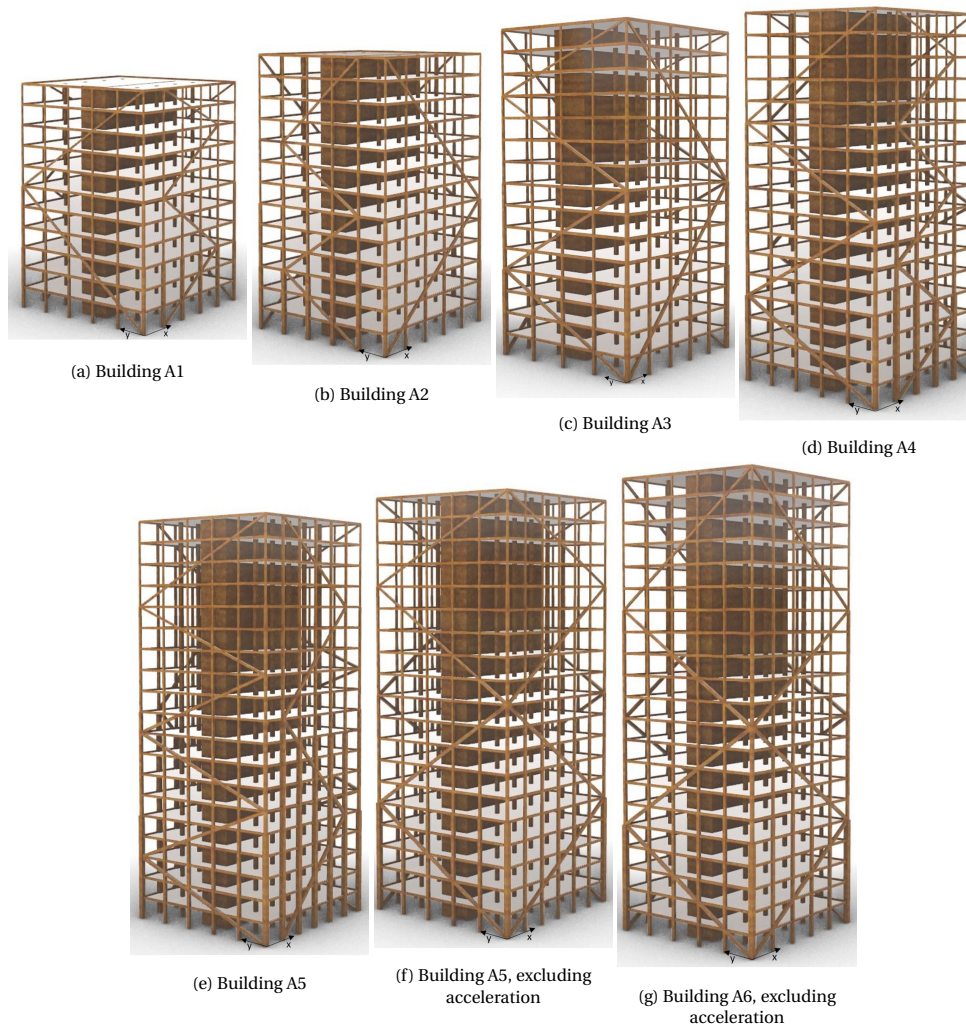


Figure 6.20: Buildings A1 to A6: The Pareto optimal buildings with the lowest construction costs

Optimal buildings for various building heights							
	Including acceleration					Excluding acceleration	
	A1	A2	A3	A4	A5	A5	A6
Amount of floors	11	13	15	17	19	19	21
Height	42.5	50.3	58.4	65.7	72.8	72.8	81.2
Grid size X-direction	5.76	5.76	5.76	5.76	4.8	4.8	5.76
Grid size Y-direction	5.76	5.76	7.2	5.76	5.76	5.76	5.76
Number of diagonals in X-direction	2	1	1	3	2	2	2
Number of diagonals in Y-direction	1	2	2	2	3	2	2
Positioning of diagonals in X-direction	1	0	0	1	1	0	0
Positioning of diagonals in Y-direction	0	1	0	0	0	0	0
Length of steel plate in X-direction	600	800	1000	600	1200	1200	1200
Length of steel plate in Y-direction	1000	1000	1400	1600	1000	800	1600

Figure 6.21: Found parameters for buildings A1 to A6, and A6 and A7 excluding acceleration criteria

Building types B

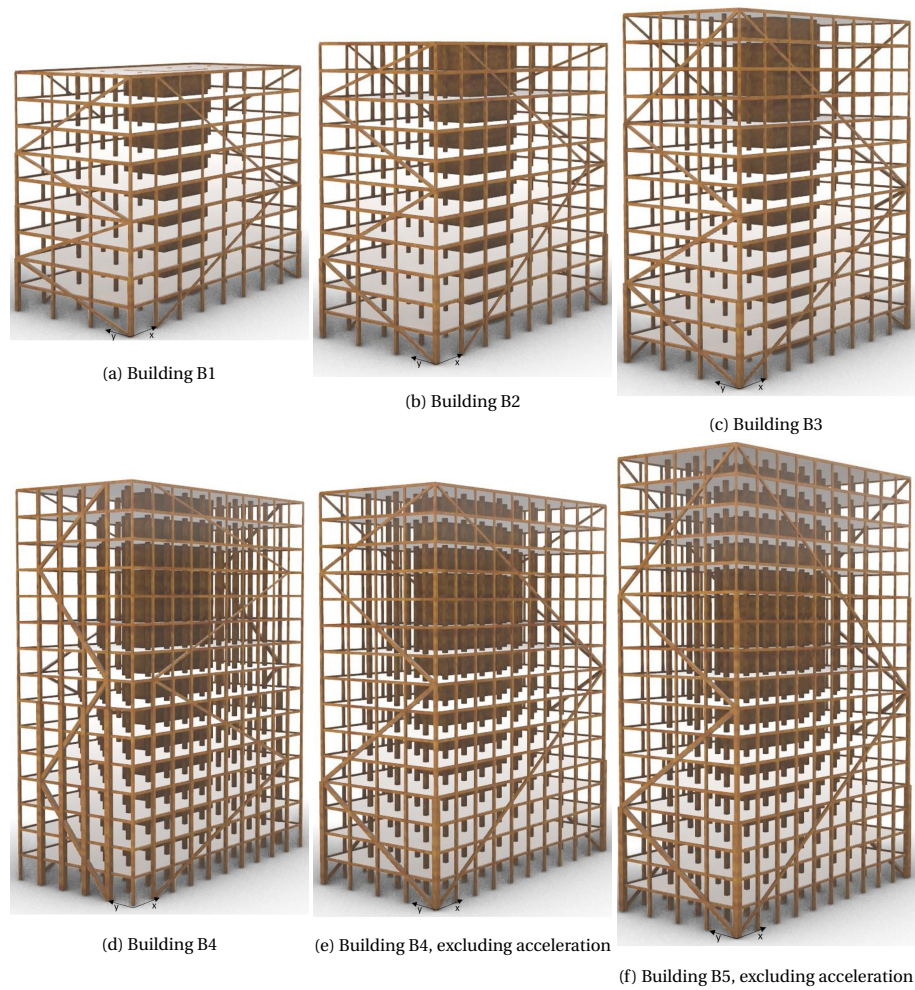


Figure 6.22: Buildings B1 to B5: The Pareto optimal buildings with the lowest construction costs.

Optimal buildings for various building heights						
	Including acceleration				Excluding acceleration	
	B1	B2	B3	B4	B4	B5
Amount of floors	9	11	13	15	15	17
Height	35.0	42.8	50.6	56.9	57.1	64.8
Grid size X-direction	5.4	5.4	5.4	4.32	4.32	4.32
Grid size Y-direction	7.2	7.2	7.2	4.32	5.4	5.4
Number of diagonals in X-direction	1	1	1	2	1	1
Number of diagonals in Y-direction	2	2	2	2	2	2
Positioning of diagonals in X-direction	1	1	0	1	0	0
Positioning of diagonals in Y-direction	0	0	0	1	0	0
Length of steel plate in X-direction	800	1000	1000	1400	800	1000
Length of steel plate in Y-direction	600	800	800	1400	800	600

Figure 6.23: Found parameters for buildings B1 to B4 and B4 and B5 excluding acceleration criteria.

6.4.1. Unity Checks

As discussed in Chapter 5, the tool dimensions the generated buildings based on the SLS and ULS requirements. Subsequently, the generated building designs are verified by determining the unity checks for the along-wind and cross-wind acceleration, connection strength, wind friction and the force in the tension ties. If these unity checks are all below 1.0, the building design is verified and is accepted by the genetic algorithm as an individual result. So, because of this MDO Architecture, a generated building design is always first optimized for ULS and SLS and thereafter checked based on the mentioned verification criteria. This MDO architecture is based on the hypothesis that for timber buildings between 50 and 70 meters, the SLS and ULS requirements are normative. This section analyses the unity checks of the verification criteria, to investigate the consequences of the defined MDO architecture.

Acceleration

As mentioned in Section A.4.2, there is an along-wind response, cross-wind response and a torsional response to wind which cause acceleration of the building. Van Oosterhout (1996) argues that the torsional response is not normative for the considered building type [153]. So, only the along-wind response and the cross-wind response are investigated further.

Along-wind Response The along-wind response is calculated in a custom node in the tool. The calculation is based on the requirements set in the Eurocode. The total mass of the building consist of the dead load of the building element, the dead load of the façade and the live loads times a factor $\psi_2 = 0.3$

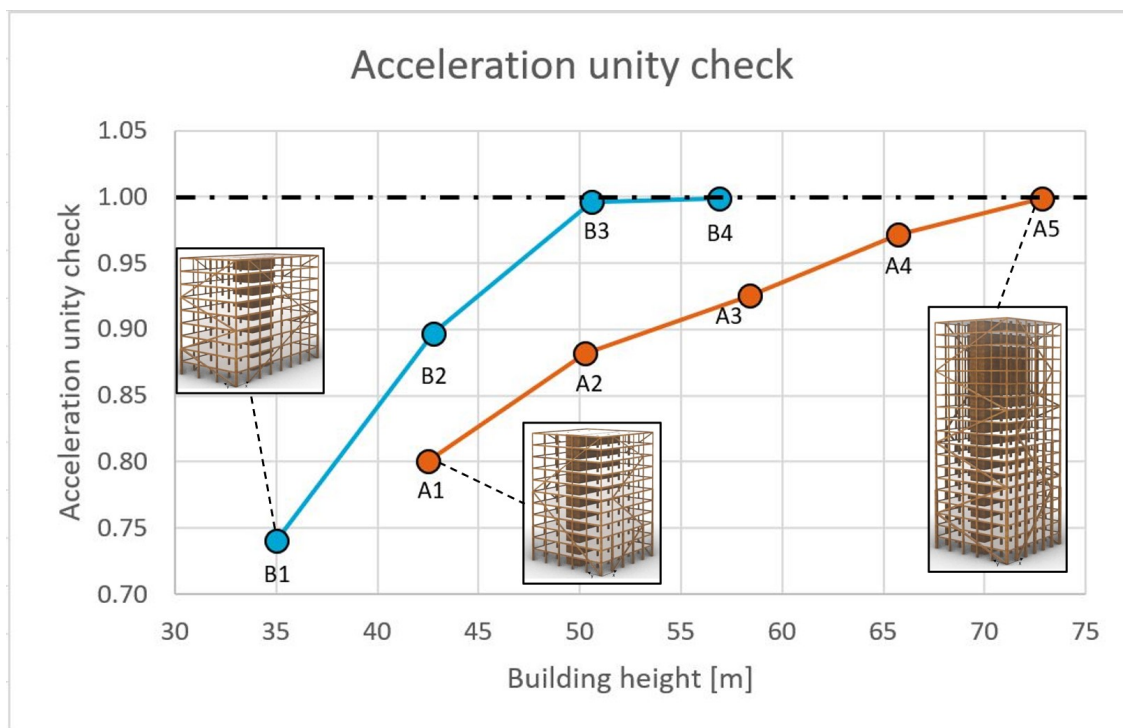


Figure 6.24: Unity checks for acceleration for Buildings A1-A5 and B1-B4

Figure 6.24 shows the unity checks for acceleration for nine analysed design situations. These results are based on a wind force caused by a terrain category of 3 and a wind zone of 1. For buildings A5 and B4, the unity check reaches 1.0. This indicates that the acceleration criteria for the along-wind response for these building is normative. For buildings A1 to A4, B1 to B3 the acceleration criteria for the along-wind response is not normative.

The along-wind response is calculated according to the requirements set in the Eurocode, see Section A.4.2. According to this calculation the acceleration of the top level of the building can only be decreased by increasing the total mass of the building. So, for buildings where the acceleration criteria for the along-wind response are normative, the tool increases the total building weight to meet these acceleration requirements. To accomplish this, the tool decreases grid sizes and increases the amount of diagonals. This is clearly visible

for Building B4, in Figure 6.22d. The grid sizes are decreased to 4.32 in both X- and Y-direction, and the number of diagonals is set to 2 in both directions. The structure of this obtained building is far from optimal. So, to be able to gain more insight, optimal building designs are generated for buildings A5, A6, B4 and B5 where the acceleration unity check is excluded from the calculation. Figure 6.25 shows the results of this analysis.

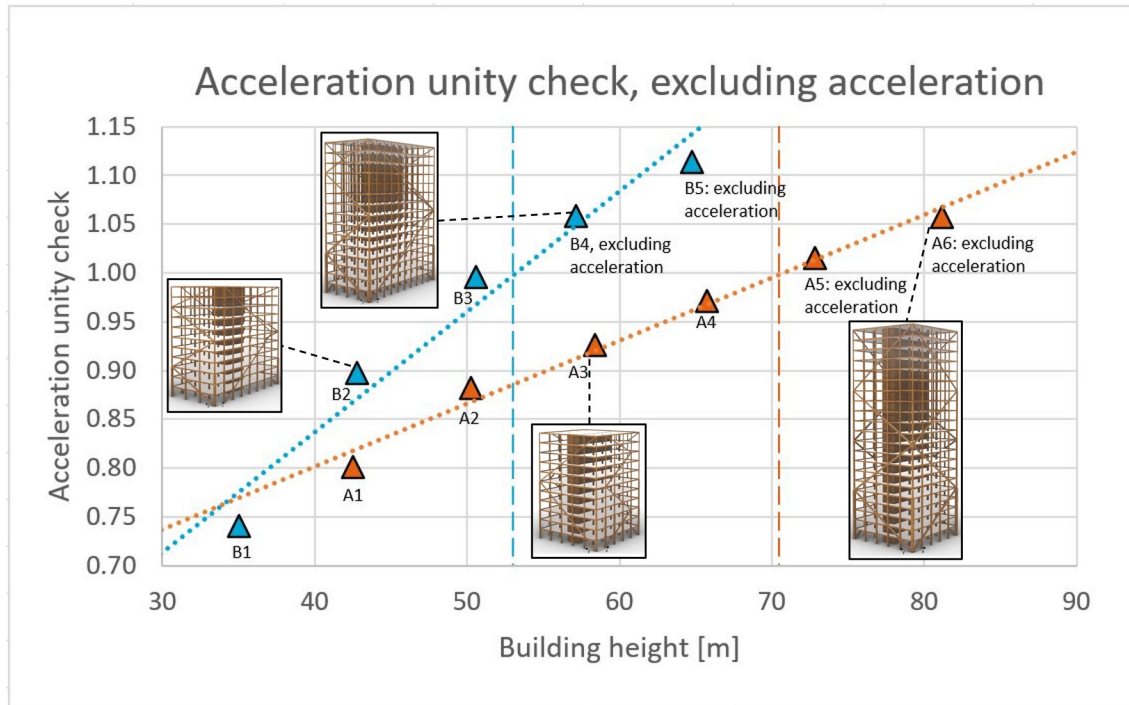


Figure 6.25: Unity checks for acceleration for Buildings A1 to A6 and B1 to B5, when the unity check for acceleration is excluded

Figure 6.25 shows a roughly linear relation between building height and unity check for acceleration. For the building type A, the acceleration is normative for a building height over 71 meters. For building type B, when the building is over 53 meters tall, the acceleration is normative. It is expected that acceleration is normative for a different building height for these buildings because of the different slenderness of the buildings. To investigate this statement, the relation between acceleration and slenderness is analysed, see Figure 6.26

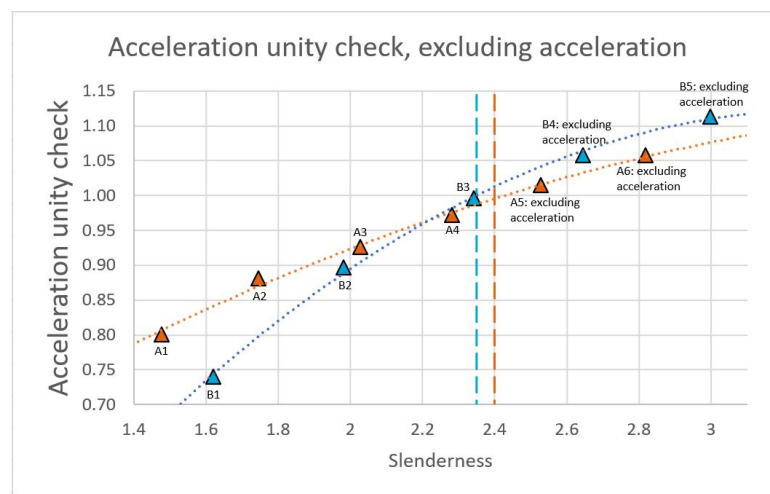


Figure 6.26: Unity checks for acceleration for Buildings A1-A6 and B1-B5 compared to the slenderness, when the unity check for acceleration is excluded

As Figure 6.26 shows, for building type A the acceleration is normative for a slenderness greater than 2.3. For building type B this is the case for a slenderness greater than 2.35. Based on these graphs, it can be concluded that there is a direct relation between slenderness and acceleration for this building type.

Design considerations When the along-wind response of the building is normative, some design alterations can be made to reduce the acceleration.

- **Increasing the total mass of the building** This can be done by replacing timber floors with concrete floors, as is done in the Mjøstårnet reference project.
- **Decreasing the slenderness of the building.** A decrease in slenderness of the building and thus the stability system, increases the stiffness of the stability system.
- **Accurate estimation of damping coefficient** A more accurate analyses than the empirical formulas given in the Eurocode might prove that the timber building is more resilient against acceleration. Various researches have proven that a damping coefficient of the building (D) of 0.01 as defined in the Eurocode is a conservative assumption. The research of Feldmann et al. (2016) showed an average structural damping ratio of 0.02 for tall timber structures up to 100m [49]. A damping ratio of 0.019 was used for the design of Mjøstårnet[8].

The replacement of timber floors with concrete floors results in an increase in building mass. The self-weight for a 300 mm thick concrete floor is $23.5 \text{ kN/m}^3 \cdot 0.3 \text{ m} = 7.05 \text{ kN/m}^2$. The weight of a Kerto-Ripa floor was found to be 2.28 kN/m^2 in the Mjøstårnet verification. So, replacing a Kerto-Ripa floor with a concrete floor results in an additional dead load of $7.05 - 2.28 = 4.77 \text{ kN/m}^2$. For buildings A5, A6, B4 and B5 where the acceleration criteria are excluded, an additional load is required to satisfy the acceleration criteria. The required amount of concrete floors are calculated for these buildings, see Figure 6.27.

Required additional weight				
	Building A5	Building A6	Building B4	Building B5
Building mass present [kN]	46585	57255	39798	45407
Required building mass[kN]	47285	62077	42107	50553
Required additional building mass [kN]	710	4822	2309	5146
Required concrete floor area [m^2]	149	1010	484	1079
Required levels of concrete floors	0.18	1.22	0.52	1.16

Figure 6.27: Grid sizes Building A3 and B3.

The premise that adding concrete floors results in a design which satisfies the acceleration criteria is based on the along-wind calculation as mentioned in NEN-EN 1990-1-1 [80]. However, a modal analysis must be performed on the model to verify the acceleration requirements more accurately. Here, adding some concrete floors to a timber building might have a big impact on the analysis. However, if the total added mass is low, it is expected to not cause big changes.

Based on these three design considerations, it is assumed that a building which exceeds the acceleration limits slightly, can be adapted to satisfy the requirements. So, for buildings A5, A6, B4 and B5 a separate optimization is done in the tool where the acceleration criteria are excluded from the analysis. The obtained results are shown in following Figures, depicted using a triangle.

Cross-wind response The cross-wind response of the building is negligible. For building B5 in X-direction the unity check is 0.032 and in Y-direction the unity check is 0.004. So, the cross-wind response is not further analysed.

Tension tie

The forces in the tension ties can be transferred by the beams. For building B5 the utilization factor for the tension ties for wind in X-direction is 0.0044. In Y-direction this utilization factor is 0.0194. The transfer of these forces through the connections is not analysed in the tool.

Connection strength

Figure 6.28 shows the unity check regarding the strength of steel plate and dowels connections in the stability system.

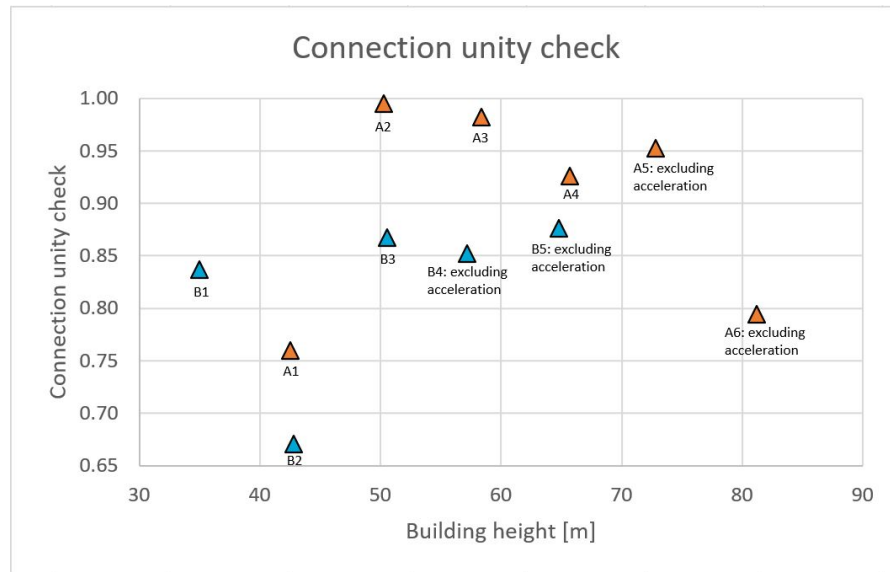


Figure 6.28: Unity checks for connection strength for Buildings A1-A6 and B1-B5

Two statements can be made regarding Figure 6.28. Firstly, some unity checks are significantly lower than the expected 1.0. This is expected to be caused by the discrete input of the length of the steel plate. Since this input parameter is discrete, it can be the case that when choosing a steel plate length which is 200 mm shorter, the unity check will be over 1.0. Secondly, for less tall buildings, the connection unity check is found to be lower. This is expected due to the fact that an increase of steel plate length of 200 mm has a bigger effect on the increase of the connection unity check. This statement was analysed for Building A1. The effect of a reduction of length of steel plate in Y-direction from 1000 to 800 mm was analysed. This steel plate length reduction caused the connection unity check to increase from 0.76 to 1.12 proving the statement.

Utilization factor

Figure 6.29 shows a Box-plot of the average utilization factor of the stability system X- and Y-direction for buildings A1-A6 and B1-B5 excluding acceleration. This is based on the average of all element groups in ULS design with a wind force from the left. As can be seen the average utilization factor of all elements is roughly 0.57. This is due to the discrete amount of element dimensions, and the grouping of elements.

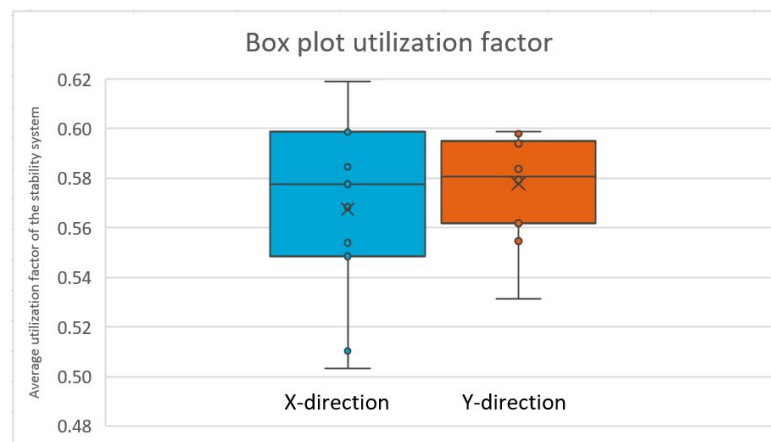


Figure 6.29: Average utilization factor for buildings A1-A6 and B1-B5 excluding acceleration

Deflection

Each building is designed based on the SLS and ULS requirements. The ULS check assures all elements are dimensioned such that they can transfer all present forces and moments. This is done by defining an utilization factor of 1.0. The SLS check is based on the maximum horizontal deflection of the building. To gain insight into which unity check is normative, the 'deflection unity check' is introduced. First, the stability system is optimized based on the ULS requirements. Next, the horizontal deflection of this stability is determined and using the maximum horizontal deflection of $\frac{h}{825}$ as specified in Annex A.4.3, the 'deflection unity check' is determined.

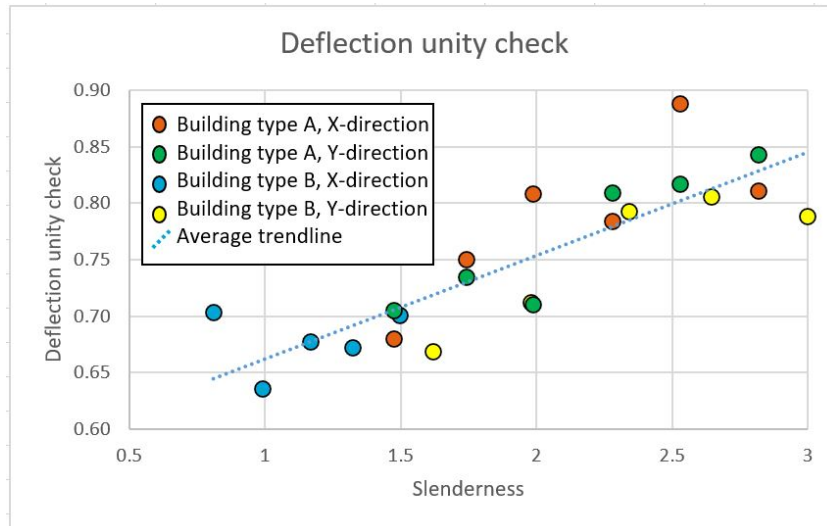


Figure 6.30: Unity checks for deflection for Buildings A1-A6 and B1-B5

Figure 6.30 shows the unity checks for the deflection regarding building types A and B in X- and Y-direction. This deflection is compared to the slenderness of the considered building. All unity checks are smaller than 1.0 indicating that the ULS is normative in all building designs. The linear trendline for all obtained points seems to indicate a relation between deflection and slenderness. If indeed a linear relation is present, the SLS check will be normative over the ULS check at a certain slenderness.

6.4.2. Angle of diagonals

In Section 6.3.1, it was concluded that a diagonal angle of roughly 45° will result in a structure with the smallest timber volume. This analysis was based on a 150 meter tall building with a slenderness of $\frac{150}{43.2} = 3.5$.

For building A1-A6 and B1-B5, the diagonal angle of the Pareto optimal building is analyzed, see Figure 6.31. The diagonal angles for both building types in X- and Y-direction are visualized, each containing different dimensions and loads.

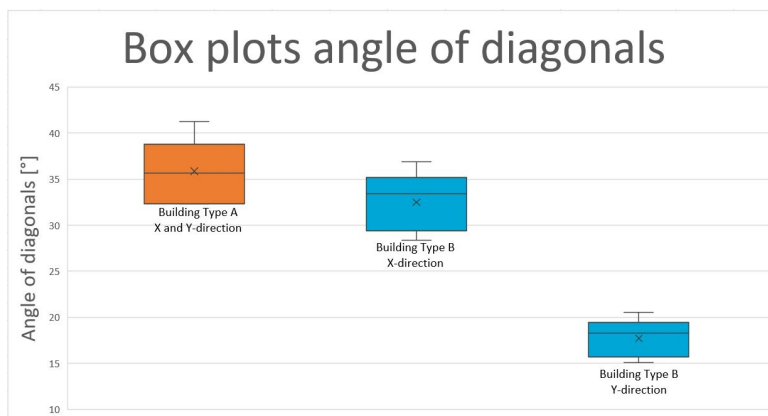


Figure 6.31: Box plot of the found diagonal angle in X- and Y-direction

Figure 6.31 shows the dependence of the stability system dimensions and wind forces on the optimal diagonal angle. The optimal diagonal angle is found to be dependent on the dimensions of the stability system and the wind forces on it. Thus, the floor plan influences the diagonal angle. For a square floor plan, the optimal diagonal angle is roughly 36%. While for a rectangular floor plan with a ratio of 2:1, the optimal diagonal angle is 33% in the long direction and 18% in the short direction. So, a lower optimal diagonal angle is obtained when the forces are larger and the width of the stability system is smaller. This is also true for Mjøstårnet, where the diagonals are positioned under an angle of 27.4° in the short dimension.

6.4.3. Comparison to reference projects

In this Section, the given properties for three case-studies are compared with the obtained properties for the optimized timber building designs. Accordingly, conclusions can be made regarding the accuracy of the tool, and the performance of the created designs. Tupenaite (2019) and Jackson (2019) analysed the total investment costs, timber volume and steel mass of these three reference projects: Treet, Mjøstårnet and 25 King [85], [145].

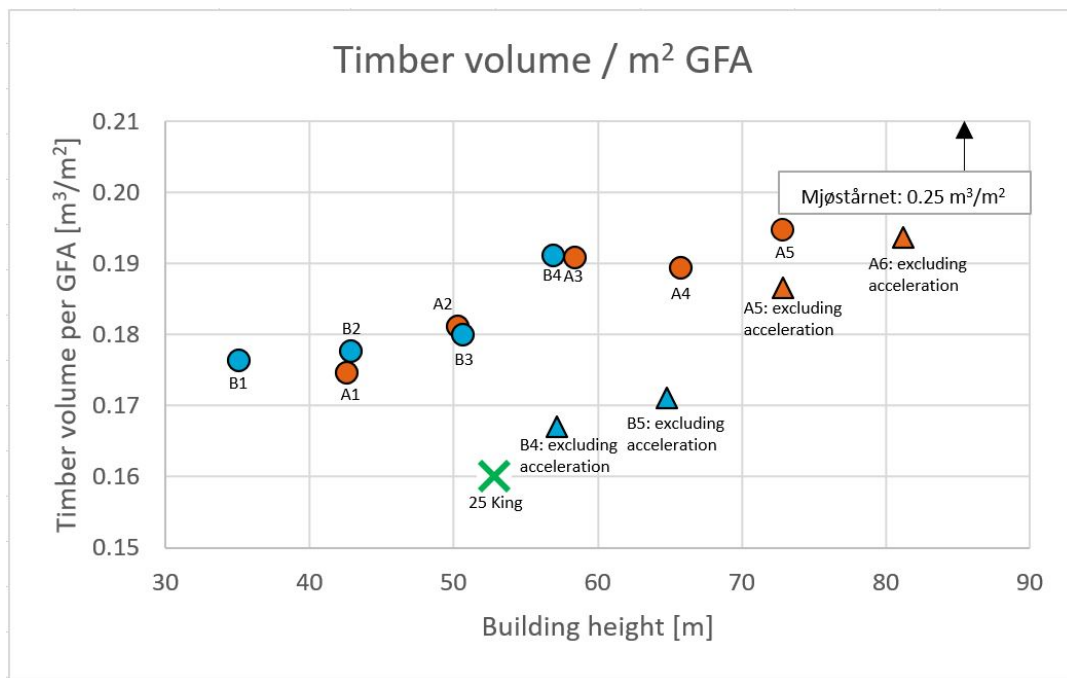


Figure 6.32: Timber volume per m^2 GFA compared to reference projects

Figure 6.32 show the relation between timber volume per m^2 of gross floor area and building height. Approximately similar results are obtained for building types A and B and 25 King. A similar relation is expected to be found between timber volume per m^2 of gross floor area and building height for Mjøstårnet and the optimized timber buildings, since their design approach is similar. However, this relation differs significantly. This does not imply that the tool creates inaccurate results, since there are five possible factors which differ regarding Mjøstårnet and the optimized timber buildings, that may influence the found results.

- The slenderness of Mjøstårnet, with a width of 17 meters and a height of 85.4 meters is 5, resulting in extra glulam elements required for stabilisation of the building.
- Mjøstårnet contains concrete floors on the six top floors, which increase the total gravitational loads. Thus, thicker columns and beams are required compared to the optimized timber buildings.
- Mjøstårnet is taller, and the effect of wind forces on a structure is not linear.
- The CLT core covers 25% of the floor area in Mjøstårnet. However, a value of 15% is assumed in the tool.
- The function of Mjøstårnet is residential, where the created buildings using the tool create an office building. Acoustical and acceleration requirements are stricter for a residential function compared to an office function



Figure 6.33: Steel weight per m² GFA compared to reference project

Figure 6.33 visualizes the steel weight per m² gross floor area. Madsen (2019) mentions a steel weight of 106916 kg for Mjøstårnet, thus a steel weight per m² gross floor area of $\frac{106916}{11322} = 9.44 \text{ kg/m}^2 \text{ GFA}$ [97]. This value of steel mass per m² of gross floor area for Mjøstårnet is slightly favourable over the timber buildings obtained using the tool. Although the method for calculation of connections in the tool is questionable, the obtained steel mass per m² of gross floor area is shown to be reasonable.

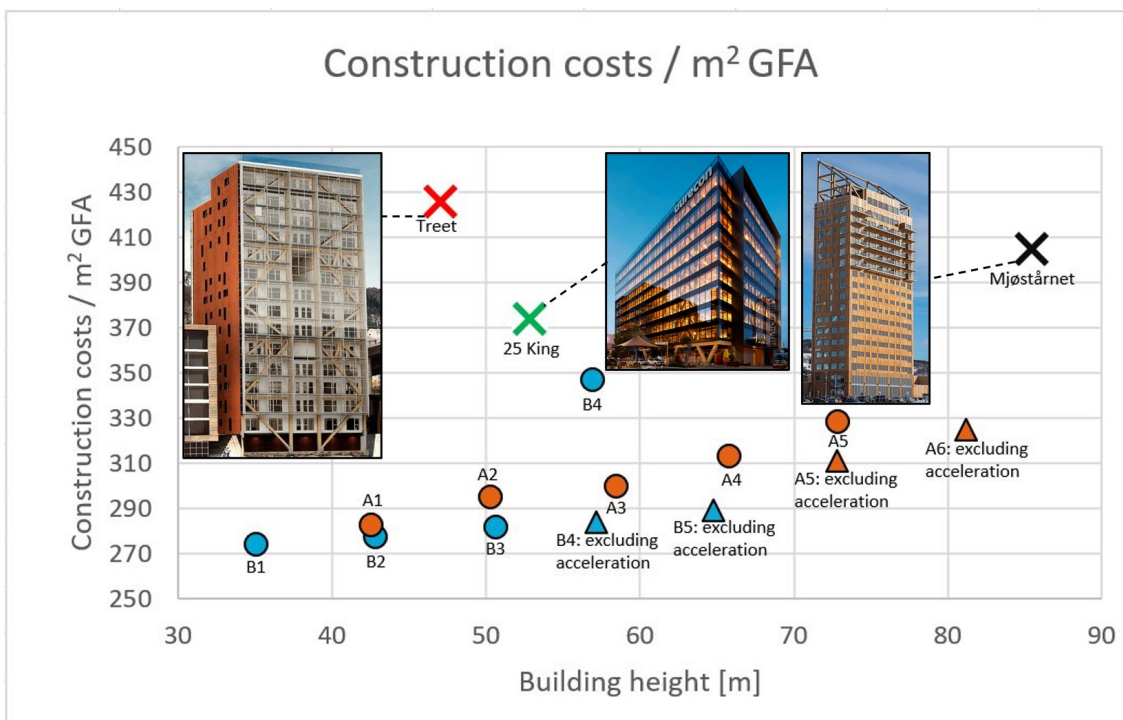


Figure 6.34: Construction costs per m² GFA compared to reference projects

Figure 6.34 shows the comparison regarding construction costs per m^2 of gross floor area and building height for the optimized timber buildings and the reference projects. For the reference projects, the construction costs of the structural system is assumed to equal 9.8% of the total investment costs, as was found for Mjøstårnet using the MAMO calculation in Section 5.12.2. The timber buildings which are created in the tool best resemble Mjøstårnet. So, Mjøstårnet is expected to show roughly the same relation between construction costs per m^2 of gross floor area and building height. However, Mjøstårnet is found to be more expensive than expected. This is argued to be due to the fact that the timber volume in Mjøstårnet is significantly larger than for the optimized building designs, as was shown in Figure 6.32.

The optimized building designs also show favourable results considering construction costs compared to 25King and Treet. Thus, based on these results it can be concluded that this type of stability system is the most favourable. However, it must be noted that direct cost comparison between buildings is difficult, because of the varying boundary conditions. Hourly wages, quality of the building, transportation distances and building norms are boundary conditions which differ for each building. Also, Treet and Mjøstårnet are residential building, which implies stricter design regulations. Lastly, in Australia, where the 25King building is located, the design restrictions regarding fire are much stricter.

6.4.4. Comparison to case studies

The tool obtains the shadow costs and construction costs for all analysed timber buildings. These results are divided by the gross floor area to obtain the shadow costs per m^2 of gross floor area and the construction costs per m^2 of gross floor area. In Figure 6.35 the construction costs per m^2 of gross floor area are compared with the results from "The Square" and "The Rectangle", on which building type A and B are respectively based.



Figure 6.35: Construction costs per m^2 GFA for building types A and B

Figure 6.35 shows the relationship between construction costs per m^2 of gross floor area and the building height, when the acceleration is excluded from the analysis. The construction costs for building type B are smaller than for building type A. But for building type A, higher buildings are attainable.

The construction costs per m^2 of gross floor area for building type B is 4.5 % higher than the concrete variant: The Rectangle. For building type A, the construction costs per m^2 of gross floor area is 7.6% higher than The Square.

The construction costs for buildings A4, A5 and B4 are significantly larger than the construction costs for their counterparts where the acceleration is excluded from the analysis. For these three buildings, the cheapest design can be created when the design is made excluding the acceleration from the analysis and taking the correct design considerations. This will result in a cheaper building than including the acceleration in the analysis and taking no additional measurements to decrease the acceleration.

For the comparison of the shadow costs, carbon sequestration calculation method 1 is used. This method excludes carbon sequestration in the shadow cost calculation. Figure 6.36 shows the comparison of the shadow costs per m^2 of gross floor area.

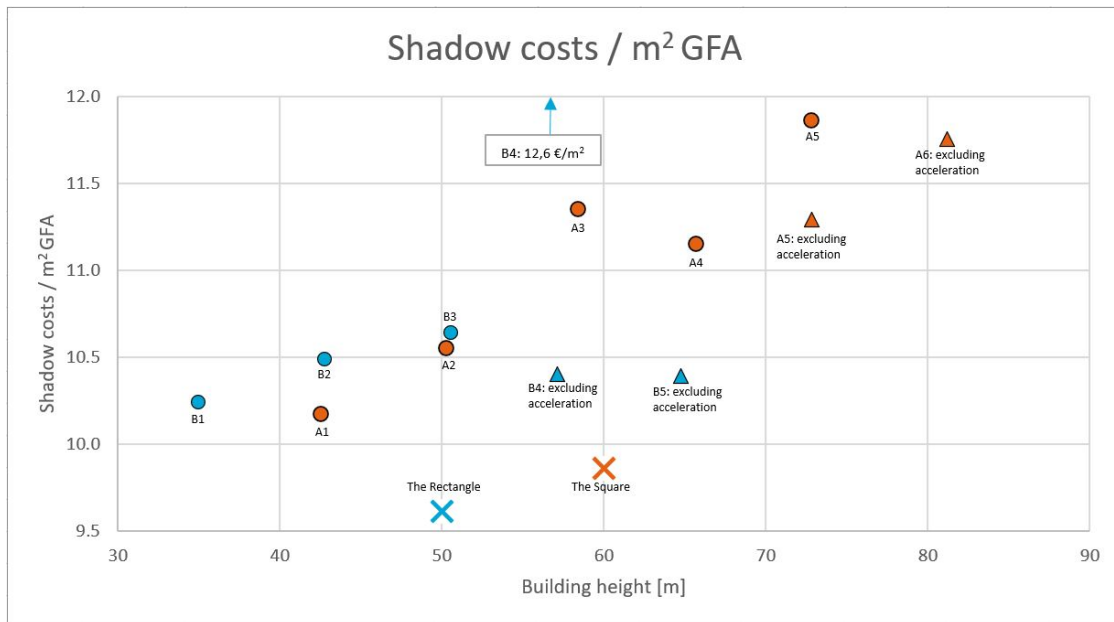


Figure 6.36: Shadow costs per m^2 GFA for building types A and B, using carbon sequestration calculation method 1.

Two observations are made based on Figure 6.36. Firstly, for which building type the shadow costs per m^2 of gross floor are favourable depends on the building height.

Secondly, carbon sequestration is not included in the calculation of the shadow costs of the timber buildings. Hence, the shadow costs per m^2 of gross floor are found to be smaller for the concrete buildings than the timber building designs. However, it could be the case that the shadow costs for timber buildings are favourable if the Pareto optimal timber building designs were chosen which have the lowest shadow costs.

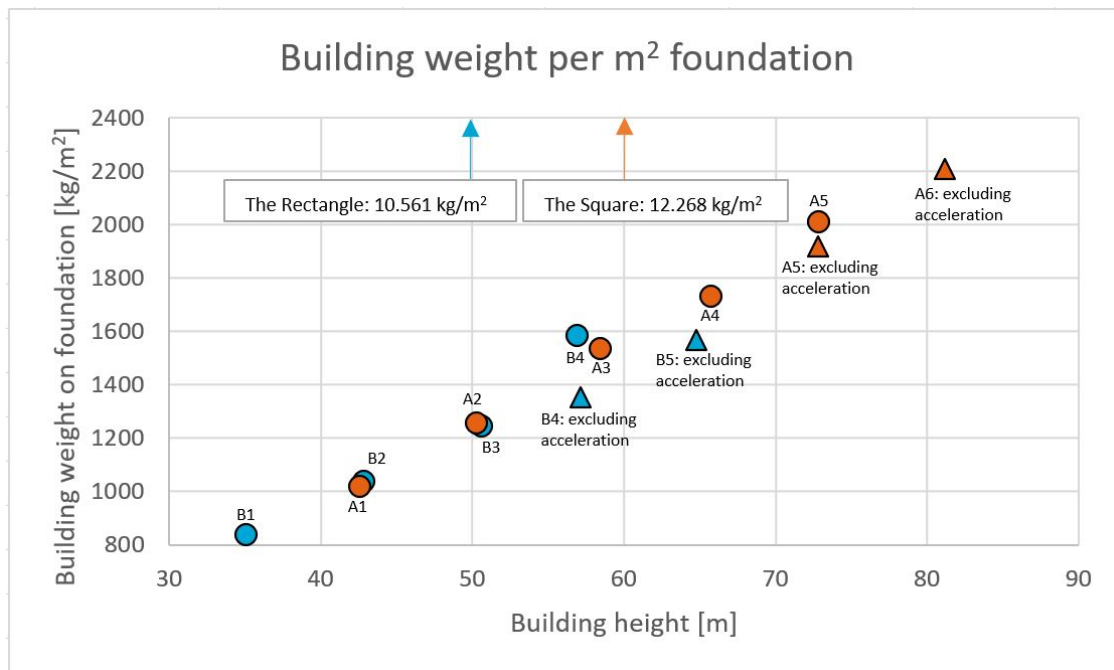


Figure 6.37: Building weight on foundation for Buildings A1-A6, B1-B5, The Square and The Rectangle.

Figure 6.37 depicts the building weight on the foundation for the timber buildings. The building weight included in this calculation consists of the dead-loads of all the structural elements and the facade, and the live-loads times a ψ_2 factor of 0.3. For the facade a dead load of 2 kN/m^2 is used. A clear linear relation is found between building weight on foundation and building height.

The concrete buildings are found to be around 8 times heavier than the timber buildings. This weight difference has an effect on the construction costs of the foundation. Calculation of the building weight of the concrete case-study buildings is found in Annex D.3.

The construction costs of the foundation consists of water management and construction of the ground floor and foundation piles. The weight difference only effects the costs of the foundation piles. According to Tom Borst, a senior structural engineer at Arcadis, for a 8 times lighter building, the costs of the foundation piles can be reduced with 60%. So for Building A3, this results in a reduction of construction costs of $\text{€}160.000 \cdot 0.6 = \text{€}96.000$. For The Square, the construction costs of the foundation are $\text{€}580.000$. So, for building A3 the construction costs of the foundation are $\text{€}484.000$

For Building B3, this implies a reduction of construction costs of $\text{€}175.000 \cdot 0.6 = \text{€}105.000$. For The Rectangle, the construction costs of the foundation are $\text{€}640.000$. So, for building A3 the construction costs of the foundation are $\text{€}535.000$. These construction costs of the foundation are used to compare the construction costs of the concrete and timber building, see Figure 6.38.

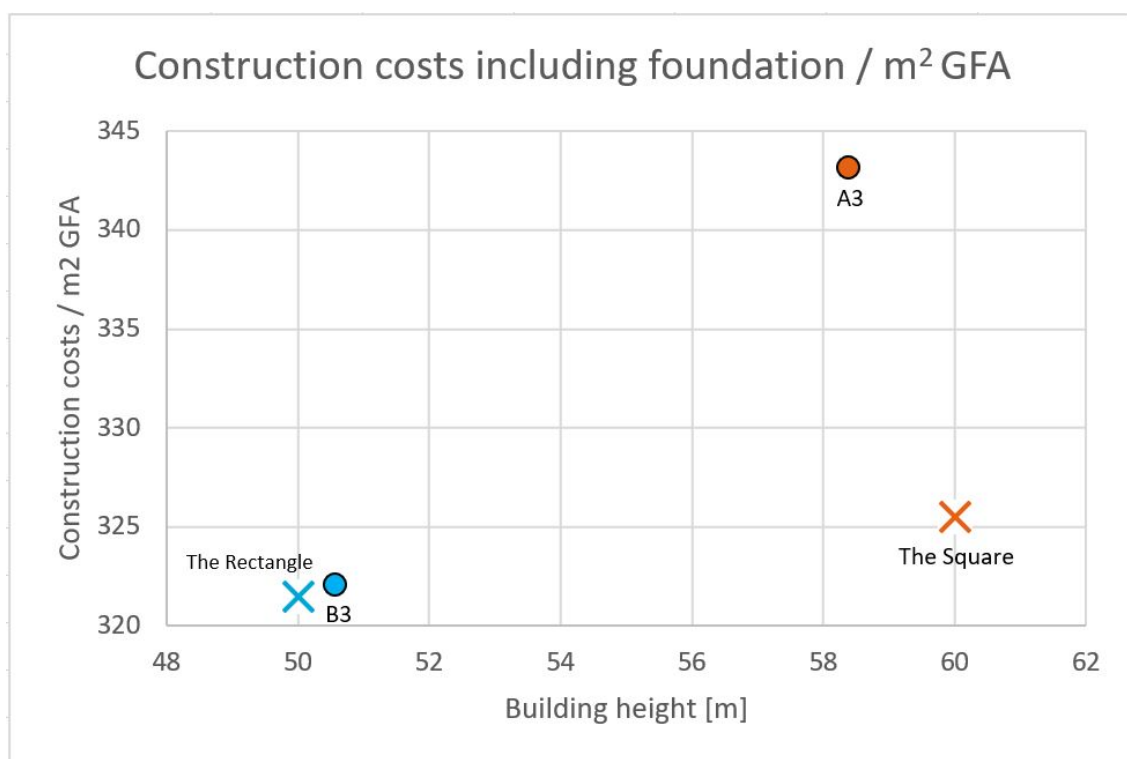


Figure 6.38: Construction costs per m^2 GFA for building types A and B including foundation.

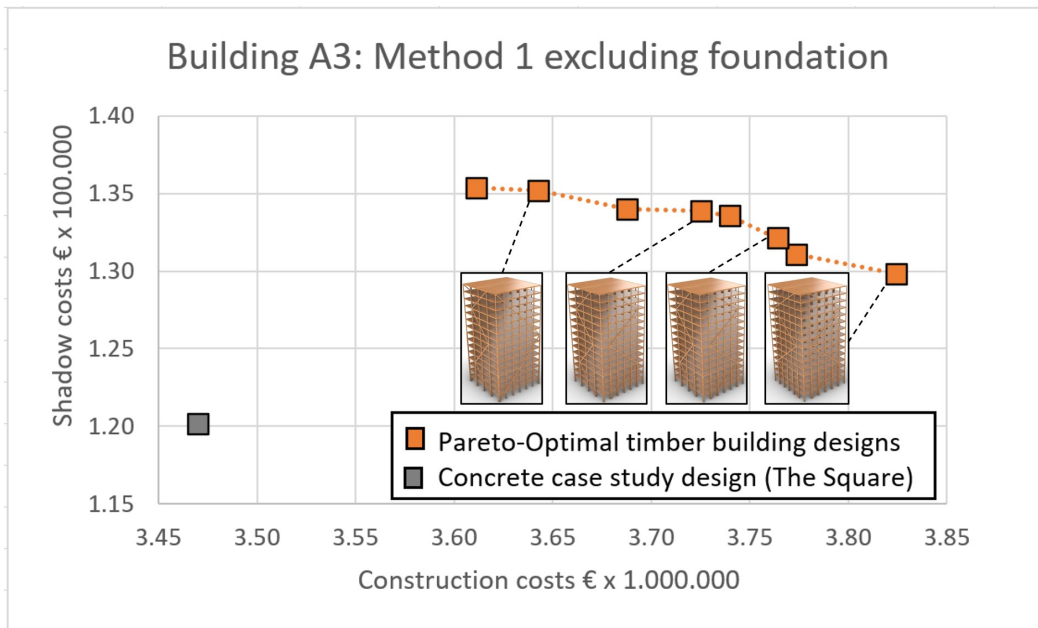
The construction costs for Building B3 is comparable to The Rectangle, while the construction costs for Building A3 and The Square differ with roughly 6%. This indicates that Building B3 is competitive with The Rectangle for construction costs, while Building A3 is not competitive with The Square.

6.5. Case study analysis

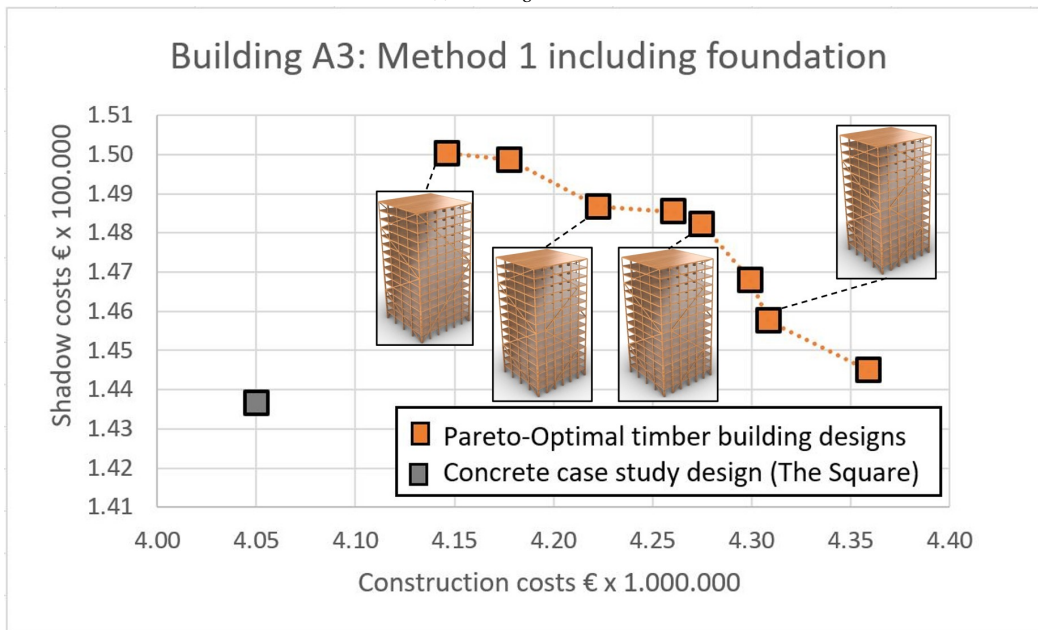
In this section, the Pareto optimal timber designs considering the shadow costs and construction costs are obtained using the tool for the design situations which "The Square" and "The Rectangle" represent. The aim of this section is to examine for what design situation, timber building design can be competitive compared to concrete design.

6.5.1. Construction costs and shadow costs comparison

Figure 6.39 shows the comparison between building A3 and "The Square" for carbon sequestration calculation method 1.



(a) Excluding foundation.



(b) Including foundation.

Figure 6.39: Comparison of shadow cost and construction costs for "The Square" and Building A3 excluding and including foundation, using carbon sequestration calculation method 1.

Figure 6.40 shows the comparison between building B3 and "The Rectangle" for carbon sequestration calculation method 1. In this method, the carbon sequestration is not included in the assessment of the shadow costs.

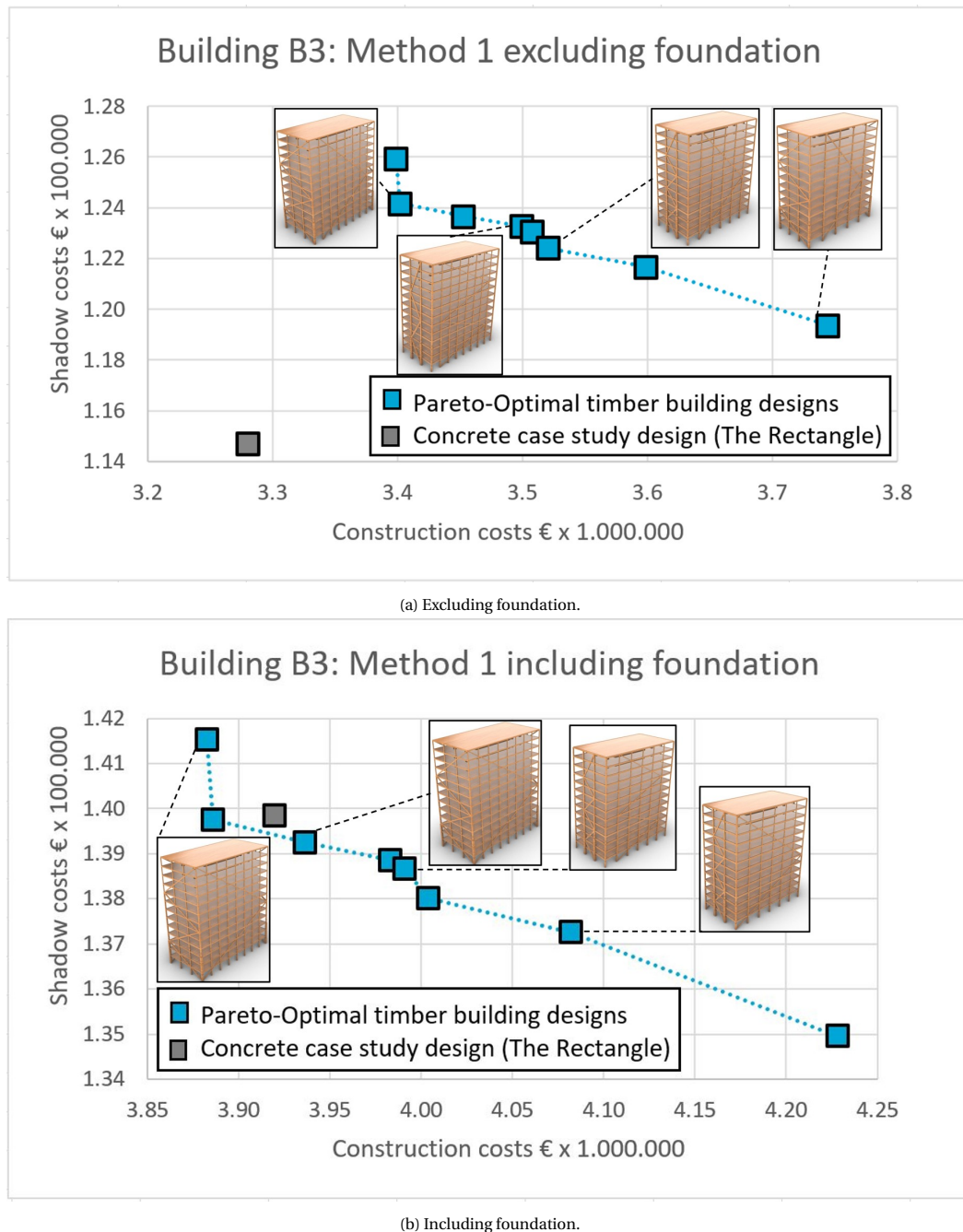


Figure 6.40: Comparison of shadow cost and construction costs for "The Rectangle" and Building B3 excluding and including foundation, using carbon sequestration calculation method 1.

Some conclusions can be made based on Figures 6.39 and 6.40. Firstly, for both design situations, a Pareto front consisting of eight Pareto optimal building designs is found. Secondly, when regarding the visualization of Pareto optimal designs, various diagonal layouts and grid sizes are found to be optimal. Next, when the foundation is included in the calculations, the competitiveness of the timber building improves for both shadow costs and construction costs. This is the case because the timber buildings are approximately eight times lighter than the concrete buildings, see Section 6.4.4. According to Tom Borst, a senior structural engineer at Arcadis, when a building weighs eight times less, 60% less foundation piles are required. However,

in order to obtain a structurally safe building design, a check using load combination ULS1, see Section 4.6 should be performed to check the tensile forces in the foundation for the timber building. A decrease in the amount of required foundation piles effects both the shadow costs and the construction costs. For Building B3, this inclusion of the foundation results in lower construction costs and shadow costs compared to concrete alternative. Secondly, it was found that timber building design alternatives for the design situation which "The Rectangle" represents are more competitive than timber building design alternatives for the design situation which "The Square" represents.

The cause of this competitiveness for timber buildings for the design situation which "The Rectangle" over the design situation which "The Square" represents is argued to be caused by the width of the stability system. For a stability system located in the façade with a smaller width, a stiffer stability system is required, thus resulting in more shadow and construction costs per meter length. Building A3 consists of four medium-width-façades, while Building B3 consists of two short-width-façades and two long-width-façades. It is expected that the decrease in shadow and construction costs for these long-width-façades is larger than the increase in shadow and construction costs for these short-width-façades, compared to a façade with a medium width. This effect is assumed to explain why Building B3 was found to be competitive with the analysed concrete design alternative, while Building A3 was found not to be competitive.

Based on the obtained results it is recommended to consider timber building design alternatives in the design process for the design situation which "The Rectangle" represents. However, it must be noted that marketability also plays a role and various boundary conditions lead to this conclusion. These factors makes it incorrect to conclude that a timber building is a cheaper option than a concrete building for the design situation which "The Rectangle" represents in reality.

Parallel coordinates plot

As is shown in Figures 6.39 and 6.40, various diagonal layouts and grid sizes are found to be optimal. To gain more insight in these combination of input parameters leading to Pareto-optimal timber designs, parallel coordinates plots are created building A3 and B3, see Figure 6.41. This parallel coordinates plot visualizes the input parameters found for the Pareto optimal building designs using coloured lines.

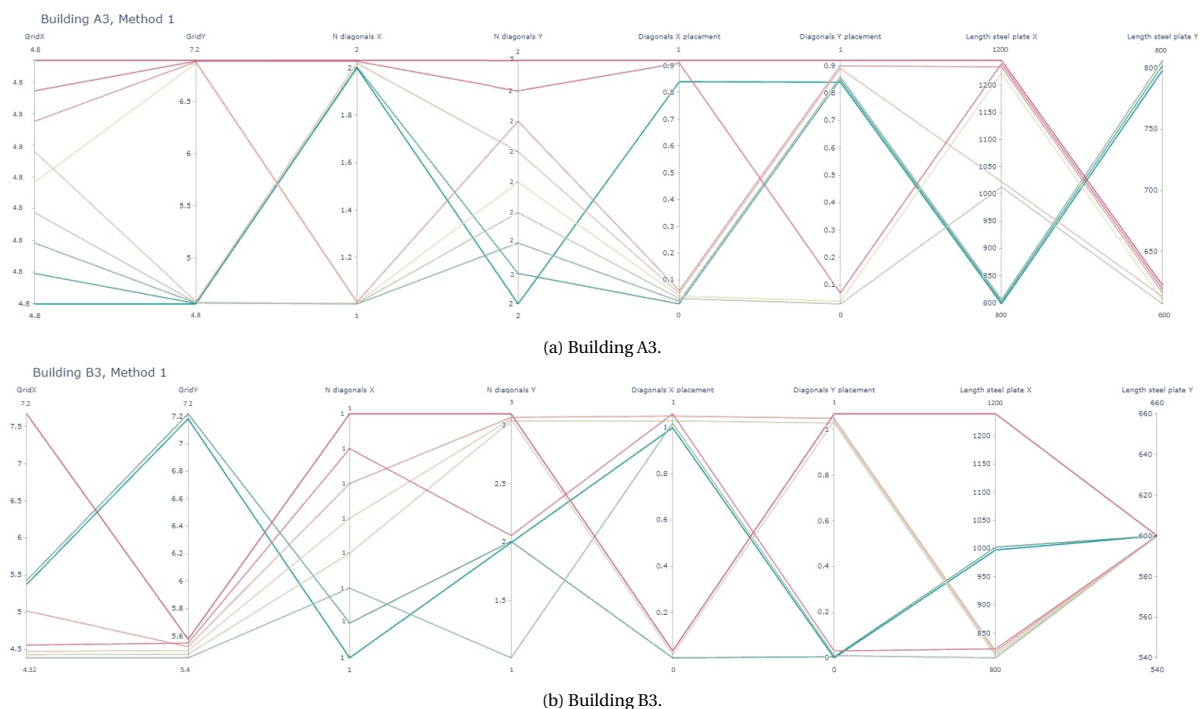


Figure 6.41: Parallel coordinates plot of the input parameters of the Pareto optimal timber building designs for Building A3 and B3, using carbon sequestration calculation method 1

*To make sure lines do not overlap, some lines do not intersect at the exact value. For example for the diagonals X placement, a line intersects at around 0.82. This should be at 1.0.

Figure 6.41a shows the parallel coordinates plot for the optimal building designs for Building A3. For Building A3, the dimensions and load on the stability system are similar in X- and Y-direction. However, the optimal parameters for grid sizes and steel plate length in X- and Y-direction differ. This difference in steel plate length is caused by the methodology used for calculation of connection strength. The steel plate length in the connections is defined as the average steel plate length in the model. A certain percentage of the connections present may fail on strength for this steel plate length, see the first bullet point in Section 5.1.2.. This percentage is set to 33%, as was observed for Mjøstårnet in Section 5.12.1. This percentage accounts for the connections in both X- and Y-directions, which can lead to a different optimal value in both directions.

Figure 6.41b shows the parallel coordinates plot for the optimal building designs for Building B3. The results clearly show the increased stiffness that is required for the stability system in Y-direction compared to the stability system in X-direction. It is found that the amount of times the diagonal crosses the full width of the façade back and forth in X-direction is 1 for all designs. The amount of times the diagonal crosses the full width of the façade back and forth in Y-direction is either 1, 2 or 3. Furthermore, the steel plate length in X-direction is 600mm for all pareto optimal designs, while it varies between 800 and 1200mm in Y-direction.

For both Building A3 and B3 the optimal grid sizes in X-direction are smaller than the grid sizes in Y-direction. This difference is assumed to be caused by the fact that the span of the beams is equal to the length of the grid X, while the span of the floor elements is equal to the length of grid Y.

Building elements

This section evaluates how much each building element amounts to the total construction costs and shadow costs. This is done for The Square, The Rectangle and the Pareto optimal timber building A3 and B3 with the lowest construction costs, see Figure 6.39b and Figure 6.40b

Construction costs Figure 6.42 shows the construction costs per building element for the concrete case-study buildings. Figure 6.43 depicts the construction costs per building element for the Pareto optimal timber buildings A3 and B3 with the lowest construction costs.

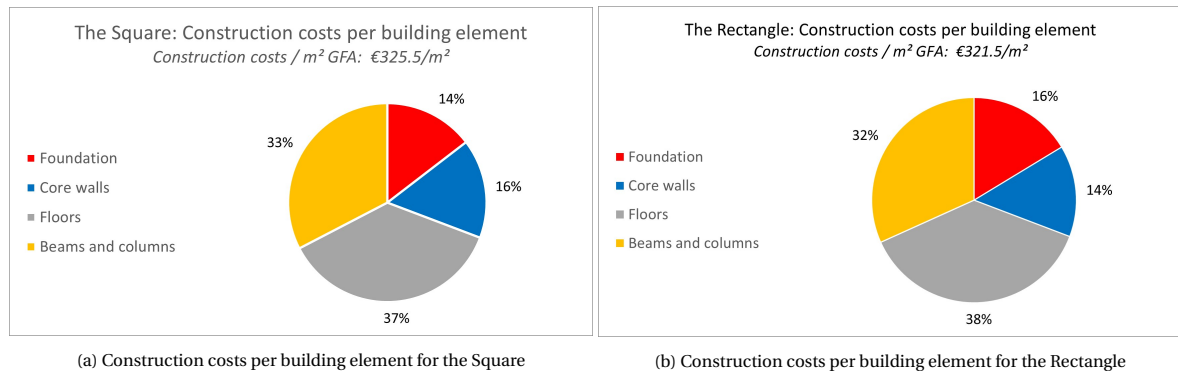


Figure 6.42: Construction costs per building element for the concrete buildings: The Square and The Rectangle

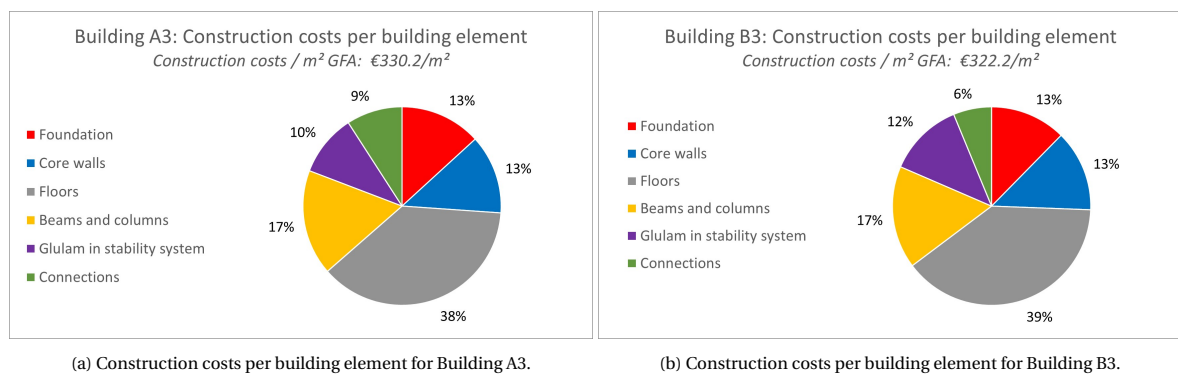


Figure 6.43: Construction costs per building element for the timber buildings: Building A3 and B3

Figure 6.42 and 6.43 show the percentage of the total construction costs over the building elements. For timber buildings, the construction costs for foundation and core walls together is 26% of the total construction costs. For concrete buildings this is roughly 30%. The percentage of total construction costs for the floors are corresponding for both building materials. For the timber buildings, the construction costs for columns, beams and diagonals in the stability system and the connections are roughly 18.5% of the total construction costs. The inner columns are 17% of the total construction costs. For the concrete buildings, the beams and columns consist of roughly 32.5% of the total construction costs.

Shadow costs Figure 6.44 shows the shadow costs per building element for the concrete case-study buildings. These shadow costs are calculated using the MPGcalc 1.2 software, see Annex D.2 [3]. Figure 6.45 depicts the shadow costs per building element for the Pareto optimal timber buildings A3 and B3 with the lowest shadow costs. This calculation is performed following carbon sequestration calculation method 1, see Section 4.5.3. In this method the effect of carbon sequestration is not included in the calculation of the shadow costs.

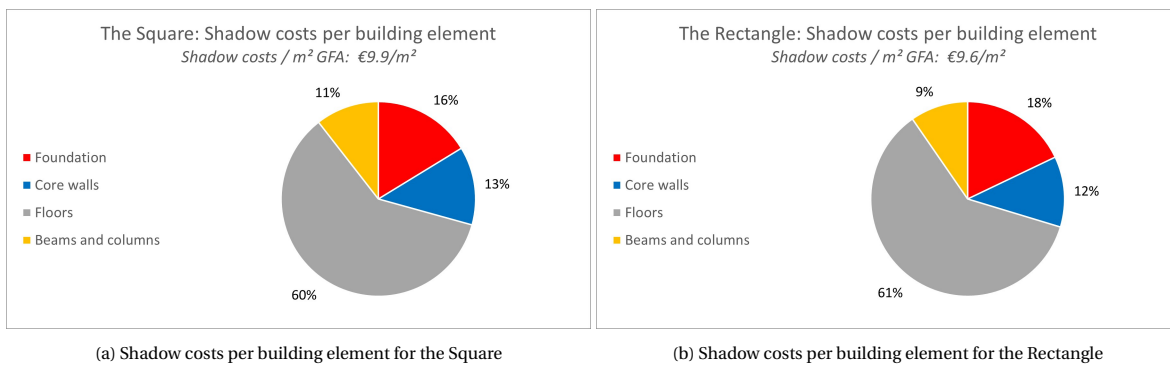


Figure 6.44: Shadow costs per building element for the concrete buildings: The Square and The Rectangle

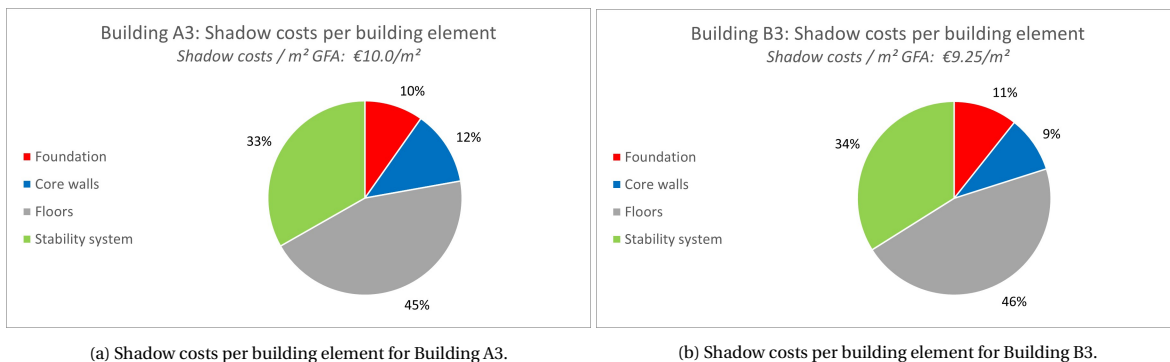


Figure 6.45: Shadow costs per building element for the timber buildings: Building A3 and B3

Again, the impact of the foundation is lower for the timber buildings than for the concrete buildings regarding their shadow costs. This is reasonable since 60% less foundation piles are required for a timber building, due to the low mass. Also, the shadow costs for the floors and core walls are lower for the timber building. However, the stability system of the timber building amounts for one third of the total shadow costs due to the large amount of steel and glulam.

Based on these results and the scope and assumptions of this research, it is suggested that a building with a concrete core stability system and timber floors, beams and columns can result in a design which combines the best parts of both building materials. This type of building is expected to show lower shadow costs than the analysed buildings.

When carbon sequestration calculation method 2 or 3 is used, the shadow costs for all timber elements will decrease. The shadow costs will drop significantly for the floors and the core walls. The shadow costs for the stability system will also decrease, but less due to the shadow costs for the steel connections. Then, it is expected that the shadow costs of fully timber buildings are much lower than for concrete buildings.

6.5.2. Carbon sequestration calculation methods

For both Building A3 and Building B3, the effect of the calculation method of carbon sequestration as defined in Section 4.5.3 are analysed. This concerns the following three methods:

- **Method 1:** Exclusion of carbon sequestration. This is according to NEN-EN 15804 guidelines, which are used in the Netherlands to determine the environmental impact.
- **Method 2:** Inclusion of carbon sequestration and re-emittance. This is argued to be the most accurate calculations method by Hawkins (2021) in the IStructE guide [65].
- **Method 3:** Inclusion of carbon sequestration and BECCS. This is a potential scenario in the future where the carbon from biomass is captured and stored. Since the lifespan of a building is aimed at 50-years. This might be implemented for the timber buildings which are constructed soon.

So, there will be six situations for which separate optimizations are ran, see Figure 6.46.

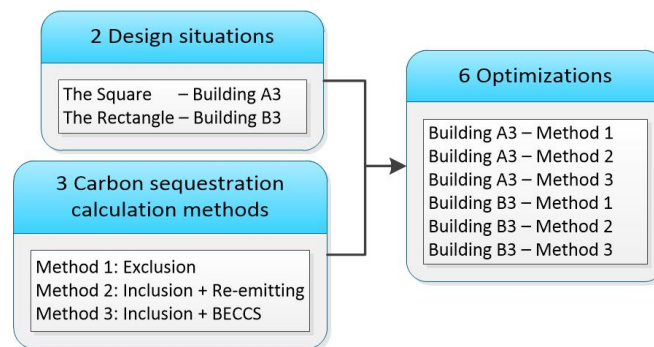


Figure 6.46: Analysed design situations

For every calculation method an independent optimization is ran using the tool. The results are shown in Figure 6.47 and 6.48 for both Building A3 and B3.

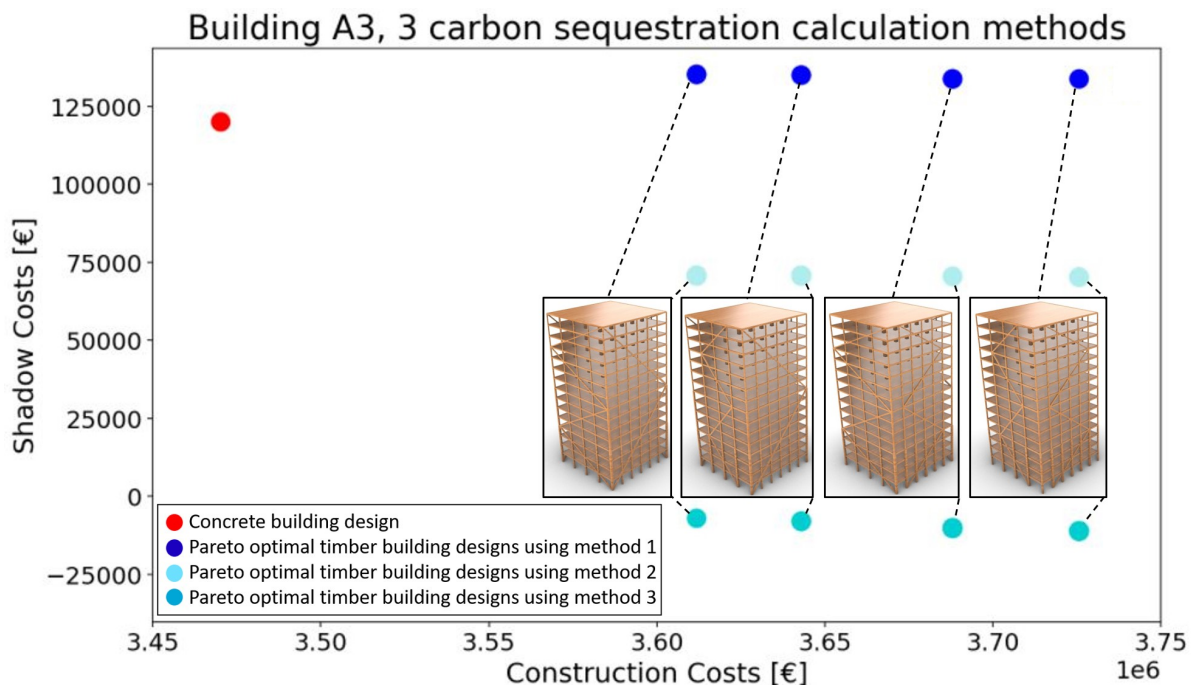


Figure 6.47: Comparison of shadow cost and construction costs for "The Square" and Building A3*.

*Only a part of the Pareto front is depicted. The four Pareto optimal building designs with the lowest construction costs are shown in order to increase the readability of the Figure.

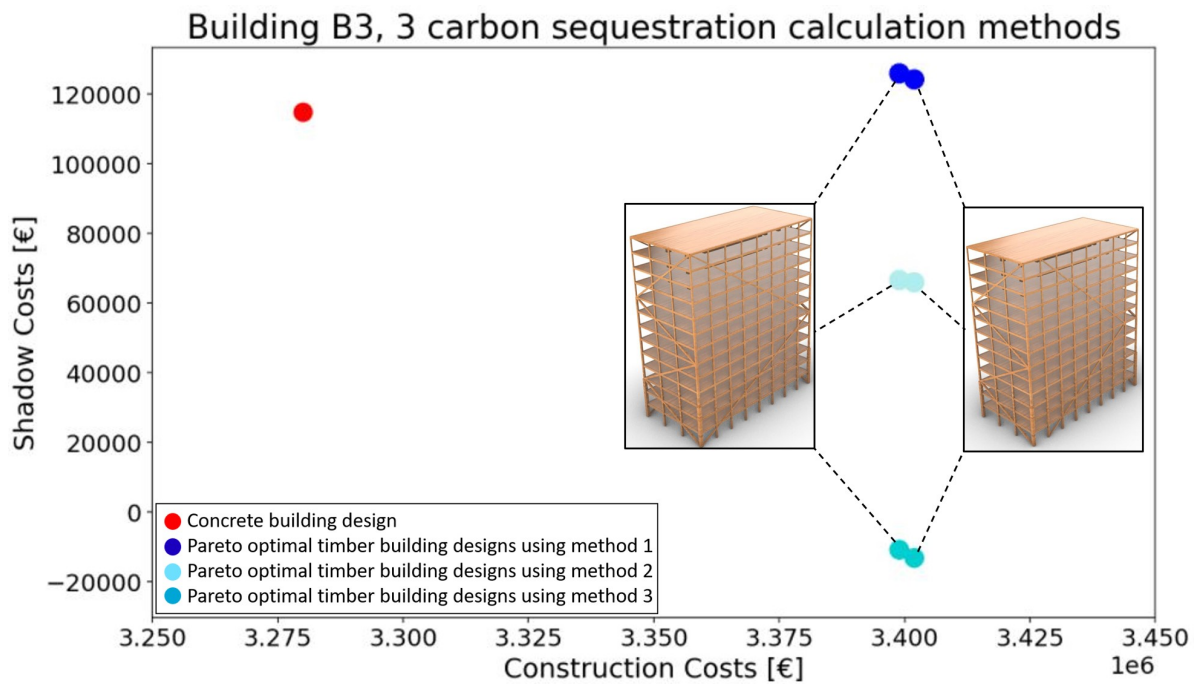


Figure 6.48: Comparison of shadow cost and construction costs for "The Rectangle" and Building B3**.

**Only a part of the Pareto front is depicted. The two Pareto optimal building designs with the lowest construction costs are shown in order to increase the readability of the Figure.

Several conclusions can be made based on Figure 6.47 and Figure 6.48. Firstly, the obtained shadow costs for the Pareto optimal timber designs for the three calculation methods accurately resembles Figure 4.26. Secondly, regardless of the method for calculation of carbon sequestration, the same Pareto optimal building design with the lowest construction is obtained. Lastly, the used method for carbon sequestration calculation in the determination of the shadow costs has a massive impact regarding the comparison of the environmental impact between a concrete and timber building. Three different assessment methods for the inclusion of carbon sequestration are defined in this research. The use of timber and concrete in the structural system was found to provide comparable results when the effect of carbon sequestration is disregarded as is done in carbon sequestration method 1. The inclusion of the effect of carbon sequestration in the calculation of the shadow costs as is done in calculation method 2, results in a reduction of shadow costs of approximately 40% compared to a similar concrete building. Lastly, the inclusion of the effect of carbon sequestration in combination with carbon capture and storage at the end-of-life stage of the building, as calculated using carbon sequestration method 3, can even result in a negative carbon footprint of the structural system.

6.6. Conclusion

- Multi-Objective Genetic Algorithm** For both case studies, approximately 14.000 timber building designs make up the design space. In Section 6.2.1 it is found that a full generation, evaluation, and verification of a timber building design takes 1.22 seconds on average using a 2.4 GHz processor. Furthermore, the Octopus plug-in is found to efficiently determine Pareto optimal building designs. As half of the Pareto optimal building designs are obtained when only 6.25% of all possible building designs have been analysed. No errors or unrealistic results were obtained when using the tool.
- Grid size** For both Building A3 and B3 the optimal grid sizes in X-direction are smaller than the grid sizes in Y-direction, see Figure 6.41a and Figure 6.41b. This difference is assumed to be caused by the fact that the span of the beams is equal to the length of the grid X, while the span of the floor elements is equal to the length of grid Y. Thus, the construction and shadow costs decrease more for short beam spans than for short floor plate spans.
- Steel plate length** A longer steel plate in the steel plate and dowel connections in the stability system results in a stiffer connection. Due to this stiffer connection, the stability system will act more as a moment frame rather than a truss system. This results in a decrease in cross section sizes of the timber elements, which decreases the timber volume of the stability system, see Figure 6.10. Since the cross section sizes of timber elements decrease for the ULS check, the influence of the SLS check increases compared to the ULS check, see Figure 6.13. The definition of an average steel plate length in millimetres and using the obtained strength and stiffness properties of this connection in the calculations of the structural system was found to provide accurate results. This approach for the determination of required steel plate length was found to provide a steel weight which is in line with the steel weight found in the reference project Mjøstårnet.
- Diagonal angle** The optimal diagonal angle is found to be dependent on the dimensions of the stability system and the wind forces on it. Thus, the floor plan dimensions influence the optimal diagonal angle. For a square floor plan, the optimal diagonal angle is roughly 36%. While for a rectangular floor plan with a ratio of 2:1, the optimal diagonal angle is 33% in the long direction and 18% in the short direction, see Figure 6.31. So, a lower optimal diagonal angle is obtained when the forces are larger and the width of the stability system is smaller. This is also true for Mjøstårnet, where the diagonals are positioned under an angle of 27.4° in the short dimension.
- Diagonal layout** Based on the analysis in Section 6.3.2 it is concluded that a diagonal layout where the diagonals cross the columns and beams in the same point is preferred over a diagonal layout where the diagonals, beams and columns do not cross in the same point. A more efficient transfer of forces is obtained if the diagonals, beams, and columns cross in the same point. A more efficient transfer of forces leads to small bending moments in the structure leading to smaller required cross sectional dimensions and thus a cheaper structure.
- Utilization factor** The average utilization factor for a structural system grouped in 12 element groups was found to be around 0.6, disregarding the beams. No relation was found between this average utilization factor and the slenderness, positioning of diagonals or the steel plate length. The normative utilization of the beams in the stability system is found to be below 0.25 for all analysed stability systems, see Section 6.3.2. This is due to the design choice to dimension the beams in the stability system similarly as the beams in the gravitational system.
- Deflection** Each stability system is optimized based on the SLS and ULS requirements. To gain insight into which unity check is normative, the 'deflection unity check' is introduced. First, the stability system is optimized based on the ULS requirements. Next, the horizontal deflection of this stability is determined and using the maximum horizontal deflection of $\frac{h}{825}$, as specified in Annex A.4.3, the 'deflection unity check' is determined. For the analysed Pareto optimal buildings, the deflection unity check was never found to be over 1.0, See Figure 6.30. So the horizontal deflection is never normative. Based on Figure 6.30, this research suggests the presence of a linear relation between slenderness and deflection unity check. This implies that the deflection becomes normative, instead of the utilization factor, at a certain slenderness. This is suggested to occur at a slenderness of approximately 4.5, by extrapolating the linear trend-line.

- **Acceleration** According to Figure 6.26, the along-winds acceleration is normative for a slenderness greater than 2.35 for a timber office building with a braced tube structure. This result is based on a terrain category of 3 and a wind zone of 1. The slenderness of building B3 is slightly below this limit. When acceleration becomes normative, the results created by the tool become infeasible. The tool will use small grid sizes and big cross sections to create a model with sufficient mass to satisfy the acceleration criteria. This results in infeasible building designs. It is argued that increasing the total mass by replacing Kerto-Ripa floors with concrete floors is a feasible design choice to satisfy the acceleration requirements as given in NEN-EN 1990-1-1.
- **Normative design criteria** For both Building A3 and Building B3 the ULS check and the connection unity check are found to be normative in Pareto optimal building designs. The effect of the Cross-wind response and the tension forces in the tension ties are found to be negligible.
- **Building weight and foundation** For the obtained Pareto optimal timber buildings, there is a linear relation found between the building weight and building height. The mass of the Pareto optimal timber building designs is approximately 8 times smaller compared to concrete design alternatives, see Figure 6.37. This mass includes the live-loads times a ψ_2 factor of 0.3 and the dead-loads of all the structural elements and the façade. Tom Borst, a senior structural engineer at Arcadis argues that this lower building weight on the foundation results in a reduction of required foundation piles of 60%. Including this reduction of foundation piles in the construction costs calculation results in a comparable construction costs per m^2 of gross floor area for Building B3 and the concrete design alternative.
- **Construction costs** The construction costs per m^2 of gross floor area for building type B are found to be more competitive to its concrete alternative than building type A is to its concrete alternative, see Figure 6.35. Including the reduction of foundation piles in the construction costs calculation results in a comparable construction costs per m^2 of gross floor area for Building B3 and the concrete design alternative. The construction costs per m^2 of gross floor area for the Pareto optimal design with the lowest construction costs for Building A3 are 2.7% higher than the concrete design alternative, see Figure 6.38.
- **Shadow costs** The following statements are made for carbon sequestration calculation method 1. The shadow costs per m^2 of gross floor area for Pareto optimal timber building designs are approximately 5 to 10 % higher than for concrete design alternatives when disregarding the foundation, see Figure 6.36. When the foundation is included in the shadow costs calculation, the shadow costs per m^2 of gross floor area for Pareto optimal timber building designs are found to be similar to concrete design alternatives.
- **Carbon sequestration calculation methods** The obtained shadow costs using the three defined carbon sequestration calculation methods are comparable with the expectations as proposed by Hawkins (2021) [65]. Figure 4.26 shows Hawkins expectations. When comparing these expectations to Figures 6.47 and Figures 6.48 the order sizes are found to be comparable. The use of timber and concrete in the structural system was found to provide comparable results when using carbon sequestration method 1. The inclusion of carbon sequestration in the calculation of the shadow costs as is done in calculation method 2 results in a decrease in shadow costs of approximately 40% as is seen in Figure 6.47 and Figure 6.48. The usage of carbon sequestration method 3 results in a negative carbon footprint of the structural system for the analysed buildings.
- **Building elements** The percentage of construction costs per building element are approximately similar for timber and concrete building designs. For carbon sequestration calculation method 1, the percentage of shadow costs per building element are smaller for the foundation, core walls and floors for the timber building. The stability system of the timber building encompasses one-third of the total shadow costs. It is suggested that a building with a concrete core stability system and timber floors can result in a design that combines the best parts of both building materials, see Section 6.5.1.

7

Discussion

This research aims to identify design situations where timber high-rise design can be competitive to concrete design alternatives using a Multidisciplinary Design Optimization approach. This is accomplished by developing a tool within Rhinoceros, using Grasshopper software. This tool aims to indicate in which design situations timber high-rise can be competitive to a concrete design alternative, considering the combination of properties for shadow costs and construction costs. The tool is tested using a case study, which provides insights required to answer the research questions. The optimal timber building designs referred to as Building B3 were found to be competitive with the analysed concrete design alternative. For Building A3 this was not the case. Based on this result, two conclusions can be made considering all boundary conditions of this tool as discussed below. Firstly, it can be concluded that a design situation with a rectangular floor plan is favourable over a design situation with a square floor plan. Secondly, it can be concluded that a design situation with a building height of 50 meter is favourable over a design situation with a building height of 60 meter.

In this approach, several design choices and assumptions are made which can influence the results. These possible influences on the results, limitations, and general findings are reported below. This is done considering the developed tool in Section 7.1. Next, in Section 7.2 the results are discussed.

7.1. Discussion of tool

MDO Tool

- The tool optimizes a timber building considering the combination of properties for shadow costs and construction costs, taking into account the structural and architectural constraints. Because of the scope of this approach, a Pareto-optimal building design according to the tool might not be optimal in reality. Since the tool does not consider certain effects such as the optimization of other building elements, the building physics, maintenance, and implementation of installation.
- As discussed in Chapter 5, the tool dimensions the generated buildings based on the SLS and ULS requirements. Subsequently, the generated building designs are verified by determining the unity checks for the along-wind and cross-wind acceleration, connection strength, wind friction, and the forces in the tension ties. The tool excludes the building designs which do not meet the verification criteria from further analysis. However, an approach including an iterative process, where the design is adapted until it meets the verification criteria, might increase the number of obtained Pareto optimal designs. However, this approach is expected to increase computational time significantly, since an iterative process requires a new calculation for each iteration.
- The tool is verified in Section 5.12, by comparing Mjøstårnet to a model version using the tool. This comparison is performed regarding the structural, economical, and environmental discipline. Based on this comparison the tool is concluded to be accurate for a design in the conceptual design phase. The tool is verified for one reference project since only one reference project exists for which a fair comparison can be made. However, since the verification is based on one reference project, the certainty of this verification is limited. To add certainty, some individual elements of the building are verified. This is done for the connections, the core and the stability system, in Annex B.1, B.7, and B.8 respectively.

- While the columns, beams, and diagonals in the stability system are grouped into thirteen groups, only one connection is defined to represent all connections in the stability system in each direction. Definition of only one average connection results in inaccuracies in building design. Grouping connections and designing the connection based on their location in the stability system and their required strength and stiffness results in a more accurate design.
- The tool positions the diagonals according to the "number of diagonals" and "placement of diagonals" parameter. This approach does not take into account the intersection of diagonals with beams and columns, which does influence the results according to Section 6.3.2.
- The tool optimizes the timber buildings based on their gross floor area as opposed to their net floor area. This results in a preference for smaller grid sizes. The effect of smaller grid sizes on the marketability of a building is not considered but can be an incentive to set additional requirements in the tool.

Structural discipline

- For all building elements, two or more load combinations are used for calculation in the tool. These load combinations, as defined in Section 4.6.1, are assumed to be normative for the considered building elements.
- The Optimize Cross Section component of the Karamba3D plug-in is used to dimension the columns and diagonals in the stability system. This component is verified in Annex A.6. Although the Optimize Cross Section component provides accurate results overall, there are two disadvantages regarding using this tool in timber building design. Firstly, the tool uses the requirements as specified in Eurocode 3 for steel structures for the determination of buckling. Secondly, this component is based on materials for which the compressive and tensile design strength are similar. But, for engineered timber, the maximum tension design strength of the material is roughly 80% of the maximum compression design strength in the strong direction. To create a structurally safe structure, the compressive design strength is set equal to the tensile design strength. This way, the compression design strength is smaller than in reality, but this conservative assumption might be required since buckling is not accurately regarded.
- All columns, beams, and diagonals in the structural system are grouped in thirteen different groups. Elements for which the optimal cross sections are expected to be comparable are grouped. The normative element in each group is found and the required cross section is calculated. Then, this cross section is applied to the full group. This results in an over dimensioning of building elements, but increases the modularity and buildability, thus providing realistic results.
- Only square cross sections are considered for dimensioning of columns and diagonals in the stability system, excluding the corner columns. This may result in over dimensioning of building elements.
- The steel plate and dowel connection is dimensioned assuming a straight transfer of forces. However, some steel plate and dowel connections transfer forces under an angle. The effect of this is not considered in the tool.
- A wind force that acts on the building under an angle compared to the façade is not analysed in the calculation of the stability system. Only wind forces that act orthogonally on the building surface are considered.
- Some structural design considerations are not analysed in this tool. This includes torsional and cross wind acceleration, earthquake resistance, façade deflection, the wind suction on the façade, and robustness.

Architectural discipline

- All floor elements are dimensioned such that they satisfy the acoustical requirements for vibrations. However, the acoustical requirements for connections are not analysed. This may affect the construction costs since acoustical damping of connections is a big challenge in timber buildings.

Environmental discipline

- Generally, the embodied energy and the operational energy consist of 30% and 70% respectively of the total energy consumption during the lifetime of a building. However, with the rise of energy-neutral buildings, the emissions caused by operational energy decreases, thus increasing the relative impact of embodied energy. The impact of the usage of sustainable materials is thus increasing. In this research, only the embodied energy of the structural system is considered. So, the optimization of the shadow costs only considers a small part of the total energy consumption during the lifetime of a building.
- Calculation of the environmental performance is affected greatly by the used EPD data. EPD data provided by manufacturers can vary greatly for the same material. Therefore, it is crucial to assess this data thoroughly, and use EPD data that is independently researched. The used EPD data is mentioned in Annex C.1.

Economical discipline

- The economical discipline considers the construction costs using the MAMO (*Materiaal, Arbied, Materieel, Onderaanneming*) rules for budgeting. Accordingly, the construction costs are calculated by summing the costs for materials, labor, equipment, and subcontracting. However, the following cost influencers are not considered in this calculation.
 - **Market** The market is dependent on competition, supply, and demand.
 - **Construction time** A faster construction time results in a reduction of construction costs. Because of the high running costs of construction, and since the building can be rented out earlier [47].
 - **Number of repetitions** It should be aimed to use as many identical building elements as possible since fewer errors are made by factory workers for repetitive tasks [59].
 - **Bulk** Average prices drop when a greater quantity is bought.
 - **Availability** The availability of sustainably harvested engineered timber fluctuates, which impacts the costs.
- For the calculation of indirect costs in the concrete buildings, three categories are included. For each category, a percentage is set, which is multiplied by the total direct costs, to obtain the indirect costs. These categories and their percentage are mentioned below:
 - General implementation costs: 10%
 - General costs, profit, and risk: 9%
 - risk further plan elaboration: 5%

So, the total indirect costs are equal to the total direct costs multiplied by 24%. It is debatable if the inclusion of these factors provides a fair comparison between the concrete and timber buildings.

- This research only analysis the construction costs of the structural system. The structural system considers only a small part of the total investment costs. For Mjøstårnet the construction costs of the structural system were found to amount to 9.8% of the total investment costs, see Section 5.12.2.

7.2. Discussion of results

For the design situation based on the concrete building "The Rectangle", the Pareto optimal timber building designs, referred to as Building B3, are found to be competitive with "The Rectangle". This is a questionable result since timber buildings are usually mentioned to be 5 to 10% more expensive compared to concrete buildings. The optimization process is expected to decrease these construction costs for timber buildings, but not up to this extent. It is argued that the assumptions made for the economical discipline as mentioned above are inaccurate.

Market value Apart from the construction costs, a difference in market value between the two buildings might influence economical considerations. Market value differences are expected to be caused by the following factors.

- The obtained Pareto optimal designs for Building B3 with lower construction costs compared to The Rectangle, have a grid size of 5.4m and 7.2m, see Figure 6.41b. The Rectangle has grid sizes of 7.2m and 8.6m. This lack of open space decreases the market value of a timber building.
- A timber building is regarded as sustainable and might increase the public opinion regarding the sustainability of a company, thus increasing the market value.
- Several studies have shown exposed timber has several health benefits for occupants, such as reduced heart rate, blood pressure, and stress levels, and improvement of emotional state and level of self-expression of inhabitants [14]. This increases the market value.

Optimal buildings The obtained Pareto optimal buildings using the tool might not prove to be the most optimal in practice for several reasons:

- The tool concerns four disciplines while the Architecture, Engineering, and Construction industry consists of various disciplines. Furthermore, the tool only concerns the structural system, not all building elements present in a building.
- While the elements in the stability system and all columns are grouped, the steel plate and dowel connections in the stability system are not grouped. Grouping of connections increases the accuracy of the model.
- Several design considerations are outside the scope of this research: the acoustical requirements for connections, marketability, additional cost influences, torsional and crosswind acceleration, earthquake resistance, façade deflection, wind force under an angle, the wind suction on the façade and the robustness.
- In timber design, some building regulations are still missing or are very conservative causing overdimensioning of timber structures. These consist of the damping coefficient of the building, the regulations for floor vibrations, and the regulation disregarding the exclusion of carbon sequestration in the assessment methods for shadow costs.

Case-study results The accuracy of results obtained using the tool is decreased due to:

- The buildings which are created using the tool are based on discrete input parameters, limiting the accuracy and size of the design space.
- The developed tool provides results satisfactory for design in the conceptual design phase when verified by modelling Mjøstårnet and comparison of this model to the actual building, see Section 5.12. So, the tool is only verified based on one reference project.
- The complete Pareto front is only found when performing a brute force calculation, so there is always the possibility that some Pareto optimal buildings are present but not identified
- The building designs used in Section 6.3 are based on an optimization with generation and population size of 30. According to Section 6.2, this implies approximately half of the Pareto optimal building designs are found. This decreases the accuracy of the analysis performed in Sections 6.3 and 6.4.
- The stiffness of connections are included in the ULS and SLS check of the stability system. So, the stability system will act as something between a truss system and a moment frame.
- The beams in the stability system are set to have the same dimensions as the beams in the stability system. This is found to result in overdimensioning of the beams in the stability system, as found in Section 6.3.2.
- The obtained thickness's of the CLT plates in the core sizes are smaller than the thickness found in the 25King and Mjøstårnet reference projects. For 25King this is expected to be caused due to the stricter fire regulation norms in Australia. The cause for this in Mjøstårnet is unclear.

8

Conclusion

This research aims to identify timber high-rise designs that can be competitive to concrete design alternatives using the Multidisciplinary Design Optimization method. A tool is developed in Grasshopper, which generates, validates, and optimizes timber building designs. Using this tool, it can be determined in which design situation timber high-rise can be competitive to a concrete design alternative, considering the combination of properties for shadow costs and construction costs. The tool is verified using a reference project and tested using two case studies, which provides insights required to answer the research question and sub-questions.

In this chapter, the conclusions based on the conducted research are presented. These conclusions provide an answer to the research questions.

8.1. Answer to research questions

First the sub-questions are answered, which provides knowledge, data, and conclusions. Conjointly, these sub-questions answer the main research question.

8.1.1. Sub-questions

1. (a) How can the MDO method be applied to this design problem?

For the development of the MDO tool, four separate layers are created, as proposed by Jansen (2014) tool [86]. The Grasshopper visual programming language, which runs within the Rhinoceros CAD application forms the basis for the tool development. Since the start of the development of the tool, the trade-off between accuracy and computational time was considered. The following design choices were made to decrease the computational time:

- **The building model is simplified.** This is done by grouping building elements, taking average values for connection design, and setting verification requirements that prevent the need for an iterative process for the design of one building.
- **The building simulation methods are simplified.** The building simulation methods for the environmental and economical performance are calculated using simple formulas. The stability system is calculated in 2D using the Karamba3D plug-in. The dimensioning of the other parts of the structural system is done using custom nodes based on Python.
- **Reducing design variables.** The number of design variables are reduced by using discrete variables. Furthermore, the chosen input for which the tool optimizes the building is carefully selected.
- **Simplifying the MOGA.** In Section 6.2.1 the effect of chosen generation and population size and accuracy of the results is analysed. It was found that half of the Pareto optimal building designs are obtained when only 6.25% of all possible building designs have been evaluated.

All these design choices decrease the computational time of the developed tool, while the accuracy remains acceptable for design in the conceptual design phase. It was found that a full generation, evaluation, and verification of a timber building design requires 1.22 seconds on average using a 2.4 GHz processor.

(b) What are the limitations of the use of MDO for this design problem?

The use of MDO for this design problem is limited by the simplifications required to create a generic model which can be optimized. Furthermore, these simplifications decrease the computational time and complexity of the tool. The most significant simplifications are:

- Discrete input is used for optimization of the building.
- Building elements are grouped to decrease the complexity of the building design. Elements in such groups are optimized for the most normative case in the group.
- All steel plate and dowel connections in the stability system have similar properties, for which the tool optimizes.
- For the diagonals and columns, except the corner columns, only square cross sections are considered in the optimization.

(c) Which design considerations require thorough examination when designing a timber building?

- **Timber is an anisotropic material** The strength perpendicular to the grain is significantly smaller than parallel to the grain.
- **Acoustics** Main challenges are the human-induced vibrations in floors and connections
- **Low self-weight** This can result in problems with wind-induced acceleration.
- **Connection design** Several design considerations must be made considering changes in moisture content, shear strength, tensile strength perpendicular to the grain, fire design, and costs.

(d) What type of structural system is appropriate for a 50 to 70 meter high fully timber building? A braced tube structure, as is used in the only three fully timber buildings which reach a height over 45 meter: Treet, Mjøstårnet, and 25 King.**(e) How can the optimization goal of each discipline be defined and modelled?**

The architectural and structural disciplines are defined as constraints in this research. The building must meet all regulations regarding daylight, storey height, acoustics, and structural safety.

The environmental discipline only considers the embodied energy. An environmental performance is calculated, see Equation 8.1, based on the Milieu Prestatie Gebouwen (MPG) calculation. Furthermore, three calculation methods for the assessment of carbon sequestration are defined, see Section 4.5.3. These calculation methods affect the Environmental Product Deceleration (EPD) data which is used to determine the environmental performance.

$$\text{Environmental Performance} = \text{EPD data} \cdot \text{Material quantity} \cdot \text{Shadow price per unit} \quad (8.1)$$

Regarding the economical discipline, only the construction costs are considered. For the determination of the economical performance, the MAMO (*Materiaal, Arbied, Materieel, Onderaanneming*) rules for budgeting are used. Accordingly, the construction costs are calculated by summing the costs for materials, labor, equipment, and subcontracting.

2. (a) **How can an integrated MDO tool be developed which provides accurate results for this design problem?** Using Grasshopper, timber building designs are generated, evaluated and optimized. This process starts with the definition of a set of design situation dependent input and input for which the tool optimizes. Using this input, and a minor structural calculation, the geometry of the building is obtained. This geometry indicates the location of building elements and connections. Next, the cross section sizes of the elements in the structural system are determined using custom node calculations and Karamba3D's Optimize Cross Section component. This results in a database with all required timber elements and connections. Using this database, the economical and environmental performance can be determined. After the building is checked for several verification criteria, the obtained results for economical and environmental performance are transferred to the optimization component. For this optimization component, the Octopus plug-in is used. This plug-in uses the SPEA-2 Multi-Objective Genetic Algorithm to predict the input which creates an optimal timber building design. By defining this new input, a new iteration starts. This cycle of creating new generations stops when the solution reaches the convergence criteria, or after a set amount of iterations, called the maximum iteration number.

3. (a) **Which assumptions and design choices affect the comparison between timber and concrete building design and how significant are the resulting differences?** The exclusion of carbon sequestration from the calculation of shadow costs has a big effect on the comparison between timber and concrete building design. The chosen generation and population size can have a huge effect on the accuracy of the obtained Pareto optimal timber building designs.
- (b) **What design criteria are normative for timber building design?** Considering the boundary conditions and scope of this research the ULS is found to be normative for a slenderness up to 2.35. The along-wind acceleration becomes normative for a slenderness greater than 2.35. If the acceleration is disregarded, and if the assumption of a linear relation between deflection and slenderness is correct, the SLS is found to be normative over ULS for a slenderness of approximately 4.5

8.2. Research question

The main research question is:

"For which design situation can a timber braced tube system be economically and environmentally competitive with a concrete design alternative for a 50 to 70 meter tall building?"

For the design situation based on the concrete building "The Rectangle", the Pareto optimal timber building designs, referred to as Building B3, were found to be competitive with "The Rectangle". For the other analysed design situation, the Pareto optimal timber building designs referred to as Building A3, were not found to be competitive with the concrete building "The Square". Considering the boundary conditions and scope of this research, it can be concluded that a design situation with a rectangular floor plan is favourable over a design situation with a square floor plan and a design situation with a building height of 50 meter is favourable over a design situation with a building height of 60 meter.

The conclusion presented above includes the foundation of the building. The mass of the Pareto optimal timber building designs is approximately eight times smaller compared to the concrete design alternative, which results in a reduction of required foundation piles.

Considering the boundary conditions and scope of this research, the ULS is found to be normative for a slenderness up to 2.35. The along-wind acceleration becomes normative for a slenderness greater than 2.35. If the acceleration is disregarded, and if the assumption of a linear relation between deflection and slenderness is correct, the SLS is found to be normative over ULS for a slenderness of approximately 4.5

The following structural aspects influence the design of the braced tube stability system:

- A longer steel plate in the steel plate and dowel connections in the stability system results in a stiffer connection. Due to this stiffer connection, the stability system acts more as a moment frame rather than a truss system. This results in a decrease in cross section sizes of the timber elements, which decreases the timber volume of the stability system.
- The building elements in the stability system are grouped into thirteen groups. The required cross section is calculated for the normative element in the group and this cross section is applied to the full group. An average utilization factor of 57% is found for the building elements in the stability system, excluding the beams.
- The optimal diagonal angle is dependent on the dimensions of the stability system and the wind forces acting on it. Thus, the floor plan influences the diagonal angle. For a square floor plan, the optimal diagonal angle is roughly 36%. While, for a rectangular floor plan with a ratio of 2:1, the optimal diagonal angle is 33% in the long direction and 18% in the short direction.
- A diagonal layout where the diagonals cross the columns and beams at the same point is preferred as it will lead to a more efficient transfer of forces. A more efficient transfer of forces leads to smaller bending moments in the structure resulting in smaller required cross sectional dimensions and thus a cheaper structure. A more optimal diagonal layout is found to reduce the timber volume between 5% and 14% when analysed for two stability systems.

The shadow costs for the Pareto optimal timber building design and the concrete alternatives are approximately equal. There are two possibilities for the reduction of shadow costs:

- The stability system of the timber building encompasses one-third of the total shadow costs. This is mostly due to the steel present in the connections. It is suggested that a building with a concrete core stability system and timber floors can result in a design that combines the best parts of both building materials.
- The used method for carbon sequestration calculation in the determination of the shadow costs has a considerable impact regarding the comparison of the environmental impact between a concrete and timber building. Three different assessment methods for the inclusion of carbon sequestration are defined in this research. The use of timber and concrete in the structural system was found to provide comparable results when using carbon sequestration method 1. The inclusion of the effect of carbon sequestration in the calculation of the shadow costs as is done in calculation method 2, results in a reduction of shadow costs of approximately 40% compared to a similar concrete building. The inclusion of the effect of carbon sequestration in combination with carbon capture and storage at the end-of-life stage of the building, as calculated using carbon sequestration method 3, can even result in a negative carbon footprint of the structural system.

9

Recommendations

9.1. Recommendations for future research

To be able to answer the research questions within the timeframe as set for a graduation thesis, some scope limitations and assumptions have been made. This leads to possibilities for future research which are summed below:

- In this research a braced tube system is used as the stability system. The effect of different stability systems on the results is interesting to analyse. In Section 6.5.1, it is suggested that a building with a concrete core stability system, and timber floors, beams and columns can result in a sustainable design with low shadow costs. This combination is argued to combine the best parts of both building materials.
- In this research, one connection is defined for all connections in the stability system. Grouping connections and designing the connection based on their location in the stability system and their required strength and stiffness is expected to result in a more optimal and accurate design. Future research can regard these effects of the grouping of connections and the effect of their stiffness and strength on the stability system.
- In this research Kerto-Ripa floor plates are used. The implementation of CLT plates as floors will provide other results, because of the two-way spanning capabilities of CLT plates.
- In this research four disciplines have been considered. The addition of other disciplines using the developed tool as a basis may provide new insights as to what designs are favoured.
- In this research the tool positions the diagonals according to the "number of diagonals" and "placement of diagonals" parameter. This approach does not take into account the intersection of diagonals with beams and columns. In future research, another approach can be defined which aims to find solutions where the diagonals intersect with beams and columns. This will result in a decrease of required connections and a more efficient transfer of forces.
- In this research the stiffness of connections was included in the ULS and SLS check of the stability system. Future research can analyse the results of this methodology for designing as opposed to not considering the stiffness of connections in the ULS and SLS check.

9.2. Recommendations for policy makers

This research assumes the presence of a feedback loop that causes a lack of implementation of timber high-rise, see Figure 9.1.

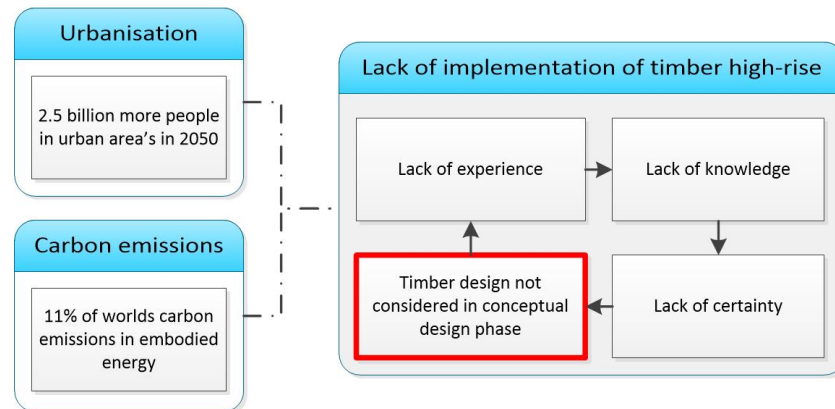


Figure 9.1: Feedback loop preventing consideration of timber high-rise design alternatives in the conceptual design phase.

It is argued that the created tool can aid with identifying design situations where timber high-rise design can be competitive with concrete high-rise design. However, additional measures might be required to significantly increase the implementation of timber high-rise design. Policy makers have a key role in this, so special recommendations are made for policy makers.

Dutch Government The construction industry is considered to be supplier-driven, highly fragmented, and risk-averse. Furthermore, most firms invest little in research and development and absorptive capacity [17]. An incentive is required for the construction industry to take the risk associated with constructing using timber. The Dutch government can create a financial incentive, as it has done for electric cars. According to the "Algemene Rekenkamer" (2019), the Dutch government spends €2000 to emit a ton of CO₂ less, by promoting electric cars [122].

For building B3, when using carbon sequestration calculation method 2, a reduction of 100 tons of CO₂ emissions is found. If the Dutch government also spends €2000 to emit a ton of CO₂ less in the building industry, a cost reduction of €200.000 is found for Building B3, reducing the total construction costs of the structural system by approximately 6 percent. This can be the incentive required for an increase in the implementation of timber buildings.

Regulation revision In timber design, some building regulations are still missing or are very conservative causing overdimensioning of timber structures. These regulations limit the design in timber and are arguably too conservative. It is recommended to research these regulations further and revise them if required.

- **Damping coefficient of the building** The Eurocode defines a damping coefficient of the building D of 0.01. Various researches have proven that this is a conservative assumption. The research of Feldmann et al. (2016) showed an average structural damping ratio of 0.02 for tall timber structures up to 100m [49]. A damping ratio of 0.019 was used for the design of Mjøstårnet [8].
- **Floor vibrations** The European standard EN 1995-1-1 combined with the Dutch national annex [74] does not provide an accurate calculation of the human-induced vibrations in the floor. This research uses two alternative guidelines that provide more accurate calculations: the Austrian standard Önorm B 1995-1-1 [71], and the HIVOSS design guidelines for the calculation of floor vibrations [67].
- **Exclusion of carbon sequestration** In the Netherlands, the environmental impact is determined using the NEN-EN 15804 norm. In this norm, the process of carbon sequestration is excluded from the calculation of the shadow costs. In the tool, this generally leads to the shadow costs of timber buildings being unfavourable over concrete buildings. The inclusion of the effect of carbon sequestration during the lifetime of a timber building results in a reduction of shadow costs of approximately 40% compared to a similar concrete building.

Bibliography

- [1] Height comparison of the hyperion tree, figure. URL <https://www.iltwmt.com/>.
- [2] *Fire safety in timber buildings Technical guideline for Europe*, 2010. URL https://eurocodes.jrc.ec.europa.eu/doc/Fire_Timber_Ch_5-7.pdf.
- [3] Mpg calc 1.2 software, 2019.
- [4] Key considerations of cross-laminated timber (clt) for high-rise construction in australia: A review. *NICMAR Journal of Construction Management*, 35(1):70–81, 2020.
- [5] Megant®- heavy duty system, 2021. URL <https://www.knapp-verbinder.com/en/produkt/megant-heavy-duty-system/>.
- [6] Cara Eckholm January 24, Okalo Ikhen, Rachel Steinberg, Cara Eckholm, Eric Jaffe, Vanessa Quirk Jaffe, Eric, Nick Bowden, Simon Brandler Brodhead, John, Vanessa Quirk, Amy Crawford, and et al. Introducing pmx: Our model for how tall timber buildings could work in cities, Jan 2020. URL <https://www.sidewalklabs.com/blog/introducing-pmx-model-tall-timber-buildings-cities/>.
- [7] Rune Abrahamsen. Mjøstårnet-18 storey timber building completed. In *Internationales Holzbau-Forum IHF*, 2018.
- [8] Rune Abrahamsen and Moelven Limtre AS. Mjøstårnet-construction of an 81 m tall timber building. In *International House Forum*, 2017.
- [9] Rune B Abrahamsen and Kjell Arne Malo. Structural design and assembly of "treet"—a 14-storey timber residential building in norway. In *World conference on timber engineering*, volume 2014, 2014.
- [10] Shafayet Ahmed and Ingrid Arocho. Analysis of cost comparison and effects of change orders during construction: Study of a mass timber and a concrete building project. *Journal of Building Engineering*, page 101856, 2020.
- [11] AIA. Document e202–2008 building information modeling protocol exhibi. 2008.
- [12] Robert Aish and Andrew Marsh. An integrated approach to algorithmic design and environmental analysis. In *Proceedings of the 2011 Symposium on Simulation for Architecture and Urban Design*, pages 149–155, 2011.
- [13] Raya A Ajouz. Optimising production costs of steel trusses: A computational approach of designing cost-effective steel trusses with welded connections. 2018.
- [14] Waugh Thistleton Architects. *100 Projects UK CLT*. Waugh Thistleton Architects, 2018.
- [15] Waugh Thistleton Architects. Waugh thistleton architects. *Murray Grove: The original Timber Tower*, 2019.
- [16] J Armstrong. Jane armstrong interview regarding timber building design in australia on 17-11-2020, Nov 2020.
- [17] Sanjay K Arora, Rider W Foley, Jan Youtie, Philip Shapira, and Arnim Wiek. Drivers of technology adoption—the case of nanomaterials in building construction. *Technological Forecasting and Social Change*, 87:232–244, 2014.
- [18] Johannes Bader and Eckart Zitzler. Hype: An algorithm for fast hypervolume-based many-objective optimization. *Evolutionary computation*, 19(1):45–76, 2011.

- [19] K Bayne and S Taylor. Attitudes to the use of wood as a structural material in non-residential building applications: Opportunities for growth. *Forest and Wood Products Research and Development Corporation, Victoria, Australia*, 2006.
- [20] BIMForum. Lod specification 2018 part i: For building information models and data. *BIMForum*, 2018.
- [21] Hans Joachim Blaß and Carmen Sandhaas. *Timber Engineering-Principles for Design*. KIT scientific publishing, 2017.
- [22] Stichting Bouwkwiteit. Bepalingsmethode milieuprestatie gebouwen en gww-werken. *Berekeningswijze voor het bepalen van de milieuprestatie van gebouwen en GWW-werken gedurende hun gehele levensduur, gebaseerd op de EN*, 15804, 2014.
- [23] Reinhard Brandner, Roberto Tomasi, Thomas Moosbrugger, Erik Serrano, and P Distch. Properties, testing and design of cross laminated timber. *A State-Of-The-Art Report by COST Action FP1402/WG2*, 2018.
- [24] Marlon Braun, Thomas Dengiz, Ingo Mauser, and Hartmut Schmeck. Comparison of multi-objective evolutionary optimization in smart building scenarios. In *European Conference on the Applications of Evolutionary Computation*, pages 443–458. Springer, 2016.
- [25] Brudder. *Brock Commons Tallwood House*. URL <https://www.naturallywood.com/emerging-trends/tall-wood/brock-commons-tallwood-house>.
- [26] Barbie Buckner. Models of the engineering design process, nasa epdc, texas, 2019.
- [27] Tim Butler and DesignMake Lendlease. International house sydney. In *Proceedings (Part II) 22nd. Int. Wood Construction Forum (IHF 2016)*. Garmisch, Germany, pages 35–45, 2016.
- [28] Ario Ceccotti. Composite concrete-timber structures. *Progress in structural engineering and materials*, 4(3):264–275, 2002.
- [29] Martin Cepelka. Splicing of large glued laminated timber elements by use of long threaded rods. 2017.
- [30] John Chapman, Thomas Reynolds, and Richard Harris. A 30 level cross laminated timber building system and analysis of the eurocode dynamic wind loads. *World*, 15:19, 2012.
- [31] Panagiotis Chastas, Theodoros Theodosiou, and Dimitrios Bikas. Embodied energy in residential buildings-towards the nearly zero energy building: A literature review. *Building and environment*, 105: 267–282, 2016.
- [32] Cobouw. revolutionaire bouwers dolblij met stikstof: dit kan weleens dé motor van verandering zijn, Oct 2019. URL <https://www.cobouw.nl/duurzaamheid/nieuws/2019/10/van-stikstofnegatief-naar-biobased-en-modulair-dit-kan-weleens-de-motor-van-verduurzaming-z>
- [33] Jeronimus Leonardus Coenders. Networkeddesign: next generation infrastructure for computational design. 2011.
- [34] G Comello. Nationaal digitaal houtbouwcongres 2020, presentation: "de realisatie van het hoogste hybride gebouw van nederland: Haut amsterdam", Oct 2020.
- [35] World Green Building Council. Bringing embodied carbon upfront: Coordinated action for the building and construction sector to tackle embodied carbon. 2019.
- [36] R.L. de Jong. Tall timber buildings. 2017.
- [37] Kalyanmoy Deb, Amrit Pratap, Sameer Agarwal, and TAMT Meyarivan. A fast and elitist multiobjective genetic algorithm: Nsga-ii. *IEEE transactions on evolutionary computation*, 6(2):182–197, 2002.
- [38] Héctor Díaz, Luis F Alarcón, Claudio Mourgues, and Salvador García. Multidisciplinary design optimization through process integration in the aec industry: Strategies and challenges. *Automation in Construction*, 73:102–119, 2017.

- [39] P Dubas and T Gehri, E amd Steurer. Modelling of steel-timber composite connections: Validation of finite element model and parametric study. *Holzbau*, Publication No. 81-1, 1981.
- [40] C Eastman, W Newstetter, and M McCracken. *Design knowing and learning: Cognition in design education*. Elsevier, 2001.
- [41] Tomás Mendez Echenagucia, Mario Sassone, Arianna Astolfi, Louena Shtrepi, and Arthur Van Der Harten. Multi-objective acoustic and structural design of shell structures for concert halls. In *Proceedings of IASS Annual Symposia*, volume 2014, pages 1–10. International Association for Shell and Spatial Structures (IASS), 2014.
- [42] Joyce El Kouarti. Build better, stronger, faster with clt. *US Department of Agriculture*, 4, 2017.
- [43] Ministerie van Economische Zaken en Klimaat. Klimaatakkoord, 2019.
- [44] Stora Enso. Clt stairs by stora enso product brochure, 2017.
- [45] Omar Espinoza, Vladimir Rodriguez Trujillo, Maria Fernanda Laguarda Mallo, and Urs Buehlmann. Cross-laminated timber: Status and research needs in europe. *BioResources*, 11(1):281–295, 2016.
- [46] A Falk, Ph Dietsch, and J Schmid. Cross laminated timber—a competitive wood product for visionary and fire safe buildings. In *Proceedings of the Joint Conference of COST Actions FP1402 & FP1404, Stockholm, ISBN*, pages 978–91, 2016.
- [47] Azadeh Fallahi. *Innovation in hybrid mass timber high-rise construction: A case study of UBC's Brock commons project*. PhD thesis, University of British Columbia, 2017.
- [48] Paul Fast, Bernhard Gafner, Robert Jackson, and Jimmy Li. Case study: an 18 storey tall mass timber hybrid student residence at the university of british columbia, vancouver. In *WCTE 2016-World Conference on Timber Engineering, Vienna, Austria*, 2016.
- [49] Angela Feldmann, Haoyu Huang, W Chang, Richard Harris, Philipp Dietsch, Martin Gräfe, and Carsten Hein. Dynamic properties of tall timber structures under wind-induced vibration. In *World Conference on Timber Engineering (WCTE 2016)*, 2016.
- [50] Forest Flager, Benjamin Welle, Prasun Bansal, Grant Soremekun, and John Haymaker. Multidisciplinary process integration and design optimization of a classroom building. *Journal of Information Technology in Construction (ITcon)*, 14(38):595–612, 2009.
- [51] Charlie Fong. he sakyamuni pagoda of fogong temple, ying county, shanxi province, china. is a wooden chinese pagoda built during the khitan-led liao dynasty., 2019. URL <https://commons.wikimedia.org/wiki/File:Pagodaoffogongtemple2019.jpg>. File: Pagodaoffogongtemple2019.jpg.
- [52] Tamara SFA Franca, C Elizabeth Stokes, and Juliet D Tang. Durability of cross laminated timber against termite damage. In *In: Proceedings, 61st international convention of society of wood science and technology and Japan wood research society. Monona, WI: Society for Wood Science and Technology. 10 p.*, 2018.
- [53] W Frehe. Interview walter frehe 23-03-2021, Mar 2021.
- [54] David Jason Gerber. *The parametric affect: Computation, innovation and models for design exploration in contemporary architectural practice*. GSD, 2009.
- [55] David Jason Gerber and Shih-Hsin Eve Lin. Designing in complexity: Simulation, integration, and multidisciplinary design optimization for architecture. *Simulation*, 90(8):936–959, 2014.
- [56] Jannik Giesekam, John R Barrett, and Peter Taylor. Construction sector views on low carbon building materials. *Building Research & Information*, 44(4):423–444, 2016.
- [57] RPT Gijzen. Modular cross-laminated timber buildings. 2017.
- [58] Annie Gosselin, Pierre Blanchet, Nadia Lehoux, and Yan Cimon. Main motivations and barriers for using wood in multi-story and non-residential construction projects. *BioResources*, 12(1):546–570, 2017.

- [59] Stefan Christoffer Gottlieb and Kim Haugbølle. The repetition effect in building and construction works: A literature review. 2010.
- [60] Michael C Green and J Eric Karsh. *The case for tall wood buildings: how mass timber offers a safe, economical, and environmentally friendly alternative for tall building structures*. MgbARCHITECTURE+DESIGN, 2012.
- [61] Sebastian Gyllensten and Axel Modig. The 200 m timber tower-a study on the possibilities of constructing a 200 meter tall timber building. 2020.
- [62] P Ham and KC Terwel. Structural calculations of high rise structures. *TU Delft, Delft, Netherlands.[course reader]*, 2017.
- [63] Mohamed Hamdy, Anh-Tuan Nguyen, and Jan LM Hensen. A performance comparison of multi-objective optimization algorithms for solving nearly-zero-energy-building design problems. *Energy and Buildings*, 121:57–71, 2016.
- [64] A Hassanieh, HR Valipour, MA Bradford, and C Sandhaas. Modelling of steel-timber composite connections: Validation of finite element model and parametric study. *Engineering Structures*, 138:35–49, 2017.
- [65] Will Hawkins. Timber and carbon sequestration. *Climate emergency, thestructuralengineer.org*, 2021.
- [66] Darrall Henderson, Sheldon H Jacobson, Alex W Johnson, F Glover, and GA Kochenberger. Handbook of metaheuristics. *Chapter The Theory and Practice of Simulated Annealing*, 57:287–319, 2003.
- [67] HIVOSS. *Trillingen van vloeren Ontwerprichtlijn*. 2007.
- [68] JCD Hoenderkamp. Critical loads of lateral load resisting structures for tall buildings. *The structural design of tall buildings*, 11(3):221–232, 2002.
- [69] Pekka Huovila. *Buildings and climate change: status, challenges, and opportunities*. UNEP/Earthprint, 2007.
- [70] Elias Hurmekoski. How can wood construction reduce environmental degradation? *European Forest Institute, Joensuu*, 2017.
- [71] Austrian Standards Institute. Design of timber structures—part 1-1: General—common rules and rules for buildings, national specifications for the implementation of Önorm en 1995-1-1, national comments and national supplements. Önorm b 1995-1-1:2015. 2015.
- [72] Nederlands Normalisatie Instituut. Eurocode 1: Belastingen op constructies - deel 1-1: Algemene belastingen - volumieke gewichten, eigen gewicht en opgelegde belastingen voor gebouwen, 2002.
- [73] Nederlands Normalisatie Instituut. Eurocode 1: Belastingen op constructies - deel 1-4: Algemene belastingen - windbelasting. 2002.
- [74] Nederlands Normalisatie Instituut. Eurocode 5: Ontwerp en berekening van houtconstructies - deel 1-1: Algemeen - gemeenschappelijke regels en regels voor gebouwen, 2007.
- [75] Nederlands Normalisatie Instituut. National annex to nen-en 1990+ a1+ a1/c2: Eurocode: Basis of structural design, 2011.
- [76] Nederlands Normalisatie Instituut. Eurocode 5: Ontwerp en berekening van houtconstructies -deel 1-2: Algemeen - ontwerp en berekening van constructies bij brand, 2011.
- [77] Nederlands Normalisatie Instituut. Nta 4614-3 nl, covenant hoogbouw - deel 3: Constructieve veiligheid. 2012.
- [78] Nederlands Normalisatie Instituut. Nen-en 14080: Gelijmd gelamineerd hout en gelijmd massief hout. 2013.
- [79] Nederlands Normalisatie Instituut. Nen-en 338 - structural timber - strength classes. 2016.

- [80] Nederlands Normalisatie Instituut. Eurocode: Grondslagen van het constructief ontwerp, nen-en 1990:2002+a1:2019+nb:2019, 2019.
- [81] Nederlands Normalisatie Instituut. Eurocode 1: Belastingen op constructies - deel 1-3: Algemene belastingen - sneeuwbelasting, nen-en 1991-1-3+c1+a1:2019 nl. 2019.
- [82] Nederlands Normalisatie Instituut. Nen 5077 - noise control in buildings - determination methods for performances concerning airborne sound insulation of facades, airborne sound insulation and impact sound insulation, sound levels caused by technical services, 2019.
- [83] Nederlands Normalisatie Instituut. Eurocode 3: Ontwerp en berekening van staalconstructies - deel 1-1: Algemene regels en regels voor gebouwen, 2020.
- [84] ISO. 10137: Bases for design of structures-serviceability of buildings and walkways against vibrations. *International Standard Organisation (ISO)*, 2007.
- [85] Quentin Jackson and Jeremy Mansfield. 25 king presentation to airah. URL https://www.airah.org.au/Content_Files/Divisionmeetingpresentations/QLD/QLd-19-02-19-Quentin%20Jackson-Jeremy-Mansfield.pdf.
- [86] Dion Jansen, Anke Rolvink, Jeroen Coenders, and Mattias Schevenels. Interactive distributed optimisation for multidisciplinary design. In *Proceedings of IASS Annual Symposia*, number 16, pages 1–8. International Association for Shell and Spatial Structures (IASS), 2014.
- [87] Marek Johanides, Lenka Kubíncová, David Mikolášek, Antonín Lokaj, Oldřich Sucharda, and Petr Mynarčík. Analysis of rotational stiffness of the timber frame connection. *Sustainability*, 13(1):156, 2021.
- [88] Carin Johansson. Low-frequency impact sound insulation of a light weight wooden joist floor. *Applied Acoustics*, 44(2):133–147, 1995.
- [89] Helena Johnsson. *Systematic design of glulam trusses*. PhD thesis, Luleå tekniska universitet, 2001.
- [90] Knauf Gips KG. Environmental product declaration plasterboard knauf diamant gkfi, 2016.
- [91] A Koezjakov, D Urge-Vorsatz, W Crijns-Graus, and M Van den Broek. The relationship between operational energy demand and embodied energy in dutch residential buildings. *Energy and Buildings*, 165: 233–245, 2018.
- [92] Esmee Koopman. Rationalising the structural material choice process for high rise buildings in the netherlands. 2020.
- [93] Hubert Kuijpers. *Constructie-uitdagingen in houtbouw*, 2020.
- [94] Aryani Ahmad Latiffi, Juliana Brahim, Suzila Mohd, and Mohamad Syazli Fathi. Building information modeling (bim): exploring level of development (lod) in construction projects. In *Applied Mechanics and Materials*, volume 773, pages 933–937. Trans Tech Publ, 2015.
- [95] KK Law. *Brock Commons Tallwood House*. URL <https://www.naturallywood.com/emerging-trends/tall-wood/brock-commons-tallwood-house>.
- [96] Fernanda Leite, Asli Akcamete, Burcu Akinci, Guzide Atasoy, and Semiha Kiziltas. Analysis of modeling effort and impact of different levels of detail in building information models. *Automation in construction*, 20(5):601–609, 2011.
- [97] Christopher Irving Lykke Madsen and Kjetil Henrik Sydow. Miljøvurdering av mjøstårnet. B.S. thesis, NTNU, 2019.
- [98] Laurent Magnier and Fariborz Haghghat. Multiobjective optimization of building design using trnsys simulations, genetic algorithm, and artificial neural network. *Building and Environment*, 45(3):739–746, 2010.
- [99] Kumar Mahesh, Perumal Nallagownden, and Irraivan Elamvazuthi. Advanced pareto front non-dominated sorting multi-objective particle swarm optimization for optimal placement and sizing of distributed generation. *Energies*, 9(12):982, 2016.

- [100] Ali M Malkawi. Developments in environmental performance simulation. *Automation in Construction*, 13(4):437–445, 2004.
- [101] Ali M Malkawi. Performance simulation: research and tools. *Performative architecture: beyond instrumentality*, pages 85–96, 2005.
- [102] Emilio Martín-Gutiérrez, Javier Estévez-Cimadevila, and Dolores Otero-Chans. Durability of joints made with threaded steel rods glued in chestnut timber—an experimental approach. *Composites Part B: Engineering*, 108:413–419, 2017.
- [103] Carlos Martins, Pedro Santos, Pedro Almeida, Luís Godinho, and Alfredo Dias. Acoustic performance of timber and timber-concrete floors. *Construction and Building Materials*, 101:684–691, 2015.
- [104] Robert L McGavin, Tony Dakin, and Jon Shanks. Mass-timber construction in australia: Is clt the only answer? *BioResources*, 15(3):4642–4645, 2020.
- [105] Bas Meeuwissen. Kerto ripa roof and floor elements, 2017.
- [106] Sinan Mengana and Tassos Mousiadis. Parametric bim: Energy performance analysis using dynamo for revit, 2016.
- [107] MetsaWood. Kerto-riipa tm long-span engineered timber solutions. 2012.
- [108] Kaisa Miettinen. Some methods for nonlinear multi-objective optimization. In *International conference on evolutionary multi-criterion optimization*, pages 1–20. Springer, 2001.
- [109] Moelven. Moelven töreboda – modern timber and hybrid systems. URL https://www.nacka.se/4a586f/globalassets/arbete-foretagande/dokument/foretagande/nyheter-foretagande/halvdagsseminarium/johan-ahlen_moelven-toreboda_byggaitra_170901.pdf.
- [110] Manu Moudgil. *Feasibility study of using cross-laminated timber core for the UBC Tall Wood building*. PhD thesis, University of British Columbia, 2017.
- [111] Standards Norway. Ns-en-1991-1-4 eurocode 1: Actions on structures - part 1-4: General actions - wind actions, 2009.
- [112] United Nations Department of Economic and Social Affairs (UN DESA). World urbanization prospects. the 2018 revision, highlights. 2018.
- [113] Frederick Institute of Technology. Connections in timber structures. 2006. URL <http://staff.fit.ac.cy/eng.ma/BATECH08/Connections.pdf>.
- [114] Oscar Ortiz, Francesc Castells, and Guido Sonnemann. Sustainability in the construction industry: A review of recent developments based on lca. *Construction and building materials*, 23(1):28–39, 2009.
- [115] Martin Bo Uhre Pedersen. Dowel type timber connections strength modelling. 2001.
- [116] Bennie Potjes. Kostenmodel staalskeletbouw. URL <https://www.bouwenmetstaal.nl/tools/aspecten/kosten/kostenmodel/>.
- [117] Alessandro Prada, Andrea Gasparella, and Paolo Baggio. A comparison of three evolutionary algorithms for the optimization of building design. In *Applied Mechanics and Materials*, volume 887, pages 140–147. Trans Tech Publ, 2019.
- [118] Cornelius Preidel, Simon Daum, and André Borrmann. Data retrieval from building information models based on visual programming. *Visualization in Engineering*, 5(1):1–14, 2017.
- [119] Michael H Ramage, Henry Burr ridge, Marta Busse-Wicher, George Fereday, Thomas Reynolds, Darshil U Shah, Guanglu Wu, Li Yu, Patrick Fleming, Danielle Densley-Tingley, et al. The wood from the trees: The use of timber in construction. *Renewable and Sustainable Energy Reviews*, 68:333–359, 2017.
- [120] Thillaigovindan Ramesh, Ravi Prakash, and KK Shukla. Life cycle energy analysis of buildings: An overview. *Energy and buildings*, 42(10):1592–1600, 2010.

- [121] Birgit Rasmussen and Teresa Carrascal García. Acoustic regulations for offices-comparison between selected countries in europe. In *INTER-NOISE and NOISE-CON Congress and Conference Proceedings*, volume 259, pages 8141–8150. Institute of Noise Control Engineering, 2019.
- [122] Algemene Rekenkamer. Fiscale stimulering van elektrische auto's, Jun 2019.
- [123] Alan Richardson. *Reuse of materials and byproducts in construction: waste minimization and recycling*. Springer Science & Business Media, 2013.
- [124] James N Richardson, Guy Nordenson, Rebecca Laberenne, Rajan Filomeno Coelho, and Sigrid Adrienssens. Flexible optimum design of a bracing system for façade design using multiobjective genetic algorithms. *Automation in construction*, 32:80–87, 2013.
- [125] Adam Blake Robertson. *A comparative life cycle assessment of mid-rise office building construction alternatives: laminated timber or reinforced concrete*. PhD thesis, University of British Columbia, 2011.
- [126] Rothoblaas. Plates and connectors for timber - buildings, structures and outdoors, 2019. URL <https://issuu.com/rothoblaas/docs/2-plates-and-connectors-for-timber>.
- [127] Nina Rundsvveen. *Mjøstårnet*. Mar 2019. URL <https://commons.wikimedia.org/wiki/File:Mj\T1\ostårnet.jpg>.
- [128] Ruukki. Environmental product declaration structural steel construction products, 2014.
- [129] Marc Schluessel, Rijun Shrestha, and Keith Crews. Acoustic performance of timber and timber-concrete composite floors. In *World Conference on Timber Engineering*, 2014.
- [130] Matthias Schmid. Acoustic performance of timber concrete composite floors. In *INTER-NOISE and NOISE-CON Congress and Conference Proceedings*, volume 2005, pages 900–909. Institute of Noise Control Engineering, 2005.
- [131] Kay-Uwe Schober and Thomas Tannert. Hybrid connections for timber structures. *European Journal of Wood and Wood Products*, 74(3):369–377, 2016.
- [132] Kristina Shea, Robert Aish, and Marina Gourtovaia. Towards integrated performance-driven generative design tools. *Automation in Construction*, 14(2):253–264, 2005.
- [133] Karol S Sikora, Daniel O McPolin, and Annette M Harte. Shear strength and durability testing of adhesive bonds in cross-laminated timber. *The Journal of Adhesion*, 92(7-9):758–777, 2016.
- [134] EC Slooten. Feasibility study of a wood-concrete hybrid super tall building and optimization of its wind-induced behaviour, 2018.
- [135] Jaroslaw Sobieszczanski-Sobieski, Alan Morris, and Michel Van Tooren. *Multidisciplinary design optimization supported by knowledge based engineering*. John Wiley & Sons, 2015.
- [136] Chris Stark, Mike Thompson, Climate Change Committee, et al. Net zero the uk's contribution to stopping global warming. 2019.
- [137] CCB Stathopoulos. Wind effects on buildings and structures. *Nature*, 199, 2007.
- [138] Bioeconomy Strategy. A sustainable bioeconomy for europe: strengthening the connection between economy, society and the environment. *European Commission.-2018.-URL: https://ec.europa.eu/research/bioeconomy/pdf/ec_bioeconomy_strategy_2018.pdf*, 2018.
- [139] Fredrik Svalestuen, Vegard Knotten, Ola Lædre, and Jardar Lohne. Planning the building design process according to level of development. 2018.
- [140] Catarina Thormark. A low energy building in a life cycle—its embodied energy, energy need for operation and recycling potential. *Building and environment*, 37(4):429–435, 2002.
- [141] Bas Tonn. Interview heko spanten regarding construction costs clt elements, Mar 2021.

- [142] R. Treels. Berekeningsmethoden dynamische responsies hoogbouw, Nov 2019. URL <https://www.cementonline.nl/berekeningsmethoden-dynamische-responsies-hoogbouw>.
- [143] SN Tucker and MD Ambrose. Embodied energy of dwellings. *no. September*, pages 1–7, 1997.
- [144] Çetin Tünger. *Comparing designers' cognitive behaviors in geometry-based and parametric 3D modeling environments*. PhD thesis, Bilkent University, 2014.
- [145] Laura Tupėnaitė, Viktorija Žilėnaitė, Loreta Kanapeckienė, Seyed Masoud Sajjadian, Tomas Gečys, Lina Sakalauskienė, and Jurga Naimavičienė. Multiple criteria assessment of high-rise timber buildings. *Engineering Structures and Technologies*, 11(3):87–94, 2019.
- [146] IEAthe UNEP. 2019 global status report for building and construction: Towards a zero-emission, efficient and resilient buildings and construction sector, 2019.
- [147] Till Vallée, Thomas Tannert, Rahul Meena, and Simon Hehl. Dimensioning method for bolted, adhesively bonded, and hybrid joints involving fibre-reinforced-polymers. *Composites Part B: Engineering*, 46:179–187, 2013.
- [148] Walter van Adrichem. Informatiesessie 'stabieliteit - hout in utiliteitsbouw', 2021. URL <https://www.youtube.com/watch?v=TM2bUkjjtBM>.
- [149] LAHM Van Berlo and F Bomhof. Creating the dutch national bim levels of development. In *Computing in Civil and Building Engineering (2014)*, pages 129–136. 2014.
- [150] Ton van de Veeken. Ketendenken en grondig nadenken over bouwprocessen leidt tot besparingen op de bouwplaats: interview met c. de bruijn (op+). *Bouwkostenkunde & Huisvestingseconomie (NVBK)*, februari, 2005.
- [151] A. L. M. van Eekelen, J. J. Rip, and P. L. Wentzel. *Hogere bouwkunde Jellema 10, Bouwproces : ontwerpen*. ThiemeMeulenhoff., 2002.
- [152] Joris van Maastrigt. Quantifying life cycle environmental benefits of circular steel building designs: development of an environmental assessment tool for reuse of steel members in building designs for the netherlands. 2019.
- [153] Geert PC van Oosterhout. The wind-induced dynamic response of tall buildings, a comparative study. *Journal of wind engineering and industrial aerodynamics*, 64(2-3):135–144, 1996.
- [154] SCF Van Oss. Hoe hoger, hoe duurder? onderzoek naar de invloed van de bouwhoogte op de investeringskosten van kantoorgebouwen in nederland. 2007.
- [155] Arthur van Rhijn. Possibilities of timber high-rise: A parametric study on the possibilities of timber high-rise in the netherlands. 2020.
- [156] David A Van Veldhuizen and Gary B Lamont. Multiobjective evolutionary algorithms: Analyzing the state-of-the-art. *Evolutionary computation*, 8(2):125–147, 2000.
- [157] Wouter van Wijnen. Sustainable timber structures: Quantitative research evaluating the potential effects of carbon sequestration and cascading strategies in the netherlands based on a comparison of the dutch and european life cycle assessment methodologies. 2020.
- [158] Robert Vierlinger. Octopus. URL <https://www.grasshopper3d.com/group/octopus>.
- [159] Cindy Vissering. Sbr kennispaper- bepaling van de milieuprestatie van gebouw en gww-werken (mpg). *SBRCURnet*, 2015.
- [160] De Groot Vroomshoop. Interview de groot vroomshoop regarding construction costs of glulam, Mar 2021.
- [161] Steve Watts and D Langdon. The economics of high-rise as per 2nd quarter 2010. *CTBUH Journal Issue III Tall Buildings in Numbers*, pages 44–45, 2010.

- [162] Okke Willebrands. Differential vertical shortening in timber-concrete high-rise structures. 2017.
- [163] woodworkingnetwork. Canadian 'wood first' move stirs ire of cement, steel industries, 2013. URL <https://www.woodworkingnetwork.com/wood-market-trends/woodworking-industry-news/production-woodworking-news/Canadian-Wood-First-Move-Stirs-Ire-of-Cement-Steel-Industries-234959731.html>.
- [164] Jonathan A Wright, Heather A Loosemore, and Raziye Farmani. Optimization of building thermal design and control by multi-criterion genetic algorithm. *Energy and buildings*, 34(9):959–972, 2002.
- [165] Fabiano de Aquino Ximenes, Brendan H George, Annette Cowie, Justin Williams, and Georgina Kelly. Greenhouse gas balance of native forests in new south wales, australia. *Forests*, 3(3):653–683, 2012.
- [166] MIZUKI YAMADA. The criteria to motions in tall building. In *Proceedings Pan Pacific Tall Buildings Conference*, pages 233–244, 1975.
- [167] Chunfeng Yang, Haijiang Li, Yacine Rezgui, Ioan Petri, Baris Yuce, Biaosong Chen, and Bejay Jayan. High throughput computing based distributed genetic algorithm for building energy consumption optimization. *Energy and Buildings*, 76:92–101, 2014.
- [168] Gustavo Zavala, Antonio J Nebro, Francisco Luna, and Carlos A Coello Coello. Structural design using multi-objective metaheuristics. comparative study and application to a real-world problem. *Structural and Multidisciplinary Optimization*, 53(3):545–566, 2016.
- [169] Qingfu Zhang and Hui Li. Moea/d: A multiobjective evolutionary algorithm based on decomposition. *IEEE Transactions on evolutionary computation*, 11(6):712–731, 2007.
- [170] Eckart Zitzler, Kalyanmoy Deb, and Lothar Thiele. Comparison of multiobjective evolutionary algorithms: Empirical results. *Evolutionary computation*, 8(2):173–195, 2000.
- [171] Eckart Zitzler, Marco Laumanns, and Lothar Thiele. Spea2: Improving the strength pareto evolutionary algorithm. *TIK-report*, 103, 2001.
- [172] Tigist Znabei. A post-tensioned cross-laminated timber core for buildings. 2020.

A

Theory

A.1. Properties and costs of timber

A.1.1. Structural properties

As already mentioned, timber is an an-isotropic material. The material properties of an an-isotropic material are different in the three axes. For a timber log, these three axes are the axial, radial and circumferential axes. For example, when looking at C50 softwood. The characteristic value of the compression stresses are $\frac{f_{c,0,k}}{f_{c,90,k}} = \frac{29}{3.2} = 9$ times higher parallel to the grain compared to perpendicular to the grain. For tensile stresses, the characteristic value is $\frac{f_{t,0,k}}{f_{t,90,k}} = \frac{30}{0.4} = 75$ times higher parallel to the grain compared to perpendicular to the grain [74]. Isotropic materials have the same material properties in all three axes. Isotropic materials are preferred as building materials, because of the more diverse application possibilities and easier prediction of behaviour.

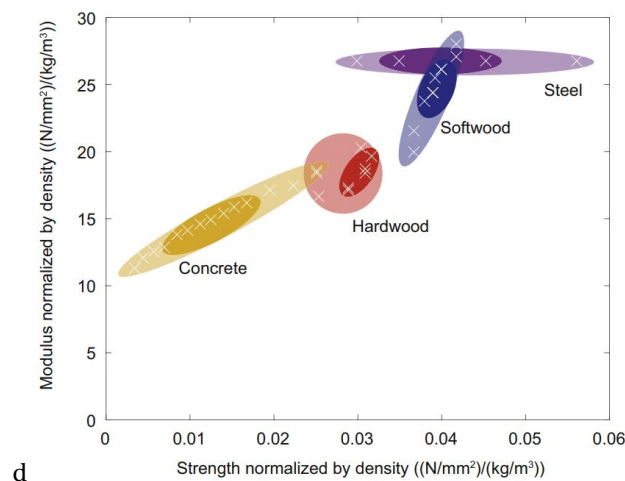


Figure A.1: Comparison between compression strength normalised by density and modulus of elasticity normalised by density, for various building materials [119].

Timber is a competitive building material when the timber properties parallel to the grain are normalized by density. Figure A.1 shows the strength-to-weight and elastic modulus-to-weight ratio's for the most common building materials. It can be concluded that when loads are resisted only by compression and tension, timber shows equal performance to traditional building materials. Timber is an efficient solution for application in the gravitational load resisting system in buildings, because of the lower self weight than steel and concrete.

Timber even shows favourable results over concrete and steel when comparing the weight to bending strength ratio parallel to the grain, see Figure A.2.

Material Properties of different materials			
Material	Bending strength $f_m(N/mm^2)$	Density $\rho(kg/m^3)$	Ratio ρ/f_m
Glulam GL30C	30	390	13
Steel S235	235	7850	33.4
Reinforced concrete	40	2400	60

Figure A.2: Material properties of different materials

A.1.2. Sustainability

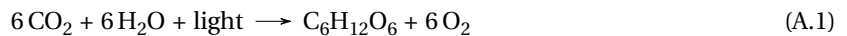
To determine the sustainability of timber, the greenhouse gas CO_2 will be used as a comparison between building materials. Considering the CO_2 emissions, timber is regarded as a sustainable material compared to other common building materials. Two reasons can be named for this. To begin with, a relatively low primary energy consumption is needed to produce a cubic meter of timber compared to other building materials. Secondly, the construction of a timber building will result in carbon sequestration.

Primary energy consumption

The primary energy consumption is the energy needed in the full process of production of the building material. This primary energy consumption can be converted to a primary CO_2 consumption.

Carbon sequestration

The growth of a tree results in the storage of carbon dioxide outside of the atmosphere during its lifetime. During the forming of the biomass, a process called photosynthesis takes place, see Formula A.1. During this process carbon dioxide, water and light are turned into $C_6H_{12}O_6$, a simple sugar, and oxygen. The carbon is stored in the form of $C_6H_{12}O_6$ in the biomass, while the oxygen is emitted. Only when the biomass is burned or rots, this Carbon dioxide will be released in the atmosphere [21].



By dividing the primary CO_2 consumption of timber with the carbon sequestration, the total emission per m^3 of timber can be found. Finding one exact value is difficult, since the both production of timber and the determination of carbon sequestration are a complex processes. Different research papers produce different results. In this research, the results as reported by the European Commission (2018) are used [138]. The European Commission bases their results on the research conducted by Hurmekoski (2017) [70]. This research concludes an average reduction of 2.1 tons of CO_2 emissions per ton of used timber compared to non-wood products. However, the estimation vary greatly between an increase of 2.33 to a reduction of 15 tons of CO_2 emissions per ton of used timber. Assuming the use of spruce, with a density of $0.45 \text{ ton}/m^3$, a reduction of 0.95 tons per m^3 of timber is found. This value is corresponding to values reported by various sources.

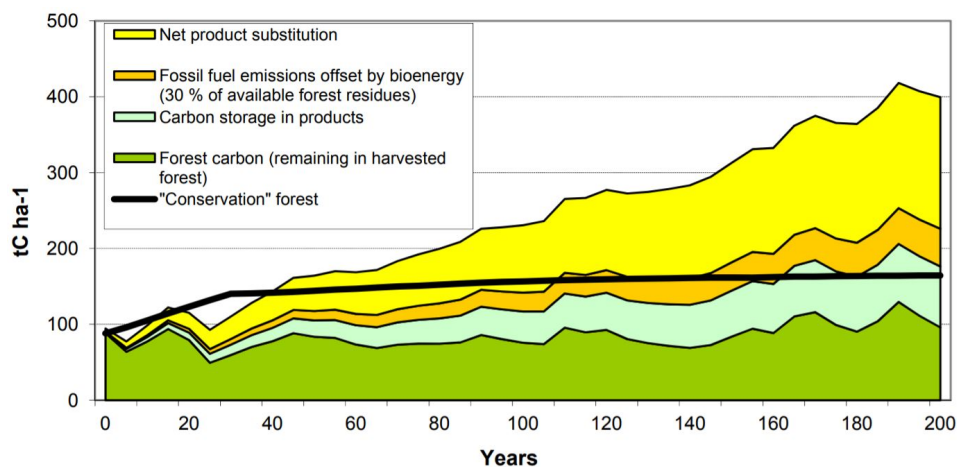


Figure A.3: Carbon emission effects over 200 years for a sustainably harvested forest [165].

One of the mentioned preconceptions concerning timber construction is the notion that harvesting of trees will reduce the forests and thus the total potential for CO_2 sequestration by the forest. Figure A.3 shows the tonnes of carbon per hectare of forest over a 200 year period when the forest sustainably managed. The first years a reduction of stored carbon in the forest can be identified. However, the stored carbon per hectare of forest and in the created timber products is 4 times higher after 200 years.

Comparing environmental impact of a building solely on CO_2 emission is an oversimplification of this problem. To thoroughly examine the environmental impact of a building, a Life Cycle Analysis (LCA) should be done following the ISO 14040 guidelines [114] for all building materials. In such a LCA, 11 environmental cost indicators (MKI's) are mentioned. The global warming potential for 100 years is one of these impact categories which is base on emissions of CO_2 and other greenhouse gases [159].

A.1.3. Durability

Another preconception concerning timber is a limited potential lifespan. However, various studies have shown that the same lifespan can be achieved for timber as for traditional building materials [120], [125]. Special attention must be given to the following aspects to assure a high potential lifespan of timber:

- **The effect of moisture content on timber** Important concerning the durability of timber is the moisture content. Since the properties of timber vary with a varying moisture content. Proper design is necessary to prevent the possibility of wetting of the timber. When timber elements are exposed to wetting, the correct preservatives protection can create a durable material.
- **Termite and insect damage** Treated CLT can withstand termite damage perfectly: [52]. The European standard DIN 68800-2 (6.3b) states that "the exclusive use of glued laminated timber, cross laminated timber, artificially dried building timber or wood-based panels with a moisture content u above 20 percent in service is sufficient to avoid structural damage by insects". Thus it can be assumed that CLT is invulnerable to insect attacks. [14]
- **Corrosion resistance of metallic fasteners in timber connections.** The corrosion resistance of metallic fasteners in timber connections must be considered to ensure a durable connection design [21]. Hidden steel connections can provide both a protections against corrosion and against loss of strength caused by fire [102].
- **Creep of the material** The biggest worry in durability or life-time expectancy of timber is creep. When not properly considered in design, it will cause the building to warp. Especially when the core is from concrete and the rest of the building is made from timber. Differences in creep must be carefully considered.
- **Adhesives** The durability of PUR and PRF adhesives have been tested showing sufficient durability compared to timber[133].
- **Direct sunlight** Direct sunlight must be minimized since it might result in a faster degradation of timber [119].

The Pagoda of Fogong Temple shown in Figure 4.6 best shows the durability of timber construction. Even without most of these design considerations, this temple is still intact after almost a thousand years.

A.1.4. Fire safety

Another major preconceptions concerning timber high-rise is the fire safety. To provide sufficient fire safety, the structural integrity of the building must be ensured for a sufficient amount of time for the occupants to be evacuated. Providing fire safety consists of two main principles. At first the reaction to fire of the material and secondly the fire resistance of the material.

Reaction to fire

This concerns the ignitability, heat release, burning droplets, smoke production an flame spread of the building material. Untreated timber is a combustible material and produces smoke when burning. When timber materials are properly treated, a non-smoke producing material can be created. (B-s1,d0 rating)

Fire resistance

The fire resistance can be described by the amount of time a building element exposed to fire can guarantee its required structural and separating function.

The charring process that occurs when a timber element is burning helps provide this fire resistance. During a fire, the outside of a timber element begins to char, and this charring layer provides insulation to the fire to the inner part of the timber element. This inner part of the timber element will then provide the structural integrity of the building. The strength loss of this inner part is considerably small when compared to the strength loss of steel in a fire, see Figure A.4.

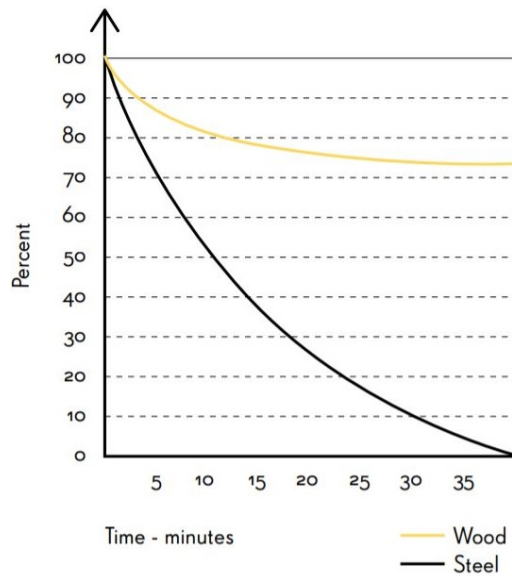


Figure A.4: Percentage of initial strength during a fire [14].

The charring happens from the outside to the inside of the material. For structural calculations during a fire, a charring rate is given in the Eurocode. Eurocode 5 gives a charring rate of 0.7 mm/minute for glulam, LVL and CLT [76]. This charring process starts at temperatures of 300 degrees Celcius for CLT.

Self-extinguishing of timber



Figure A.5: Timber beam supporting melted steel beams after a fire in American factory

Figure A.5 shows the aftermath of a fire in an American factory. A timber beam is shown which supports two melted steel beams. This picture clearly shows the self-extinguishing behaviour of timber. When the fire has run out of fuel, the timber will extinguish itself. Although timber is combustible, it will not provide sufficient fuel for the fire to keep burning. Meanwhile, the steel beams heat up due to their high thermal conductivity and loses its strength.

A.1.5. Acoustics

Because of the low self-weight of timber, often additional measurements must be taken to comply with the acoustical requirements. These acoustic issues are most challenging in timber floors, specifically at low frequencies [103]. Several possibilities of improvement of the acoustic properties of floors showed their benefits in different studies:

- Increasing stiffness of the floors [88].
- Concrete toppings or floating screed [129].
- Increase mass of floor [28].
- Suspended ceilings [130].

There are several suppliers that supplies timber floor systems which use one or multiple of these aforementioned techniques for improving the acoustic properties. Various methods are used to increase the mass of the floor. For example, foam concrete or a honey-comb system using special grains or sand to add mass to the floors. When the building has a residential function, acoustic damping of the walls is also required. Drywalls are often used to guarantee this required acoustic damping.

A.1.6. Additional properties

Heat conductivity

The heat conductivity λ of timber is between 0.13 and 0.20 W/(m·K) for steel this is $\lambda = 60$ W/(m·K) [21].

Effect on well-being

Several studies have shown exposed timber has several health benefits for occupants, such as reduced heart rate, blood pressure and stress levels. Furthermore, it improves the emotional state and level of self-expression of inhabitants [14].

Impact resistance

In 2016, the U.S. Department of Defense researched the resistance to impact of CLT and other building materials. Blast tests were conducted which showed the bowing of absorption of the materials. CLT showed excellent properties, it absorbed most of the energy of the blast, causing only limited damage of the material [42].

Earthquake Resistance

Timber shows favourable properties in earthquake design because of its high ductility. Furthermore, Feldman et al. (2016) did various vibration tests on buildings and concluded that the damping ratio of a timber structure has superior capacities to dissipate vibration compared to concrete or steel structures

Creaking

Another concern regarding timber is the creaking noise it might produce. Again this is a preconception based on unprocessed timber materials. Working on various timber projects in Australia Armstrong did not experience problems with creaking in timber design using processed timber materials [16].

Nitrogen emissions

Recently in the Netherlands, the government started taking measures to reduce nitrogen emissions. The construction sector was one of the industries where measurements were taken, although it only accounts for 2.4 percent of the total emissions. According to van den Dobbelen, timber buildings can create a nitrogen positive construction, resulting in the storage of nitrogen. Furthermore, the increase in prefabricated buildings will help reduce the amount of transportation, and the amount of diesel-powered equipment. This will both aid with the reduction of nitrogen emissions [32].

Construction process

The construction process of timber buildings provides several benefits.

- Building with timber simplifies the prefabrication.
- When using CLT panels, erection is easier, quieter and safer. This reduces the amount of personnel for erection of the superstructure by 50 to 70 % [14].
- Less on-site waste is created, see Figure A.6.



Figure A.6: The total collected waste after a week of erection of the CLT frame at Murray Grove [14].

A.1.7. Costs

The construction costs for timber design are often assumed to be between 5% to 10% higher than building design using traditional building materials. Ahmed found in a research conducted in 2020 that the construction cost for a hybrid timber building is 6.43% higher compared to a traditional concrete building. The considered hybrid timber building has 18 floors and consists of a timber superstructure with a concrete core [10]. One reason for these higher costs is the higher costs per building volume for timber products. The costs for production of CLT is around 30-40% higher by building volume than traditional building materials [14]. However, other factors improve the construction costs using timber materials, such as the lightness, accuracy and workability of the timber. Lastly, when comparing a CLT structure to in-situ concrete frames, 80-85% less deliveries are required [14].

Putting costs in perspective

An increase in timber building industry can help the development of infrastructure, manufacturers and knowledge of timber, resulting in a decrease in construction costs. Furthermore, sustainability goals set by governments may result in economical stimulation for sustainable designs, increasing the incentive to construct using timber. Moreover, a timber structure will result in a light building, which might decrease foundation costs. Lastly, the construction time of a CLT building is approximately 20% faster than for a comparable reinforced concrete building [14]. Because of this reduction in construction time, the building can begin earning back the construction costs sooner.

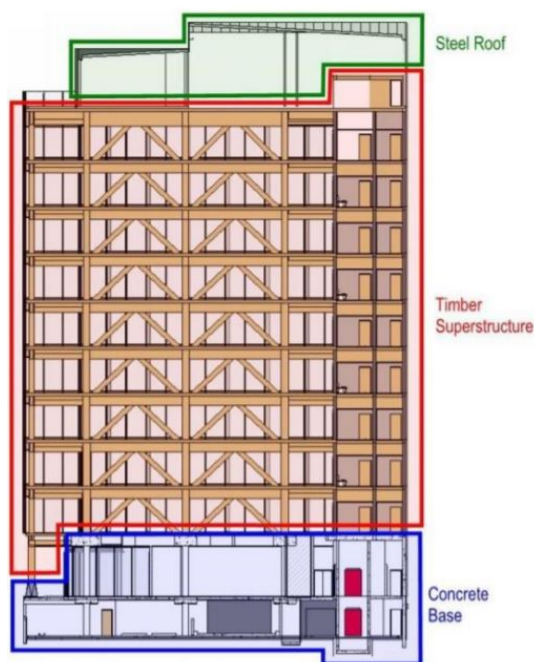
A.2. Reference projects

A.2.1. Introduction

Various timber high-rise buildings have been completed, these completed buildings can provide information and insight. This section will cover a comparison between five completed timber high-rise buildings projects.

A.2.2. 25 King

25 King is a 47 meter high office building in Australia. The stability of this full timber building is provided by the core and diagonals in the façade. Since the building site is a declared termite area, the ground floor does not contain timber elements. Connectors similar to Knapp connectors are used to connect the beams and columns, see Figure A.8. The columns are connected by placing them on top of each other, and screwing the timber parts together, see Figure A.7c. For connection of the columns and diagonals in the facade, a steel plate and dowel connection is used, see Figure A.7b. The timber elements are fully exposed in the building. To provide sufficient fire safety, a sprinkler system is present in the building.



(a) Section [85].



(b) Steel plates and dowel connection of diagonals [85].



(c) Connection [85].



(d) Construction [85].

Figure A.7: 25 King

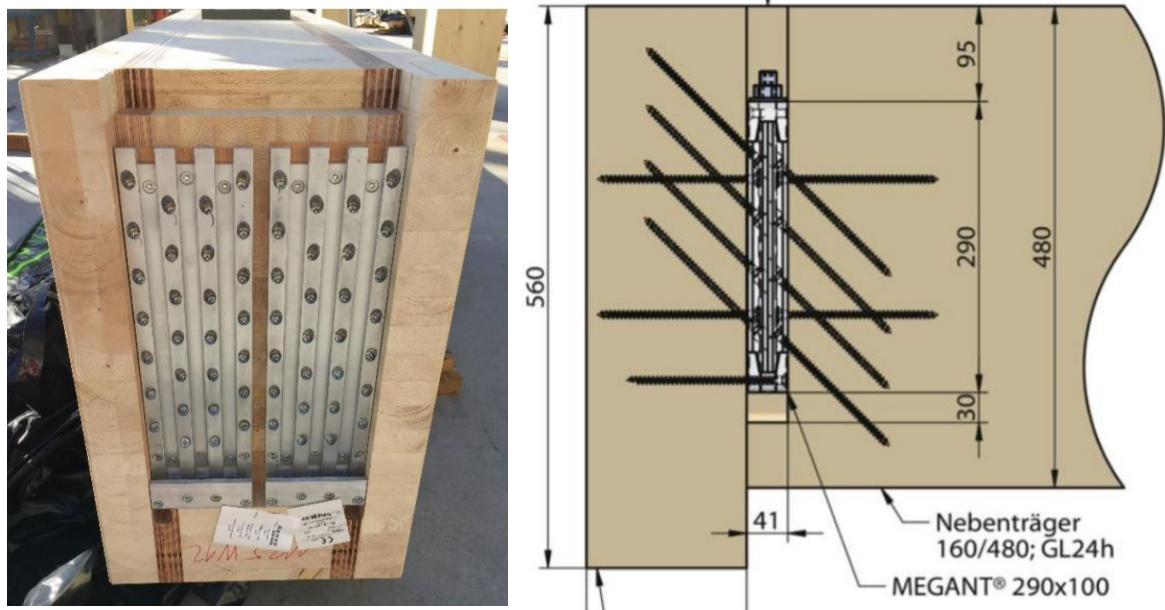


Figure A.8: Beam-column connection [85].

A.2.3. Treet

The Treet building in Norway is a 14-storey high timber building. It makes use of a power storey. This power storey essentially functions as an outrigger. Every fourth level a power storey is constructed composed of glulam trusses. For the glulam trusses, GL30c and GL30h is used. This Power level takes the loads of the floors above it. For the connection in these glulam trusses, a steel plate and dowel connection is used. The building is composed of a CLT core and walls, but these have no load-bearing function [9].



(a) Exterior [9].

(b) Structure [9].

Figure A.9: Treet

A.2.4. Murray Grove Stadthaus

Murray Grove is considered the first fully timber high-rise building in the world. The building has a residential function and is constructed using CLT panels. KLH CLT panels used for the core, floor slabs, load bearing walls, stairs and lift cores. For the walls, 128 mm thick CLT is used. For the floors, 146 mm thick CLT is used. The CLT elements are connected using angle brackets, mechanical fixings and steel ties. The timber structure is encapsulated using gypsum panels. This increases the fire resistance with 30 minutes [145].



Figure A.10: Murray Grove Stadthaus

A.2.5. Mjøstårnet

Mjøstårnet is a 18-storey high timber building in Norway that was completed in March 2019, see Figure A.11a.

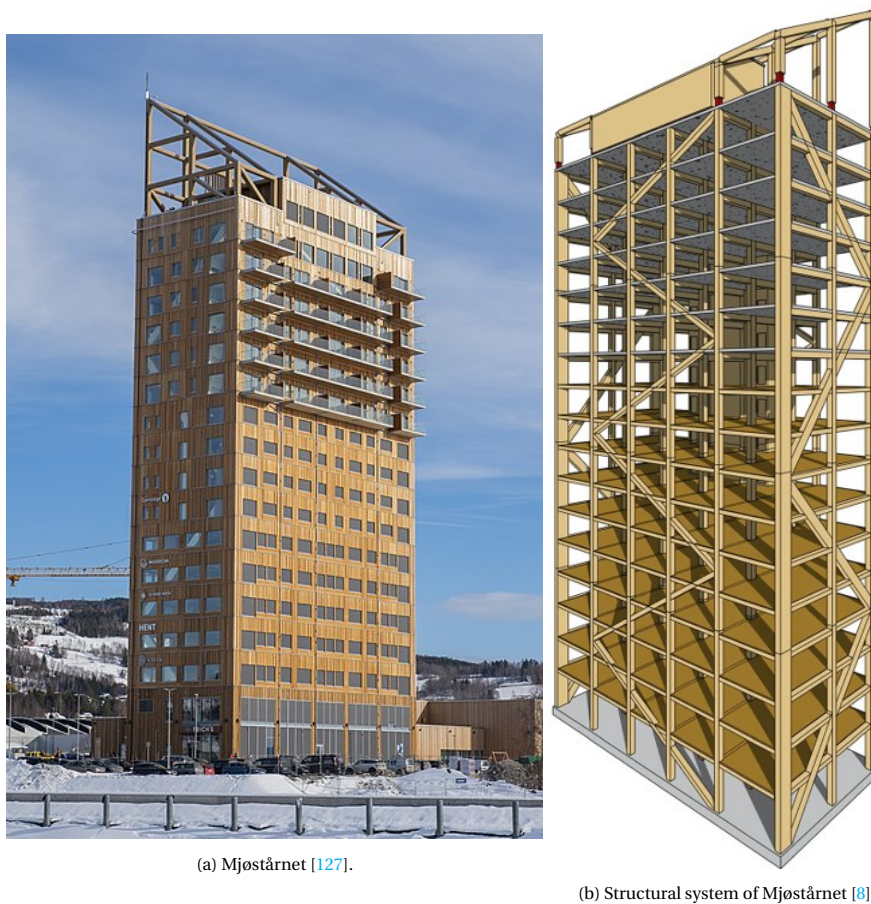
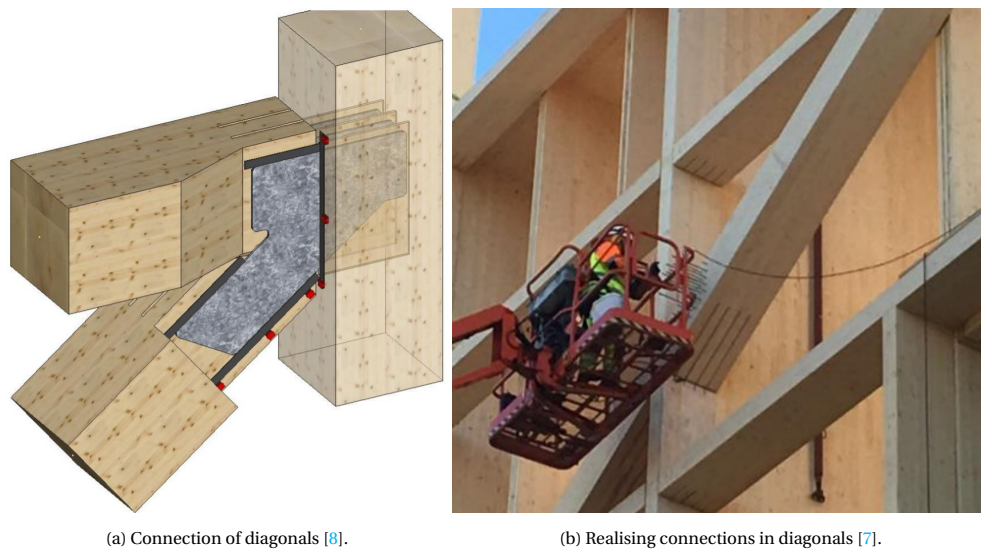


Figure A.11: Mjøstårnet

Now, in 2021, Mjøstårnet is considered the world's tallest timber building, with a height of 85.4 meters. The

main structural system consists of glulam elements, making up the trusses along the façade, the columns and the beams of the building. CLT walls are also used for vertical transfer of forces, see Figure A.11b. However, they do not contribute to the horizontal stability of the building [8]. For the diagonals, steel plates and dowel connections are used, see Figure A.12a. In this connection, intumescent fire strips are used in gaps and slots.



(a) Connection of diagonals [8].

(b) Realising connections in diagonals [7].

Figure A.12: Connection of diagonals in Mjøstårnet

The first ten floors are constructed using prefab glulam, floor and façade elements. The higher floors are created using concrete to provide the necessary comfort criteria [145].

The maximum horizontal deflection at the top of the building is 140 mm. The glulam elements are connected by use of slotted-in steel plates and dowels. This is a high capacity connection which is commonly used in bridges and large buildings. Glulam with strength class GL30c and GL30h is used. The used CLT plates have a bending strength of $f_{mk} = 24$ MPa. For the connections, powder coated S355 steel is used together with acid-proof steel dowels[8].

A.2.6. Brock Commons Project

The Brock Commons Project is a 18 storey hybrid residential high-rise building. The complete building was erected within 70 days [145].



(a) Installation of glulam Columns [25].

(b) Exterior [95].

Figure A.13: Brock Commons Project

This building consists of two concrete cores and a concrete base. From the third floor up, glulam and PSL columns and CLT panels are used. For the glulam columns, GL24h is used. The CLT panels are connected to the core using steel angles screwed to the CLT and bolted to the concrete walls. CLT panels are used for the floors. Because of their twoway spanning abilities, no beams are required. For the connection between the columns and the floors, steel is used which is adhered to the columns using epoxy resin and bolted between each floor slab. The completely structure is encapsulated using gypsum panels. Furthermore, a sprinkler system is present [47].

A.3. Connection types

A.3.1. Steel plate and dowels

This connection type is based on the mechanical fastener technique. One or multiple steel plates are inserted in the center of the timber element. Steel dowels are placed through these steel plates in pre-drilled holes in the timber [155].

Strength

This connection has three main failure mechanisms:

1. Failure of dowels

Pedersen (2001) gives seven failure modes for the dowels in a steel plates and dowel connection [115], see Figure A.14. It is assumed the timber and the steel can reach plasticity. The dowel is assumed to be rigid-plastic.

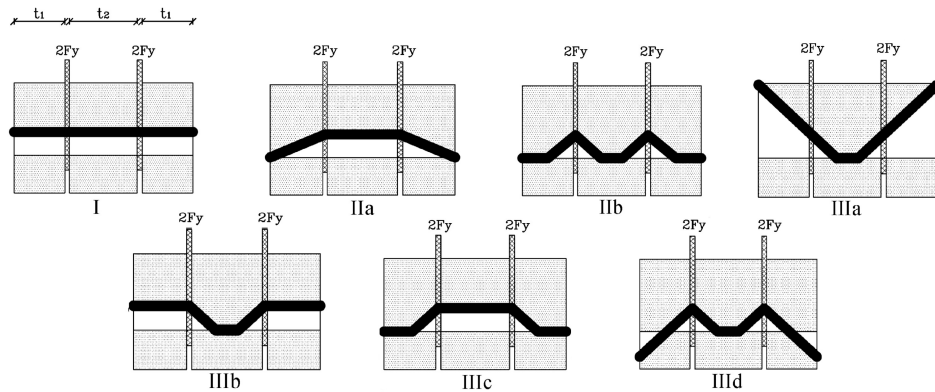


Figure A.14: Failure modes steel plate and dowel connection [115].

These failure modes can be calculated using:

$$F_{\text{failure}} = \min \begin{cases} \frac{1}{4} (2t_1 + t_2) \cdot d \cdot f_h & \text{Mode I} \\ \left(-\frac{1}{2}t_1 + \frac{t_2}{4} + \sqrt{\frac{1}{2}t_1^2 + \frac{M_y}{d \cdot f_h}} \right) \cdot d \cdot f_h & \text{Mode IIa} \\ \sqrt{4 \cdot M_y \cdot d \cdot f_h} & \text{Mode IIb} \\ \left(\frac{1}{2}t_1 + \frac{1}{2}\sqrt{t_1^2 + \frac{2 \cdot M_y}{d \cdot f_h}} \right) \cdot d \cdot f_h & \text{Mode IIIa} \\ \left(\sqrt{\frac{M_y}{d \cdot f_h}} + \frac{1}{2}t_1 \right) \cdot d \cdot f_h & \text{Mode IIIb} \\ \left(\sqrt{\frac{M_y}{d \cdot f_h}} + \frac{1}{4}t_2 \right) \cdot d \cdot f_h & \text{Mode IIIc} \\ \left(-\frac{1}{2}t_1 + \sqrt{\frac{1}{2}t_1^2 + \frac{M_y}{d \cdot f_h}} + \sqrt{\frac{M_y}{d \cdot f_h}} \right) \cdot d \cdot f_h & \text{Mode IIId} \end{cases}$$

t = wood thickness in mm

d = dowel diameter in mm

$f_{h,k}$ = embedment strength in N/mm, calculated using Formula A.2.

M_y = plastic yield moment of the dowel in N/mm^2 . For a circular dowel it can be calculated using Formula A.3.

$$f_{h,k} = 0.082(1 - 0.01d) \cdot \rho_k \quad (\text{A.2})$$

ρ_k = wood density

d = dowel diameter

$$M_y = W_y f_y = \frac{1}{6} d^3 f_y \quad (\text{A.3})$$

d = dowel diameter
 f_y = yield strength of steel dowel

Only a part of the dowel columns is effective. This effective number of dowel columns can be found using:

$$n_{ef} = \min(n_{columns}; n_{columns}^{0.9} \cdot (\frac{\alpha_1}{13d})^{1/4}) \quad (A.4)$$

$n_{columns}$ = number of dowel columns parallel to the grain

Using this, the maximum force in the dowels is determined using:

$$F_{max,dowels} = n_{ef} \cdot 4 \cdot F_{failure} \cdot n_{rows} \quad (A.5)$$

2. Failure in tension or compression of net timber area

Since steel plates and dowels are placed in the timber, the timber area is reduced. This net timber area still must resist the tension and compression forces. The following equations are used:

$$F_{max,c} = f_{c,0,k} \cdot A_{net,timber} \quad (A.6)$$

$$F_{max,t} = 0.4 \cdot f_{t,0,k} \cdot A_{net,timber} \quad (A.7)$$

3. Failure of steel plate

Another possible failure is failure of the steel plate. For this, there are various failure mechanisms

(a) Steel plate reaches yield strength.

$$F_{max,plates,1} = f_y \cdot t_{steel\ plates} \cdot b_{steel\ plates} \quad (A.8)$$

$t_{steelplates}$ = total thickness of the steel plates

$b_{steelplates}$ = width of the steel plates

(b) Block shear and plug shear failure, as given in the Eurocode [74], see Figure A.15:

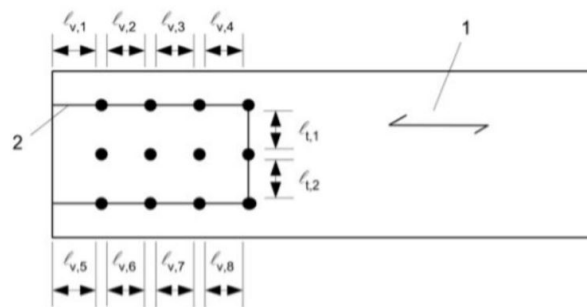


Figure A.15: Block shear failure $l_{v,i}$ and $l_{t,i}$ [74].

$$F_{max,blockplug} = \max \begin{cases} 1.5 A_{net,t} \cdot f_{t,0,k} \\ 0.7 A_{net,v} \cdot f_{v,k} \end{cases} \quad (A.9)$$

$$L_{net,v} = \sum_i l_{v,i}$$

$$L_{net,t} = \sum_i l_{t,i}$$

$$A_{net,t} = L_{net,t} \cdot t$$

$$A_{net,v} = L_{net,v} \cdot t$$

t = thickness of timber element, perpendicular to steel plate

(c) Net area of steel plate fails in tension.

$$F_{\max, \text{plates}, 2} = \frac{0.9 \cdot f_u \cdot A_{\text{net}}}{\gamma_{M,2}} \tag{A.10}$$

f_u = ultimate tensile strength
 A_{net} = net section

Distancing

For the placement of dowels in the steel plate, the requirements mentioned in the Eurocode must be met. The Eurocode gives minimum end distances, edge distances, and spacings for steel plates and dowel connections. These differ based on the diameter of the dowels and the direction of the load, see Figure A.16 and Figure A.17.

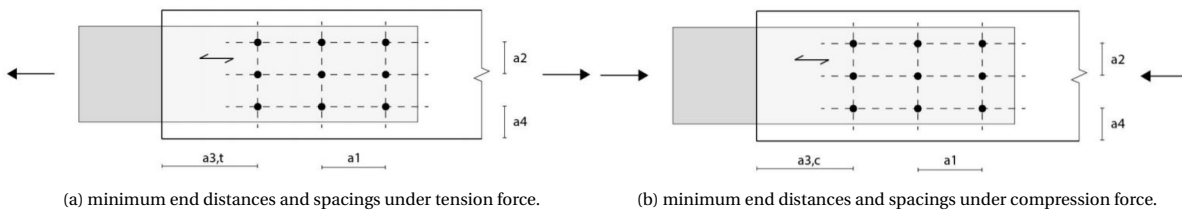


Figure A.16: minimum end distances and spacings.

Minimum end distance and spacing		
Considered end distance or spacing	Angle	Minimum end distance or spacing
α_1 (parallel to grain)	$0^\circ \leq \alpha \leq 360^\circ$	$(3 + 2 \cos \alpha) \cdot d$
α_2 (perpendicular to grain)	$0^\circ \leq \alpha \leq 360^\circ$	$3 \cdot d$
$\alpha_{3,t}$ (loaded end)	$-90^\circ \leq \alpha \leq 90^\circ$	$\max(7 \cdot d; 80)$
$\alpha_{3,c}$ (unloaded end)	$90^\circ \leq \alpha \leq 150^\circ$	$\max(\alpha_{3,t} \sin \alpha ; 3d)$
	$90^\circ \leq \alpha \leq 150^\circ$	$3 \cdot d$
	$210^\circ \leq \alpha \leq 270^\circ$	$\max(\alpha_{3,t} \sin \alpha \cdot d; 3d)$
$\alpha_{4,t}$ (loaded edge)	$0^\circ \leq \alpha \leq 180^\circ$	$\max((2 + 2 \sin \alpha) \cdot d; 3 \cdot d)$
$\alpha_{4,t}$ (unloaded edge)	$180^\circ \leq \alpha \leq 360^\circ$	$3 \cdot d$

Figure A.17: Minimum end distances and spacings under compression force.

Stiffness

Slip modulus The stiffness of the connections depends on the properties of the timber and the diameter of the dowel. The total stiffness of the dowels can be determined by summing the stiffness's of a single dowel. By calculating the slip modulus K_{ser} the stiffness of a single dowel can be determined, see Formula A.11.

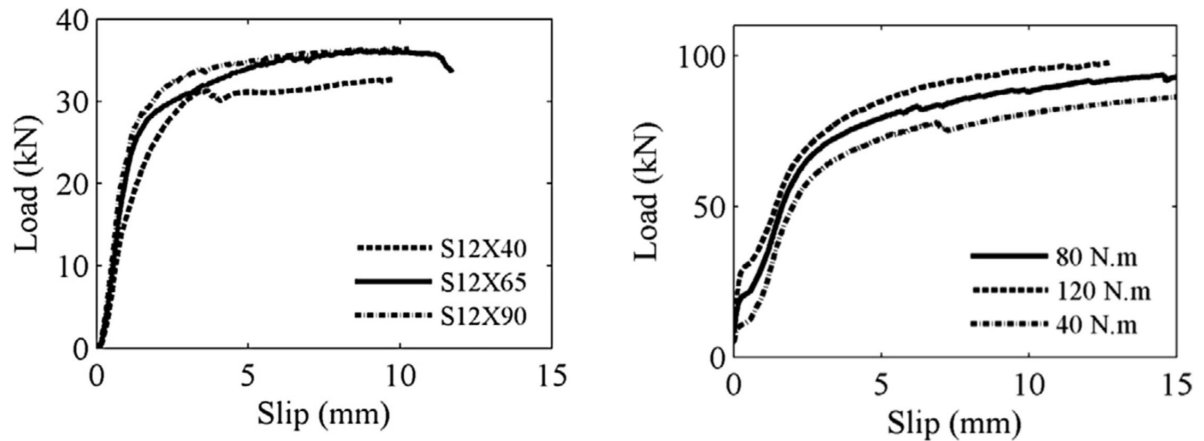
$$K_{ser} = \rho_m^{1.5} \cdot d / 23 \tag{A.11}$$

K_{ser} = slip modulus per shear plane of a single dowel
 ρ_m = mean density value of timber
 d = diameter of a dowel

The following Formula calculates the design value of the instantaneous slip modulus for timber-to-timber connections.

$$K_u = \frac{2}{3} \cdot K_{ser} \tag{A.12}$$

An important aspect to consider is the initial slip of a connection. The hole diameter in the steel and timber is equal to the dowel diameter and a tolerance. This tolerance will result in initial slip. Figure A.18a



(a) Load-slip response of three steel-timber composite bolted connections [64].

(b) Load-slip response of three post-tensioned steel-timber composite bolted connections [64].

Figure A.18

shows an load-slip response of a bolted steel-timber connection. Here, the initial slip is a negligible fraction of the total slip under load. So, in this research it is assumed Formula A.11 can be used to determine the slip of a connection. However, it must be noted that according to Dubas (1981) initial slip found in laboratory research is often smaller than in practice, due to higher precision [39].

There are two options to decrease initial slip:

1. **Post-tensioning the bolts.** This post-tensioning force in the high-strength bolts, increases the initial stiffness of the connections. Thus increasing the required load for initial slip in the connection, see Figure A.18b.
2. **Using Computer Numerical Control (CNC) machinery.** This CNC machinery can be used to drill the holes in wood and steel. This way, the tolerances and thus the initial slip in the connection can be minimized or even be absent. In CNC implementation, self-drilling dowels are used.

Translational Stiffness According to Eurocode 5, timber-to-timber connections can be calculated using Formula A.12. For timber-to-steel connections, this value for K_{ser} may be multiplied with 2 to obtain the instantaneous slip modulus per steel dowel in the connection. The translational stiffness is found by summing this slip modulus with all dowels, see Formula A.13.

$$K_{t,u} = 2 \cdot n \cdot K_u \quad (\text{A.13})$$

$K_{t,u}$ = translational stiffness

K_u = design value of instantaneous slip modulus

n = number of dowels

Rotational Stiffness According to Johanides et al. (2021), the rotational stiffness can be obtained by obtaining the translational stiffness of dowel i multiplied with the square of the radial length of dowel i to the center of mass of all dowels, see Formula A.14 [87].

$$K_{r,ser} = \sum_{i=1}^n K_{ser} \cdot r_i^2 \quad (\text{A.14})$$

$K_{r,ser}$ = rotational stiffness

K_{ser} = slip modulus of a single dowel

r_i = radial length of dowel i to the center of mass of all dowels

A.4. Structural design considerations

A.4.1. Loads

Four types of loads are elaborated on in this Section: wind load, dead loads, live loads, and snow loads.

Wind load

The wind load is determined according to NEN-EN 1991-1-4 [73]. Assumed: Flat roof, No round corners.

For determination of the extreme wind load on the façade, Formula A.15 is used.

$$Q_w = c_s c_d \cdot c_f \cdot q_p(z_e) \tag{A.15}$$

$c_s c_d$ = building factor

c_f = force coefficient for the structure

$q_p(z_e)$ = peak velocity pressure at height z_e

For buildings consisting of bracing and stability walls under 100 meters tall. If the height is smaller than four times the building depth in the direction of the wind, a value of 1.0 can be used for $c_s c_d$ [73]. If this requirement is not met, the building factor is assumed to equal 1.1.

The force coefficient can be determined using the external pressure coefficients for suction and pressure. For the calculation of the main load bearing system, the external pressure coefficient $c_{pe,10}$ is used. Figure A.20 shows these external pressure coefficients for the zones depicted in Figure A.19.

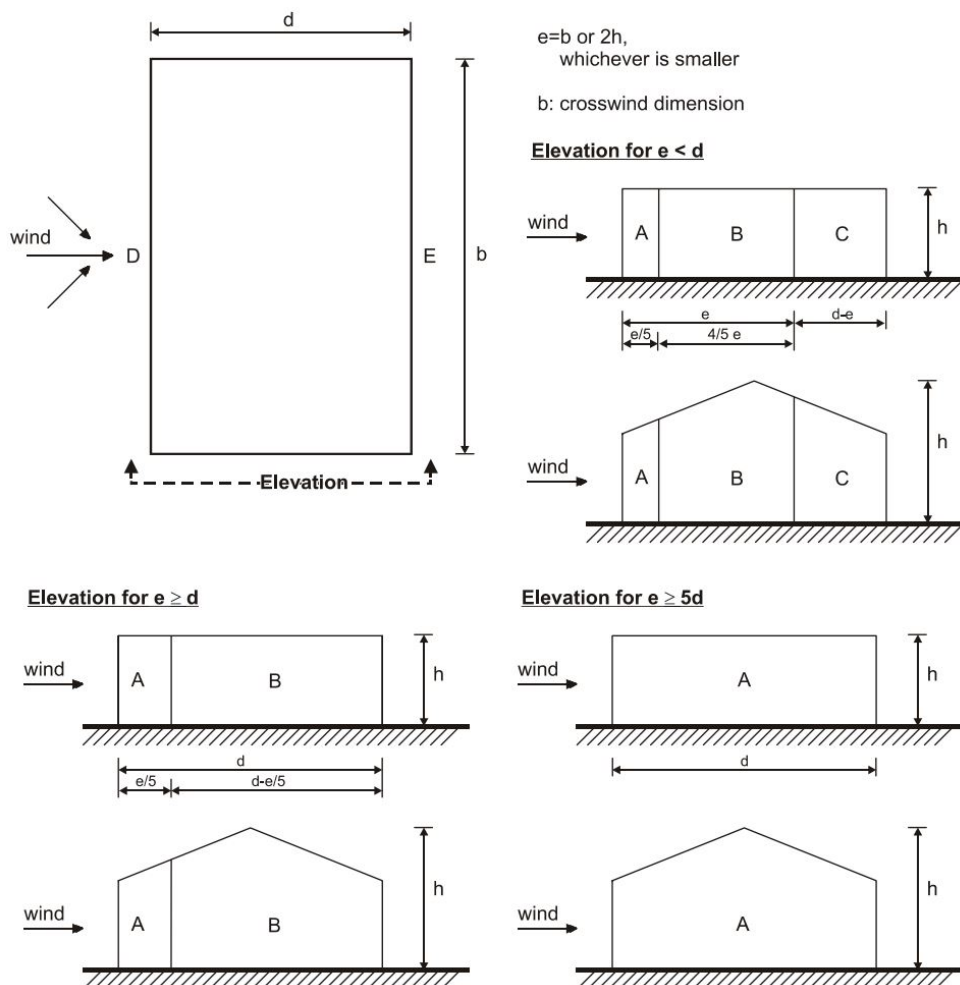


Figure A.19: External pressure coefficients [73].

External pressure coefficients $c_{pe,10}$ and $c_{pe,1}$ for different building zones										
Zone	A		B		C		D		E	
h/d	$c_{pe,10}$	$c_{pe,1}$								
5	-1.2	-1.4	-0.8	-1.1	-0.5		+0.8	+1.0		-0.7
1	-1.2	-1.4	-0.8	-1.1	-0.5		+0.8	+1.0		-0.5

Figure A.20: External pressure coefficients $c_{pe,10}$ and $c_{pe,1}$ for different building zones [73].

For values of $\frac{h}{d}$ between 1 and 5, linear interpolation can be used to find the correct value. Furthermore, because of a lack of correlation of wind suction and pressure, for values of $\frac{h}{d} \leq 1$, the resulting forces must be multiplied with 0.85. For values of $\frac{h}{d} \geq 5$, a multiplication factor of 1 is used. A linear interpolation is applied for intermediate values.

The peak velocity pressure, $q_p(z_e)$, is calculated with

$$q_p(z) = (1 + 7 \cdot I_v(z)) \cdot \frac{1}{2} \cdot \rho \cdot v_m^2(z) \quad (\text{A.16})$$

ρ = air density = 1.25 kg/m^3 .

$I_v(z)$ = turbulence intensity, found using Formula A.17

$v_m(z)$ = mean wind value at height z above the terrain, determined using Formula A.18

$$I_v(z) = \frac{k_l}{c_0(z) \cdot \ln\left(\frac{z}{z_0}\right)} \quad (\text{A.17})$$

k_l = turbulence factor = 1.0

$$v_m(z) = c_r(z) \cdot c_0(z) \cdot v_b \quad (\text{A.18})$$

$c_r(z)$ = terrain roughness factor, calculated using Formula A.19

$c_0(z)$ = orography factor = 1.0

v_b = basic wind speed, determined in Formula A.21

Roughness length for different terrain categories.			
Terrain category	Terrain type	z_0	z_{min}
0	Sea or coastal environment	0.005	1
I	Lakes or flat horizontal environment without obstacles	0.01	1
II	Environment with some obstacles	0.05	2
III	Environment with regular obstacles	0.3	5
IV	Environment where at least 15% of the environment is covered with buildings with an average height above 15 meters.	1.0	10

Figure A.21: Roughness length for different terrain categories [73].

c_r is calculated using:

$$c_r(z) = k_r \cdot \ln\left(\frac{z}{z_0}\right) \quad (\text{A.19})$$

k_r = terrain factor, calculated using Formula A.20

z_0 = roughness length found in Formula A.21

$$k_r = 0.19 \cdot \left(\frac{z_0}{0.05}\right)^{0.07} \quad (\text{A.20})$$

z_0 = terrain roughness length, given in Figure 4.30

The basic wind speed v_b , required in Formula A.18 is determined using:

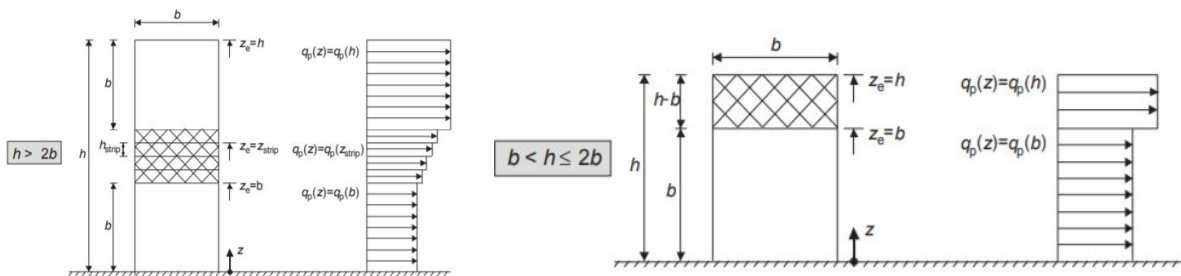
$$v_b = c_{dir} \cdot c_{season} \cdot v_{b,0} \tag{A.21}$$

- c_{dir} = directional factor = 1.0
- c_{season} = seasonal factor = 1.0
- $v_{b,0}$ = as found in Figure A.22

$(v_{b,0})$ for different wind zones			
Wind zone	I	II	III
$(v_{b,0})$ (m/s)	29.5	27.0	24.5

Figure A.22: $v_{b,0}$ for different wind zones [73].

Figure A.23a applies if the height is larger than twice the width of the building.



(a) If the height is larger than twice the width of the building (b) If the height is smaller than twice the width of the building and larger than the width of the building.

Figure A.23: Distribution of the peak velocity pressure over the building.

Wind friction The friction on surfaces parallel to the wind force direction must also be taken into account.

$$F_{fr} = c_{fr} \cdot q_p(z_e) \cdot A_{fr} \tag{A.22}$$

- F_{fr} = wind friction force in kN
- c_{fr} = friction coefficient, see Figure A.24
- $q_p(z_e)$ = peak velocity pressure at height z_e in kN/m^2
- A_{fr} = area of surface parallel to wind force direction in m^2

Friction coefficient c_{fr} for exterior surfaces	
Surfaces	Friction coefficient c_{fr}
Smooth (e.g. steel)	0.01
Rough (e.g. rough concrete)	0.02
Very rough (e.g. wrinkled facade elements)	0.04

Figure A.24: Friction coefficient c_{fr} for exterior surfaces [73].

This wind friction can be neglected if the total area of all surfaces parallel to the wind force direction are smaller than four times the total area of all surface perpendicular to the wind force direction.

Accordingly, see Figure A.25, the wind friction can be neglected if:

$$2hd + db \leq 8hb \tag{A.23}$$

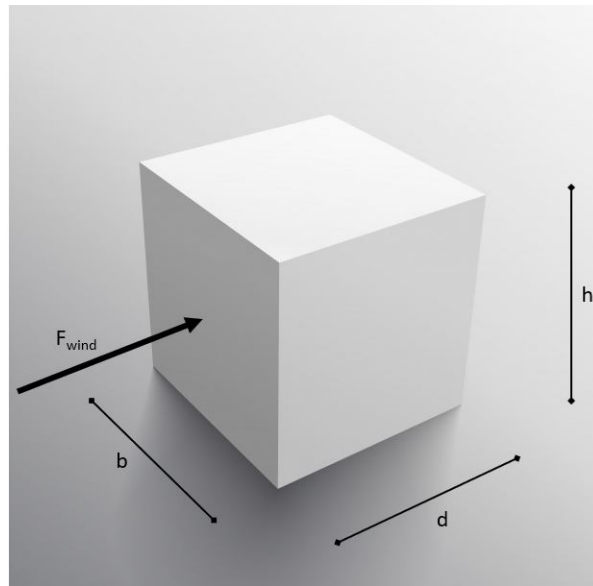


Figure A.25: Wind Friction.

The lowest height will be normative. A minimum height of 50 meters is assumed in this research paper. So, a height of 50 meters will be used. This gives:

$$100d + db \leq 400b \quad (\text{A.24})$$

So,

$$d \leq \frac{400b}{100 + b} \quad (\text{A.25})$$

Assuming the width of the building is minimally 20 meters. It is found that the wind friction can be neglected if the length of the building $d \leq 66.7$ meters. It is assumed such a building shape will not be optimal, so the wind friction is neglected in the calculations.

Dead load

The dead load on the structure consists of the self-weight of the load-bearing structure and skin of the building. This self-weight is multiplied by the gravitational constant g to find the dead load. $g = 10 \text{ m/s}^2$ is used for simplification of the calculations.

Live load

The live loads are defined in the Eurocode. These live loads are determined according to the function of the considered space. This live load is 1.75 kN/m^2 for residential use and 2.50 kN/m^2 for office spaces [72]. The use of light partition walls can be added to this live load. Depending on the used partition wall, a different live load is used. For this research a load of 0.50 kN/m^2 is used to take these partition walls into account. For the upper two floors, this full live load is added. For the other floors, the factor ψ_0 is used to determine the live loads.

Snow load

For the snow load, a load of 0.56 kN/m^2 is used applied to the roof of the building [81]. This snow load is assumed to be larger than the maximum rain load on the roof of the building.

A.4.2. Serviceability Limit State

When a structure satisfies the serviceability limit state, it is ensured the structure will serviceable and perform its intended function throughout its lifetime. The following subsections will cover the aspects the structure must satisfy to ensure its serviceability.

Horizontal deformation

The maximum horizontal deformation of the total building is given in the national annex of EN 1990:

$$u_{max} = \frac{h}{500} \quad (\text{A.26})$$

h = building height

Part of the horizontal deformation is caused by the rotational stiffness of the foundation. However, the rotational stiffness of the foundation is not considered in the structural model. Therefore a stricter equation for determination of the maximum horizontal deformation is determined [62], see Formula A.27. Second-order effects, as discussed in Annex A.4.3 also effect the horizontal deformation.

$$u_{max} = \frac{h}{750} \quad (\text{A.27})$$

Vertical deformation

For the floors, a maximum vertical deformation is specified.

$$w_{inst} = \frac{l}{300} \quad (\text{A.28})$$

w_{inst} = deflection due to permanent load immediately after permanent load is applied.

l = length of floor

$$w_{net,fin} = \frac{l}{250} \quad (\text{A.29})$$

$w_{net,fin}$ = long term deflection under permanent loading

See Figure A.26.

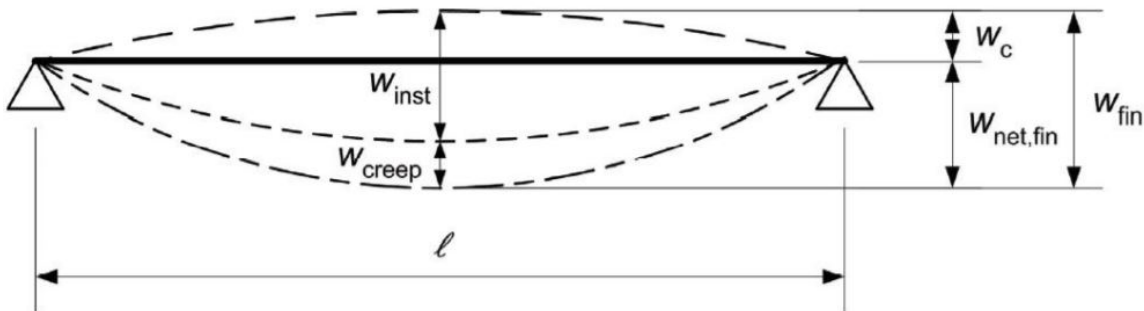


Figure A.26: Determination of total vertical deformation [75]

The creep factor k_{def} is 0.6 for glulam, CLT and LVL. The creep is taken into account by calculating the final modulus of elasticity, using the following equation:

$$E_{mean,final} = \frac{E_{mean}}{1 + k_{def}} \quad (\text{A.30})$$

$$u_{fin} = u_{fin,G} + u_{fin,Q_1} + \sum u_{fin,Q_i} \quad (\text{A.31})$$

For the permanent load:

$$u_{fin,G} = u_{inst,G} (1 + k_{def}) \quad (\text{A.32})$$

For the leading variable load:

$$u_{fin,Q_1} = u_{inst,Q_1} (1 + \psi_{2,1} k_{def}) \quad (\text{A.33})$$

For the other variable loads:

$$u_{fin,Q_i} = u_{inst,Q_i} (\psi_{0,i} + \psi_{2,1} k_{def}) \quad (\text{A.34})$$

Acceleration

Because of the relatively low structural weight of timber high-rise, accelerations caused by wind are important to analyse. These accelerations can cause nausea to the users of the buildings. Various vibrations and their effects are listed in Figure A.27.

Human perception levels		
Range	Acceleration (m/s^2)	Effect
1	< 0.05	Humans cannot perceive motion.
2	0.05-0.10	Sensitive people can perceive motion; hanging objects may move slightly.
3	0.10-0.25	Majority of people will perceive motion, level of motion may effect. desk work, long-term exposure may produce motion sickness.
4	0.25-0.40	Desk work becomes difficult or almost impossible, ambulation still possible.
5	0.40-0.50	People strongly perceive motion, difficult to walk naturally, standing people may lose balance.
6	0.50-0.60	Most people cannot tolerate motion and are unable to walk naturally.
7	0.60-0.70	People cannot walk or tolerate motion.
8	> 0.85	Objects begin to fall and people may be injured.

Figure A.27: Human Perception Levels [166].

The maximum allowed acceleration for buildings is given in the NEN-EN 1990-1-1 [80], see figure A.28.

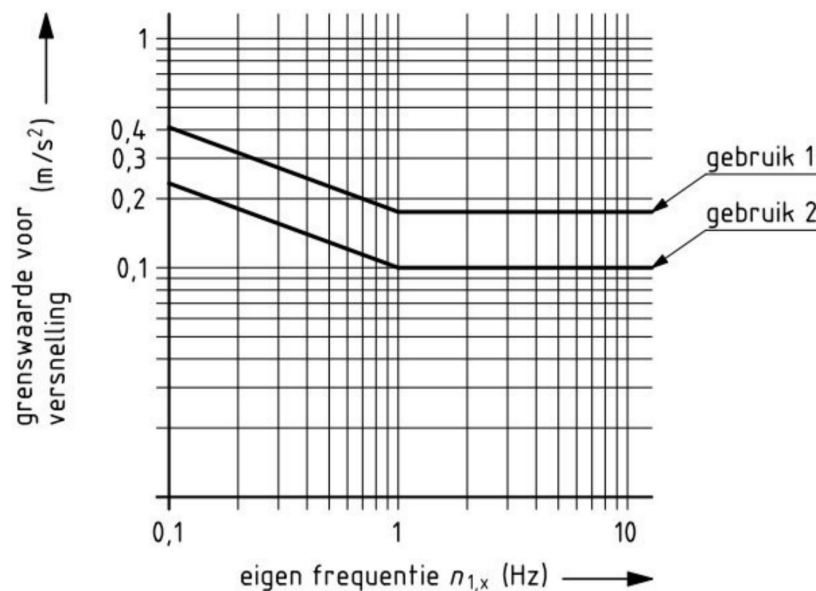


Figure A.28: Maximum allowed acceleration for a building as specified in NEN-EN 1990-1-1 [84].

Van Rhijn (2020) determined the acceleration for timber high-rise using various lateral stability systems. All found results were within the maximum acceleration limits for office buildings, without needed alternations. So, it can be concluded that the maximum allowed acceleration for office buildings is often achievable without additional adjustments. However, Van Rhijn found that all 70 meter high buildings did not satisfy the acceleration requirements for residential buildings. For residential buildings with a building height of less than 50 meters, roughly all buildings did satisfy the requirements [155]. A critical note must be made on this research, since it does not include torsional vibration of the building.

A building can have three types of responses when exposed to wind loads. Van Oosterhout (1996) analysed these responses and found three different possible responses, see Figure A.29, each being normative depending on the structural shape [153].

- **Along-wind response:** Normative when the building width is considerably larger than the building depth.

- **Cross-wind response:** Normative for cylindrical or square buildings
- **Torsional response:** Normative for asymmetrical shapes regarding mass and stiffness of the building.

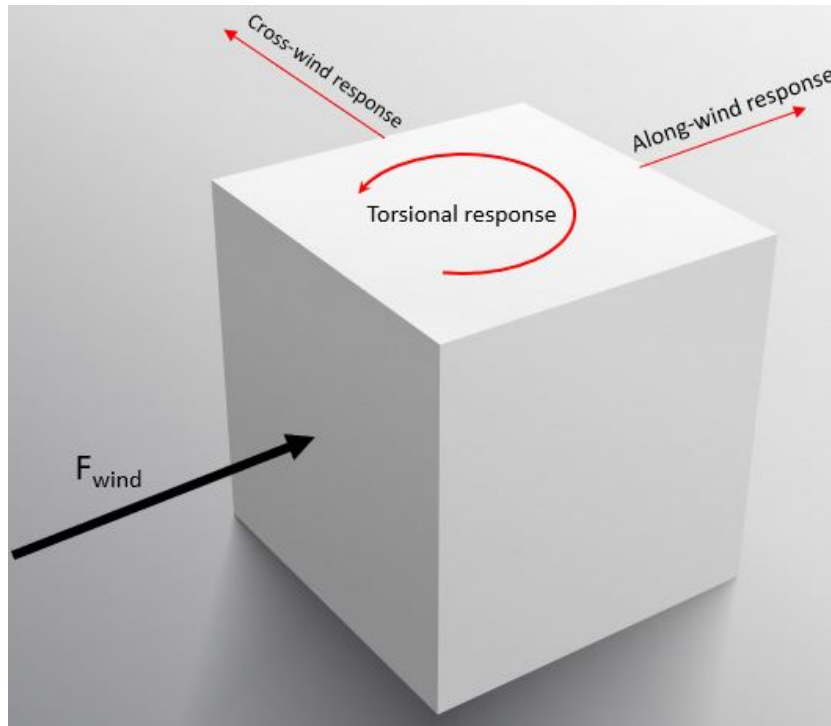


Figure A.29: Possible building response caused by wind load.

Based on this, the along-wind response, or the cross-wind response is assumed to be normative depending on the design situation.

Torsional response To accurately account for the total vibrations in a building, the bending vibration in X- and Y-direction must be calculated and both must be added to the torsional vibration of the building to obtain the total vibration of the building. For buildings below 70 meters, the 1990-1-1 does not include the calculation of the torsional vibration in the calculation of the total vibration, if the mass of the building is equally distributed over the height. For buildings over 70 meters, the NTA 4614-3 provides additional information for high-rise buildings over 70 meters [77]. It includes guidelines on correctly determining the torsional vibration.

Along-wind response

$$n_{1,x} = \frac{46}{h} \quad (\text{A.35})$$

$n_{1,x}$ = first natural frequency of the building

h = height of the structure

$$a_{wind} = 1.6 \cdot \frac{\phi_2 \cdot \rho_{vw,1} \cdot c_{pe} \cdot b_m}{\rho_l} \quad (\text{A.36})$$

a_{wind} = acceleration of top level of the building.

ϕ_2 = dynamic factor for vibrations caused by wind, calculated using Formula A.37.

$\rho_{vw,1}$ = value for varying part of the wind pressure, determined using Formula A.38.

c_{pe} = sum of external wind pressure coefficients.

b_m = width of the building perpendicular to the direction of the wind.

ρ_l = total mass of the building.

$$\phi_2 = \sqrt{\frac{0.0344 (n_{1,x})^{-2/3}}{D(1 + 0.12n_{1,x}h)(1 + 0.2n_{1,x}b_m)}} \quad (\text{A.37})$$

ϕ_2 = dynamic factor for vibrations caused by wind
 D = damping coefficient of the building
 $n_{1,x}$ = first natural frequency of the building
 h = height of the structure
 b_m = width of the building perpendicular to the direction of the wind.

$$\rho_{vw,1} = 100 \cdot \ln\left(\frac{h}{0.2}\right) \quad (\text{A.38})$$

$\rho_{vw,1}$ = value for varying part of the wind pressure.
 h = height of the structure

For D , the damping coefficient of the building, the Eurocode gives a value of 0.01 for buildings with a natural frequency lower than 1 Hz. However, this damping coefficient is considered to be on the conservative side. It is expected that due to the weak soil in the Netherlands and the use of pile foundations will result in higher damping coefficient in Dutch buildings [142]. Furthermore, timber connections influence the damping of the structure. According to Stathopoulos (2007) the damping ratio for timber frame towers is higher than for solid timber towers, because the connection enable small movements between the elements [137].

The research of Feldmann et al. (2016) showed an average structural damping ratio of 0.02 for tall timber structures up to 100m [49]. A damping ratio of 0.019 was used for the design of Mjøstårnet [8]. So, the 0.01 structural damping ratio as given in the Eurocode is a conservative assumption.

Cross-wind response The Eurocode does not specify a calculation of the cross-wind response of a building. However, it does elaborate on a calculation of the vortex shedding effect, and whether this effect must be taken into account. This vortex shedding effect is caused by wind turbulence, and will be used to account for cross-wind response in this research.

$$v_{crit} \geq 1.25 \cdot v_m(z) \quad (\text{A.39})$$

$v_m(z)$ = mean wind velocity at the top of the building.
 v_{crit} = critical wind velocity for vortex shedding, determined using Equation A.40

$$v_{crit} = \frac{b \cdot n_{1,x}}{S_T} \quad (\text{A.40})$$

b = building width
 $n_{1,x}$ = first natural frequency of the building, calculated using Equation A.35
 S_T = Strouhal number, equal to $0.15 \cdot \frac{\text{Buildingdepth}}{\text{Buildingwidth}}$

To calculate the Strouhal number, for simplification reasons, the normative factor of 0.15 is used.

Inter storey drift

The inter-storey drift gives a maximum horizontal displacement between two subsequent floors. The inter-storey drift is defined as:

$$\delta = (\Delta_2 - \Delta_1) / h \leq \frac{1}{400} \quad (\text{A.41})$$

Δ_1 = horizontal displacement of a specific floor
 Δ_2 = horizontal displacement of floor above floor Δ_1
 h = storey height

A.4.3. Ultimate Limit State

Normal force

Normal force parallel to the grain.

$$\sigma_{c,0,d} = \frac{N_{Ed}}{A} \leq f_{c,0,d} \quad (\text{A.42})$$

$$\sigma_{t,0,d} = \frac{N_{Ed}}{A} \leq f_{t,0,d} \quad (\text{A.43})$$

Normal force perpendicular to the grain.

$$\sigma_{c,90,d} \leq k_{c,90} \cdot f_{c,90,d} \quad (\text{A.44})$$

$$\sigma_{t,90,d} \leq k_{t,90} \cdot f_{t,90,d} \quad (\text{A.45})$$

Shear

$$\tau_d = \frac{3}{2} \frac{V_d}{A} \leq f_{v,d} \quad (\text{A.46})$$

k_{cr} = reduction factor caused by cracks, for prismatic cross sections $k_{cr} = 1.0$

Bending moment

$$\sigma_{m,d} = \frac{M_d}{W} \leq f_{m,d} \quad (\text{A.47})$$

Where M_d is the design bending moment, W is the moment of resistance, and $f_{m,d}$ is the design bending strength.

Combined moment and axial tension

$$\frac{\sigma_{t,0,d}}{f_{t,0,d}} + \frac{\sigma_{m,y,d}}{f_{m,y,d}} + k_m \frac{\sigma_{m,z,d}}{f_{m,z,d}} \leq 1 \quad (\text{A.48})$$

$$\frac{\sigma_{t,0,d}}{f_{t,0,d}} + k_m \frac{\sigma_{m,y,d}}{f_{m,y,d}} + \frac{\sigma_{m,z,d}}{f_{m,z,d}} \leq 1 \quad (\text{A.49})$$

Combined moment and axial compression

$$\left(\frac{\sigma_{c,0,d}}{f_{c,0,d}} \right)^2 + \frac{\sigma_{m,y,d}}{f_{m,y,d}} + k_m \cdot \frac{\sigma_{m,z,d}}{f_{m,z,d}} \leq 1.0 \quad (\text{A.50})$$

$$\left(\frac{\sigma_{c,0,d}}{f_{c,0,d}} \right)^2 + k_m \frac{\sigma_{m,y,d}}{f_{m,y,d}} + \frac{\sigma_{m,z,d}}{f_{m,z,d}} \leq 1.0 \quad (\text{A.51})$$

k_m = Factor for re-distribution of stresses and the effect of inhomogeneities in the cross section.

For solid timber, glulam and LVL $k_m = 0.7$. For other timber products or when $h/b > 4$, $k_m = 1.0$.

Second order effect

The second order effect accounts for the combination of wind loads and gravitational loads. When, a wind load causes horizontal deflection of the building, the center of gravity of the building will shift relative to the foundation. This shift of the center of gravity of the building will result in a displacement of the gravitational loads relative to the base of the building. This leads to an additional moment in the base of the building, see Figure A.30. This effect is known as the second order effect or the P- Δ effect. Slooten (2018) and Gijzen (2017) both analysed timber high-rise structure and reported an additional 10% of deflection caused by second-order effects [57], [134].

These second-order effects influence the horizontal deflection. The maximum horizontal deflection was determined to be $\frac{h}{750}$, see Equation A.27. To account for this additional 10% of deflection caused by second-order effects, the maximum horizontal deflection is given in Equation A.52.

$$u_{max} = \frac{h}{825} \quad (\text{A.52})$$

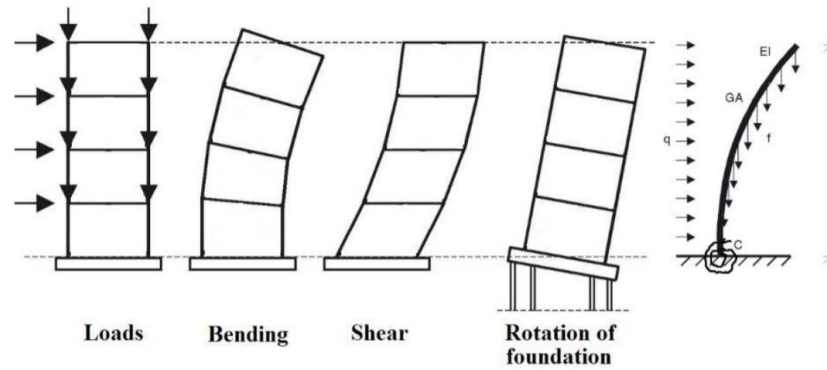


Figure A.30: Simple model of second order effects [68].

Global initial sway imperfections

Imperfections in the materials can create an initial skew of the frame. This skew of the frame will provide additional horizontal forces on the structure in the façade of the building. NEN-EN 1993-1-1 is used to determine the global initial sway imperfection [83].

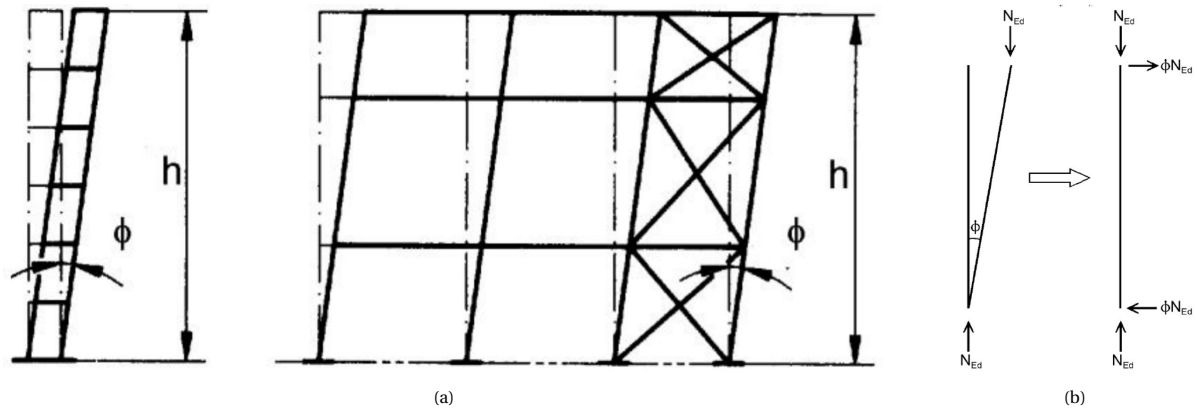


Figure A.31: Global initial sway imperfection [83].

$$\phi = \phi_0 \cdot \alpha_h \cdot \alpha_m \quad (\text{A.53})$$

ϕ_0 = basic value, $\phi_0 = \frac{1}{200}$

α_h = reduction factor for height h applicable to columns: $\alpha_h = \frac{2}{\sqrt{h}}$, but $\frac{2}{3} \leq \alpha_h \leq 1.0$

h = height of the structure

α_m = reduction factor for the number of columns in a row $\sqrt{0.5 \cdot (1 + \frac{1}{m})}$

m = number of columns in a row which carry a vertical load $N_{Ed} \geq 50\%$ of the average vertical load

The additional horizontal force on the structure in the façade of the building is equal to the vertical force on the considered column multiplied by ϕ .

Buckling

In the case of a compression force, buckling can occur.

$$\sigma_{c,0,d} \leq k_c \cdot f_{c,0,d} \quad (\text{A.54})$$

k_c = instability factor, determined by:

$$k_c = \frac{1}{k + \sqrt{k^2 - \lambda_{rel}^2}} \quad (\text{A.55})$$

$$k = 0.5 \cdot (1 + \beta_c \cdot (\lambda_{rel} - 0.3) + \lambda_{rel}^2) \quad (\text{A.56})$$

β_c = factor. For glulam and LVL $\beta_c = 0.1$

λ_{rel} = relative slenderness, determined by:

$$\lambda_{rel} = \frac{\lambda}{\pi} \sqrt{\frac{f_{c,0,k}}{E_{0.05}}} \quad (\text{A.57})$$

$E_{0.05}$ = 5% value of the modulus of elasticity

λ = slenderness of the column, determined using:

$$\lambda = \frac{l_{eff}}{i} \quad (\text{A.58})$$

l_{eff} = buckling length

i = radius of gyration, given in:

$$i = \frac{I}{A} \quad (\text{A.59})$$

I = moment of inertia

A = cross sectional area

The moment of inertia for CLT can be calculated using:

$$I_{net} = b \cdot \sum_{i=1}^n \left(\frac{t_i^3}{12} + t_i \cdot a_i^2 \right) \quad (\text{A.60})$$

n = number of lamella in loaded direction

b = one meter wide strip

t_i = thickness of the lamellae i

a_i = distance of the middle of the lamellae to the centre of gravity of the cross section

The following unity check is done when $\lambda_{rel} \leq 0.3$

$$u.c. = \left(\frac{\sigma_{c,0,d}}{f_{c,0,d}} \right)^2 + \frac{\sigma_{m,y,d}}{f_{m,y,d}} + k_m \cdot \frac{\sigma_{m,z,d}}{f_{m,z,d}} \leq 1.0 \quad (\text{A.61})$$

$$u.c. = \left(\frac{\sigma_{c,0,d}}{f_{c,0,d}} \right)^2 + \frac{\sigma_{m,z,d}}{f_{m,z,d}} + k_m \cdot \frac{\sigma_{m,y,d}}{f_{m,y,d}} \quad (\text{A.62})$$

For the used columns, a square cross section is assumed, so

$$u.c. = \left(\frac{\sigma_{c,0,d}}{f_{c,0,d}} \right)^2 + (1 + k_m) \cdot \frac{\sigma_{m,d}}{f_{m,d}} \quad (\text{A.63})$$

If $\lambda_{rel} > 0.3$:

$$u.c. = \frac{\sigma_{c,0,d}}{k_{c,y} \cdot f_{c,0,d}} + \frac{\sigma_{m,y,d}}{f_{m,y,d}} + k_m \cdot \frac{\sigma_{m,z,d}}{f_{m,z,d}} \quad (\text{A.64})$$

$$u.c. = \frac{\sigma_{c,0,d}}{k_{c,z} \cdot f_{c,0,d}} + \frac{\sigma_{m,z,d}}{f_{m,z,d}} + k_m \cdot \frac{\sigma_{m,y,d}}{f_{m,y,d}} \quad (\text{A.65})$$

For the used columns, a square cross section is assumed, so

$$u.c. = \frac{\sigma_{c,0,d}}{k_c \cdot f_{c,0,d}} + (1 + k_m) \cdot \frac{\sigma_{m,d}}{f_{m,d}} \quad (\text{A.66})$$

Robustness

The Eurocode NEN-EN 1991-1-7 gives design guidelines for creating sufficient robustness in a structure in case of local structural failure. This local structural failure can be caused by vehicle impact or an explosion. There are two strategies to guarantee sufficient global strength of a structure in case of local structural failure.

- tension ties
- secondary load paths: The structure is designed in such a way that neighbouring structural elements are able to take the additional forces caused by the local failure. A secondary load path is created.

The verification of the robustness of the structure is outside the scope and is not verified in the tool.

Internal wind pressure

Apart from wind loads on the building, the internal wind pressure must also be considered. This internal wind pressure acts on walls inside the building. For determination of these internal wind loads, Formula A.15 is used. Here, the force coefficient is found by summing the internal pressure coefficient for suction and pressure. This gives $0.2 - -0.3 = 0.5$ according to NEN-EN 1991-1-4 [73].

A.4.4. Fire safety

As section A.1.4 discusses, when properly designed, a timber structure can provide sufficient fire safety. This is the result of the charring process that occurs when a timber element is burning. The outside of this timber element begins to char, and this charring layer provides insulation to the fire to the inner part of the timber element, see Figure A.32.



Figure A.32: Charring of timber [2].

Providing fire safety consists of two main principles. At first the reaction to fire of the material and secondly the fire resistance of the material.

"Bouwbesluit 2012" gives the required fire resistance for structural elements. For this building, the main load bearing system must maintain its structural function at least 120 minutes. The secondary load bearing system, such as floors, must maintain their structural function for at least 90 minutes.

Furthermore, if the fire load in a fire compartment is below $500 \text{ MJ}/\text{m}^2$, the fire resistance can be reduced with 30 minutes. Since timber is combustible, it is assumed this fire load below $500 \text{ MJ}/\text{m}^2$ can not be achieved, So, the reduction will not be used. In other timber buildings, for example in Mjøstårnet, a sprinkler system is used to decrease the fire load below $500 \text{ MJ}/\text{m}^2$.

Fire safety strategy The reduced cross section method is used to assure structural safety during a fire. When a timber element is burning, it begins charring. This charring layer provides insulation to the fire to the inner part of the timber element. This inner part of the timber element that is protected is called the effective cross section. Using the reduced cross section method, the dimensions if this effective cross section is determined, see Figure A.33.

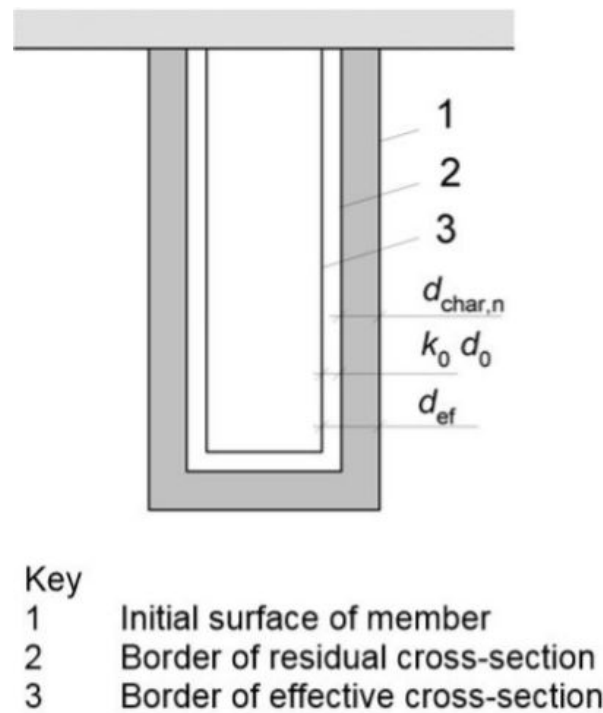


Figure A.33: Reduced cross section method [74].

This effective cross section must be able to fulfil its structural function. There are two strategies to make sure this effective cross section has sufficient dimensions to fulfil its structural function.

- **Exposed fire safety strategy** The dimensions of the timber element are increased to increase the dimensions of the effective cross section.
- **Gypsum encapsulated strategy** Gypsum boards is added to the timber element to increase the dimensions of the effective cross section.

Exposed fire safety strategy To determine the effective cross section for unprotected timber the following formula is used:

$$d_{ef} = d_{char,n} + k_0 \cdot d_0 \quad (\text{A.67})$$

d_{ef} = effective charring depth

k_0 = factor for unprotected surfaces. When $t \geq 20 \text{ min}$, $k_0 = 1.0$

d_0 = 7 mm

$d_{char,n}$ = Notional charring depth, determined using:

$$d_{char,n} = \beta_n \cdot t \quad (\text{A.68})$$

β_n = notional charring rate in mm/min
 t = time in minutes

For glulam with a characteristic density $\geq 290 \text{ kg/m}^3$, a notional charring rate β_n of 0.7 mm/min can be used. For CLT a notional charring rate β_n of 0.65 mm/min can be assumed.

Gypsum encapsulated strategy Gypsum boards are used to protect the timber. The time until the timber starts to char can be determined using:

$$t_{ch} = 2.8 \cdot h_p - 14 \quad (\text{A.69})$$

h_p = thickness of the cladding
 t = time after which the timber starts to char in minutes

When the protected timber starts to char, a multiplication factor k_3 is used. This factor is equal to 2 and increases the charring rate.

$$t_a = \min \left\{ \frac{2 \cdot t_f}{k_3 \cdot \beta_n} + t_f \right\} \quad (\text{A.70})$$

h_p = time after which notional charring rate β_n will be used
 t = time in minutes the timber is protected

The difference in charring speed between the two strategies with unprotected and protected timber is shown in Figure A.34.

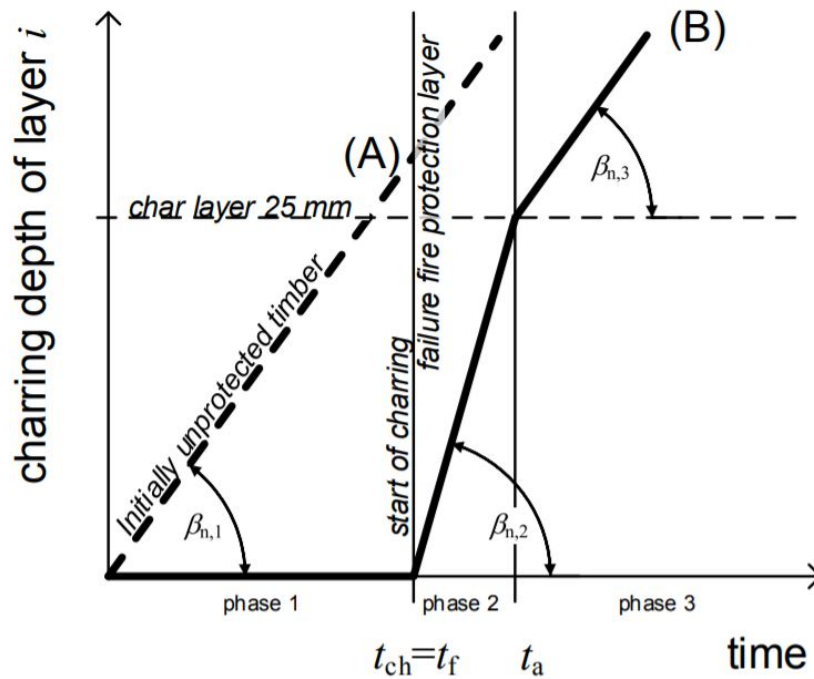


Figure A.34: Charring rates for unprotected (A) and protected (B) timber [46].

This reduced cross sections needs to be verified.

$$R_{d,t,fi} = \eta \cdot \frac{R_{20}}{\gamma_{M,fi}} \quad (\text{A.71})$$

$R_{d,t,fi}$ = design value for load bearing capacity under fire conditions
 η = conversion factor used when verifying connections
 R_{20} = 20% fractile value of the resistance, calculated using Formula A.73.
 $\gamma_{M,fi}$ = partial safety factor of material during fire. $\gamma_{M,fi} = 1.0$ for timber

$$R_{20} = k_{fi} \cdot f_k \tag{A.72}$$

R_{20} = 20% fractile value of the resistance
 k_{fi} = factor which is 1.15 for laminated timber
 f_k = characteristic resistance

The total loads on the structure can be reduced in a fire situation. For this, the following formula is used:

$$E_{d,fi} = \eta_{fi} \cdot E_d \tag{A.73}$$

E_d = design value of the loads under normal conditions
 $\eta_{fi} = 0.45$

A.5. Level Of Development

The Level of Development and estimating (LOD) determines the exactness of a design, from estimated approximation to exact representation[96]. The LOD defines what geometric and non-geometric data is included in the BIM model. The LOD also helps describing the usability and limitations of this data [94]. The American Institute of Architects (AIA) was the first to define the LOD in 2008 [11]. These definitions were extended by the BIMForum in 2018 [20]. The definition of LOD is still unclear, as a result of the vague terms used in the LOD definitions [149]. For this project, the LOD specifications as defined by BIMForum in 2018 are used [20], see Figure A.35.

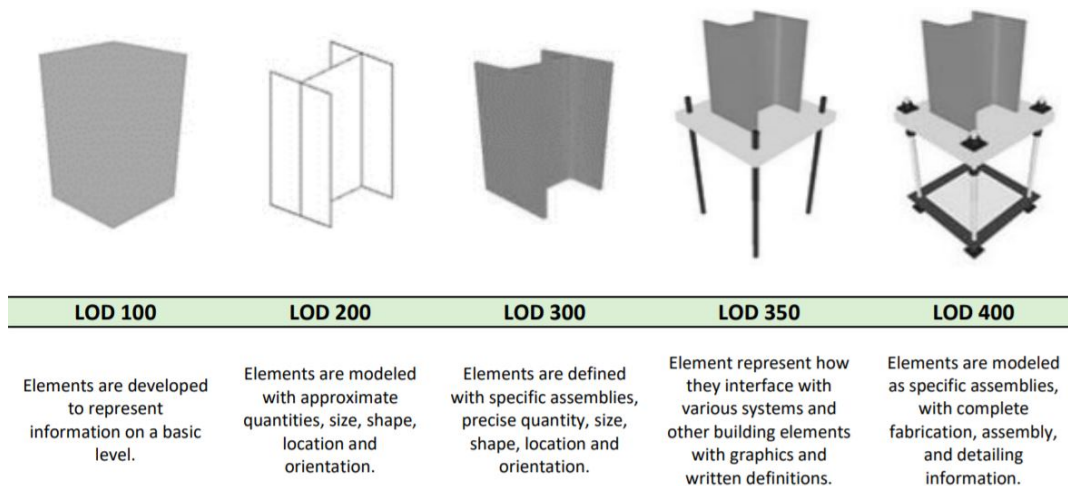


Figure A.35: Levels of Development [20].

According to Svalestuen et al. (2018), a LOD of 100 or 200 is sufficient in the conceptual design phase [139]. So, in this research, a LOD of 200 will be used. According to BIMForum, at LOD 200, elements are generic placeholders, and results are considered approximate. Elements can be identified as the components they represent or can be volumes of spaces [20].

A.6. Optimize Cross Section

Figure A.36 shows the Karamba3D's Optimize Cross Section component. This component aims to size each member for axial forces, bending moments, shear, local buckling and torsion through an iterative process. It does so through a finite element analysis and is based on the requirements as specified in Eurocode 3 for steel structures.

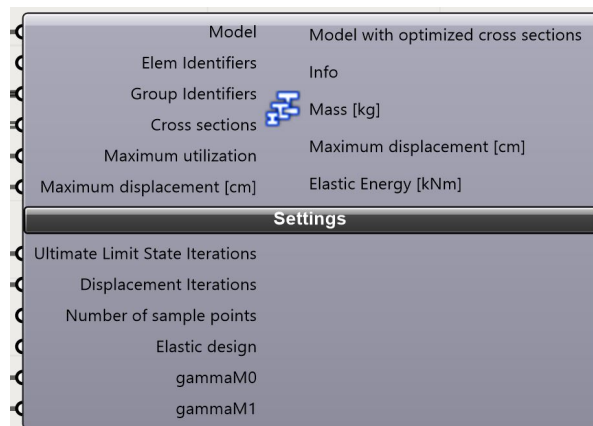


Figure A.36: Karamba3D's Optimize Cross Section component.

The Optimize Cross Section component requires the following input:

- **The Karamba3D model.**
- **The identifiers of the members.** These members can be individual or grouped. When members are grouped, all members will have the same cross section as the normative member of the group. Section 5.7.1 mentions how the grouping of members is done.
- **A list of cross sections.** This list contains the material properties of the cross sections.
- **A maximum utilization and maximum displacement value.** Two components are required, one for the ULS check where the maximum utilization equals the maximum unity check. And one for the SLS check where the maximum displacement is set to the total height of the building divided by 750.
- **A set amount of iterations.**
- **gammaM0 and gammaM1** These values account for the k_{mod} and the γ_m factor. $k_{mod} = 0.8$ and $\gamma_m = 1.25$. This gives a factor of gammaM0 of

$$\gamma_{M0} = \frac{1 \cdot \gamma_m}{k_{mod}} = \frac{1 \cdot 1.25}{0.8} = 1.5625 \quad (\text{A.74})$$

So gammaM0 and gammaM1 are set to 1.5625 to

One cycle of this iterative process can be divided into three separate steps.

1. Using the initial cross section, the forces and moments at a number of points along all elements are determined.
2. For these elements of group of elements, the first sufficient cross section is selected which satisfies all requirements for axial forces, bending moments, shear, local buckling and torsion
3. If the cross sections as determined in step 1 and step 2 are identical or the maximum number of iterations is reached, the algorithm stops. Otherwise, the found cross sections in step 2 are set as the input cross sections in step 1.

Generally, five of these cycles are sufficient to obtain the required cross sections which satisfy the maximum displacement requirements. However, there is no guarantee that the iteration converges.

A.6.1. Verification

Karamba3D's Optimize Cross Section component is tested by creating four simple models, which can easily be verified with hand calculations, see Figure A.37. In this picture, a red arrow indicates a force, and a purple area a bending moment. The component is created for isotropic materials. The verification is performed by analyzing the optimal cross sections as obtained using the component for the four simple models. This cross section is compared to the cross section as required using a hand calculation. This way, the component is verified for several failure mechanisms, see Figure A.38

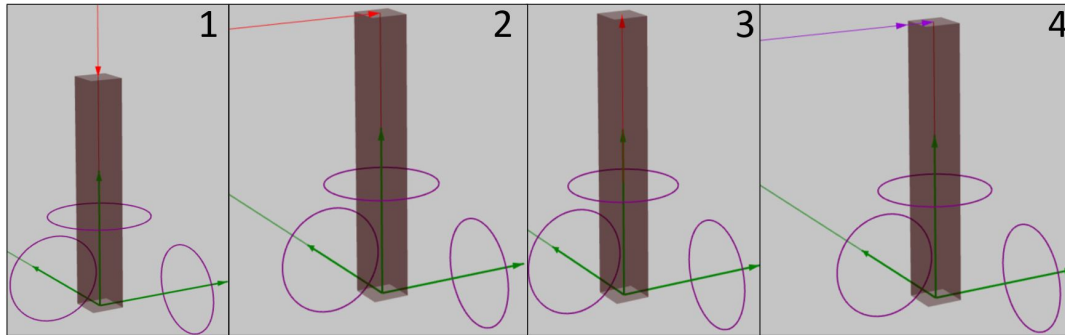
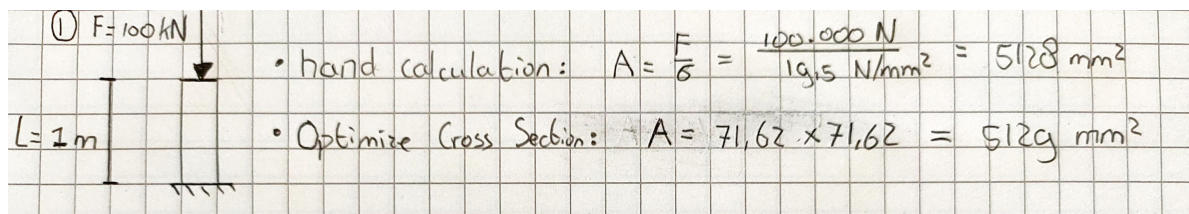
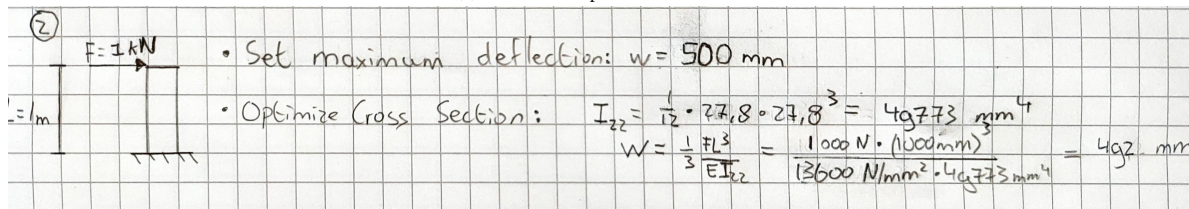


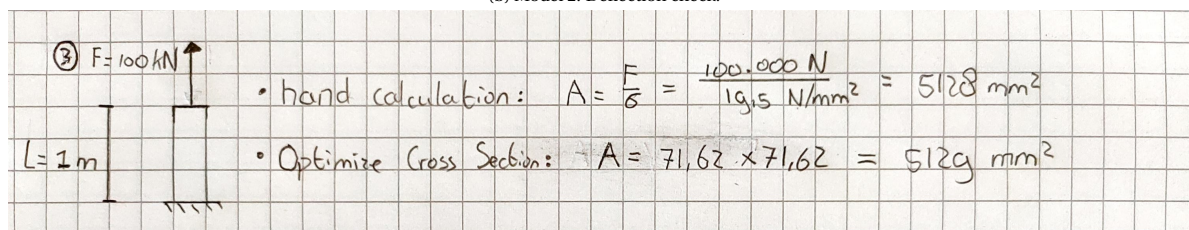
Figure A.37: Verification of Karamba3D's Optimize Cross Section component.



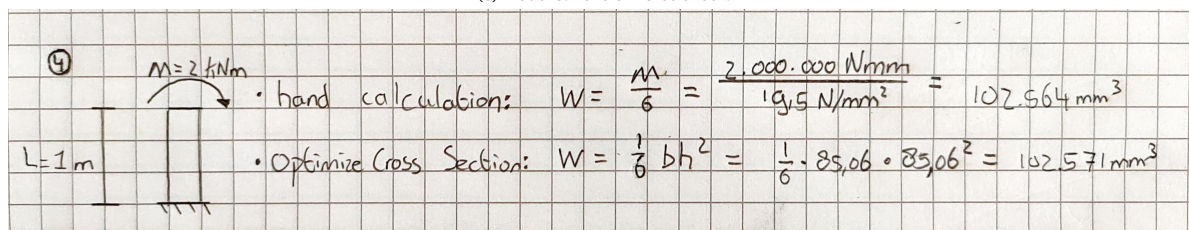
(a) Model 1: Compression force check.



(b) Model 2: Deflection check.



(c) Model 3: Tension force check.



(d) Model 4: Bending moment check.

Figure A.38: Verification of four failure mechanisms

Figure A.38 clearly shows the accuracy of the component for determining optimal cross sections for four failure mechanisms, which confirms the feasibility for implementation of the component for orthotropic materials. However, two disadvantages are found for implementation of this component. Firstly, The component uses a yield strength in strong and weak direction, thus assuming the compressive and tensile design strengths are similar. However, for engineered timber, the maximum tension design strength of the material is roughly 80% of the maximum compression design strength in the strong direction. Secondly, the component analyses the elements on buckling based on the design using steel elements in NEN-EN 1993-1-1. These calculations differ compared to the buckling calculations for timber structures. To account for these two disadvantages, the yield strength is assumed to equal the maximum tensile design strength. This way, the compression design strength is smaller than in reality, but this conservative assumption might be required since buckling is not accurately regarded.

B

Calculation of Building Elements

B.1. Steel plate and dowel connection

B.1.1. Custom node calculation

General calculations	
	Used formula
Charring depth after fire of 120 minutes	$d_{120} = 7 + 0.7 \cdot t_{res}$
t_1	$t_1 = d_{120}$
Reduced width of section	$w_{red} = w - 2 \cdot t_1$
Reduced depth of section	$d_{red} = w_{red}$
a_1	$a_1 = 5 \cdot d_{dowel}$
a_2	$a_2 = 3 \cdot d_{dowel}$
$a_{3,t}$	$a_{3,t} = \max(7 \cdot d_{dowel}, 80)$
$a_{3,c}$	$a_{3,c} = 3 \cdot d_{dowel}$
$a_{4,t}$	$a_{4,t} = 3 \cdot d_{dowel}$
Edge distance	$d_{edges} = 2 \cdot a_{4,t}$
Number of dowel columns	$[Cols] = \frac{w_{red} - d_{edges}}{a_2} + 1$
Minimum required plate length	$[Rows] = \frac{length_{steelplate} - a_{3,t} - a_{4,t}}{a_1}$

Figure B.1: Steel plate dowel connection general calculation

Net timber area failure	
	Used formula
Netto timber area	$A_{net} = w^2 - (w \cdot Cols \cdot d_{dowel}) - (d_{red} \cdot N_{steelplates} \cdot t_{steelplate})$
Maximum compression force	$F_{max,c1} = f_{c,0,k} \cdot A_{net} / 1000$
Maximum tension force	$F_{max,t1} = 0.4 \cdot f_{t,0,k} \cdot A_{net} / 1000$

Figure B.2: Net timber area failure calculation

Steel plate failure	
	Used formula
Maximum compression force	$F_{max,c2} = f_y \cdot N_{steelplates} \cdot t_{steelplate} \cdot d_{red} / 1000$
Maximum tension force	$F_{max,t2} = f_y \cdot N_{steelplates} \cdot t_{steelplate} \cdot d_{red} / 1000$

Figure B.3: Steel plate calculation

Steel plate failure	
	Used formula
Maximum tension force	$F_{max,t5} = \frac{0.9 \cdot f_u / 1000 \cdot (N_{steelplates} \cdot Thickness_{steelplate} \cdot (d_{red} - Cols \cdot d_{dowel}))}{\gamma_{m2}}$

Figure B.4: Steel plate failure calculation

Dowel failure	
	Used formula
Embedment strength	$f_h = 0.082 \cdot (1 - 0.01 \cdot d_{dowel}) \cdot \rho_k$
t_2	$t_2 = \frac{Width_{diagonal,red}}{(N_{steelplates} - 1)}$
Plastic yield moment of dowel	$M_y = (1/6) \cdot d_{dowel}^3 \cdot f_y$
Dowel failure mechanism 1	$F_{dowel1} = 0.25 \cdot (2 \cdot t_1 + t_2) \cdot d_{dowel} \cdot f_h / 1000$
Dowel failure mechanism 2	$F_{dowel2} = \left(-\frac{t_1}{2} + \frac{t_2}{4} + \sqrt{\frac{1}{2}t_1^2 + \frac{M_y}{d_{dowel} \cdot f_h}} \right) \cdot d_{dowel} \cdot f_h / 1000$
Dowel failure mechanism 3	$F_{dowel3} = \sqrt{4 \cdot M_y \cdot d_{dowel} \cdot f_h} / 1000$
Dowel failure mechanism 4	$F_{dowel4} = \left(\frac{1}{2}t_1 + \frac{1}{2}\sqrt{t_1^2 + \frac{2 \cdot M_y}{d_{dowel} \cdot f_h}} \right) \cdot d_{dowel} \cdot f_h / 1000$
Dowel failure mechanism 5	$F_{dowel5} = \left(\sqrt{\frac{M_y}{d_{dowel} \cdot f_h}} + \frac{1}{2}t_1 \right) \cdot d_{dowel} \cdot f_h / 1000$
Dowel failure mechanism 6	$F_{dowel6} = \left(\sqrt{\frac{M_y}{d_{dowel} \cdot f_h}} + \frac{1}{4}t_2 \right) \cdot d_{dowel} \cdot f_h / 1000$
Dowel failure mechanism 7	$F_{dowel7} = \left(-\frac{1}{2}t_1 + \sqrt{\frac{1}{2}t_1^2 + \frac{M_y}{d_{dowel} \cdot f_h}} + \sqrt{\frac{M_y}{d_{dowel} \cdot f_h}} \right) \cdot d_{dowel} \cdot f_h / 1000$
Effective number of dowels	$n_{ef} = \min(Rows; Rows^{0.9} \cdot \left(\frac{\alpha_1}{13 \cdot d_{dowel}} \right)^{1/4})$
Maximum compression force	$F_{max,c3} = 4 \cdot n_{ef} \cdot Cols \cdot \min(F_{dowel1}, F_{dowel2}, F_{dowel3}, F_{dowel4}, F_{dowel5}, F_{dowel6}, F_{dowel7})$
Maximum tension force	$F_{max,t3} = 4 \cdot n_{ef} \cdot Cols \cdot \min(F_{dowel1}, F_{dowel2}, F_{dowel3}, F_{dowel4}, F_{dowel5}, F_{dowel6}, F_{dowel7})$

Figure B.5: Dowel failure calculation

Connection failure	
	Used formula
Maximum compression force	$F_{c,max,connection} = k_{mod} \cdot \frac{\min(F_{max,c1}, F_{max,c2}, F_{max,c3})}{\gamma_{m2}}$
Maximum tension force	$F_{t,max,connection} = k_{mod} \cdot \frac{\min(F_{max,t1}, F_{max,t2}, F_{max,t3}, F_{max,t4}, F_{max,t5})}{\gamma_{m2}}$

Figure B.6: Connection failure calculation

Block and plug shear failure	
	Used formula
Length timber area in tension	$l_t = d_{red} - d_{edges} - Cols \cdot d_{dowel}$
Net timber area in tension	$A_{net,t} = l_t \cdot (t_1 + t_1 + t_2)$
Maximum tension force	$F_{bs,1} = 1.5 \cdot A_{net,t} \cdot f_{t,0k} / 1000$
Length timber area in shear	$l_v = 5 \cdot d_{dowel} \cdot (Rows - 1) + \max(7 \cdot d_{dowel}, 80)$
Net timber area in shear	$A_{net,v} = l_v \cdot (t_1 + t_2 + t_1)$
Maximum shear force	$F_{bs,2} = 0.7 \cdot A_{net,v} \cdot f_{vk} / 1000$
Maximum tension force	$F_{max,t4} = \max(F_{bs,1}, F_{bs,2})$

Figure B.7: Block and plug shear failure calculation

Timber failure during fire	
	Used formula
Maximum compression force	$F_{c,max,fire} = \frac{f_{c,0,k} \cdot 1.1 \cdot (w_{red})^2}{\eta_{fi}} / 1000$
Maximum tension force	$F_{t,max,fire} = \frac{f_{t,0,k} \cdot 1.1 \cdot (w_{red})^2}{\eta_{fi}} / 1000$

Figure B.8: Fire failure calculation

Member resistance	
	Used formula
Maximum compression force	$F_{c,max,member} = \frac{f_{c,0,k} \cdot k_{mod} \cdot w_{red}^2}{\gamma_{m2}} / 1000$
Maximum tension force	$F_{t,max,member} = \frac{f_{t,0,k} \cdot k_{mod} \cdot w_{red}^2}{\gamma_{m2}} / 1000$

Figure B.9: Member failure calculation

Total maximum force	
	Used formula
Maximum compression force	$F_{max,compression} = \min(F_{c,max,connection}, F_{c,max,fire}, F_{c,max,member})$
Maximum tension force	$F_{max,tension} = \min(F_{t,max,connection}, F_{t,max,fire}, F_{t,max,member})$

Figure B.10: Normative failure calculation

Translational stiffness	
	Used formula
Slip modulus of a dowel	$K_{ser} = \rho_m^{1.5} \cdot \frac{d_{dowel}}{23}$
Translational stiffness in SLS	$K_{ser,SLS,total} = 2 \cdot N_{steelplates} \cdot K_{ser} \cdot n_{ef}$
Translational stiffness in ULS	$K_{ser,ULS,total} = \frac{2}{3} \cdot K_{ser,SLS,total}$

Figure B.11: Translational stiffness calculation

According to Johanides et al. (2021), the rotational stiffness can be obtained by obtaining the translational stiffness of dowel i multiplied with the square of the radial length of dowel i to the center of mass of all dowels, see Formula B.1 [87].

$$K_{r,ser} = \sum_{i=1}^n K_{ser} \cdot r_i^2 \quad (B.1)$$

$K_{r,ser}$ = rotational stiffness

K_{ser} = slip modulus of a single dowel

r_i = radial length of dowel i to the center of mass of all dowels

For every connection, in the custom node, the center of all dowels is obtained, and the distance in X- and Y-direction to this center point is determined for all dowels. By using Pythagoras, the radial length of each dowel is determined. Using this approach the rotational stiffness of the steel plate and dowel connection is found.

B.1.2. Verification

The verification of the steel plate and dowel connection is performed by checking the compressive stress.

Reference

Using the case presented in the presentation "*Materialen met Toekomst: Hout in Utiliteit*" by Walter van Adrichem [148], see Figure B.12.



Figure B.12: Checked steel plate and dowel connection [148].

The following assumptions are made

- Diameter dowel = 20 mm
- Thickness steel plate = 12 mm
- Dowel rows = 11
- Dowel columns = 4
- Number of steel plates = 3
- width of timber element = 600 mm

Additional input parameters

- $f_{t,0,k} = 24 \text{ N/mm}^2$
- $f_{c,0,k} = 30 \text{ N/mm}^2$
- $f_{v,k} = 3.5 \text{ N/mm}^2$
- $\rho_k = 430 \text{ kg/m}^3$
- $\rho_{mean} = 460 \text{ kg/m}^3$
- $\gamma_m = 1.25$
- $k_{mod} = 0.8$
- $f_y = 460 \text{ N/mm}^2$
- $f_u = 560 \text{ N/mm}^2$
- $t_{res} = 120 \text{ min}$
- $\eta_{fi} = 0.45$ Fire reduction factor

Custom node calculation

A compressive stress of 4.9 N/mm^2 is found, see Figure B.13.

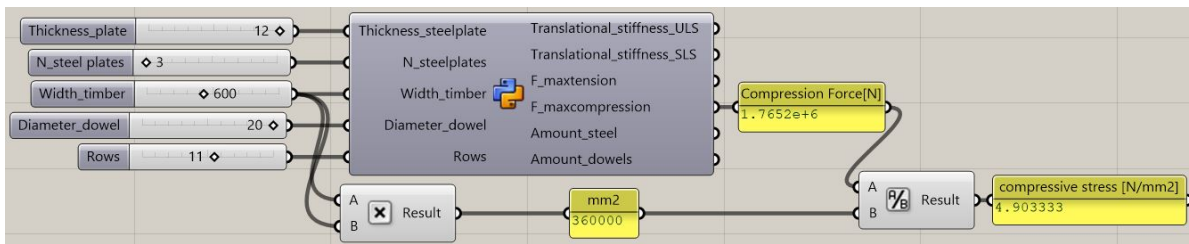


Figure B.13: Steel plate and dowel connection calculated in Grasshopper using GHPython component.

Hand calculation

Figure B.14 and B.15 show sections of this steel plate dowel connection with 3 columns and 5 rows of dowels.

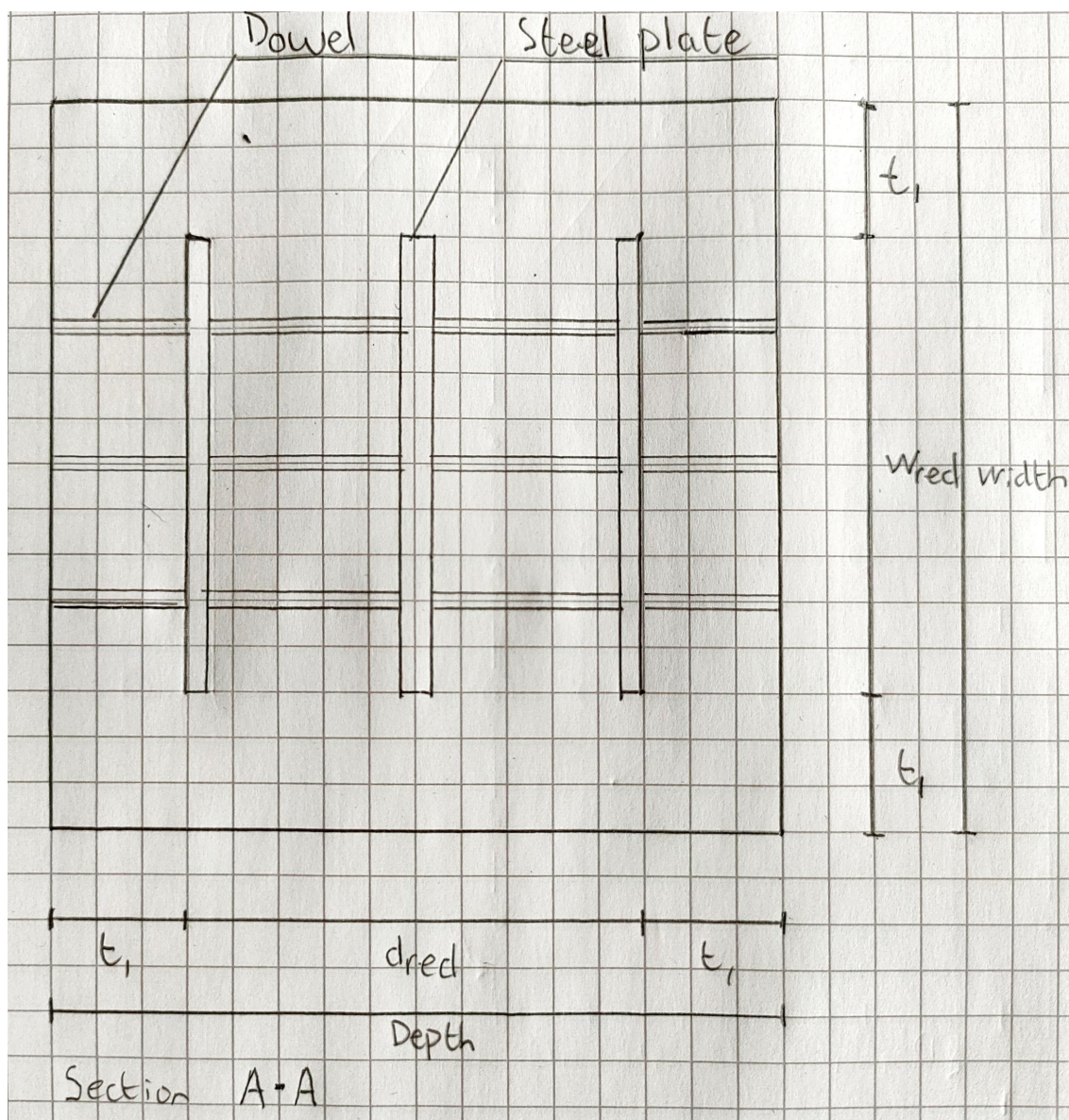


Figure B.14: Steel plate dowel connection cross section

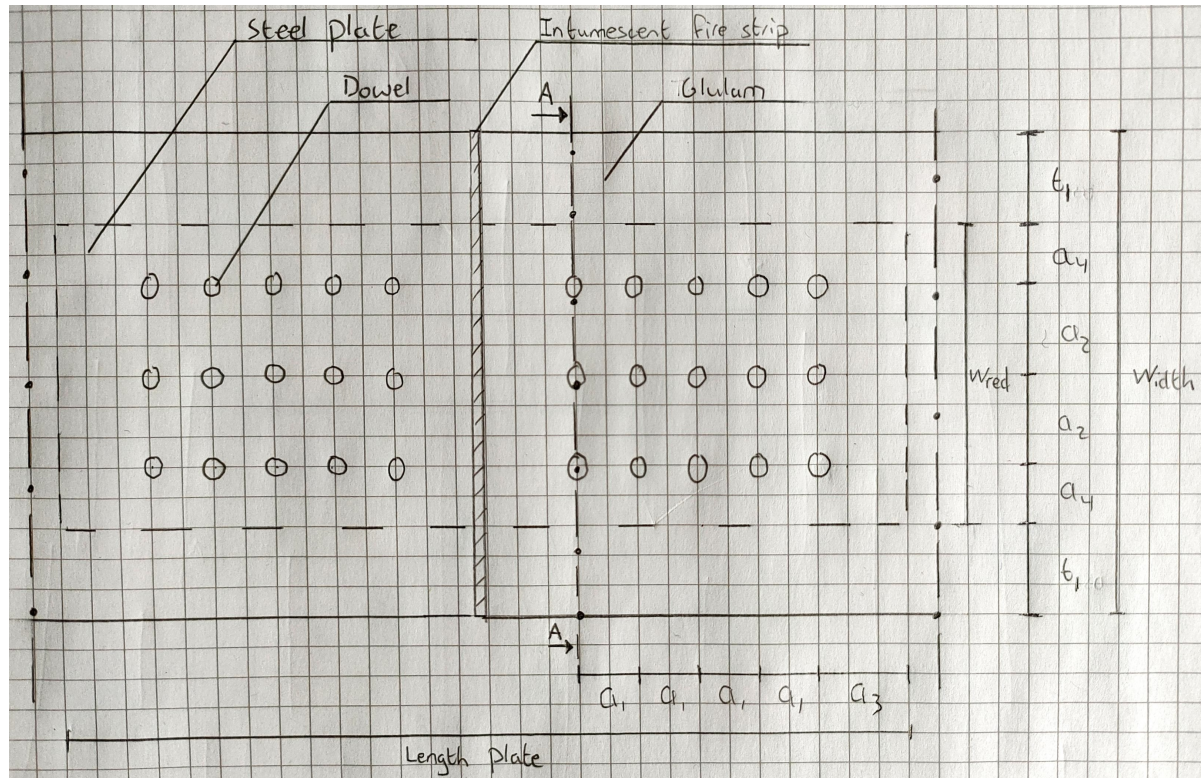


Figure B.15: Steel plate dowel connection notations.

General calculations		
	Used formula	Result
Charring depth after fire of 120 minutes	$d_{120} = 7 + 0.7 \cdot t_{res}$	91 mm
t_1	$t_1 = d_{120}$	91 mm
Reduced width of section	$w_{red} = w - 2 \cdot t_1$	418 mm
Reduced depth of section	$d_{red} = w_{red}$	418 mm
a_1	$a_1 = 5 \cdot d_{dowel}$	100 mm
a_2	$a_2 = 3 \cdot d_{dowel}$	60 mm
$a_{3,t}$	$a_{3,t} = \max(7 \cdot d_{dowel}, 80)$	140 mm
$a_{3,c}$	$a_{3,c} = 3 \cdot d_{dowel}$	60 mm
$a_{4,t}$	$a_{4,t} = 3 \cdot d_{dowel}$	60 mm
Edge distance	$d_{edges} = 2 \cdot a_{4,t}$	120 mm
Minimum required plate length	$\lceil Rows \rceil = \frac{length_{steelplate} - a_{3,t} - a_{4,t}}{a_1}$	11

Figure B.16: Steel plate dowel connection general calculation

Net timber area failure		
	Used formula	Result
Netto timber area	$A_{net} = w^2 - (w \cdot Cols \cdot d_{dowel}) - (d_{red} \cdot N_{steelplates} \cdot t_{steelplate})$	296952 mm ²
Maximum compression force	$F_{max,c1} = f_{c,0,k} \cdot A_{net} / 1000$	8909 kN
Maximum tension force	$F_{max,t1} = 0.4 \cdot f_{t,0,k} \cdot A_{net} / 1000$	2850 kN

Figure B.17: Net timber area failure calculation

Steel plate failure		
	Used formula	Result
Maximum compression force	$F_{max,c2} = f_y \cdot N_{steelplates} \cdot t_{steelplate} \cdot d_{red}/1000$	6922 kN
Maximum tension force	$F_{max,t2} = f_y \cdot N_{steelplates} \cdot t_{steelplate} \cdot d_{red}/1000$	6922 kN

Figure B.18: Steel plate calculation

Dowel failure		
	Used formula	Result
Embedment strength	$f_h = 0.082 \cdot (1 - 0.01 \cdot d_{dowel}) \cdot \rho_k$	28.2 N/mm ²
t_2	$t_2 = w_{red}$	418 mm
Plastic yield moment of dowel	$M_y = (1/6) \cdot d_{dowel}^3 \cdot f_y$	613333 Nmm
Dowel failure mechanism 1	$F_{dowel1} = 0.25 \cdot (2 \cdot t_1 + t_2) \cdot d_{dowel} \cdot f_h/1000$	84.6kN
Dowel failure mechanism 2	$F_{dowel2} = \left(-\frac{t_1}{2} + \frac{t_2}{4} + \sqrt{\frac{1}{2}t_1^2 + \frac{M_y}{d_{dowel} \cdot f_h}} \right) \cdot d_{dowel} \cdot f_h/1000$	74.1kN
Dowel failure mechanism 3	$F_{dowel3} = \sqrt{4 \cdot M_y \cdot d_{dowel} \cdot f_h}/1000$	37.2 kN
Dowel failure mechanism 4	$F_{dowel4} = \left(\frac{1}{2}t_1 + \frac{1}{2}\sqrt{t_1^2 + \frac{2 \cdot M_y}{d_{dowel} \cdot f_h}} \right) \cdot d_{dowel} \cdot f_h/1000$	54.5 kN
Dowel failure mechanism 5	$F_{dowel5} = \left(\sqrt{\frac{M_y}{d_{dowel} \cdot f_h}} + \frac{1}{2}t_1 \right) \cdot d_{dowel} \cdot f_h/1000$	44.3 kN
Dowel failure mechanism 6	$F_{dowel6} = \left(\sqrt{\frac{M_y}{d_{dowel} \cdot f_h}} + \frac{1}{4}t_2 \right) \cdot d_{dowel} \cdot f_h/1000$	77.5 kN
Dowel failure mechanism 7	$F_{dowel7} = \left(-\frac{1}{2}t_1 + \sqrt{\frac{1}{2}t_1^2 + \frac{M_y}{d_{dowel} \cdot f_h}} + \sqrt{\frac{M_y}{d_{dowel} \cdot f_h}} \right) \cdot d_{dowel} \cdot f_h/1000$	33.7 kN
Effective number of dowels	$n_{ef} = \min(Rows; Rows^{0.9} \cdot \left(\frac{\alpha_1}{13 \cdot d_{dowel}} \right)^{1/4})$	6.82
Maximum compression force	$F_{max,c3} = 4 \cdot n_{ef} \cdot Cols \cdot \min(F_{dowel1}, F_{dowel2}, F_{dowel3}, F_{dowel4}, F_{dowel5}, F_{dowel6}, F_{dowel7})$	3675 kN
Maximum tension force	$F_{max,t3} = 4 \cdot n_{ef} \cdot Cols \cdot \min(F_{dowel1}, F_{dowel2}, F_{dowel3}, F_{dowel4}, F_{dowel5}, F_{dowel6}, F_{dowel7})$	3675 kN

Figure B.19: Steel plate failure calculation

Block and plug shear failure		
	Used formula	Result
Length timber area in tension	$l_t = d_{red} - d_{edges} - Cols \cdot d_{dowel}$	218 mm
Net timber area in tension	$A_{net,t} = l_t \cdot (t_1 + t_1 + t_2)$	130800 mm ²
Maximum tension force	$F_{bs,1} = 1.5 \cdot A_{net,t} \cdot f_{t,0k}/1000$	4709 kN
Length timber area in shear	$l_v = 5 \cdot d_{dowel} \cdot (Rows - 1) + \max(7 \cdot d_{dowel}, 80)$	1140 mm
Net timber area in shear	$A_{net,v} = l_v \cdot (t_1 + t_2 + t_1)$	684000 mm ²
Maximum shear force	$F_{bs,2} = 0.7 \cdot A_{net,v} \cdot f_{vk}/1000$	1676 kN
Maximum tension force	$F_{max,t4} = \max(F_{bs,1}, F_{bs,2})$	4709 kN

Figure B.20: Dowel failure calculation

Steel plate failure		
	Used formula	Result
Maximum tension force	$F_{max,t5} = \frac{0.9 \cdot f_u/1000 \cdot (N_{steelplates} \cdot Thickness_{steelplate} \cdot (d_{red} - Cols \cdot d_{dowel}))}{\gamma_{m2}}$	4906 kN

Figure B.21: Connection failure calculation

Connection failure		
	Used formula	Result
Maximum compression force	$F_{c,max,connection} = k_{mod} \cdot \frac{\min(F_{max,c1}, F_{max,c2}, F_{max,c3})}{\gamma_{m2}}$	1764 kN
Maximum tension force	$F_{t,max,connection} = k_{mod} \cdot \frac{\min(F_{max,t1}, F_{max,t2}, F_{max,t3}, F_{max,t4}, F_{max,t5})}{\gamma_{m2}}$	1368 kN

Figure B.22: Block and plug shear failure calculation

Timber failure during fire		
	Used formula	Result
Maximum compression force	$F_{c,max,fire} = \frac{f_{c,0,k} \cdot 1.1 \cdot (w_{red})^2}{\eta_{fi}} / 1000$	12813 kN
Maximum tension force	$F_{t,max,fire} = \frac{f_{t,0,k} \cdot 1.1 \cdot (w_{red})^2}{\eta_{fi}} / 1000$	10250 kN

Figure B.23: Fire failure calculation

Member resistance		
	Used formula	Result
Maximum compression force	$F_{c,max,member} = \frac{f_{c,0,k} \cdot k_{mod} \cdot w_{red}^2}{\gamma_{m2}} / 1000$	2516 kN
Maximum tension force	$F_{t,max,member} = \frac{f_{t,0,k} \cdot k_{mod} \cdot w_{red}^2}{\gamma_{m2}} / 1000$	2013 kN

Figure B.24: Member failure calculation

Total maximum force		
	Used formula	Result
Maximum compression force	$F_{max,compression} = \min(F_{c,max,connection}, F_{c,max,fire}, F_{c,max,member})$	1764
Maximum tension force	$F_{max,tension} = \min(F_{t,max,connection}, F_{t,max,fire}, F_{t,max,member})$	1368

Figure B.25: Normative failure calculation

Translational stiffness		
	Used formula	Result
Slip modulus of a dowel	$K_{ser} = \rho_m^{1.5} \cdot \frac{d_{dowel}}{23}$	8579 kN/m
Translational stiffness in SLS	$K_{ser,SLS,total} = 2 \cdot N_{steelplates} \cdot K_{ser} \cdot n_{ef}$	351052 kN/m
Translational stiffness in ULS	$K_{ser,ULS,total} = \frac{2}{3} \cdot K_{ser,SLS,total}$	234035 kN/m

Figure B.26: Translational stiffness calculation

$$\frac{1764000}{600 \cdot 600} = 4.9 N/mm^2 \tag{B.2}$$

The hand calculation, the Python node and the presentation by Walter van Adrichem all find a compressive stress of roughly $5.0 N/mm^2$. So, the calculation for the steel plate and dowel connection is verified.

B.2. Knapp connection

For the determination of the required Knapp connectors, the strength, dimensions and prices as specified on the Knapp website are used [5]. Using this data, formula's can be determined for price and surface area estimation based on the required characteristic strength of the connection, see Figure B.27 and Figure B.28.

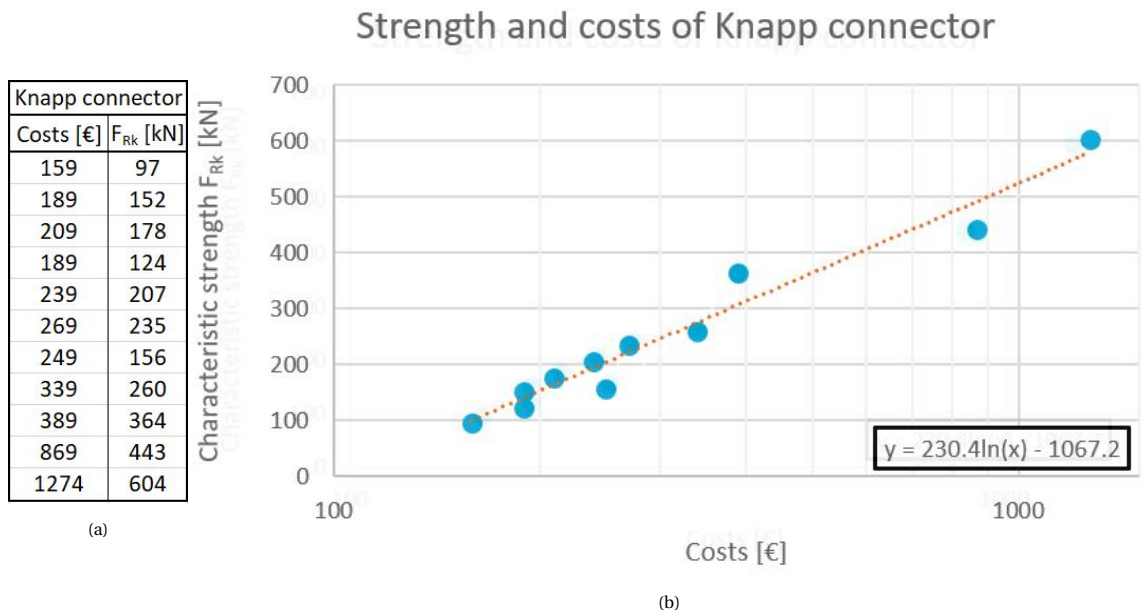


Figure B.27: Characteristic strength and costs of Knapp connection [5].

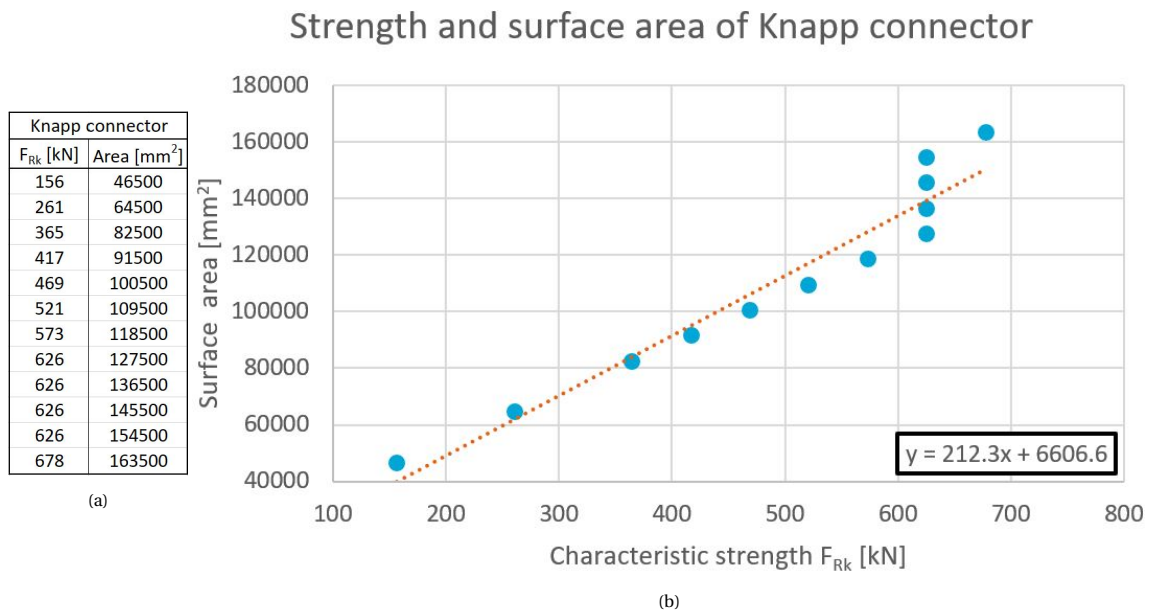


Figure B.28: Characteristic strength and surface area of Knapp connection [5].

B.3. Floors

The design of the floors is based on calculations of vibrations, shear and tension.

B.3.1. Vibrations

The European standard EN 1995-1-1 combined with the Dutch national annex [74] does not provide an accurate calculation of the human induced vibrations in the floor. There are two alternative guidelines that provide more accurate calculations: the Austrian standard Önorm B 1995-1-1 [71], and the HIVOSS design guidelines for calculation of floor vibrations [67].

Eigen frequency

The HIVOSS design guidelines gives a calculation method for floor plates and for beams. For these floor plates, a two-way spanning capability is assumed. Because of the one-way spanning capabilities of a Kerto-Ripa floor, the calculation method for beams is used.

According to the HIVOSS design guidelines, the eigenfrequency is determined using:

$$f_1 = \frac{2}{\pi} \sqrt{\frac{3EI}{0.49\mu l^4}} \quad (\text{B.3})$$

f_1 = first eigenfrequency in Hz

E = modulus of elasticity about an axis perpendicular to the span in N/mm^2

I = second moment of inertia about an axis perpendicular to the span in m^4

μ = divided floor mass in kg/m

l = span in m

According to the Austrian standard Önorm B 1995-1-1, the eigenfrequency is determined using:

$$f_1 = \frac{\pi}{2l^2} \sqrt{\frac{EI}{\mu}} \quad (\text{B.4})$$

The parameters in these two formulas are the same. However, the factor with which the formula is multiplied is different. By rewriting both formulas, the factor k can be found:

$$f_1 = k \sqrt{\frac{EI}{\mu l^4}} \quad (\text{B.5})$$

For the HIVOSS guidelines this factor $k = 1.575$. For the Austrian standard Önorm B 1995-1-1 this factor $k = 1,571$. Since the Austrian standard Önorm B 1995-1-1 gives the most conservative result, the eigenfrequency will be determined using Formula B.4.

Criteria minimal eigenfrequency

Austrian standard Although both guidelines for calculation give roughly the same first eigenfrequency, the criteria for minimal eigenfrequency differ. Tabelle NA 7.5 is used in the Austrian standard Önorm B 1995-1-1, for determination of the minimum value of the eigenfrequency, see Figure B.29. For floors in offices, floor class I must be used, so a minimum eigenfrequency of 8 Hz is required.

Eigenfrequency and deflection criteria according to Austrian standard Önorm B 1995-1-1		
	Floorclass I	Floorclass II
Eigenfrequency	$f_1 \geq 8 \text{ Hz}$	$f_1 \geq 6 \text{ Hz}$
Deflection	$w_{stat} \leq 0.25 \text{ mm}$	$w_{stat} \leq 0.5 \text{ mm}$

Figure B.29: Austrian standard Önorm B 1995-1-1, Tabelle NA 7.5 [71].

HIVOSS guidelines The HIVOSS guidelines uses the $ES - RMS_{90}$ value. This value shows the 90 percentile upper limit of a step RMS value of the speed of a significant step. It gives a maximum value of $ES - RMS_{90}$ of 3.2 for an office function. Furthermore it gives a damping D , which is 7 % for an office with open spaces and a timber floor. By calculating the eigenfrequency and the modal mass, the value of $ES - RMS_{90}$ can be found using Figure B.30. The modal mass can be calculated using:

$$M_{mod} = 0.5\mu l \tag{B.6}$$

- M_{mod} = modal mass
- μ = divided floor mass in kg/m
- l = span in m

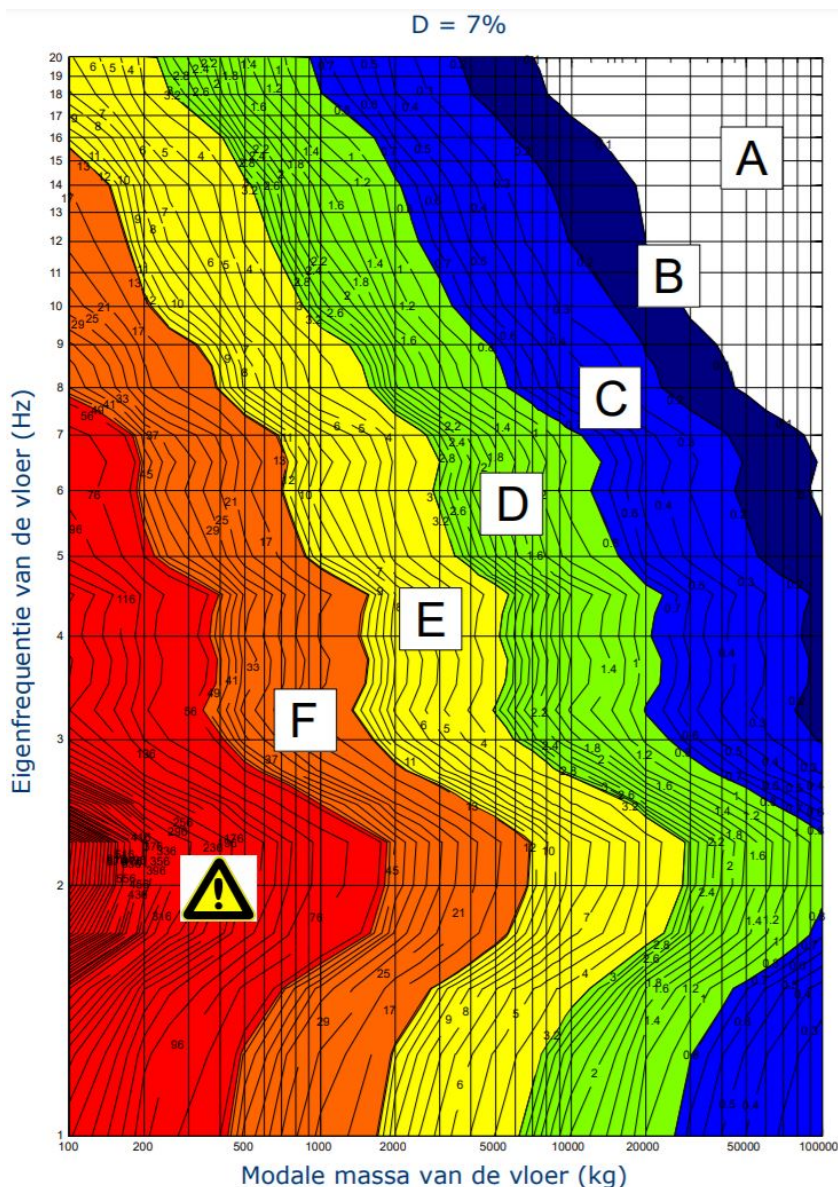


Figure B.30: Determination of $ES - RMS_{90}$ [67].

By combining the two Criteria for the eigenfrequency, a conservative result can be found. This implies that the eigenfrequency will be determined using Formula B.4. The eigenfrequency must be greater than 8 Hz, and furthermore, the modal mass of the floor must have a $ES - RMS_{90}$ smaller than 3.2, determined using Figure B.30.

Maximum immediate deformation

Furthermore, the floor must also fulfil the requirement set for the maximum immediate deformation caused by walking as the The Austrian standard Önorm B 1995-1-1 gives, see Figure B.29. This maximum immediate deformation is 0.25 mm. For determination of this value a footstep is modelled as a point load of 1 kN:

$$w_{\text{stat}} = \frac{Fl^3}{48(EI)l b_r} \quad (\text{B.7})$$

w_{stat} = maximum immediate deformation in m
 F = immediate vertical displacement due to a point load in N
 E = modulus of elasticity about an axis perpendicular to the span in N/mm^2
 I = second moment of inertia about an axis perpendicular to the span in m^4
 l = span in m
 b_r = effective width

Assuming the floor has no transversal stiffness, the factor b_r can be assumed to be equal to the centre to centre distance of two floor plates.

B.3.2. Shear and tension

The floor system transfers the wind forces to the stability system. This creates tension forces in the tension ties and shear between floors and between floors and beams. The forces in the tension ties are checked in the Post Optimization Verification, see Section 5.10. The shear forces are transferred using screws. These screws are included in the model in calculation of the construction costs and shadow costs. Using the wind force in X and Y direction, these forces can be calculated, see Figure B.31.

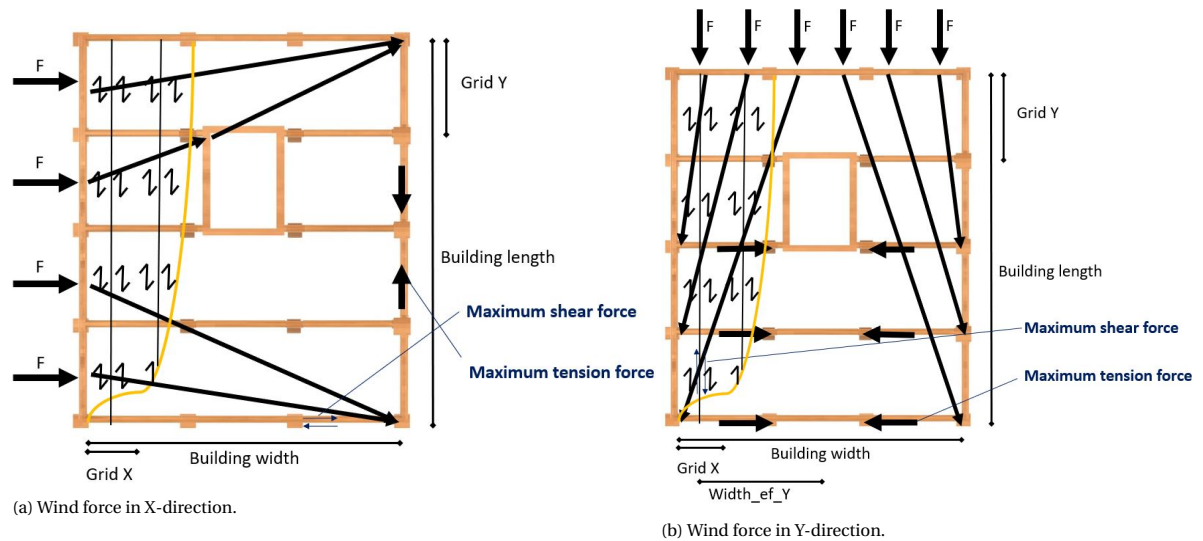


Figure B.31: Calculation of maximum shear force and tension force.

The forces F in Figure B.31 in Y-direction are obtained using Formula B.8. For this, the known q -load in Y-direction and N_1 is used. N_1 is calculated using Formula B.9. This same procedure is used to calculate the force F in X-direction.

$$F = \frac{q_y}{N_1} \quad (\text{B.8})$$

$$N_1 = \frac{\text{Building}_{\text{length}}}{\text{Grid}_Y} \quad (\text{B.9})$$

The shear force between floor plate and beams is largest in X-direction, while the shear force between floor plates is largest in Y-direction. Calculations for these two forces are shown below. Furthermore, the calculation of tension forces in the tension ties are given for both X- and Y-direction.

Shear force between floor plate and beam in X-direction When the wind direction is along the X-axis, the forces in the floor can be modelled according to Figure B.31a.

The wind force creates shear forces between floor plate and beam. The location of the maximum shear force are shown in Figure B.31a. All forces over $Width_{eff,x}$ must pass as a shear force through the lowest floor plates to the beam. So, the maximum shear force in X-direction is:

$$Shear_{max,x} = Width_{eff,x} \cdot q_x \quad (B.10)$$

These shear forces are transferred between floor plate and beam using screws. 7 x 100 VGZ full threaded cylindrical head fastener screws by Rothoblaas are used in the design. A shear resistance per screw of $R_{v,k} = 2.68$ kN is given. The design shear resistance can be found using:

$$F_{v,d} = \frac{R_{v,k} \cdot k_{mod}}{\gamma_m} \quad (B.11)$$

Using Formula B.11, a design shear resistance of 1.7 kN is found.

The maximum shear force is found in the outer floor plate connection to the beam. A linear distribution is assumed to find the total amount of required screws in the normative floor. To find the total amount of required screws for all floors, the required amount of screws in the normative floor is multiplied with the number of floors

Shear force between floor plates in Y-direction The wind force creates shear forces between the floor plates. The maximum shear forces are shown in Figure B.31b. All forces over $Width_{eff,y}$ must pass as a shear force through the left-most plate. So, the maximum shear force in Y-direction is:

$$Shear_{max,y} = Width_{eff,y} \cdot q_y \quad (B.12)$$

These shear forces are transferred using screws. 7 x 100 VGZ full threaded cylindrical head fastener screws by Rothoblaas are used in the design. These screws are diagonal placed, because this ensures a more rigid connection, see Figure B.32.

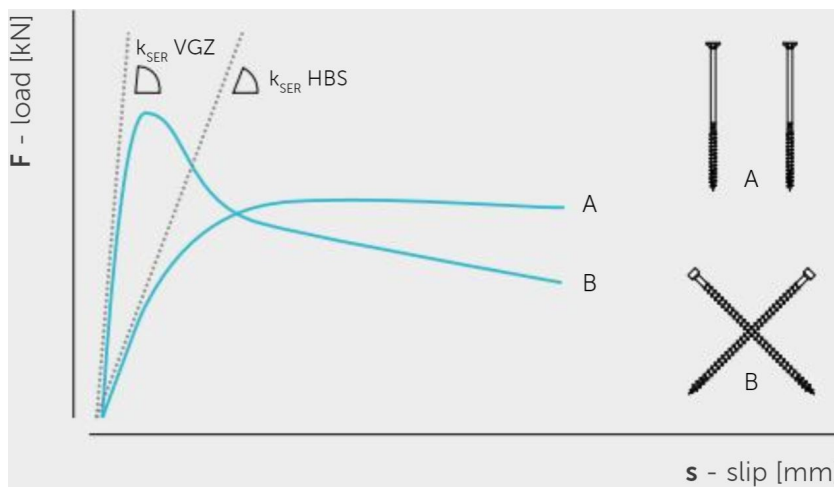


Figure B.32: Diagonal placed screws vs vertical screws [126].

The resistance of the 7 x 100 VGZ is proportional to the threaded length. Per screw, the shear resistance $R_{v,k}$ is 1.99 kN. So per two screws, the shear resistance is:

$$F_{v,d} = 2 \cdot \frac{R_{v,k} \cdot k_{mod}}{\gamma_m} \quad (B.13)$$

So, for two screws $F_{v,d} = 2.5$ kN.

Next, the maximum required amount of screws can be calculated:

$$Screws_{max} = \frac{Shear_{max,y}}{F_{v,d}} \cdot 2 \quad (B.14)$$

The outer most floor plates will require the maximum amount of screws. A linear distribution is assumed to find the amount of required screws in all floor plates. For all floors the required amount of screws in the normative floor is used.

Tension tie in X-direction In X-direction the only tension tie is situated in the beam in the façade.

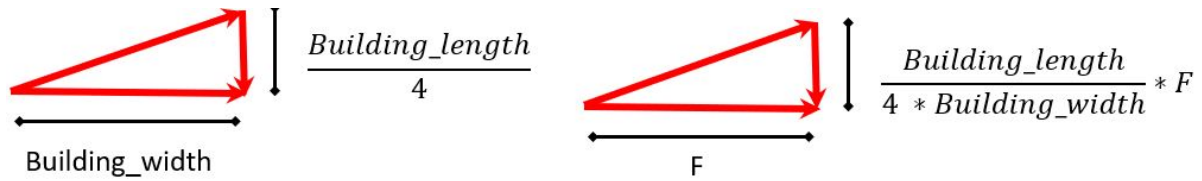


Figure B.33: Tension force in tension tie.

Figure B.33 shows the distribution of forces to the tension tie. This gives:

$$\text{Tension}_X = \frac{\text{Building}_{\text{length}}}{4 \cdot \text{Building}_{\text{width}}} \cdot F \quad (\text{B.15})$$

Tension tie in Y-direction The wind force is distributed to the tension tie according to Figure B.34. So, the force in the tension tie can be calculated using Formula B.16

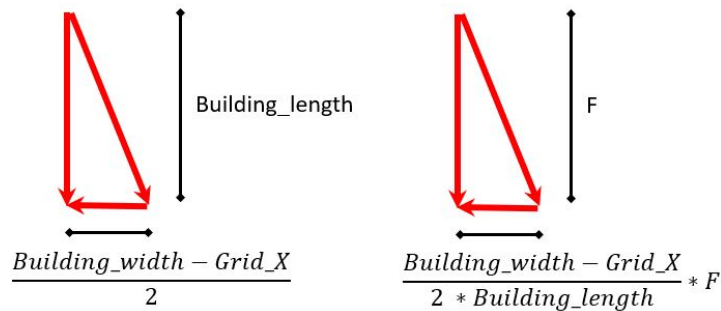


Figure B.34: Force in tension tie.

$$\text{Tension}_Y = \frac{\text{Building}_{\text{width}} - \text{Grid}_X}{2 \cdot \text{Building}_{\text{length}}} \cdot F \quad (\text{B.16})$$

B.4. Beams

B.4.1. Custom node calculation

Bending moment		
	Original formula	Rewritten formula
Unity check	$uc = \frac{\sigma_{md}}{f_{md}}$	$\sigma_{md} = uc \cdot f_{md}$
Design bending moment	$M_{Ed} = \frac{1}{8} q_{d,ULS} * (l_{beam})^2$	$M_{Ed} = \frac{1}{8} q_{d,ULS} * (grid_x)^2$
Design bending stress	$\sigma_{md} = \frac{M_{Ed}}{W_y}$	$W_y = \frac{M_{Ed}}{\sigma_{md}}$
Moment of resistance	$W_y = \frac{1}{6} * height_1 * f_{height,width} * (height_1)^2$	$height_1 = \left(\frac{6 * W_y}{f_{height,width}} \right)^{1/3}$

Figure B.35: Beam bending check.

Deformation		
	Original formula	Rewritten formula
Unity check	$uc = \frac{w_{final}}{w_{max}}$	$w_{final} = uc \cdot w_{max}$
Final mean modulus of elasticity	$E_{mean,final} = \frac{E_{mean}}{1 + k_{def}}$	
Final deflection	$w_{final} = \frac{5}{384} * \frac{q_d * (l_{beam})^4}{E_{mean,final} * I}$	$I = \frac{5}{384} * \frac{q_d * (l_{beam})^4}{E_{mean,final} * w_{final}}$
Moment of inertia	$I = \frac{1}{12} \cdot (height_2 \cdot f_{height,width}) \cdot (height_2)^3$	$height_2 = \left(\frac{12 \cdot I}{f_{height,width}} \right)^{0.25}$

Figure B.36: Beam deformation check.

Shear		
	Original formula	Rewritten formula
Unity check	$uc = \frac{\tau_d}{f_{vd}}$	$\tau_d = uc \cdot f_{vd}$
Design shear force	$V_{Ed} = \frac{q_{d,ULS} \cdot l_{beam}}{2}$	$V_{Ed} = \frac{q_{d,ULS} \cdot grid_x}{2}$
Design shear stress	$\tau_d = \frac{3 \cdot V_{Ed}}{2 \cdot A}$	$A = \frac{3 \cdot V_{Ed}}{2 \cdot \tau_d}$
Area	$A = height_3 * (height_3 \cdot f_{height,width})$	$height_3 = \sqrt{f_{height,width} * A}$

Figure B.37: Beam shear check.

Fire situation: Bending moment		
	Original formula	Rewritten formula
Unity check	$uc = \frac{\sigma_{md,fi}}{f_{md,fi}}$	$\sigma_{md,fi} = uc \cdot f_{md,fi}$
Design bending moment during fire	$M_{Ed,fi} = \frac{1}{8} q_{d,fi,ULS} * (l_{beam})^2$	$M_{Ed,fi} = \frac{1}{8} q_{d,fi,ULS} * (grid_x)^2$
Design bending stress during fire	$\sigma_{md,fi} = \frac{M_{Ed,fi}}{W_{y,fi}}$	$W_{y,fi} = \frac{M_{Ed,fi}}{\sigma_{md,fi}}$
Moment of resistance of reduced cross section	$W_{y,fi} = \frac{1}{6} \cdot (height_4 \cdot f_{height,width} - d_{ef}) \cdot (height_4 - 2 \cdot d_{ef})^2$	$height_4 = (6 \cdot W_{y,fi} \cdot f_{height,width})^{1/3} + 1.7 \cdot d_{ef}$

Figure B.38: Beam bending during fire check.

Fire situation: Shear		
	Original formula	Rewritten formula
Unity check	$uc = \frac{\tau_{d,fi}}{f_{vd,fi}}$	$\tau_{d,fi} = uc \cdot f_{vd,fi}$
Design shear force during fire	$V_{Ed,fi} = \frac{q_{d,fi,ULS} \cdot l_{beam}}{2}$	$V_{Ed,fi} = \frac{q_{d,fi,ULS} \cdot grid_x}{2}$
Design shear stress during fire	$\tau_{d,fi} = \frac{3 \cdot V_{Ed,fi}}{2 \cdot A_{fi}}$	$A_{fi} = \frac{3 \cdot V_{Ed,fi}}{2 \cdot \tau_{d,fi}}$
Area of reduced cross section	$A_{fi} = (height_5 - d_{ef})(f_{height,width} \cdot height_5 - 2 \cdot d_{ef})$	$height_5 = \sqrt{f_{height,width} \cdot A_{fi} + 1.8d_{ef}}$

Figure B.39: Beam shear during fire check.

B.5. Columns

B.5.1. Custom node calculation

Compression		
	Original formula	Rewritten formula
Unity check	$uc = \frac{\sigma_{c,0,d}}{f_{c,0,d}}$	$\sigma_{c,0,d} = uc \cdot f_{c,0,d}$
Design compressive stress	$\sigma_{c,0,d} = \frac{N_{Ed}}{A}$	$A = \frac{N_{Ed}}{\sigma_{c,0,d}}$
Area	$A = (width_1)^2$	$width_1 = \sqrt{A}$

Figure B.40: Column compression check.

Buckling (compression + bending)	
	Used formula
Area	$A = (width_2)^2$
Design compressive stress	$\sigma_{c,0,d} = \frac{N_{Ed}}{A}$
Moment of resistance	$W = \frac{1}{6} * (width_2)^3$
Design bending stress	$\sigma_{md} = \frac{M_{Ed}}{W}$
Moment of inertia	$I = \frac{1}{12} * (width_2)^4$
Radius of gyration	$i = \sqrt{\frac{I}{A}}$
Slenderness factor	$\lambda = \frac{l_{eff}}{i}$
Relative slenderness	$\lambda_{rel} = \frac{\lambda}{\pi} \sqrt{\frac{f_{c,0,k}}{E_{0.05}}}$
K factor	$k = 0.5 \cdot (1 + \beta_c \cdot (\lambda_{rel} - 0.3) + \lambda_{rel}^2)$
Reduction factor	$k_c = \frac{1}{k + \sqrt{k^2 - \lambda_{rel}^2}}$
Unity check ($\lambda_{rel} > 0.3$)	$uc = \frac{\sigma_{c,0,d}}{k_c \cdot f_{c,0,d}} + (1 + k_m) \cdot \frac{\sigma_{m,d}}{f_{m,d}}$
Unity check ($\lambda_{rel} \leq 0.3$)	$uc = \left(\frac{\sigma_{c,0,d}}{f_{c,0,d}}\right)^2 + (1 + k_m) \cdot \frac{\sigma_{m,d}}{f_{m,d}}$

Figure B.41: Column buckling check.

Fire situation: compression		
	Original formula	Rewritten formula
Unity check	$uc = \frac{\sigma_{c,0,d,fi}}{f_{c,0,d,fi}}$	$\sigma_{c,0,d,fi} = uc \cdot f_{c,0,d,fi}$
Design compressive stress in fire	$\sigma_{c,0,d,fi} = \frac{N_{Ed,fi}}{A_{fi}}$	$A_{fi} = \frac{N_{Ed,fi}}{\sigma_{c,0,d,fi}}$
Area of reduced cross section	$A_{fi} = (width_3 - 2 \cdot d_{ef})^2$	$width_3 = \sqrt{A_{fi} - 2 \cdot d_{ef}}$

Figure B.42: Column compression during fire check.

Buckling (compression + bending)	
	Used formula
Width of reduced cross section	$width_{4,fi} = width_4 - 2 * d_{ef}$
Area of reduced cross section	$A_{fi} = (width_{4,fi})^2$
Design compressive stress in fire	$\sigma_{c,0,d,fi} = \frac{N_{Ed,fi}}{A_{fi}}$
Moment of resistance in fire	$W_{fi} = \frac{1}{6} * (width_{4,fi})^3$
Design bending stress in fire	$\sigma_{md,fi} = \frac{M_{Ed}}{W_{fi}}$
Moment of inertia in fire	$I_{fi} = \frac{1}{12} * (width_{4,fi})^4$
Radius of gyration in fire	$i_{fi} = \sqrt{\frac{I_{fi}}{A_{fi}}}$
Slenderness factor in fire	$\lambda_{fi} = \frac{l_{eff}}{i_{fi}}$
Relative slenderness in fire	$\lambda_{rel,fi} = \frac{\lambda_{fi}}{\pi} \sqrt{\frac{f_{c,0,k}}{E_{0.05}}}$
K factor in fire	$k_{fi} = 0.5 \cdot (1 + \beta_c \cdot (\lambda_{rel,fi} - 0.3) + \lambda_{rel,fi}^2)$
Reduction factor in fire	$k_{c,fi} = \frac{1}{k_{fi} + \sqrt{k_{fi}^2 - \lambda_{rel,fi}^2}}$
Unity check ($\lambda_{rel,fi} > 0.3$)	$uc = \frac{\sigma_{c,0,d,fi}}{k_{c,fi} \cdot f_{c,0,d,fi}} + (1 + k_m) \cdot \frac{\sigma_{md,fi}}{f_{md,fi}}$
Unity check ($\lambda_{rel,fi} \leq 0.3$)	$uc = \left(\frac{\sigma_{c,0,d,fi}}{f_{c,0,d,fi}} \right)^2 + (1 + k_m) \cdot \frac{\sigma_{md,fi}}{f_{md,fi}}$

Figure B.43: Column buckling during fire check.

B.6. Diagonals

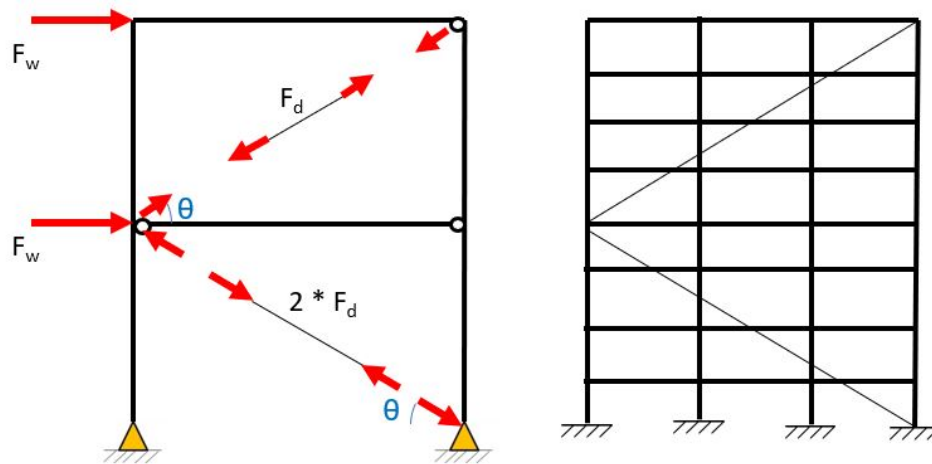


Figure B.44: Simplified model

For the calculation of the diagonals, it is assumed that the gravitational loads do not influence the forces in the diagonals. A simplified model is used to determine the forces in the diagonals as a result of the wind forces, see Figure B.44. In this model, the following assumptions are made:

- All connections are hinged connections, thus there are only axial forces in the members
- Only the outer columns are modelled.
- The diagonals are not connected to the beams at intermediate floors
- All members consist of linear elastic material
- The extensional strain in the diagonal caused by rotation $\Delta\beta$ is neglected, see Figure B.45.

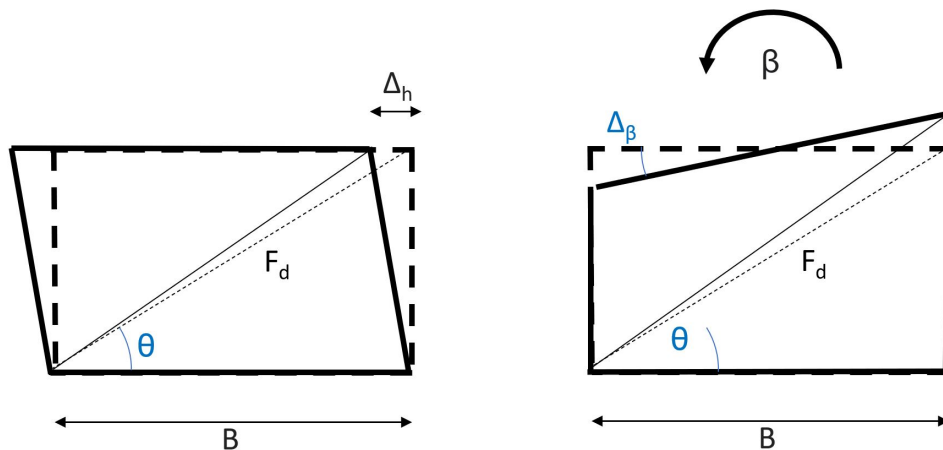


Figure B.45: Deformation caused by shear and bending

$$F_w = F_d \cos\theta \quad (\text{B.17})$$

$$F_d = A_d \sigma_d = A_d E_d \epsilon_d \quad (\text{B.18})$$

Extensional strain caused by relative lateral motion between neighbouring nodes, see Figure B.45, is found using:

$$\epsilon_d = \frac{e_d}{L_d} = \frac{\Delta_h \cdot \cos \theta}{\frac{h}{\sin \theta}} = \frac{\Delta_h \cos \theta \sin \theta}{h} \quad (\text{B.19})$$

The transverse shearing strain γ is approximated using:

$$\gamma \approx \frac{\Delta_h}{h} \quad (\text{B.20})$$

So,

$$\epsilon_d \approx \gamma \cos \theta \sin \theta \approx \frac{\gamma \sin 2\theta}{2} \quad (\text{B.21})$$

$$F_w = \frac{A_d E_d \sin 2\theta \cos \theta}{2} \gamma \quad (\text{B.22})$$

So, for the maximum value of $\sin 2\theta \cos \theta$ gives the angle for which the shear rigidity of the system is maximal, see Figure B.46. The maximum shear rigidity is found for an angle Θ of approximately 35° .

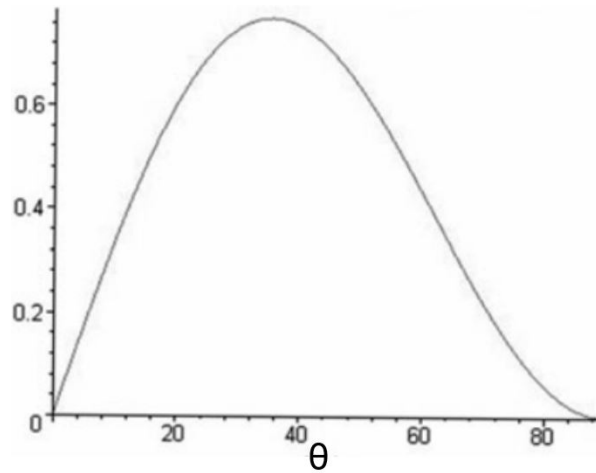


Figure B.46: Graph of $\sin 2\theta \cos \theta$

B.6.1. Force estimation

Formula B.17 can be rewritten to find the axial force in the diagonal. When the simplified model, see Figure B.44, is used, this force in the diagonal increases for every additional diagonal.

$$F_d = n \cdot \frac{F_w}{\cos \theta} \quad (\text{B.23})$$

$n = n_{th}$ diagonal counting from top to bottom.

However, this assumption is very conservative.

Furthermore, the axial forces in the outer two columns can be calculated using this simplified model. The wind loads are transferred through the diagonals to the columns where they result in a compression and tension force. This compression and tension force together create a moment balancing with the moment created by the wind loads.

This compression and tension forces increase from top to bottom. Since the forces in the diagonals increases from top to bottom, the compression and tension forces in the columns also increase is exponentially

$$F_c = n \cdot \frac{n+1}{2} \quad (\text{B.24})$$

$n = n_{th}$ diagonal counting from top to bottom.

B.7. Core

B.7.1. Custom node calculation

Loads The core must withstand gravitational loads and internal wind loads. The gravitational loads consists of loads transferred through beams or floors to the core referred to as outer loads, and loads which are caused by live loads and dead loads transferred through the stairs to the core, referred to as inner loads. The outer loads transferred through the beams, are transferred using Knapp connectors resulting in point loads on the core. The outer loads transferred through the floor elements result in two line loads, which are depicted using black arrows in Figure B.47. The inner loads are assumed to be transferred to the core as a uniformly distributed line load. Furthermore, it is assumed the stairs cover half of the core area. The transfer of the inner loads are shown with red arrows in Figure B.47.

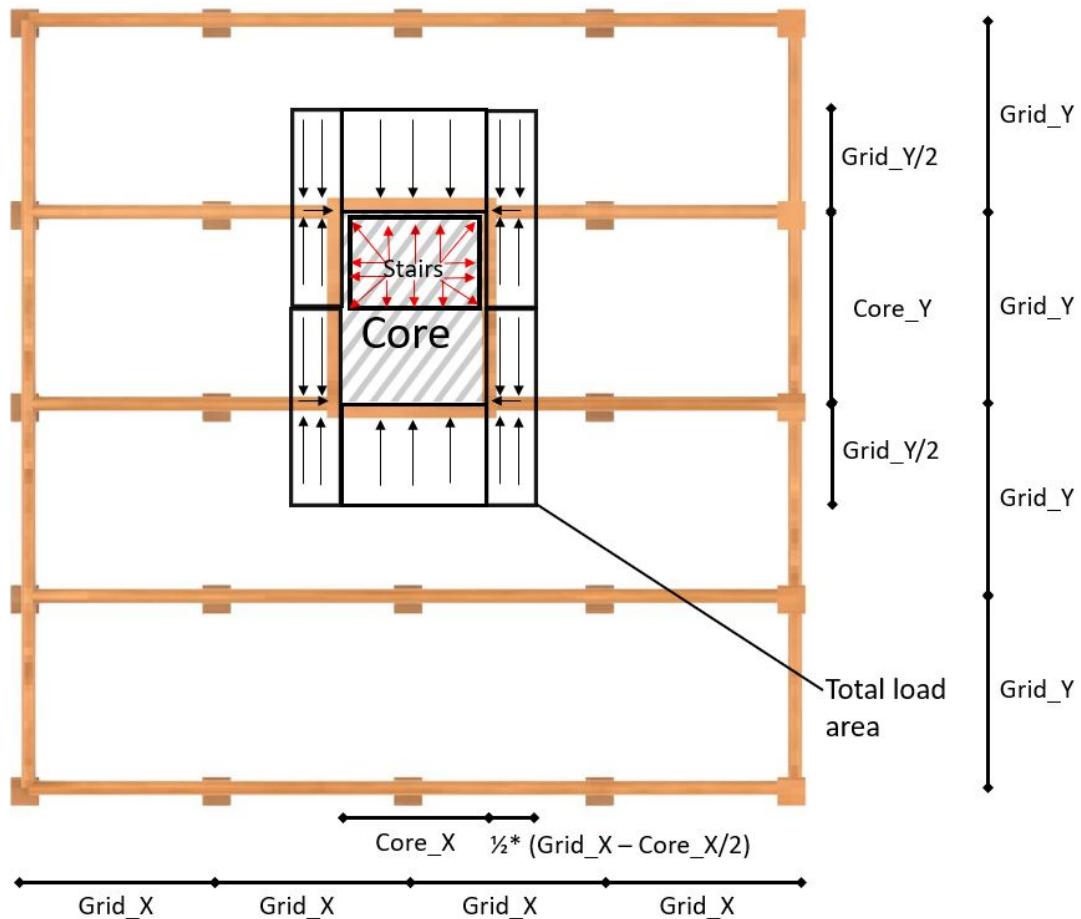


Figure B.47: Transfer of forces to the core

According to the Stora Enso design guide for CLT stairs, CLT stairs with an average thickness of 150 mm is sufficient [44]. Using a selfweight of CLT of 470 kg/m^3 , a deadload of 0.7 kN/m^2 is obtained. Stairs are placed in the category of congregation areas. Thus, a live load of 5 kN/m^2 is used. In case of a calamity, the stairs may be loaded heavily, to account for this, a factor $\psi_0 = 0.6$ is used.

Calculations Six failure mechanisms are checked to determine the thickness of the CLT plates in the core. First, two buckling checks are performed, in a normal and a fire situation. For these calculations, the inner loads are included:

- Buckling (Compression + wind load on inner walls) using $N_{d,M}$ and M_d , see Figure B.48.
- Buckling (Compression + wind load on inner walls) using $N_{d,fi,M}$ and $M_{fi,d}$, see Figure B.49.

Three calculations are performed regarding the point loads. Here the inner loads are excluded in the calculation, since their effect is negligible:

- Compression (ULS4) using N_d , see Figure B.50.
- Compression (ULS4) using $N_{d,fi}$, see Figure B.51.
- Local compressive stress at the Knapp connection (ULS2) using V_d , see Figure B.52.

Lastly, CS 8x160 screws are used in the assumed Knapp connector. These screws have a length of 160mm. The thickness of the steel plate in the connector is 50 mm. 20mm additional depth is used to prevent the screws from fully penetrating the CLT. So, a minimal thickness of CLT of $160-50+20 = 130$ mm is found, see Figure B.53

Buckling (compression + bending)	
	Used formula
Area	$A = thickness_1 * 1000$
Design compressive stress	$\sigma_{c,0,d} = \frac{NEd}{A}$
Moment of resistance	$W = \frac{1}{6} * (thickness_1 * 1000)^3$
Design bending stress	$\sigma_{md} = \frac{MEd}{W}$
Moment of inertia	$I = \frac{1}{12} * (thickness_1 * 1000)^4$
Radius of gyration	$i = \sqrt{\frac{I}{A}}$
Slenderness factor	$\lambda = \frac{l_{eff}}{i}$
Relative slenderness	$\lambda_{rel} = \frac{\lambda}{\pi} \sqrt{\frac{f_{c,0,k}}{E_{0,05}}}$
K factor	$k = 0.5 * (1 + \beta_c * (\lambda_{rel} - 0.3) + \lambda_{rel}^2)$
Reduction factor	$k_c = \frac{1}{k + \sqrt{k^2 - \lambda_{rel}^2}}$
Unity check ($\lambda_{rel} > 0.3$)	$uc = \frac{\sigma_{c,0,d}}{k_c * f_{c,0,d}} + (1 + k_m) * \frac{\sigma_{m,d}}{f_{m,d}}$
Unity check ($\lambda_{rel} \leq 0.3$)	$uc = \left(\frac{\sigma_{c,0,d}}{f_{c,0,d}}\right)^2 + (1 + k_m) * \frac{\sigma_{m,d}}{f_{m,d}}$

Figure B.48: Core buckling check.

Buckling (compression + bending)	
	Used formula
Width of reduced cross section	$thickness_{2,fi} = thickness_2 - d_{ef}$
Area of reduced cross section	$A_{fi} = (thickness_{2,fi})^2$
Design compressive stress in fire	$\sigma_{c,0,d,fi} = \frac{N_{Ed,fi}}{A_{fi}}$
Moment of resistance in fire	$W_{fi} = \frac{1}{6} * (thickness_{2,fi})^3$
Design bending stress in fire	$\sigma_{md,fi} = \frac{M_{Ed}}{W_{fi}}$
Moment of inertia in fire	$I_{fi} = \frac{1}{12} * (thickness_{2,fi})^4$
Radius of gyration in fire	$i_{fi} = \sqrt{\frac{I_{fi}}{A_{fi}}}$
Slenderness factor in fire	$\lambda_{fi} = \frac{l_{eff}}{i_{fi}}$
Relative slenderness in fire	$\lambda_{rel,fi} = \frac{\lambda_{fi}}{\pi} \sqrt{\frac{f_{c,0,k}}{E_{0.05}}}$
K factor in fire	$k_{fi} = 0.5 \cdot (1 + \beta_c \cdot (\lambda_{rel,fi} - 0.3) + \lambda_{rel,fi}^2)$
Reduction factor in fire	$k_{c,fi} = \frac{1}{k_{fi} + \sqrt{k_{fi}^2 - \lambda_{rel,fi}^2}}$
Unity check ($\lambda_{rel,fi} > 0.3$)	$uc = \frac{\sigma_{c,0,d,fi}}{k_{c,fi} \cdot f_{c,0,d,fi}} + (1 + k_m) \cdot \frac{\sigma_{md,fi}}{f_{md,fi}}$
Unity check ($\lambda_{rel,fi} \leq 0.3$)	$uc = \left(\frac{\sigma_{c,0,d,fi}}{f_{c,0,d,fi}} \right)^2 + (1 + k_m) \cdot \frac{\sigma_{md,fi}}{f_{md,fi}}$

Figure B.49: Core buckling during fire check.

Compression		
	Original formula	Rewritten formula
Unity check	$uc = \frac{\sigma_{c,0,d}}{f_{c,0,d}}$	$\sigma_{c,0,d} = uc \cdot f_{c,0,d}$
Design compressive stress	$\sigma_{c,0,d} = \frac{N_{Ed}}{A}$	$A = \frac{N_{Ed}}{\sigma_{c,0,d}}$
Area	$A = (thickness_3)^2$	$thickness_3 = \sqrt{A}$

Figure B.50: Core compression check.

Fire situation: compression		
	Original formula	Rewritten formula
Unity check	$uc = \frac{\sigma_{c,0,d,fi}}{f_{c,0,d,fi}}$	$\sigma_{c,0,d,fi} = uc \cdot f_{c,0,d,fi}$
Design compressive stress in fire	$\sigma_{c,0,d,fi} = \frac{N_{Ed,fi}}{A_{fi}}$	$A_{fi} = \frac{N_{Ed,fi}}{\sigma_{c,0,d,fi}}$
Area of reduced cross section	$A_{fi} = (thickness_4 - d_{ef})^2$	$thickness_4 = \sqrt{A_{fi}} - d_{ef}$

Figure B.51: Corecompression during fire check.

Compression at support		
	Original formula	Rewritten formula
Unity check	$uc = \frac{\sigma_{c,0,d}}{f_{c,0,d}}$	$\sigma_{c,0,d} = uc \cdot f_{c,0,d}$
Design compressive stress	$\sigma_{c,0,d} = \frac{V_{Ed}}{A}$	$A = \frac{V_{Ed}}{\sigma_{c,0,d}}$
Area	$A = thickness_5 \cdot width_{support}$	$thickness_5 = \frac{A}{width_{support}}$

Figure B.52: Core support compression check.

Depth of Knapp connector screws	
	Used formula
Thickness	$thickness_6 = 160 - 50 + 20$

Figure B.53: Knapp connector depth of screws.

B.7.2. Verification

Verification is performed using the Calculatis tool by Stora Ensa. A model of Mjøstårnet is created using the developed tool for this calculation. First, Buckling (Compression + wind load on inner walls) Using $N_{d,M} = 64.3kN$ and $M_d = 1.8kNm$.

- The custom node gives a minimal required thickness of a C24 CLT panel of 74.9 mm
- Calculatis gives a unity check of 0.84 for a C24 CLT L3s panel with a thickness of 80mm, see Figure B.54.

So, the core calculation is verified.

buckling design															
dist.	$f_{m,k}$	$f_{c,k}$	γ_m	k_{mod}	$k_{sys,y}$	$k_{sys,z}$	$l_{k,y}$	$l_{k,z}$	λ_y	λ_z	$\lambda_{rel,y}$	$\lambda_{rel,z}$	β_c	k_{tim}	k_i
[m]	[N/mm ²]	[N/mm ²]	[-]	[-]	[-]	[-]	[m]	[m]	[-]	[-]	[-]	[-]	[-]	[-]	[-]
1.45	24.00	21.00	1.30	0.60	1.10	1.00	2.900	2.900	95	10	1.54	0.16	0.2	1.00	1.00
dist.	k_y	k_z	$k_{c,y}$	$k_{c,z}$	$f_{m,y,d}$	$f_{c,d}$	$M_{y,d}$	$M_{z,d}$	$N_{c,d}$	$\sigma_{c,d}$	$\sigma_{m,y,d}$	$\sigma_{m,z,d}$	utilization		
[m]	[-]	[-]	[-]	[-]	[N/mm ²]	[N/mm ²]	[kNm]	[kNm]	[kN]	[N/mm ²]	[N/mm ²]	[N/mm ²]			
1.45	1.82	0.50	0.36	1.00	12.18	9.69	2.43	0.00	-86.89	2.17	2.60	0.00	84 %		

Figure B.54: Buckling check performed in Calculatis

B.8. Stability system

B.8.1. Verification

The tool is verified using a hand calculation. For this verification, the frame in the short direction in Mjøstårnet is modelled in the tool, see Figure B.55a. This model and the found forces are compared with a hand calculation, see Figure B.55b. For both calculations, the gravitational loads are excluded.

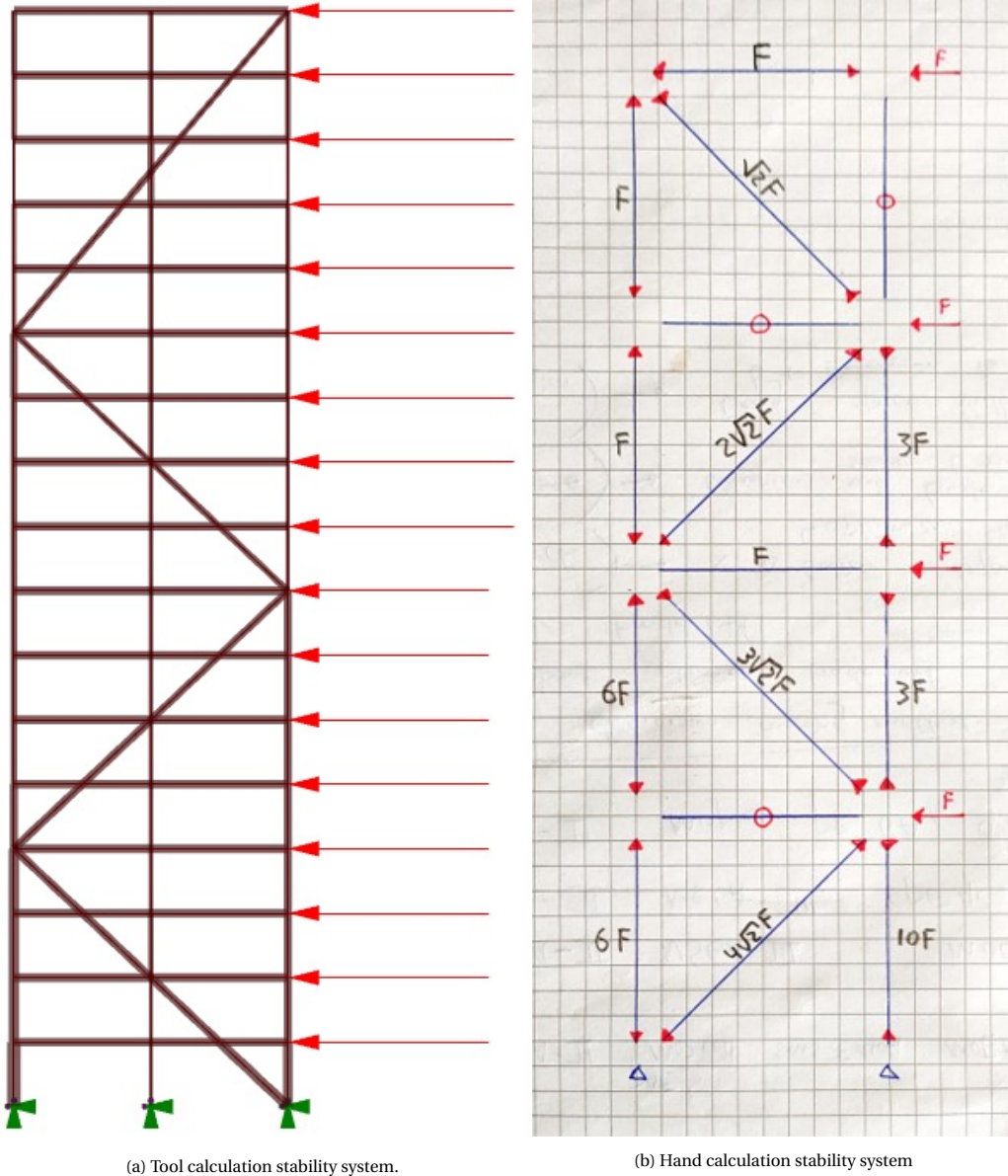


Figure B.55

Hand calculation A simplified hand calculation can be performed on the braced tube system in 2D, see Figure B.55b. To perform this calculation, a few assumptions are made:

- All connections are hinged connections.
- The wind force is evenly distributed over the height of the building and divided into point loads F .
- Only the outer columns and the beams at the height of the point loads F are included in the model.
- Gravitational loads are not considered.

The height of the stability system is 72m. To find the force F in Figure B.55b, the wind forces as obtained using the tool are used. For ULS, the tool gives a minimum wind force of 229 kN and a maximum wind force of 258 kN. These wind forces are applied at every floor of the building. There are 17 floors, so 17 forces. An average wind load of 245 kN is assumed. In the hand calculation, this wind load is divided into four forces F .

$$F = \frac{245 \cdot 17}{4} = 1041 \text{ kN} \quad (\text{B.25})$$

Verification stability system with hand calculation			
Force	Hand calculation	Model	Difference[%]
Maximum compression force in the column [kN]	$10 \cdot 1041 = 10410$	8554	22
Maximum tension force in the column [kN]	$6 \cdot 722.5 = 7521$	5514	36
Maximum force in the diagonal [kN]	$4\sqrt{2} \cdot 722.5 = 5888$	5057	16

Figure B.56: Verification of forces in stability system using a hand calculation

Comparison The hand calculation show 16 to 36% higher forces than the model, see Figure B.56. There are three reasons which can explain this difference:

1. The hand calculations assume all connections are hinged, so all forces are only transferred as normal forces.
2. The hand calculations do not include all columns and beams.
3. In the hand calculations, a force F is applied at the top of the building. When an evenly distributed wind load is transformed into these loads F , simply dividing the total load in four loads F will result in the force F at the top of the building to be overestimated, causing an overestimation of the forces.

Based on this verification it can be concluded that the forces obtained using the tool are within expected limits when checked using a hand calculation.

C

Environmental and Economical Data

C.1. Environmental performance calculation

Calculation of the environmental performance is effected greatly by the used EPD data. EPD data provided by manufacturers can vary greatly for the same material. Therefore, it is crucial to assess this data thoroughly, and use EPD data which is independently researched.

C.1.1. EPD data

EPD data connections The environmental performance of the connections is calculated by determining the total required weight of steel in the connections in the building. An EPD of steel is used to obtain the total environmental performance of the steel in the connections. The data for steel as specified in the NMD assumes 90% recycled steel as input material. However, only 40% of the steel in the market is recycled. Furthermore, NMD data assumes 49% of steel materials are re-used and 51% is recycled. However, according to Van Maastrigt (2019), only 5 to 10 % of steel is re-used [152]. The steel EPD data as provided by Ruuki is used in this research. This EPD data uses 20% recycled steel as input material. At the end-of-life stage, it assumes 90% recycling and 10% re-use [128].

All methods	stage	ADP-E	ADP-F	GWP	ODP	POCP	AP	EP
Steel	A1-A3	1.28E-05	1.33E-02	2.71E+00	9.74E-09	1.89E-03	5.48E-03	5.75E-04
	D	-1.31E-05	-6.59E-03	-1.30E+00	4.10E-08	-6.43E-04	9.16E-02	-8.78E-05
	Total	-3.00E-07	6.68E-03	1.41E+00	5.07E-08	1.25E-03	9.71E-02	4.87E-04

Figure C.1: Steel EPD data per kg material[128].

EPD data gypsum plates The gypsum boards which fire-protect the CLT core are included in the calculation of the shadow costs of the structural system. The EPD for the Knauf Diamant plasterboard is used [90].

All methods	stage	ADP-E	ADP-F	GWP	ODP	POCP	AP	EP
Gypsum board	A1-A3	2.34E-04	3.03E-02	4.22E+00	2.53E-09	5.34E-04	8.54E-03	1.85E-03
	C	4.85E-08	1.44E-03	2.42E-01	5.46E-12	-1.19E-04	6.03E-04	1.27E-04
	D	-1.59E-04	-4.27E-03	-6.37E-01	1.80E-10	-1.12E-04	-9.30E-04	-1.05E-04
	Total	7.50E-05	2.74E-02	3.83E+00	2.72E-09	3.03E-04	8.21E-03	1.87E-03

Figure C.2: Gypsum EPD data per m^2 material[90].

EPD data timber For timber elements, this research uses the EPD data as researched by Van Wijnen (2020) [157]. In this research, the EPD data from various manufacturers is researched for use in the Netherlands, according to the rules as defined for a MPG calculation. Data for the 3 different methods of including carbon sequestration is found, see Figures C.3, C.4 and C.5. LVL is used in the Kerto-Ripa plates. Thus LVL data is used to calculate the shadow costs of the Kerto-Ripa floor plates.

Method 1		ADP-E	ADP-F	GWP	ODP	POCP	AP	EP
Glulam	A1-A3	3.34E-07	1.29E-03	1.99E-01	1.61E-08	1.79E-04	1.11E-03	2.51E-04
	C	3.31E-09	1.11E-04	1.65E+00	3.36E-10	8.05E-06	7.40E-05	1.54E-05
	D* Recover	-9.33E-08	-2.36E-04	-4.34E-02	-1.41E-08	-1.79E-04	-1.15E-03	-3.74E-04
	Total	2.44E-07	1.17E-03	1.81E+00	2.34E-09	8.05E-06	3.40E-05	-1.08E-04
CLT	A1-A3	6.05E-07	1.62E-03	2.44E-01	2.66E-08	2.05E-04	1.24E-03	3.94E-04
	C	3.16E-08	1.92E-04	1.64E+00	2.86E-09	1.33E-05	1.66E-04	1.01E-04
	D* Recover	-9.33E-08	-2.36E-04	-4.34E-02	-1.41E-08	-1.79E-04	-1.15E-03	-3.74E-04
	Total	5.43E-07	1.58E-03	1.84E+00	1.54E-08	3.93E-05	2.56E-04	1.21E-04
LVL	A1-A3	1.16E-06	3.35E-03	4.17E-01	2.36E-08	2.34E-04	2.30E-03	5.03E-04
	C	5.88E-08	2.79E-04	1.79E+00	5.96E-09	4.78E-06	2.48E-04	1.14E-04
	D* Recover	-9.33E-08	-2.36E-04	-4.34E-02	-1.41E-08	-1.79E-04	-1.15E-03	-3.74E-04
	Total	1.13E-06	3.39E-03	2.16E+00	1.55E-08	5.98E-05	1.40E-03	2.43E-04

Figure C.3: EPD data used for method 1 per kg material [157].

Method 2		ADP-E	ADP-F	GWP	ODP	POCP	AP	EP
Glulam	A1-A3	3.34E-07	1.29E-03	-1.44E+00	1.61E-08	1.79E-04	1.11E-03	2.51E-04
	C	3.31E-09	1.11E-04	1.65E+00	3.36E-10	8.05E-06	7.40E-05	1.54E-05
	D* Recover	-9.33E-08	-2.36E-04	-4.34E-02	-1.41E-08	-1.79E-04	-1.15E-03	-3.74E-04
	Total	2.44E-07	1.17E-03	1.67E-01	2.34E-09	8.05E-06	3.40E-05	-1.08E-04
CLT	A1-A3	6.05E-07	1.62E-03	-1.38E+00	2.66E-08	2.05E-04	1.24E-03	3.94E-04
	C	3.16E-08	1.92E-04	1.64E+00	2.86E-09	1.33E-05	1.66E-04	1.01E-04
	D* Recover	-9.33E-08	-2.36E-04	-4.34E-02	-1.41E-08	-1.79E-04	-1.15E-03	-3.74E-04
	Total	5.43E-07	1.58E-03	2.17E-01	1.54E-08	3.93E-05	2.56E-04	1.21E-04
LVL	A1-A3	1.16E-06	3.35E-03	-1.19E+00	2.36E-08	2.34E-04	2.30E-03	5.03E-04
	C	5.88E-08	2.79E-04	1.79E+00	5.96E-09	4.78E-06	2.48E-04	1.14E-04
	D* Recover	-9.33E-08	-2.36E-04	-4.34E-02	-1.41E-08	-1.79E-04	-1.15E-03	-3.74E-04
	Total	1.13E-06	3.39E-03	5.57E-01	1.55E-08	5.98E-05	1.40E-03	2.43E-04

Figure C.4: EPD data used for method 2 per kg material [157].

Method 3		ADP-E	ADP-F	GWP	ODP	POCP	AP	EP
Glulam	A1-A3	3.34E-07	1.29E-03	-1.44E+00	1.61E-08	1.79E-04	1.11E-03	2.51E-04
	C	3.31E-10	1.11E-05	1.65E-01	3.36E-11	8.05E-07	7.40E-06	1.54E-06
	Total	3.34E-07	1.30E-03	-1.28E+00	1.61E-08	1.80E-04	1.12E-03	2.53E-04
CLT	A1-A3	6.05E-07	1.62E-03	-1.38E+00	2.66E-08	2.05E-04	1.24E-03	3.94E-04
	C	3.16E-09	1.92E-05	1.64E-01	2.86E-10	1.33E-06	1.66E-05	1.01E-05
	Total	6.08E-07	1.64E-03	-1.22E+00	2.69E-08	2.06E-04	1.26E-03	4.04E-04
LVL	A1-A3	1.16E-06	3.35E-03	-1.19E+00	2.36E-08	2.34E-04	2.30E-03	5.03E-04
	C	5.88E-09	2.79E-05	1.79E-01	5.96E-10	4.78E-07	2.48E-05	1.14E-05
	Total	1.17E-06	3.38E-03	-1.01E+00	2.42E-08	2.34E-04	2.32E-03	5.14E-04

Figure C.5: EPD data used for method 3 per kg material [157].

C.2. Economical performance calculation

C.2.1. Construction costs per building element

The prices of glulam and CLT elements are based on interview conducted with de Groot Vroomshop and Heko Spanten respectively. These engineered timber suppliers reported the following estimated costs for production and transportation.

For glulam GL30C [160].

- €700 per m^3 for cross sections up to 240x240mm
- €900 per m^3 for cross sections up to 480x480mm
- €1100 per m^3 for cross sections up to 720x720mm
- €1300 per m^3 for cross sections up to 960x960mm
- €1500 per m^3 for cross sections up to 1200x1200mm

For CLT elements, Heko Spanten reports an estimated cost of €1000 per m^3 independent of the thickness of the CLT element. This includes the connections used for CLT elements [141].

For Kerto-Ripa floor elements, for four lengths, a data sheet from Arcadis provides the prices for production. These prices are multiplied with a factor 1.2 to account for the transport. The used prices are given in Figure C.6a. Figure C.6b shows the obtained formula for determination of the price per m^2 for a 2.4 meter wide Kerto-Ripa floor element.

Figure C.6 shows the used data and found formula for assumption of the construction costs of a Kerto-Ripa floor element. The found Formula is shown in Equation C.1.

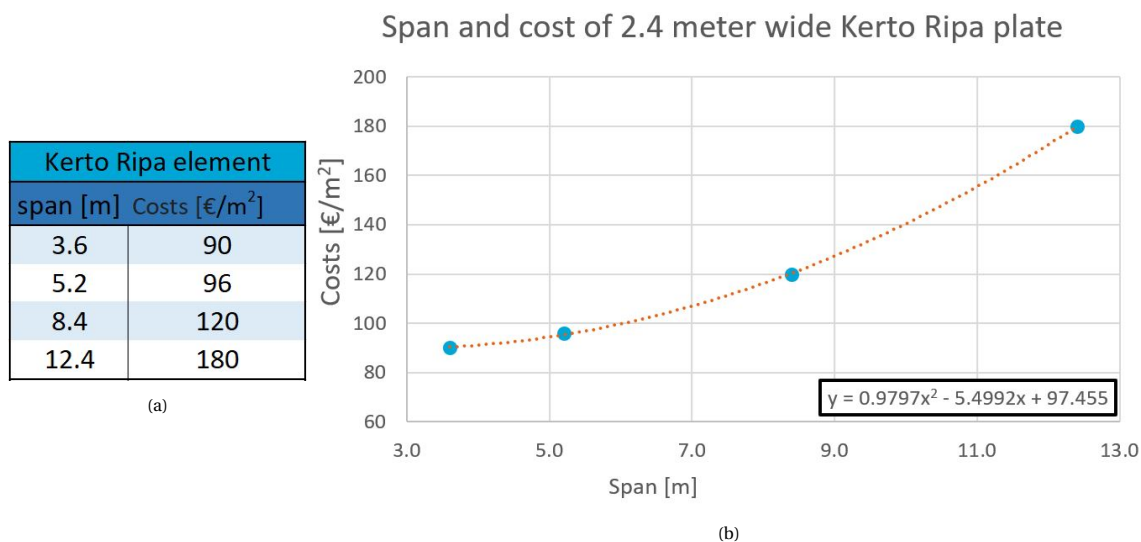


Figure C.6: Construction costs for a Kerto-Ripa plate [5].

$$Cost_{Floor} = 0.9797 \cdot L^2 - 5.4992 \cdot L + 97.455 \quad (C.1)$$

L = span of floor element in meters

C.2.2. Example of MAMO calculation

Figure C.7 visualizes the Economical Performance calculation as performed in the tool. The values used in this economical performance calculation are based on interviews conducted with Frehe (2021), who works as a cost expert for Arcadis.

D

Case Study

D.1. Construction cost calculations

Cost calculation	The Square			The Rectangle		
Item	Amount	Unit price	Total costs	Amount	Unit price	Total costs
Ground floor	829 m ²		€ 230,000	933 m ²		€ 230,000
Foundation piles			€ 160,000			€ 180,000
Water management	227	400	€ 80,000	243	400	€ 100,000
Foundation			€ 470,000			€ 510,000
Indirect costs (24%)			€ 110,000			€ 120,000
Total costs			€ 580,000			€ 630,000
Core walls	2592 m ²	200	€ 520,000	2246 m ²	200	€ 450,000
Columns	300	1500	€ 450,000	312	1500	€ 470,000
Insulated hollow core slab (260mm)	829	85	€ 70,000	933	85	€ 80,000
Uninsulated hollow core slab (260mm)	11612	65	€ 750,000	11197	65	€ 730,000
Structural topping (50mm)	12442	25	€ 310,000	12131	25	€ 300,000
Beams	3000	200	€ 600,000	2600	200	€ 520,000
Roof floor	829	65	€ 50,000	933	65	€ 60,000
Structural system			€ 2,750,000			€ 2,610,000
Indirect costs (24%)			€ 720,000			€ 680,000
Total Costs			€ 3,470,000			€ 3,290,000
Foundation + Structural system			€ 4,050,000			€ 3,920,000

Figure D.1: Cost calculation The Square and The Rectangle

D.2. MPG calculations

Below the shadow cost calculations for "The Square" and "The Rectangle" are shown. These calculations are performed using the MPGcalc 1.2 software [3].

MPGcalc 1.2



Algemene gegevens

Projectnaam:	The Rectangle excluding foundation
Plaatsnaam:	-
Variant:	kantoorgebouw basis
Status berekening:	Studieberekening
Versie productendatabase/NMD:	2.3

Gebouw

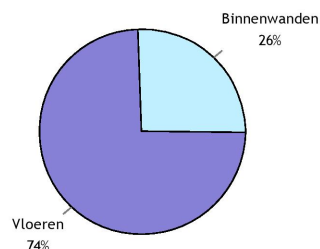
kantoorgebouw basis	
Categorie:	utiliteit nieuw; levensduur 50 jaar
Bruto vloeroppervlak:	12.131 m ²

Resultaten

Schaduwprijs:	€ 114.221 / 12... = 9,42 €/m ² BVO
Emissies:	€ 113.403 / 12... = 9,35 €/m ² BVO
Uitputting:	€ 818 / 12.131 = 0,07 €/m ² BVO

Schaduwkosten

Bouwdeel	Schaduwkosten per jaar per m ² BVO
Fundering	€ 0,-
Gevels	€ 0,-
Binnenwanden	€ 0,05
Vloeren	€ 0,14
Daken	€ 0,-
Installaties	€ 0,-
Inrichting	€ 0,-
Totaal	€ 0,19



Milieu-effecten

	Schaduwkosten	Milieu-effecten
Emissies	€ 113.403,-	
Klimaatverandering	€ 59.867,-	1.197.346 kg CO2 eq.
Aantasting ozonlaag	€ 2,-	0,0707 kg CFC-11 eq.
Humane toxiciteit	€ 27.593,-	306.592 kg 1.4-DB eq.
Zoetwater aquatische ecotoxiciteit	€ 206,-	6.880 kg 1.4-DB eq.
Mariene aquatische ecotoxiciteit	€ 3.106,-	31.060.850 kg 1.4-DB eq.
Terrestrische ecotoxiciteit	€ 811,-	13.515 kg 1.4-DB eq.
Fotochemische oxidantvorming	€ 502,-	251 kg C2H4 eq.
Verzuring	€ 13.192,-	3.298 kg SO2 eq.
Vermesting	€ 8.122,-	902 kg PO4 eq.
Uitputting	€ 818,-	
Uitputting abiotische grondstoffen	€ 1,-	4 kg Sb eq.
Uitputting fossiele energiedragers	€ 817,-	5.107 kg Sb eq.
Totaal	€ 114.221,-	

Resultaat Bouwbesluit

Schaduwkosten per jaar per m ² BVO:	€ 0,19
--	---------------

Figure D.2: Shadow cost calculation The Rectangle excluding foundation

MPGcalc 1.2



Algemene gegevens

Projectnaam:	The Rectangle including foundation
Plaatsnaam:	-
Variant:	kantoorgebouw basis
Status berekening:	Studieberekening
Versie productendatabase/NMD:	2.3

Gebouw

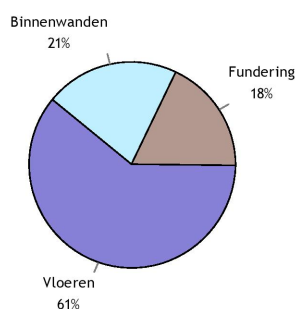
kantoorgebouw basis	
Categorie:	utiliteit nieuw; levensduur 50 jaar
Bruto vloeroppervlak:	12.131 m ²

Resultaten

Schaduwprijs:	€ 139.365 / 12... = 11,49 €/m ² BVO
Emissies:	€ 138.390 / 12... = 11,41 €/m ² BVO
Uitputting:	€ 974 / 12.131 = 0,08 €/m ² BVO

Schaduwkosten

Bouwdeel	Schaduwkosten per jaar per m ² BVO
Fundering	€ 0,04
Gevels	€ 0,-
Binnenwanden	€ 0,05
Vloeren	€ 0,14
Daken	€ 0,-
Installaties	€ 0,-
Inrichting	€ 0,-
Totaal	€ 0,23



Milieu-effecten

	Schaduwkosten	Milieu-effecten
Emissies	€ 138.390,-	
Klimaatverandering	€ 71.850,-	1.436.994 kg CO2 eq.
Aantasting ozonlaag	€ 2,-	0,0822 kg CFC-11 eq.
Humane toxiciteit	€ 34.485,-	383.167 kg 1.4-DB eq.
Zoetwater aquatische ecotoxiciteit	€ 245,-	8.164 kg 1.4-DB eq.
Mariene aquatische ecotoxiciteit	€ 3.659,-	36.587.984 kg 1.4-DB eq.
Terrestrische ecotoxiciteit	€ 911,-	15.187 kg 1.4-DB eq.
Fotochemische oxidantvorming	€ 799,-	399 kg C2H4 eq.
Verzuring	€ 16.936,-	4.234 kg SO2 eq.
Vermesting	€ 9.504,-	1.056 kg PO4 eq.
Uitputting	€ 974,-	
Uitputting abiotische grondstoffen	€ 1,-	4 kg Sb eq
Uitputting fossiele energiedragers	€ 974,-	6.086 kg Sb eq
Totaal	€ 139.365,-	

Resultaat Bouwbesluit

Schaduwkosten per jaar per m ² BVO:	€ 0,23
--	---------------

Figure D.3: Shadow cost calculation The Rectangle including foundation

MPGcalc 1.2



Algemene gegevens

Projectnaam:	The Square excluding foundation
Plaatsnaam:	-
Variante:	kantoorgebouw basis
Status berekening:	Studieberekening
Versie productendatabase/NMD:	2.3

Gebouw

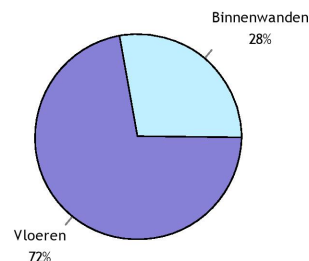
kantoorgebouw basis	
Categorie:	utiliteit nieuw; levensduur 50 jaar
Bruto vloeroppervlak:	12.442 m ²

Resultaten

Schaduwprijs:	€ 119.704 / 12... = 9,62 €/m ² BVO
Emissies:	€ 118.843 / 12... = 9,55 €/m ² BVO
Uitputting:	€ 861 / 12.442 = 0,07 €/m ² BVO

Schaduwkosten

Bouwdeel	Schaduwkosten per jaar per m ² BVO
Fundering	€ 0,-
Gevels	€ 0,-
Binnenwanden	€ 0,05
Vloeren	€ 0,14
Daken	€ 0,-
Installaties	€ 0,-
Inrichting	€ 0,-
Totaal	€ 0,19



Milieu-effecten

	Schaduwkosten	Milieu-effecten
Emissies	€ 118.843,-	
Klimaatverandering	€ 62.757,-	1.255.130 kg CO2 eq.
Aantasting ozonlaag	€ 2,-	0,0750 kg CFC-11 eq.
Humane toxiciteit	€ 28.873,-	320.813 kg 1.4-DB eq.
Zoetwater aquatische ecotoxiciteit	€ 217,-	7.233 kg 1.4-DB eq.
Mariene aquatische ecotoxiciteit	€ 3.278,-	32.780.039 kg 1.4-DB eq.
Terrestrische ecotoxiciteit	€ 851,-	14.188 kg 1.4-DB eq.
Fotochemische oxidantvorming	€ 537,-	269 kg C2H4 eq.
Verzuring	€ 13.650,-	3.413 kg SO2 eq.
Vermesting	€ 8.677,-	964 kg PO4 eq.
Uitputting	€ 861,-	
Uitputting abiotische grondstoffen	€ 1,-	4 kg Sb eq.
Uitputting fossiele energiedragers	€ 860,-	5.375 kg Sb eq.
Totaal	€ 119.704,-	

Resultaat Bouwbesluit

Schaduwkosten per jaar per m ² BVO:	€ 0,19
--	---------------

Figure D.4: Shadow cost calculation The Square excluding foundation

MPGcalc 1.2



Algemene gegevens

Projectnaam:	The Square including foundation
Plaatsnaam:	-
Variant:	kantoorgebouw basis
Status berekening:	Studieberekening
Versie productendatabase/NMD:	2.3

Gebouw

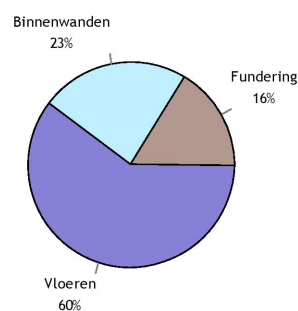
kantoorgebouw basis	
Categorie:	utiliteit nieuw; levensduur 50 jaar
Bruto vloeroppervlak:	12.442 m ²

Resultaten

Schaduwprijs:	€ 143.234 / 12... = 11,51 €/m ² BVO
Emissies:	€ 142.227 / 12... = 11,43 €/m ² BVO
Uitputting:	€ 1.007 / 12.442 = 0,08 €/m ² BVO

Schaduwkosten

Bouwdeel	Schaduwkosten per jaar per m ² BVO
Fundering	€ 0,04
Gevels	€ 0,-
Binnenwanden	€ 0,05
Vloeren	€ 0,14
Daken	€ 0,-
Installaties	€ 0,-
Inrichting	€ 0,-
Totaal	€ 0,23



Milieu-effecten

	Schaduwkosten	Milieu-effecten
Emissies	€ 142.227,-	
Klimaatverandering	€ 73.945,-	1.478.909 kg CO2 eq.
Aantasting ozonlaag	€ 3,-	0,0857 kg CFC-11 eq.
Humane toxiciteit	€ 35.366,-	392.953 kg 1.4-DB eq.
Zoetwater aquatische ecotoxiciteit	€ 253,-	8.431 kg 1.4-DB eq.
Mariene aquatische ecotoxiciteit	€ 3.793,-	37.929.689 kg 1.4-DB eq.
Terrestrische ecotoxiciteit	€ 946,-	15.763 kg 1.4-DB eq.
Fotochemische oxidantvorming	€ 816,-	408 kg C2H4 eq.
Verzuring	€ 17.140,-	4.285 kg SO2 eq.
Vermesting	€ 9.966,-	1.107 kg PO4 eq.
Uitputting	€ 1.007,-	
Uitputting abiotische grondstoffen	€ 1,-	4 kg Sb eq
Uitputting fossiele energiedragers	€ 1.006,-	6.290 kg Sb eq
Totaal	€ 143.234,-	

Resultaat Bouwbesluit

Schaduwkosten per jaar per m ² BVO:	€ 0,23
--	---------------

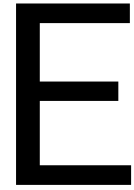
Figure D.5: Shadow cost calculation The Square including foundation

D.3. Building weight calculations

Figure D.6 shows the building weight calculations for "The Square" and "The Rectangle". It is assumed the amount of concrete in a 260 mm hollow core slabs is equal to a 160 mm full concrete floor. A density of 23.5 kN/m^3 is used for the concrete.

Building weight		The Square			The Rectangle		
Item	Dimensions [mm]	Amount	m ³ of concrete	Weight in kN	Amount	m ³ of concrete	Weight in kN
Core walls	300	2592	777.6	18274	2446	733.8	17244
Columns	530 x 530	300	84.27	1980	312	87.64	2060
Insulated hollow core slab (260mm)	260	829	132.6	3116	933	149.28	3508
Uninsulated hollow core slab (260mm)	260	11612	1857.92	43661	11197	1791.52	42101
Structural topping (50mm)	50	12442	622.1	14619	12131	606.55	14254
Beams	350 x 350	3000	367.5	8636	2600	318.5	7485
Roof floor	260	829	132.64	3117	933	149.28	3508
TOTAL weight structural system [kN]				75130	72915		
Imposed loads (follows from tool) [kN]				11197	10917		
Façade dead loads (follows from tool) [kN]				13443	12836		
Total of all loads [kN]				99770	96668		
kN per m ² foundation				120	104		
kg per m ² foundation				12268	10561		

Figure D.6: Cost calculation The Square and The Rectangle



Grasshopper Model Overview

E.1. Fixed model input parameters

The following fixed input is used in the tool:

1. Glulam type GL30C is used for beams, columns and diagonals. NEN-EN 14080 mentions properties for GL30C [78].

- $f_{m,k} = 30 \text{ N/mm}^2$
- $f_{t,0,k} = 19.5 \text{ N/mm}^2$
- $f_{c,0,k} = 24.5 \text{ N/mm}^2$
- $f_{v,k} = 3.5 \text{ N/mm}^2$
- $E_{0,mean} = 13000 \text{ N/mm}^2$
- $E_{0,05} = 10800 \text{ N/mm}^2$
- $G_{mean} = 650 \text{ N/mm}^2$
- $\rho_k = 390 \text{ kg/m}^3$
- $\rho_{mean} = 430 \text{ kg/m}^3$

2. The CLT is produced using C24 lamellas. The properties of C24 timber is given in NEN-EN 338 [79]. To obtain the strength of a CLT plate, it is assumed 3 out of 5 lamellas are positioned in the vertical direction, for the lamellas in the horizontal direction, a resistance of 0 N/mm^2 is used in the tool.

- $f_{m,k} = 24 \text{ N/mm}^2$
- $f_{c,0,k} = 21 \text{ N/mm}^2$
- $f_{v,k} = 4.0 \text{ N/mm}^2$
- $E_{0,mean} = 11000 \text{ N/mm}^2$
- $E_{0,05} = 7400 \text{ N/mm}^2$
- $G_{mean} = 690 \text{ N/mm}^2$
- $\rho_k = 350 \text{ kg/m}^3$
- $\rho_{mean} = 420 \text{ kg/m}^3$

3. Kerto-Ripa floor elements, according to a Metsa Wood brochure for Kerto-Ripa elements [107].

- $E_{deck,mean} = 10500 \text{ N/mm}^2$
- $E_{ribs,mean} = 13800 \text{ N/mm}^2$

4. Safety factors:

- $\gamma_m = 1.25$

- $\gamma_{m,fi} = 1.0$
- $k_{fi} = 1.0$
- $k_{mod} = 0.8$
- $k_{mod,fi} = 1.0$
- $k_{def} = 0.6$
- $k_m = 0.7$

5. Floor factors

- Deck E-modulus = $10500 \cdot 10^6 \text{ N/m}^2$ Kerto-Q (Deck)
- Ribs E-modulus = $13800 \cdot 10^6 \text{ N/m}^2$ Kerto-S (Ribs)
- Deck Thickness = 0.025 m
- Ribs Thickness = 0.051 m
- Imposed floor loads: 3 kN/m^2
- Kerto-Ripa floor width = 2.4 m
- Additional floor mass: 114 kg/m^2 (Floating screed: 2.4 kg/m^2 + Installations: 5 kg/m^2 + 2 Gypsum boards: 15 kg/m^2 + Variable load * combination value $\psi_{i,2} = 3.0 \text{ kN/m}^2 * 0.3 * 1000 / 9.81 = 91.7 \text{ kg/m}^2$)

6. Steel plate and dowel connection

- $f_y = 355 \text{ N/mm}^2$
- $f_u = 450 \text{ N/mm}^2$
- $h_p = 0 \text{ mm}$
- Thickness steel plate = 12 mm
- Number of steel plates per connection = 3
- Dowel diameter = 9 mm
- Timber width = 600 mm

7. Wind calculation:

- $c_{dir} = 1.0$ (Directional factor)
- $c_{season} = 1.0$ (Seasonal factor)
- $c_f = 0.85 \cdot 1.5$ (Force coefficient for the structure)
- $c_0 = 1.0$ (Orography factor)
- $k_l = 1.0$ (Turbulence factor)
- $\rho = 1.25 \text{ kg/m}^3$ (air density)
- $c_s c_d = 1.0$ (Building factor)

8. Other factors:

- Facade load = 1.5 kN/m^2
- factor height:width = 1.5 (factor between height and width of a beam)
- $t_{fire} = 120 \text{ min}$
- $\psi_2 = 0.3$ combination value used in fire design
- $\beta_n = 0.7$
- $k_0 d_0 = 7 \text{ mm/min}$
- $\beta_c = 0.1$
- $\eta_{fi} = 0.45$ Fire reduction factor

9. Input in Karamba3D Optimize Cross Section component for GL30C:

- $E_{0,mean} = 13000 \text{ N/mm}^2$
- $E_{90,mean} = 13000 \text{ N/mm}^2$
- $G_{12} = 650 \text{ N/mm}^2$
- $\nu_{12} = -1$
- $G_{31} = 650 \text{ N/mm}^2$
- $G_{32} = 650 \text{ N/mm}^2$
- $\gamma_{mean} = 4.2 \text{ kN/m}^3$
- $\alpha_{T1} = 23.4 * 10^{-6} / ^\circ\text{C}$
- $\alpha_{T2} = 32.4 * 10^{-6} / ^\circ\text{C}$
- $f_{y1} = 19.5 \text{ N/mm}^2$ *
- $f_{y2} = 0.5 \text{ N/mm}^2$

*For the yield strength, the characteristic tension strength is used in the strong and weak direction.

E.2. Input parameters Mjöstårnet model

For the determination of the wind loads on the building, the Norwegian annex to the Eurocode NS-EN 1991-1-4 is used [111].

Input parameters

- Grid X = 9.0 m
- N columns X = 3
- Grid Y = 7.2 m
- N columns Y = 6
- N diagonals X = 2
- N diagonals Y = 3
- Diagonals X placement = 0
- Diagonals Y placement = 1
- Length Steel plate X = 1200 mm
- Length steel plate Y = 1000 mm
- Maximum unity check = 1.0
- Minimum required floor area = 11000 m^2
- Free floor height = 3.2 m
- Imposed floor load = 3.0 kN/m^2
- Additional floor height = 0.44 m
- Additional floor mass = 114 kg/m^2
- Wind zone, to define the wind zone, a basic wind speed $v_b = 22.0 \text{ m/s}$ is put into the custom node for wind force calculation, following the Norwegian annex to the Eurocode NS-EN 1991-1-4
- Terrain category = 1
- Floor type = Kerto-Ripa Box floor

- Core size ratio = 0.25
- Dead load façade = 2.0 kN/m

Other assumptions

- In the dowel and steel plate connection, the dowel diameters are 8 mm
- In the dowel and steel plate connection, the thickness of the steel plate is 8 mm
- For the inner columns, GL30H is used.
- Average width of a timber element where a steel plate is located is 620 mm.
- 3 steel plates are used per connection.
- For the determination of the total amount of m^3 of used timber, it is assumed 65% of the total façade consists of panels containing 60 mm of timber.

E.3. Figures of Grasshopper model

The Grasshopper model follows the schematization of the framework.

Overview

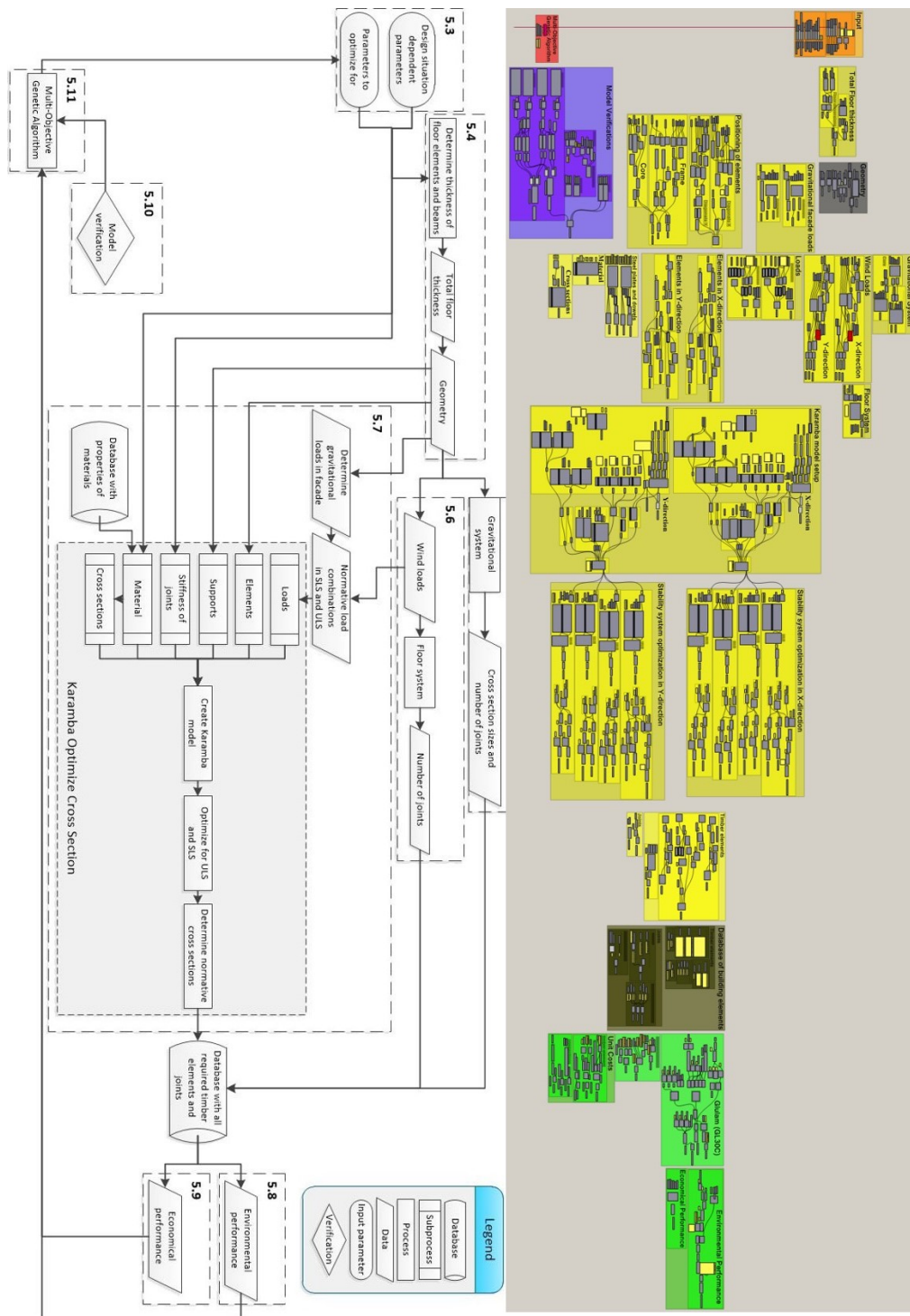


Figure E.1: Overview.

5.3 Input

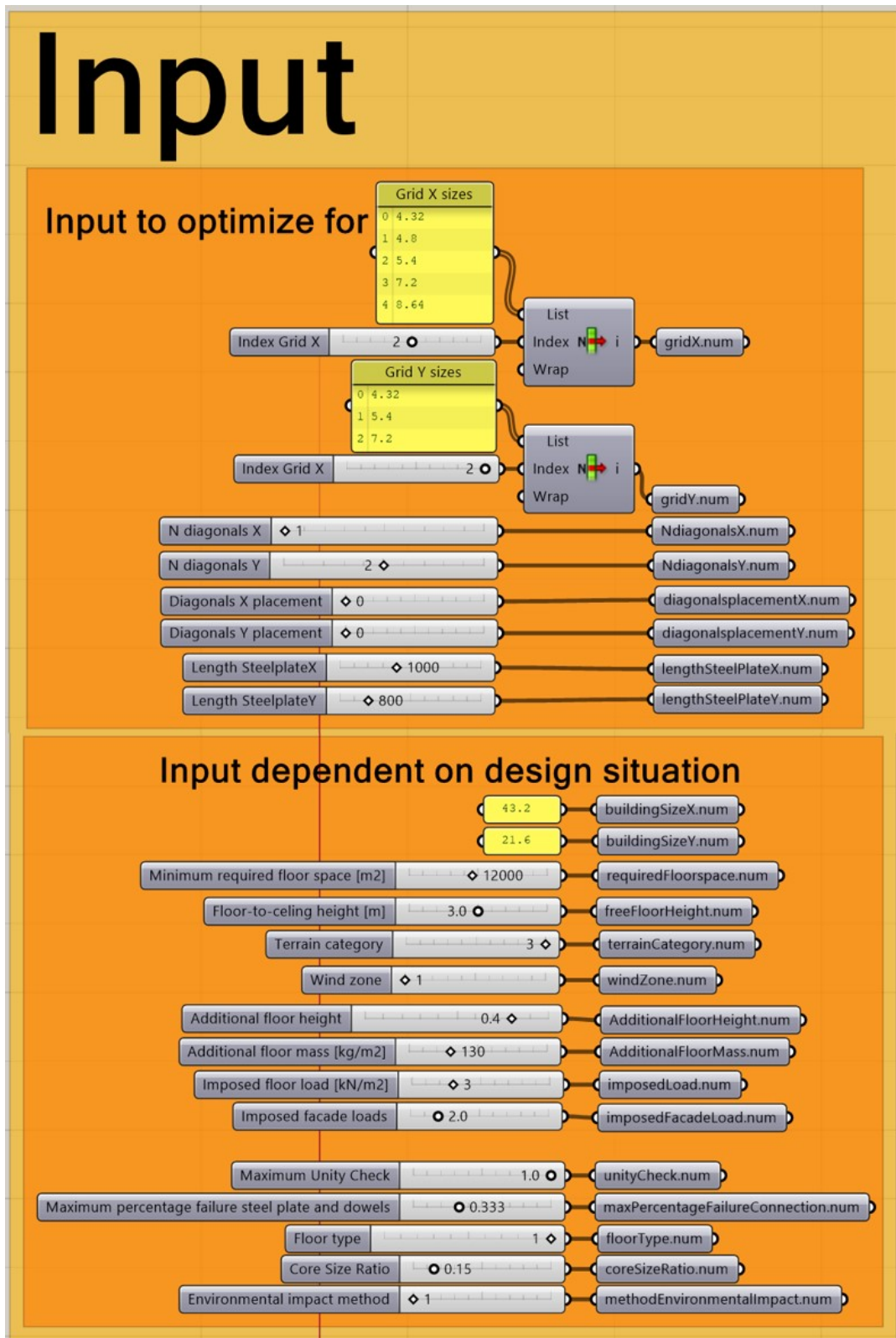


Figure E.2: Input parameters.

5.4 Building geometry

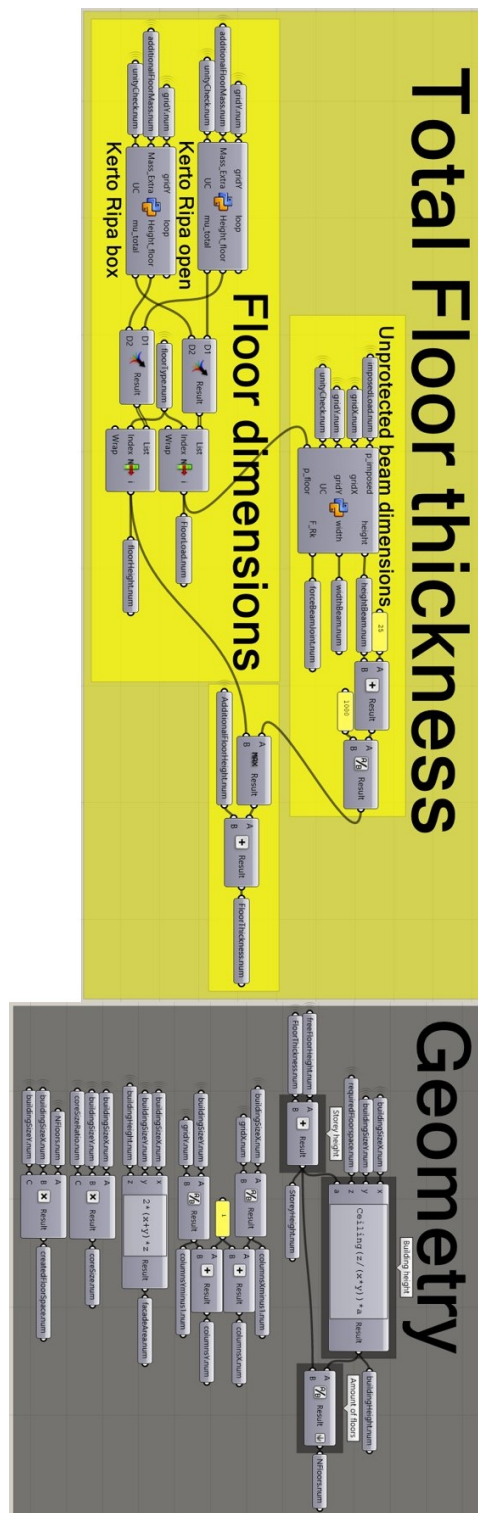


Figure E.3: Building geometry.

5.5 Gravitational system

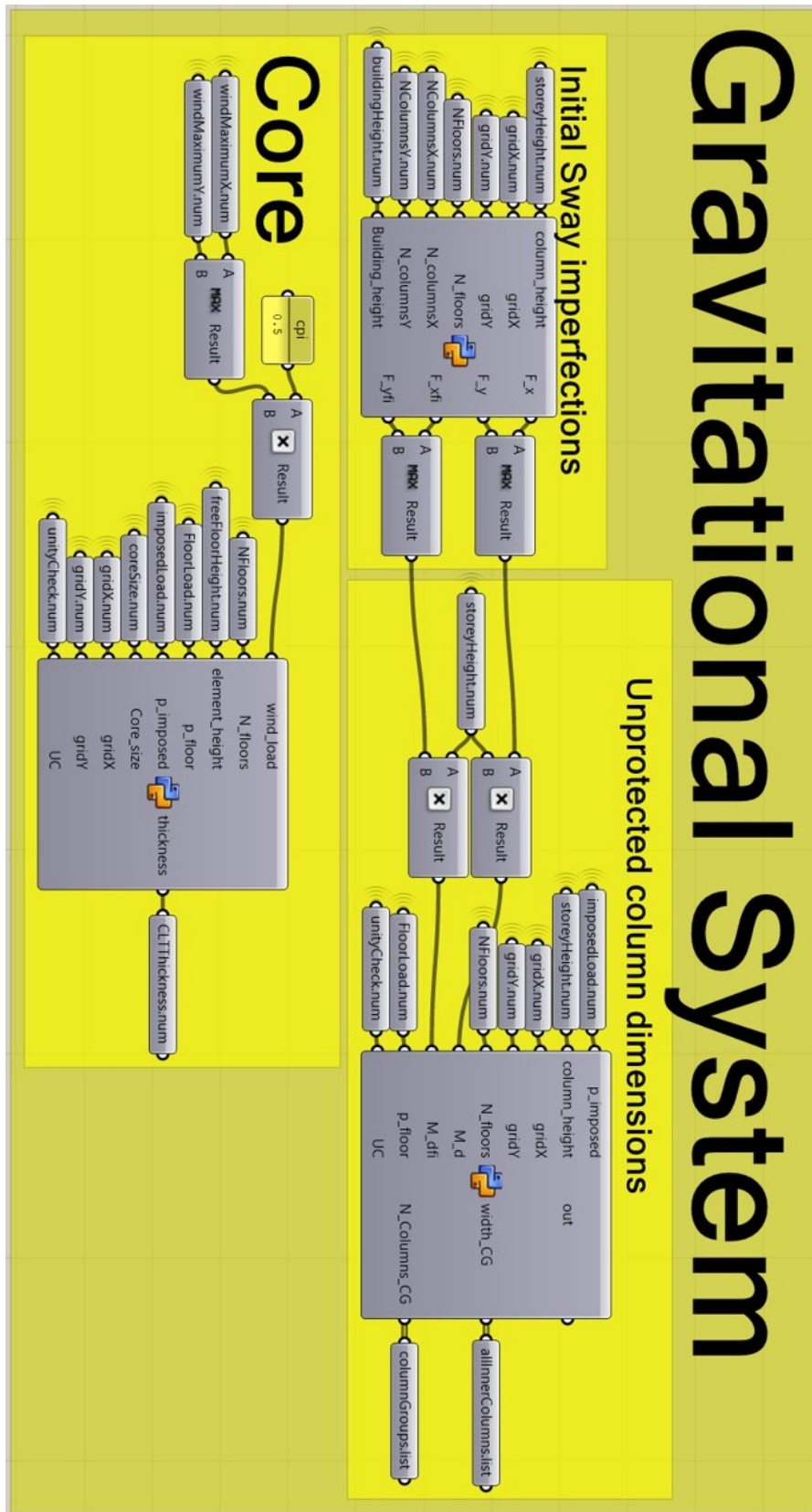


Figure E.4: Gravitational system.

5.7 Stability system

The set-up of the Karamba3D model and the analysis of the four load situations is only visualized in X-direction. In Y-direction this modelling process follows the same process.

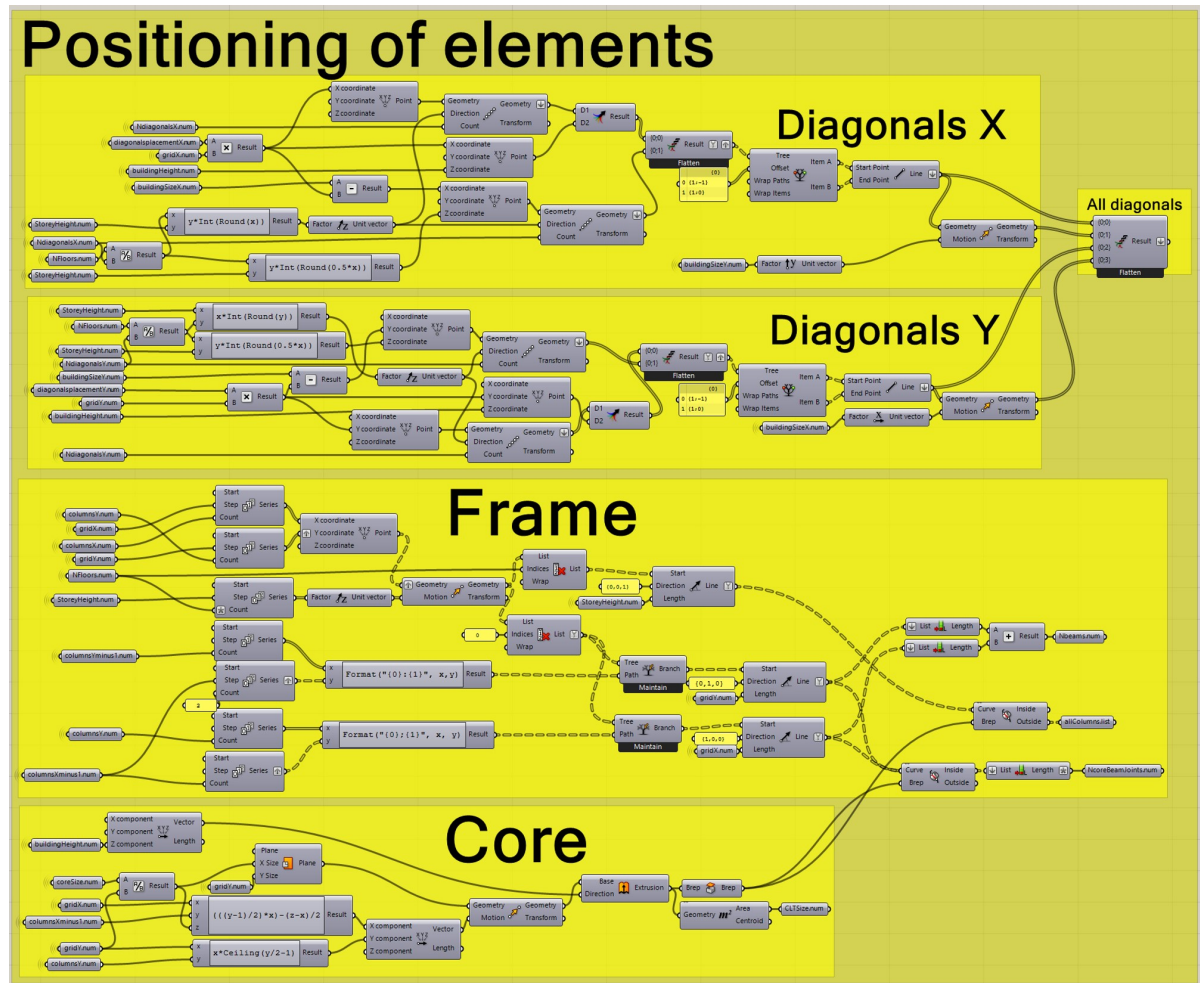


Figure E.6: Stability system: Positioning of elements.

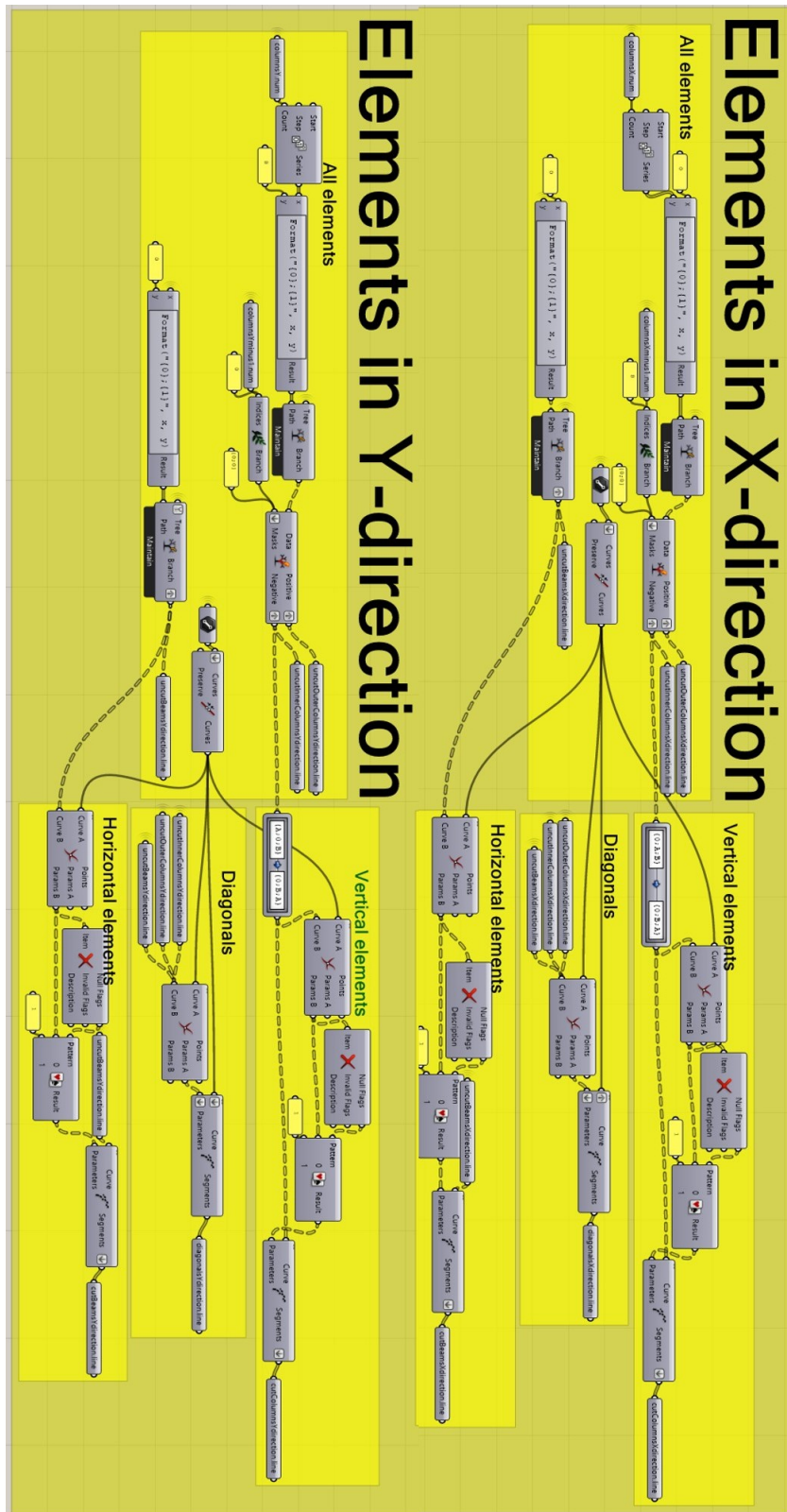


Figure E.8: Stability system: Grouping of elements.

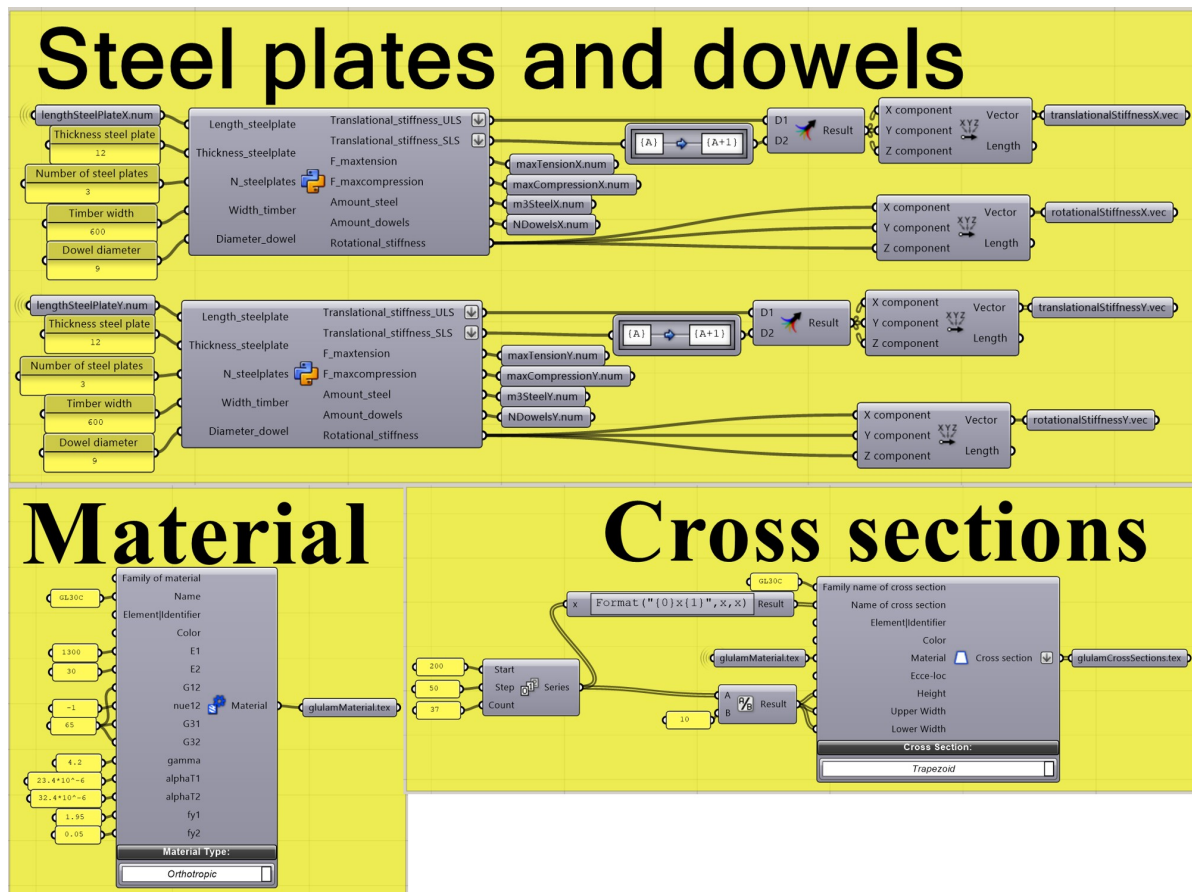


Figure E.9: Stability system: Connections, Material and Cross sections.

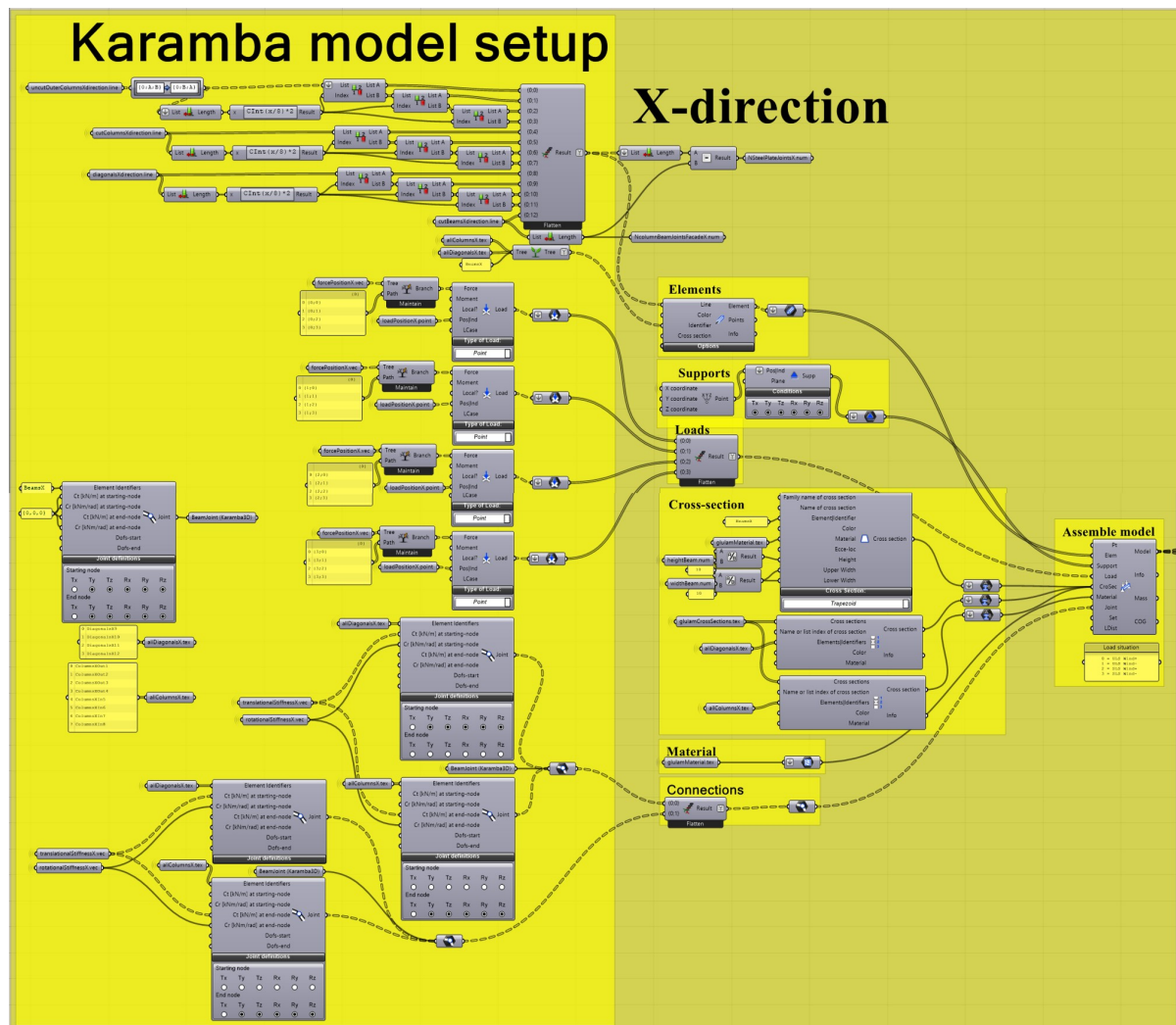


Figure E.10: Stability system: Karamba3D model setup.

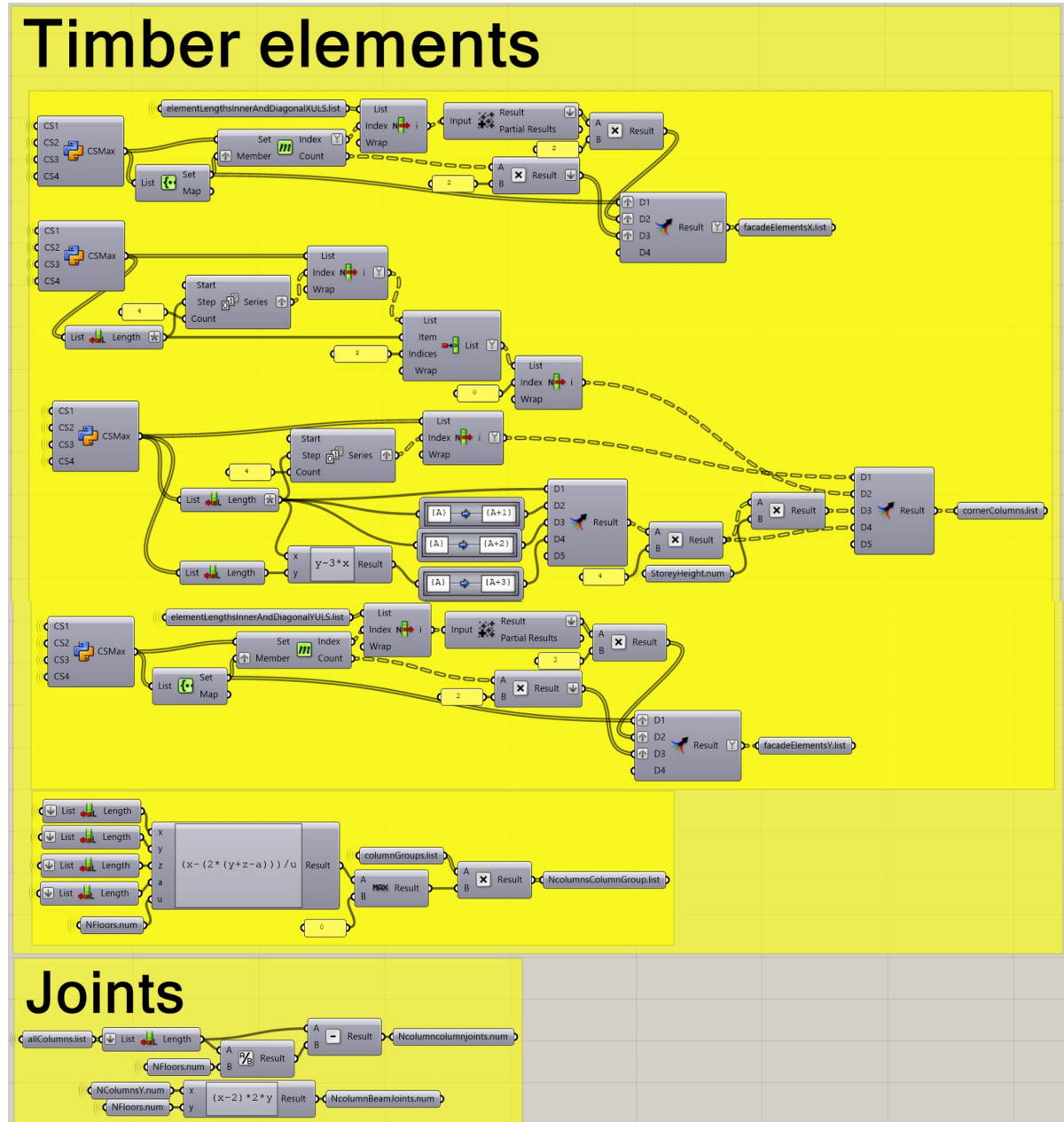


Figure E.12: Stability system: Preperation of building elements and connections for storage in database.

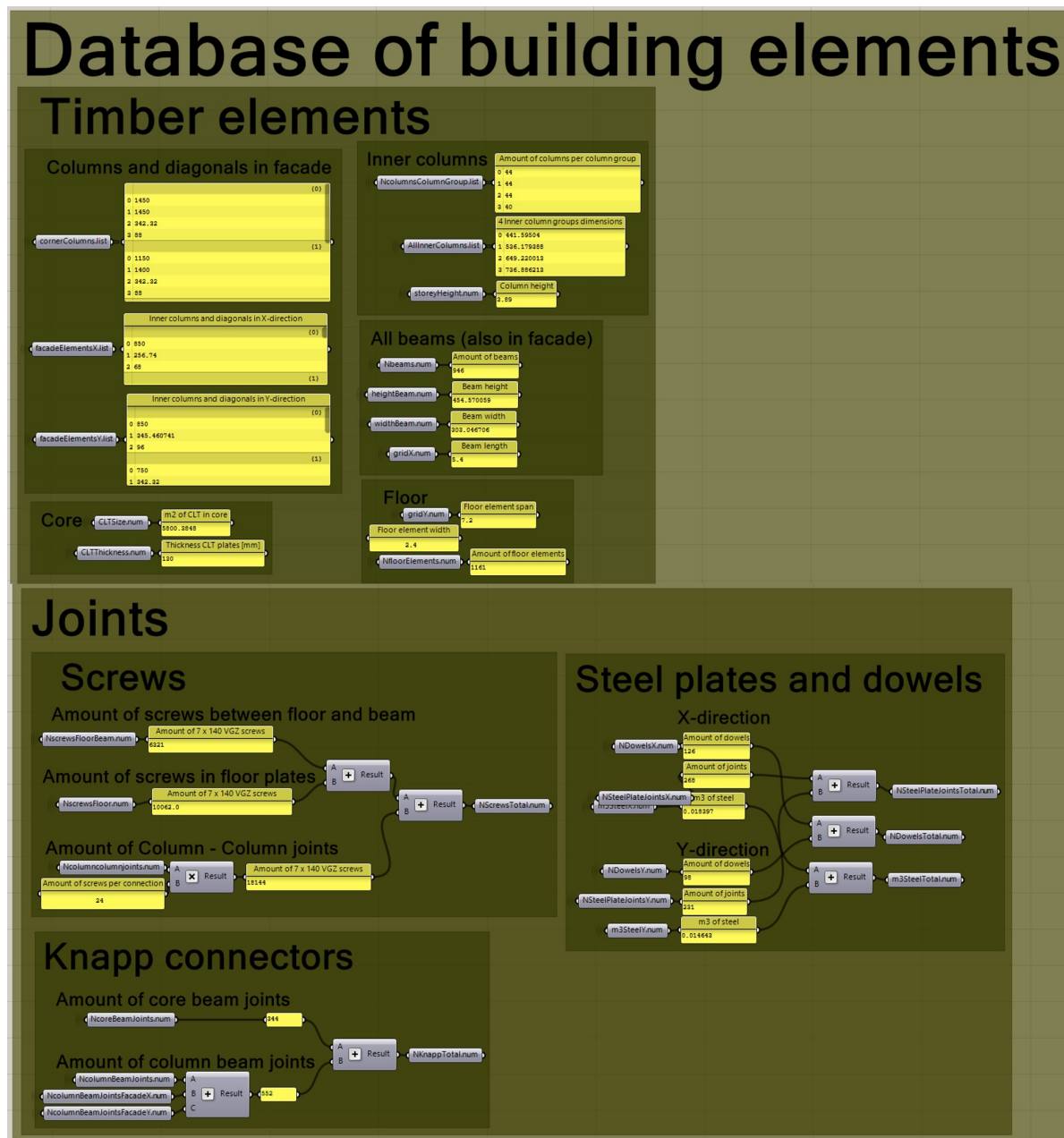


Figure E.13: Stability system: Database of building elements and connections.

5.8 Environmental performance

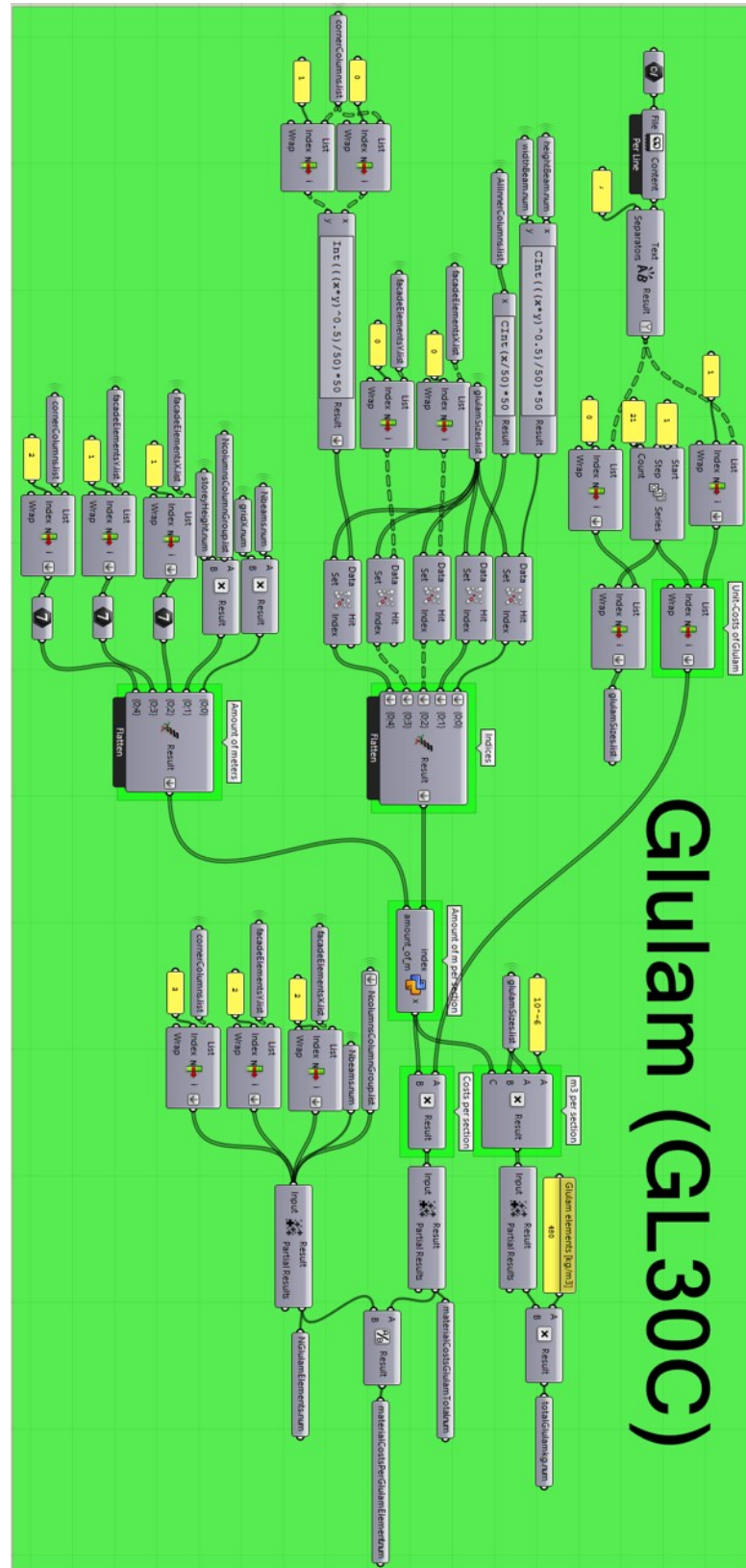


Figure E.14: Environmental performance: grouping of glulam elements.

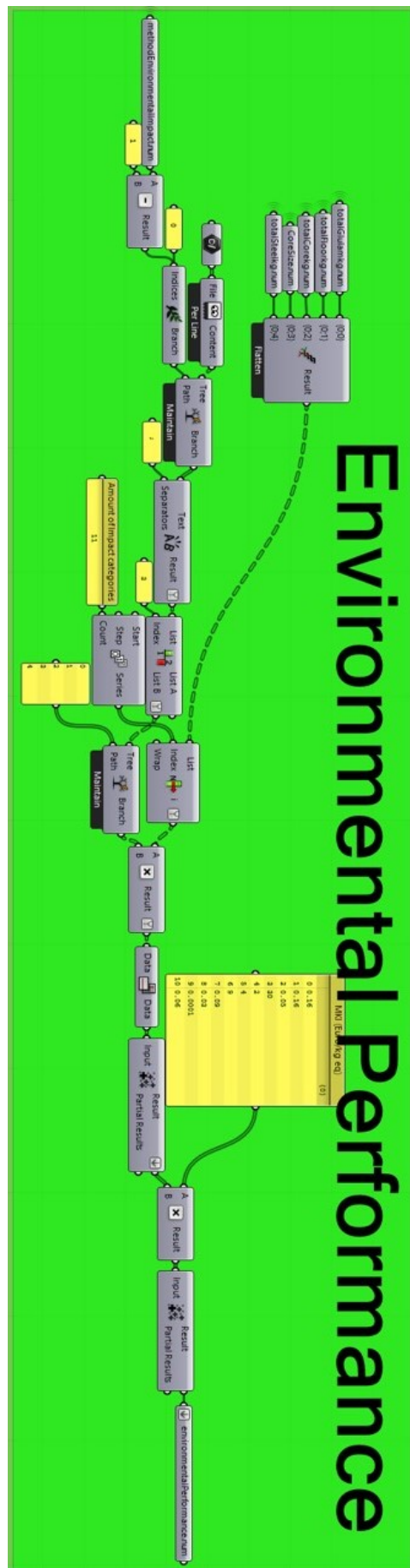


Figure E.15: Environmental performance: Shadow costs calculation.

5.9 Economical performance

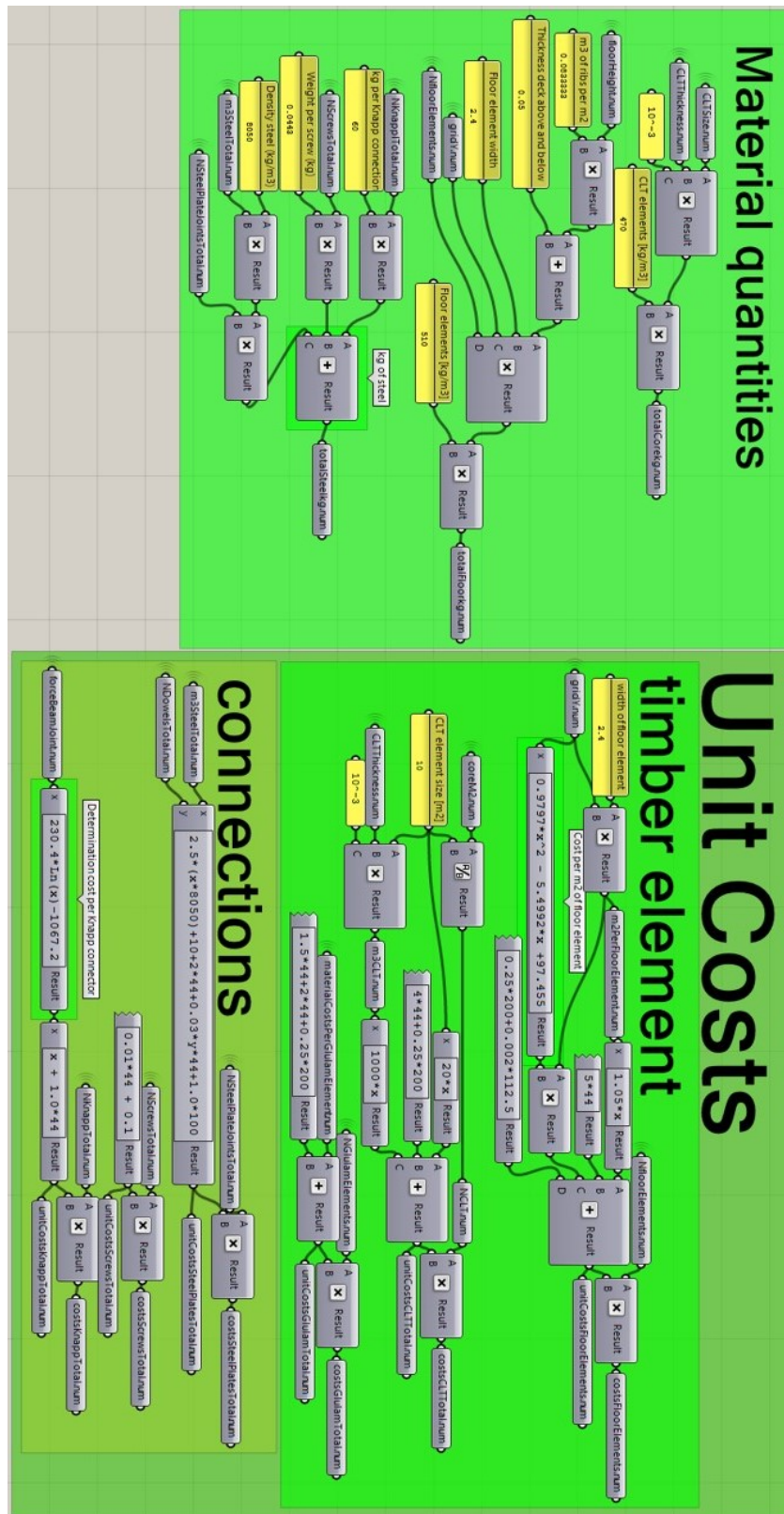


Figure E.16: Economical performance: Unit cost calculation following the MAMO methodology

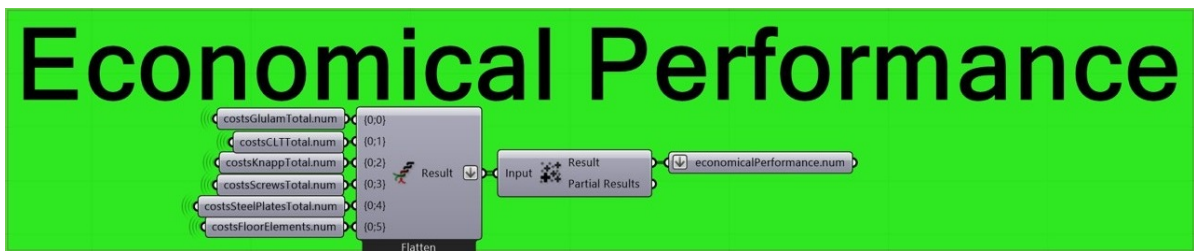


Figure E.17: Economical performance: Construction cost calculation

5.10 Post optimization verification

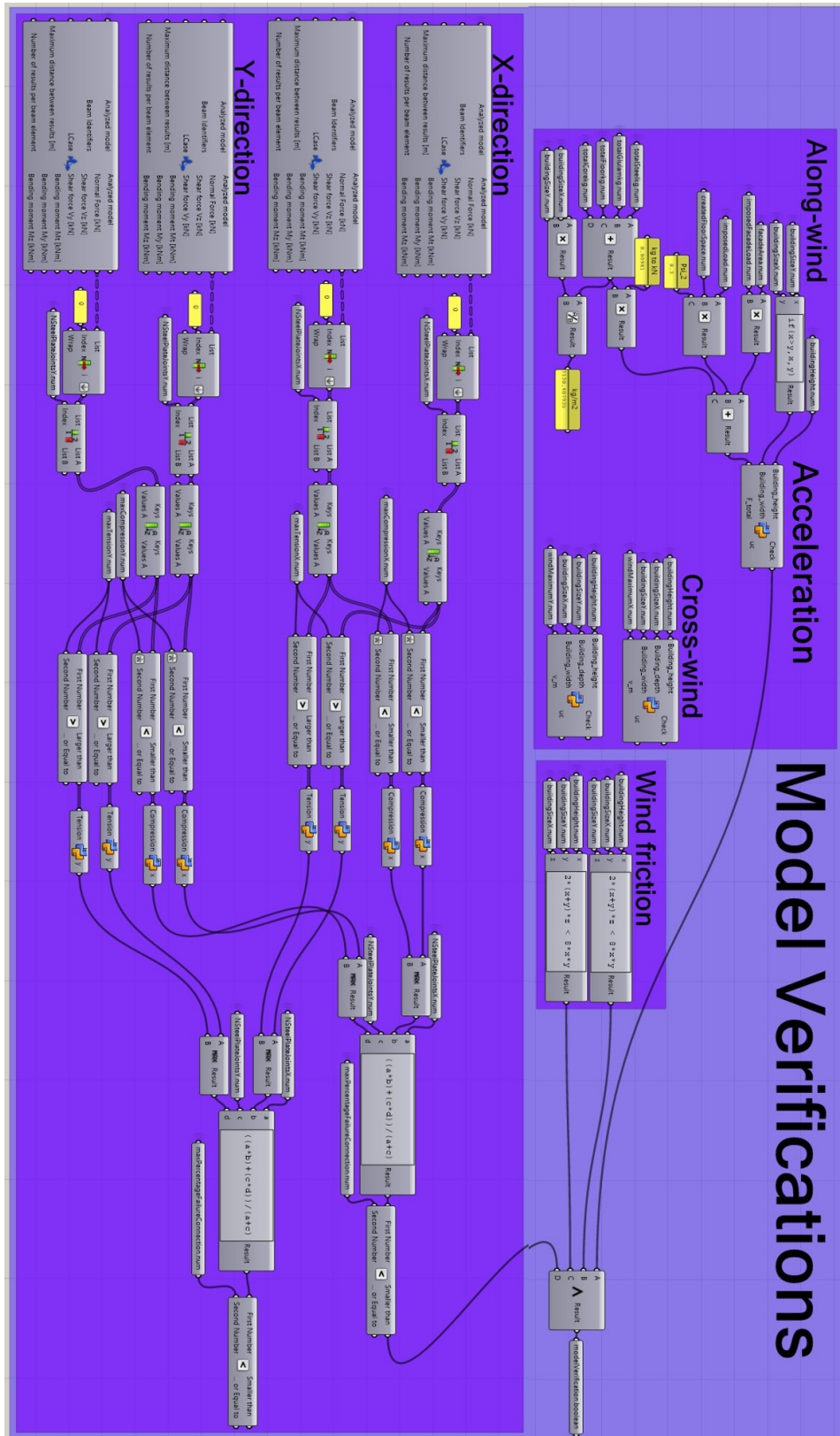


Figure E.18: Post optimization verification: Acceleration, wind friction and connection strength.

5.11 Multi-Disciplinary Design Optimization

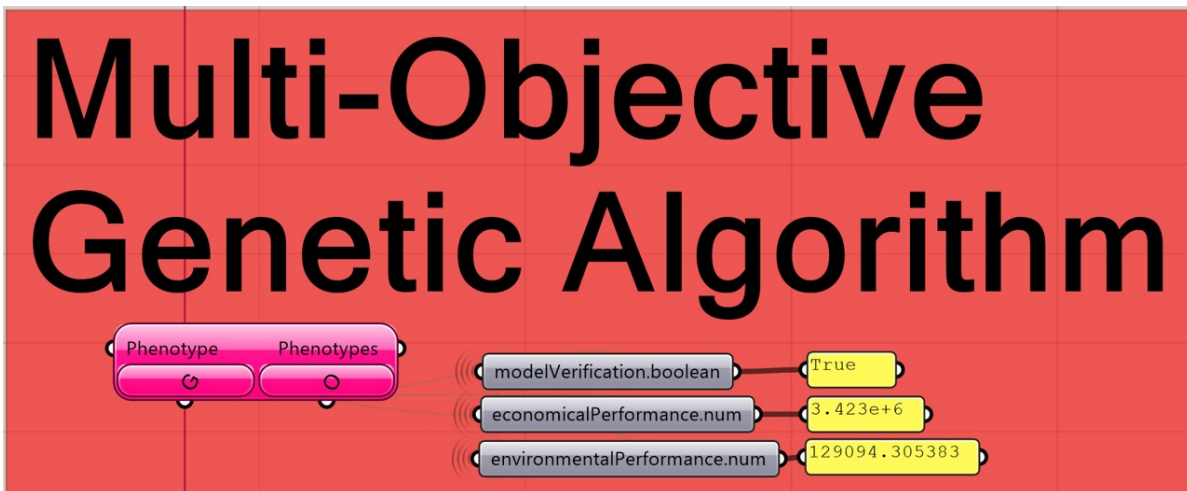


Figure E.19: Octopus plugin.

F

Interviews

Figure E1 include the professionals I contacted for interviews and crucial meetings. The interviews had an unstructured nature. The meetings with my supervisors are not included in this list.

Interviews		
Date	Person	Topics
03-09-2020	Igor Pećanac	Dynamo possibilities, computational design
03-09-2020	Michael van Telgen	Dynamo connection to RFEM, computational design
14-09-2020	Gert de Vries	Usage of timber in warehouse project, architecture
16-09-2020	Sander van Gemert	Shadow cost calculation.
23-09-2020	Toine Fokkens	Sustainability, circularity, costs.
24-09-2020	Pieter Timmerman	Timber buildings, connections and types.
25-09-2020	Wiljan Houweling	Arcadis Projects, conceptual design phase.
28-09-2020	Gerard van Engelen	Arcadis Projects, core design and conceptual design phase.
28-09-2020	Martijn Goossens	Operational energy, Vabi elements.
29-09-2020	Erwin Dam	Conceptual design phase, role of contractor.
01-10-2020	Geert Ravenshorst	Timber connection design and general timber design.
01-10-2020	Nationaal Digitaal Houtbouwcongres 2020	Timber design, reference projects
07-10-2020	Eildert Broekholt	Multidisciplinary process.
14-10-2020	Dion Jansen	MDO, Packhunt.io.
15-10-2020	Masterclass timber high-rise	Timber connections, stability systems.
16-10-2020	Kick-off meeting	-
20-10-2020	Max Hamelijnc	Connections, stability systems.
27-10-2020	Dietmar van Loon	Conceptual design phase.
29-10-2020	Paul Minartz	Creaking of connections, Nitrogen emissions.
03-11-2020	Tigist Znabei	Post-tensioning of a CLT core.
06-11-2020	Walter Frehe	Construction costs.
17-11-2020	Jane Armstrong	Timber design in Australia, creaking, fire safety, earthquake design and costs
22-01-2021	Sander van Gemert	EPD, construction cost calculations
03-02-2021	Progress meeting 1	-
04-03-2021	Heko Spanten	Information costs CLT plates
04-03-2021	De Groot Vroomshop	Information costs glulam elements
11-03-2021	Presentation Building Engineering students	-
16-03-2021	Presentation Structural Engineering students	-
23-03-2021	Walter Frehe	Case study, economical Performance, MAMO rules
29-03-2021	Sander van Gemert	Environmental performance
07-04-2021	Progress meeting 2	-
19-05-2021	Green light meeting	-
16-06-2021	Thesis defence	-

Figure E1: Unstructured interviews.